

Effective Lagrangian Perspectives on Electroweak Symmetry Breaking

THÈSE N° 6346 (2014)

PRÉSENTÉE LE 19 SEPTEMBRE 2014
À LA FACULTÉ DES SCIENCES DE BASE
LABORATOIRE DE PHYSIQUE THÉORIQUE DES PARTICULES
PROGRAMME DOCTORAL EN PHYSIQUE

ÉCOLE POLYTECHNIQUE FÉDÉRALE DE LAUSANNE

POUR L'OBTENTION DU GRADE DE DOCTEUR ÈS SCIENCES

PAR

Andrea THAMM

acceptée sur proposition du jury:

Prof. O. Schneider, président du jury
Prof. R. Rattazzi, Prof. C. Grojean, directeurs de thèse
Prof. R. Barbieri, rapporteur
Prof. T. Nakada, rapporteur
Dr A. Weiler, rapporteur



ÉCOLE POLYTECHNIQUE
FÉDÉRALE DE LAUSANNE

Suisse
2014

*Für meinen Opa
mit dem ich so oft in die Ferne geblickt habe*

Abstract

We use an effective Lagrangian approach to address the question of the dynamics of electroweak symmetry breaking in the Standard Model (SM) and its relation to the hierarchy problem. Composite Higgs models provide a solution by describing the recently discovered Higgs-like scalar particle as a composite pseudo Nambu-Goldstone boson that dissolves into its constituents above a certain high energy scale. We discuss many features of the low energy description of composite Higgs models and present an explicit realisation in a flat extra dimension showing explicitly that top partners with masses below 1 TeV are expected in a natural theory. Naturalness requires New Physics not much above the weak scale and hence motivates the search for direct and indirect evidence of physics beyond the SM at the LHC and future colliders. As an indirect probe at the LHC, we propose a dedicated analysis of single top production in association with a Higgs boson to lift the degeneracy in the sign of the top Yukawa coupling. We move on to an extensive study of WW scattering, double and triple Higgs production at future linear colliders to estimate their impact on the parameter space of a strongly interacting Higgs boson. Direct probes of New Physics at the LHC include the search for heavy vectors and fermions. We introduce a model-independent strategy to study narrow resonances which we apply to a heavy vector triplet of the SM for illustration. We conclude by summarising current constraints and the expected reach of future colliders on the parameter space of a minimal composite Higgs model. This thesis is based on the papers in Refs. [1–4].

Key words: effective Lagrangian, electroweak symmetry breaking, beyond the Standard Model physics, composite Higgs, LHC phenomenology, future colliders

Zusammenfassung

In dieser Arbeit benutzen wir die Methode der effektiven Lagrangefunktionen, um die Dynamik der elektroschwachen Symmetriebrechung im Standardmodell unter dem Gesichtspunkt des Hierarchieproblems zu untersuchen. Die Composite-Higgs-Modelle liefern eine Lösung des Hierarchieproblems, indem das kürzlich entdeckte Higgs-artige skalare Teilchen als zusammengesetztes Pseudo-Nambu-Goldstone-Boson beschrieben wird, das oberhalb einer höheren Energieskala in seine Komponenten zerfällt. Wir diskutieren die Eigenschaften zur Beschreibung des Composite-Higgs-Modells bei niedrigen Energien und liefern eine explizite Realisierung in einer flachen Extradimension und zeigen unmittelbar, dass Top-Partner mit Massen unterhalb 1 TeV auf natürliche Weise auftreten. Das Naturalness Principle verlangt eine neue Physik nicht weit oberhalb der schwachen Energieskala und motiviert deshalb die Suche am LHC und an zukünftigen Beschleunigern nach direkten oder indirekten Hinweisen auf eine Physik jenseits des Standardmodells. Als einen indirekten Test am LHC stellen wir eine zweckbestimmte Analyse der Top-Quark Produktion zusammen mit einem Higgs-Boson vor, um die Mehrdeutigkeit des Vorzeichens der Top-Yukawa-Kopplung zu klären. Weiterhin unternehmen wir eine umfassende Analyse der WW -Streuung, der Doppel- und Tripel-Higgs-Produktion an zukünftigen Linearbeschleunigern, um deren Einfluss auf den Parameterraum eines stark gekoppelten Higgs-Bosons abzuschätzen zu können. Direkte Hinweise auf eine neue Physik am LHC schließen die Suche nach schweren Vektor-Teilchen oder schweren Fermionen ein. Wir stellen außerdem eine modellunabhängige Methode zur Untersuchung schmaler Resonanzen vor, die wir zur Veranschaulichung auf schwere Vektor-Triplets des Standardmodells anwenden. Wir schließen mit einer Zusammenfassung der aktuellen Randbedingungen unter Berücksichtigung der zu erwartenden Reichweite künftiger Beschleuniger im Parameterraum eines minimalen Composite-Higgs-Modells. Diese Dissertation basiert auf den folgenden Veröffentlichungen [1–4].

Stichwörter: effektive Lagrangefunktionen, elektroschwache Symmetriebrechung, Physik jenseits des Standardmodells, composite Higgs, LHC Phenomenologie, zukünftige Beschleuniger

Contents

Abstract	v
1 Introduction	1
2 Effective Lagrangians for the Higgs boson	9
2.1 Dynamics of electroweak symmetry breaking	9
2.1.1 The linear σ -model	10
2.1.2 The non-linear σ -model	11
2.1.3 Implications of experimental evidence	13
2.2 Effective Lagrangian for New Physics effects	14
2.2.1 Higher dimensional operators	14
2.2.2 Higgs couplings	20
2.3 Electroweak precision tests	22
2.3.1 Current constraints on higher dimensional operators	22
2.3.2 Current constraints on the Higgs couplings	24
2.3.3 Oblique parameters	26
3 The Minimal Composite Higgs Model	31
3.1 The Goldstone and gauge sector: a Higgs as a pNGB	31
3.2 The fermionic sector: partial compositeness	34
3.2.1 A composite Higgs with $q_L \in \mathbf{14}$ and $t_R \in \mathbf{1}$	37
3.2.2 The Higgs potential	39
3.3 The 5D construction	41
3.3.1 Gauge degrees of freedom	42
3.3.2 Fermionic degrees of freedom	45
3.3.3 The spectrum of fermionic resonances	47
3.4 Numerical analysis	49
3.4.1 Results	51
3.5 Conclusions	56
4 Indirect Probes of NP at the LHC	59
4.1 Introduction	59
4.2 Single top and Higgs associated production	61
4.3 Signal and background study	66

4.3.1	Parton-level simulation	66
4.3.2	Final state with 3 b -tags	67
4.3.3	Final state with 4 b -tags	69
4.4	Implications on Higgs couplings	71
4.5	Conclusions	72
5	Indirect Probes of NP at Future Colliders	75
5.1	Introduction	75
5.2	Current constraints on the Higgs couplings	76
5.2.1	Direct coupling measurements	77
5.2.2	Resonance searches	77
5.3	What can be learned from single and double Higgs production?	79
5.4	What can be learned from triple Higgs production?	82
5.4.1	Symmetry structure	82
5.4.2	Quantitative analysis of $VV \rightarrow hh$	83
5.5	Quantitative analysis of $VV \rightarrow VV$ and $VV \rightarrow hh$	87
5.5.1	Identification cuts	87
5.5.2	$VV \rightarrow VV$ scattering	88
5.5.3	$VV \rightarrow hh$ scattering	92
5.5.4	Double Higgs-strahlung	98
5.6	Conclusions	105
6	Direct Probes of NP	109
6.1	Introduction	109
6.2	A Simple Simplified Model for a Heavy Vector Triplet	112
6.2.1	Basic phenomenology	116
6.2.2	Production rates parameterized	124
6.2.3	Data and Bounds	128
6.2.3.1	A first look at the LHC bounds	129
6.2.3.2	Limits on the Simplified Model parameters	131
6.2.3.3	Limit setting for finite widths	134
6.2.4	Explicit Models	141
6.2.4.1	Model A: extended gauge symmetry	141
6.2.4.2	Model B: Minimal Composite Higgs Model	143
6.2.4.3	The role of higher dimensional operators	145
6.3	A Simplified Model for Top Partners	149
6.3.1	Basic phenomenology	151
6.3.2	Data and Bounds	151
6.4	Conclusions	153
7	Conclusions	155
A	The Minimal Composite Higgs Model	159

A.1	The CCWZ chiral Lagrangian	159
A.2	$SO(5)$ generators	160
A.3	5D implementation in AdS_5 space	161
A.3.1	Gauge degrees of freedom	161
A.3.2	Fermionic degrees of freedom	163
A.4	The electroweak fit	166
B	Indirect Probes of NP at the LHC	169
B.1	Forward $Wb \rightarrow th$ scattering	169
C	Indirect Probes of NP at Future Colliders	171
C.1	Dimension-8 operators for strong scatterings	171
C.2	Double Higgs-strahlung	172
D	Direct Probes of NP	177
D.1	The tilded basis	177
D.2	Electroweak precision tests	178
D.3	Tools provided with this chapter	181
D.4	Extrapolation of experimental bounds	181
	Acknowledgements	183

1 Introduction

A matter of hierarchies. Some of the most fundamental questions currently driving particle physics are related to the Higgs boson.¹ Its peculiarity stems from the fact that it is the only fundamental scalar particle in the Standard Model (SM) and an intrinsic problem, the *hierarchy problem*, is connected to scalars. It refers to the observed hierarchy between the Higgs mass m_h , most recently measured to be 125.36 ± 0.37 (stat) ± 0.18 (syst) GeV at ATLAS [8] and $125.03^{+0.26}_{-0.27}$ (stat) $^{+0.13}_{-0.15}$ (syst) GeV at CMS [9], and the scale at which New Physics (NP) appears, m_* . In the absence of NP up to the Planck scale, m_* would have to be identified with the Planck mass $M_{\text{Pl}} = \sqrt{\hbar c/8\pi G_N} \sim 2.44 \times 10^{18}$ GeV at the onset of quantum gravity. The large separation in scales is formally preserved at tree level. The problem arises because quantum fluctuations at the scale m_* tend to spoil the hierarchy $m_h \ll m_*$. A direct way to appreciate this is to consider the Higgs mass parameter at 1-loop. Following 't Hooft's naturalness argument [10], the core question is about the observed smallness of the Higgs mass. The limit $m_h \rightarrow 0$ does not seem special from the viewpoint of short distance physics. No symmetry is enhanced in this limit. This is in clear contrast to fermions, where the chiral symmetry emerges in the massless limit. The naturalness of gauge bosons is correlated with the presence of scalar particles in the theory. Without any scalars, the gauge bosons remain massless in order to match the number of degrees of freedom. If a longitudinal component can be acquired, the naturalness of the massive vectors depends on the naturalness of the scalar mass. The same questions can be viewed from another angle. Often, a looser definition of the hierarchy problem simply questions the large energy separation between the electroweak scale $v = 246$ GeV and the Planck scale M_{Pl} . However, by itself this is not a real problem. In fact, why do we not analogously question the slightly larger energy separation between $\Lambda_{\text{QCD}} \sim 1$ GeV and M_{Pl} ? This is easily answered. In an asymptotically free theory like QCD, the strong coupling $\alpha_S(\mu)$ decreases as $\alpha_S(\mu) = \alpha_S(\Lambda_{\text{QCD}})/(1 + b \alpha_S(\Lambda_{\text{QCD}})/(2\pi) \ln(\mu/\Lambda_{\text{QCD}}))$ as

¹We refer to the recently discovered scalar particle as the Higgs boson. The scalar field has first been introduced by P. Higgs [5] and independently by G. Guralnik, C. Hagen and T. Kibble [6]. Already a few months before F. Englert and R. Brout discussed electroweak symmetry breaking to give mass to the gauge bosons without explicitly mentioning an additional scalar [7].

the energy scale μ increases. Consequently a large separation of scales can be generated naturally

$$\Lambda_{\text{QCD}} = M_{\text{Pl}} e^{-\frac{2\pi}{b\alpha_S(M_{\text{Pl}})}}, \quad (1.1)$$

and the problem of hierarchy does not arise. The crucial ingredient in this argument is the logarithmic running of $\alpha_S(\mu)$. This follows immediately from the fact that $\alpha_S(\mu)$ is a dimensionless coupling defined through a marginal operator: the kinetic term of the gluons. Furthermore notice, that the theory is promoted to a free field theory in the limit $\alpha_S \rightarrow 0$ and thus enjoys a large symmetry enhancement. But let us elaborate on the relevance of operators in the theory which lies at the heart of naturalness. Consider an operator O_Δ , with mass dimension Δ . From a Wilsonian point of view, running from a high mass scale m_* to a lower scale m_{IR} implies integrating out high energy degrees of freedom which in turn generate a perturbation [11]

$$\mathcal{L}_{\text{pert}} = c m_*^{4-\Delta} O_\Delta, \quad (1.2)$$

which leads to a relation similar to eq. (1.1) for the low energy scale

$$m_{\text{IR}} = c^{\frac{1}{4-\Delta}} m_*. \quad (1.3)$$

A priori, the parameter c is expected to be $\mathcal{O}(1)$. A hierarchy between the scales arises naturally when $4 - \Delta$ is close to zero and c algebraically small [11], i.e. $c \sim 0.1$. This is the case for a marginal or weakly relevant operator, as demonstrated in eq. (1.1) for QCD. For a highly relevant operator, $4 - \Delta \sim \mathcal{O}(1)$, no significant separation of scales is generated even for a reasonably small value of c . Exactly this is the case in the electroweak theory of the SM where the only relevant operator is the Higgs mass term $H^\dagger H$ with dimensionality $\Delta = 2$. A hierarchy can only be explained for a particularly small, very fine tuned value of the parameter c . This is typically referred to as the *fine tuning problem* and corresponds to an unnatural hierarchy in the SM.

Current status. These ideas have attracted attention for decades already before the discovery of the Higgs boson. However, electroweak precision tests (EWPT) have strongly pointed towards a Higgs-like scalar particle. In that sense, the Higgs discovery announced by the ATLAS and CMS collaborations on 4 July 2012 [12, 13] was not particularly unexpected. At the same time, the open question about the dynamics of electroweak symmetry breaking (EWSB) developed a new twist since a new scalar particle was actually discovered. Let us briefly review the need for a broken electroweak symmetry. In nature, the electroweak bosons W^\pm , Z gauging the SM group $SU(2)_L \times U(1)_Y$ are observed to be massive while the photon remains massless. The simplest way to give mass to the W^\pm , Z bosons is to couple the gauge theory to a linear σ -model, in which a complex $SU(2)$ doublet, the Higgs boson, obtains a vacuum expectation value (vev) which

breaks $SU(2)_L \times U(1)_Y$ spontaneously to the electromagnetic $U(1)_Q$ subgroup.² Current experimental data has not shown any significant deviation from the SM expectations and thus suggests the Higgs boson to play its destined role. However, explanations for EWSB without the scalar being involved in the breaking dynamics have not yet been completely refuted.

Assuming the discovered scalar particle to be involved in EWSB, a solution of the hierarchy problem requires the existence of NP at the scale m_* , not far above the weak scale. Constraints on generic NP require m_* to be at or above the TeV scale. Naturalness, on the other hand, demands low scale New Physics. A completely natural theory would, for instance, require the presence of a new set of particles and interactions at a scale

$$m_* \lesssim \frac{2\pi}{\sqrt{3}y_t} m_h \approx 450 \text{ GeV}, \quad (1.4)$$

in order to cancel the quadratically divergent top quark contribution to the SM Higgs potential.

The two main frameworks in which the hierarchy problem is usually addressed are supersymmetry and compositeness. Nature chose the observed value of the Higgs mass so delicately to push both models into regions of considerable, 1 – 10%, fine tuning and beyond their minimal realisations without clearly choosing one over the other. While a natural minimal supersymmetric model predicts the Higgs mass to be close to the Z mass, a composite Higgs model prefers a Higgs of a few hundred GeV. Nonetheless, both models can still stretch to explain the observed value. Let us briefly sketch their basic ideas.

According to the no-go theorem by Haag, Lopuszanski and Sohnius [18], in quantum field theories with a mass gap and satisfying very general conditions, supersymmetry (extending Poincaré symmetry) is the largest possible space-time symmetry of the S -matrix.³ In its minimal version, supersymmetry doubles the particle content of the SM by introducing a superpartner for each SM field.⁴ In fact, it relates fermions and bosons by packaging them into superfields which share all quantum numbers except for the spin. A complex scalar is paired on-shell with a Weyl fermion in a chiral multiplet, while a massless vector field forms a vector multiplet together with a Weyl fermion in the adjoint representation of the gauge group. Through these supermultiplets, supersymmetry extends the chiral symmetry protecting the fermion masses to the Higgs boson and consequently solves the hierarchy problem. Since none of the superpartners has been observed yet, supersymmetry must be broken. In order to preserve the cancellation of the radiative corrections, the

²Spontaneous symmetry breaking was first discussed in the context of condensed matter by Y. Nambu [14] and P. Anderson [15] and only after introduced in particle physics [7, 16, 17].

³This extends the known result by Coleman and Mandula [19] that only applies to bosonic algebras.

⁴This is not completely true as it also introduces a second Higgs doublet together with its fermionic superpartner.

breaking must be soft (i.e. through relevant operators). An upper bound on the soft masses can be inferred from the radiative corrections to the Higgs mass which the soft terms logarithmically contribute to

$$\Delta m_h^2 = m_{\text{soft}}^2 \left(\frac{\lambda}{16\pi^2} \ln \left(\frac{\Lambda_{UV}}{m_{\text{soft}}} \right) + \dots \right), \quad (1.5)$$

where λ stands for a generic dimensionless coupling, while Λ_{UV} indicates the scale at which the soft terms are generated, for instance the messenger mass in gauge mediation. m_* can be identified with the soft mass terms m_{soft} . To have a natural explanation of the Higgs mass with at most a 10% tuning, light stops and gluinos below 600 GeV and Higgsinos with masses less than 300 GeV are expected in all incarnations of supersymmetry (see for example Refs. [20–25]). Supersymmetric bounds are usually model dependent and should be interpreted with care taking the precise assumptions made in each analysis into account. Quite generically, simplified model searches for gluinos give the most robust experimental bounds up to 1 – 1.4 TeV almost independently of the nature and mass of the lightest neutralino. Since in a large class of models, the gluino pulls up the stop masses due to its one-loop contribution, the stops are expected to be heavy [25, 26]. For R-parity conserving supersymmetry, bounds reach up to around 600 GeV [27], however gaps for light stops depending on the mass and nature of the lightest supersymmetric particle in models with compressed spectra remain. For recent attempts to close these gaps see for instance Ref. [28]. For (baryonic) R-parity violating models, there are still no limits on the stop masses from LHC searches and the strongest bounds from Tevatron and LEP extend up to 100 GeV [29, 30]. Higgsino bounds are more model dependent even for R-parity conserving supersymmetry. The current most stringent Higgsino exclusion of 300 GeV requires a lightest neutralino below 50 GeV [31, 32]. Despite its growing tension with experiment in the minimal models, the supersymmetric way is still particularly attractive due to its ability to make definite predictions due to its weakly coupled nature, to provide a Dark Matter candidate, to explain gauge coupling unification and not at last due to its tight connection to string theory.

Compositeness remains a much less studied alternative which part of this thesis is devoted to. Initially proposed in Refs. [33–39] in the 1980s, a realistic framework has emerged [40–46] in the past decade in which the Higgs boson arises as a pseudo-Nambu-Goldstone Boson (pNGB) from the spontaneous breaking of a global symmetry G , of a new strongly interacting sector, to a subgroup H . The Higgs boson is composite meaning that in the far UV it is described by new degrees of freedom. Analogously to the kaon in QCD (a doublet under the isospin symmetry), the hierarchy problem does not arise. The naturalness condition in eq. (1.4) requires light states to be present in the composite sector and therefore a relatively low compositeness scale. Heavy vector resonances in composite Higgs models are already severely constrained by electroweak precision tests. $\Delta\hat{S} = m_W^2/m_\rho^2$ implies $m_\rho \gtrsim 2.6$ TeV, setting the scale of NP very high. Fermionic states are still less constrained. Partial compositeness, as discussed in detail in section

3.2, imposes a linear coupling between elementary and composite states. Since the top-loop contributes dominantly to the Higgs potential, the fermionic states coupling to the top, the so-called top partners, cancel the top contribution analogously to the stops in supersymmetry. In minimal models with the least possible amount of tuning [47], the Higgs mass is given by

$$m_h^2 \sim \frac{N_c}{2\pi^2} \frac{v^2}{f^2} m_\psi^2 g_\psi y_t, \quad (1.6)$$

where $y_t = y_L y_R / g_\psi$ is the top Yukawa coupling expressed in terms of the linear couplings y_L, y_R between elementary and composite states, which are assumed to be equal here. m_ψ denotes the top partner mass, to be identified with m_* , coupling with strength g_ψ . The ratio v^2/f^2 indicates the ratio between the weak and the composite scale and can be interpreted as a partial measure of tuning in the model. To reproduce the measured Higgs mass and avoid large fine-tuning, the coupling g_ψ is preferred to be not too strong. In fact, naturalness requires the top partner masses m_ψ to be lighter than ~ 1 TeV [1, 47–49] for a fine tuning of $\lesssim 10\%$. Although, motivated by explicit implementations, composite fermion and vector masses are expected to be the same, to achieve a mild tuning a separation of the two scales $m_\psi < m_\rho$ would be favourable. Fermionic resonances in a natural composite Higgs model, just as the stops in supersymmetry, should be well in reach of the 14 TeV run of the LHC. This is of course not the only expected experimental evidence. Indeed, light resonances also significantly affect further SM observables, mainly related to the Higgs and top quark since both couple strongest to the composite sector. Deviations in Higgs or top quark couplings could give important evidence for a strongly coupled sector.

Light new states accessible at the LHC are expected in all natural realisations of supersymmetric and composite Higgs models. The current absence of any significant hint of NP is carving a big hole into the natural parameter space and pushes both frameworks into a more and more fine-tuned region. More sophisticated non-minimal models can partially evade the most stringent bounds but often introduce many more parameters. Nevertheless, the current situation just before the 14 TeV run of the LHC is far from hopeless. Not only are significant improvements in the mass reach of direct searches for new states expected, also indirect probes of NP such as coupling and precision measurements will have an increased sensitivity. Nonetheless, the time has come to at least consider an LHC outcome without any new discovery and to evaluate the potential of future colliders with a clear physics case. Proposals for linear colliders such as the ILC [50] and CLIC [51] have been investigated for some time, while a future circular collider (FCC), with a first stage of electron positron collisions (see for instance Ref. [52]) and a second stage as a pp collider, has attracted attention only very recently. In particular, it is important to study the impact of direct versus indirect probes of NP and the wealth of information contained in them for a specific framework.

Effective Lagrangian approach. To approach the above questions with the greatest possible generality, the SM should be best viewed as an effective field theory (EFT) valid up to a certain cutoff which is parametrically larger than the scale at which the physics is probed. This is of course only valid as long as no new light states are discovered. The cutoff can be identified with the scale m_* where New Physics becomes important. If a hierarchy between the two scales exists, $m_{\text{IR}} \ll m_*$, the currently known particle content of the SM can be described as the low energy regime of a more fundamental theory whose high energy degrees of freedom at m_* have been integrated out. An effective Lagrangian is therefore an expansion in inverse powers of m_* . While the SM consists only of dimension-4 operators, higher dimensional operators characterise new effects beyond the SM (BSM). Their strengths are suppressed by inverse powers of m_* . Hence, the larger m_* , the smaller the effect of NP on the low-energy observables. Precision measurements have already set stringent bounds on the presence of NP by constraining their contribution to physical quantities. The current experimental agreement with SM predictions seems to favour a high cutoff scale which contradicts the requirement of low scale New Physics to satisfy naturalness.

An EFT approach is also of greatest value from a more practical point of view since it allows us to make model-independent predictions. Especially now, with the LHC running but no clear target to search for, the data should be interpreted as broadly as possible. Robust qualitative predictions, like the existence of a given set of particles, are common to many SM extensions but a quantitative comparison with the data requires an explicit implementation of the general idea. Technically, each model with a common prediction would need to be compared with the data. Obviously, this program can not be completed directly by the experimental collaborations because it would require tens of different models for each NP analysis and a separate presentation of the results for each of them. Moreover even if we knew the “true” NP theory, it would typically depend on so many free parameters that a direct comparison with data, obtained by scanning the multi-dimensional parameter space with numerical simulations, would be impossible. A step in the right direction is therefore a “simplified model” [53] built from an effective Lagrangian with a small number of free parameters that capture the distinct phenomenology of a class of NP models. The simplified model can easily be translated into every explicit model with the same phenomenological feature. The interpretation of the data in terms of a simplified model (where possible) makes the bounds considerably more flexible. An effective Lagrangian approach is therefore crucial to ensure constructive communication among theory and experiment and to make the most of the available data.

Outline of the thesis. This thesis is organised as follows. Chapter 2 summarises the current status of Higgs physics. We explain the necessity of EWSB in the SM in section 2.1 and introduce two commonly used effective Lagrangians, the linear and non-linear σ -model, and their respective breaking dynamics. Experiments already favour a linear σ -model with the physical Higgs boson embedded in a complex $SU(2)_L$ doublet. New physics would affect the low energy description through higher dimensional operators, written in the SILH Lagrangian, and deviations from the SM Higgs couplings, discussed in section 2.2. In section 2.3, we present the current constraints on NP effects coming from electroweak precision measurements.

Chapter 3 is devoted to composite Higgs models and is largely based on Ref. [1]. We introduce the bosonic constituents of the effective Lagrangian with the Higgs as a pNGB in section 3.1. Section 3.2 discusses the generation of the SM fermion masses and the Higgs potential through partial compositeness. We concentrate on the case where the SM quark doublet is embedded in a $\mathbf{14}$ of $SO(5)$. An explicit realisation of the minimal composite Higgs model in a flat extra dimension is studied in 3.3. Through a numerical simulation in section 3.4, we confirm the minimal tuning of this particular model and the expected small mass of around 1 TeV of the lightest top partners required for a natural theory.

Chapters 4, 5 and 6 investigate possible NP effects from an effective Lagrangian point of view. At the LHC, a wealth of indirect NP effects are currently being probed. In chapter 4, we focus on single top production in association with a Higgs boson, based on Ref. [2], to lift the degeneracy in the current best fit to the top Yukawa couplings. We present a signal and background study in 4.3 and find only the 14 TeV dataset to be able to lift the degeneracy completely.

Furthermore, we study, based on Ref. [3], indirect NP effects through Higgs precision measurements at a linear e^+e^- collider, such as the ILC or CLIC, in chapter 5. We argue in sections 5.3 and 5.4 that even small deviations in the cross sections of single and double Higgs production, or the mere detection of a triple Higgs final state, can help establish whether the Higgs is a composite state and whether or not it emerges as a pNGB from an underlying symmetry. In section 5.5, we obtain an estimate of the ILC and CLIC sensitivities on the anomalous couplings from a study of WW scattering and hh production which can be translated into a sensitivity on the compositeness scale, $4\pi f$ or equivalently on the degree of compositeness $\xi = v^2/f^2$.

In chapter 6, we present direct probes of NP at the LHC based on Ref. [4]. We construct a simplified effective Lagrangian, extending the SILH Lagrangian by the inclusion of a heavy vector triplet, which reproduces a large class of explicit models. Based on the available 8 TeV LHC analyses, we derive current limits in 6.2.3 and interpret them in 6.2.4 for vector triplets arising in weakly coupled (gauge) and strongly coupled (composite) extensions of the SM. We point out that a model-independent limit setting procedure

Chapter 1. Introduction

must be based on purely on-shell quantities as illustrated in 6.2.3.3. Section 6.3 contains a brief summary of the effective Lagrangian for top partners and their current bounds.

The conclusions are drawn in chapter 7 by comparing the sensitivities of direct and indirect probes of NP at the LHC and future colliders on the parameter space of a new strongly coupled sector.

2 Effective Lagrangians for the Higgs boson

2.1 Dynamics of electroweak symmetry breaking

The electroweak sector of the SM unifies the description of the electromagnetic and weak interactions in a gauge theory invariant under $SU(2)_L \times U(1)_Y$ [54–56]. Explicitly, the Lagrangian can be written as

$$\mathcal{L}_{EW} = -\frac{1}{4}W_{\mu\nu}^a W^{a\mu\nu} - \frac{1}{4}B_{\mu\nu}B^{\mu\nu} + i\bar{\Psi}\not{D}\Psi, \quad (2.1)$$

in terms of the field strengths $W_{\mu\nu}^a$ and $B_{\mu\nu}$

$$\begin{aligned} W_{\mu\nu}^a &= D_\mu W_\nu^a - D_\nu W_\mu^a, & D_\mu W_\nu^a &= \partial_\mu W_\nu^a + g\epsilon^{abc}W_\mu^b W_\nu^c, \\ B_{\mu\nu} &= \partial_\mu B_\nu - \partial_\nu B_\mu, \end{aligned} \quad (2.2)$$

where W_μ^a and B_μ are the $SU(2)_L$ and $U(1)_Y$ gauge bosons respectively, while $\Psi = (Q_L^i, u_R^i, d_R^i, L_L^i, e_R^i, \nu_R^i)$ is a compact notation for all SM fermions and the hypothetical right-handed neutrino in a single column vector of Weyl spinors. The index i denotes the generation. So far this Lagrangian describes only massless states. Since we encounter also massive particles in Nature we need to take their masses into account. In the following we will review two mechanisms to spontaneously break the electroweak symmetry. In each case, gauge boson masses are generated through the Higgs mechanism where the gauge vectors W^\pm and Z eat a Nambu-Goldstone boson (NGB), originating from the symmetry breaking, to obtain their longitudinal component and hence a mass. The discovery of a Higgs-like scalar particle at the LHC has added a crucial piece of information to the exploration of the electroweak sector and, although it still has not completely settled the mechanism of EWSB, the data shows a strong preference for a Higgs embedded in a linear $SU(2)_L$ doublet.

2.1.1 The linear σ -model

In the linear realisation, the physical Higgs field, h , is embedded with the three Goldstone bosons, π_1, π_2, π_3 , in a complex field

$$H = \frac{1}{\sqrt{2}} \begin{pmatrix} \pi_1 - i\pi_2 \\ v + h + i\pi_3 \end{pmatrix} \equiv \begin{pmatrix} \frac{\pi_+}{\sqrt{2}} \\ \frac{v + h + i\pi_0}{\sqrt{2}} \end{pmatrix}, \quad (2.3)$$

transforming linearly, as a doublet with hypercharge $Y = 1/2$, under $SU(2)_L \times U(1)_Y$. The potential for this Higgs doublet

$$V(H) = -\mu^2 H^\dagger H + \lambda (H^\dagger H)^2 \quad (2.4)$$

has, for $\mu^2 > 0$, a local maximum at the origin and its minimum at $H^\dagger H = v^2 = 2\mu^2/\lambda$. The physical Higgs field h thus acquires a vacuum expectation value (vev) which is conventionally given by $v = (\sqrt{2}G_F)^{-1/2} = 246$ GeV. The ground state of the Lagrangian turns out not to be invariant under the full gauge group but to preserve its subgroup, the electromagnetic $U(1)_Q$ whose generator is given by the electric charge $Q = T^3 + Y$. The non-zero Higgs vev is responsible for the spontaneous breakdown of the gauge symmetry and, at the same time, for the generation of the gauge boson and fermion masses. The Higgs kinetic term

$$\mathcal{L}_H = (D_\mu H)^\dagger D^\mu H \quad (2.5)$$

generates mass terms for the gauge bosons and a mass mixing between the W^3 and B through the covariant derivative

$$D_\mu = \partial_\mu - igW_\mu^a T^a - ig'Y B_\mu, \quad T^a = \frac{\sigma^a}{2}. \quad (2.6)$$

Rotating the neutral sector to the mass eigenstate basis

$$\begin{aligned} A_\mu &= \sin\theta_W W_\mu^3 + \cos\theta_W B_\mu, \\ Z_\mu &= \cos\theta_W W_\mu^3 - \sin\theta_W B_\mu, \end{aligned} \quad (2.7)$$

where θ_W denotes the weak mixing angle given by $\tan\theta_W = g'/g$, and defining $W_\mu^\pm = (W_\mu^1 \mp W_\mu^2)/\sqrt{2}$ gives the masses

$$m_W^2 = \frac{g^2 v^2}{4}, \quad m_Z^2 = \frac{(g^2 + g'^2)v^2}{4}. \quad (2.8)$$

The photon, as the generator of the preserved symmetry, remains massless. Fermion mass terms are generated through Yukawa couplings of the form

$$\mathcal{L} = -\lambda_{ij}^d \left(\bar{Q}_L^{(i)} \right) H d_R^{(j)} - \lambda_{ij}^u \bar{Q}_L^{(i)} H^c u_R^{(j)} + \text{h.c.}, \quad (2.9)$$

2.1. Dynamics of electroweak symmetry breaking

where i, j are generation indices and $H^c = i\sigma_2 H^*$. The λ 's denote the Yukawa couplings. The quark mass matrix is thus predicted explicitly in terms of the vev as

$$m_{ij}^d = \frac{1}{\sqrt{2}} \lambda_{ij}^d v, \quad m_{ij}^u = \frac{1}{\sqrt{2}} \lambda_{ij}^u v. \quad (2.10)$$

Lepton masses arise analogously. Note that no neutrino masses are generated in the SM at the level of dimension-4 operators. The right-handed neutrino is a possible beyond the SM extension to explain the recently observed, small neutrino masses (see for example Ref. [57] for an extensive review).

Using the expression of the weak mixing angle leads to the following relation among the charged and neutral masses

$$\frac{m_W^2}{m_Z^2 \cos^2 \theta_W} \equiv \rho = 1. \quad (2.11)$$

In the limit $g' \rightarrow 0$, the masses become equal. This is a consequence of the $SO(4)$ symmetry of the Higgs potential in eq. (2.4) which depends only on the combination $H^\dagger H = 1/2 (\pi_1^2 + \pi_2^2 + \pi_3^2 + h^2)$. $SO(4)$ is isomorphic to $SU(2)_L \times SU(2)_R$ of which $SU(2)_L$ and the third component of $SU(2)_R$ are gauged. To make this symmetry structure more explicit, we can define

$$\mathcal{H} = (i\sigma^2 H^*, H), \quad (2.12)$$

transforming as $\mathcal{H} \rightarrow U_L^\dagger \mathcal{H} U_R$ under $SU(2)_L \times SU(2)_R$, where U_L and U_R are the respective independent transformation matrices. The vacuum is only invariant under the diagonal, custodial, subgroup $SU(2)_{L+R}$ where $U_L = U_R$. W_μ^a transforms as a triplet under $SU(2)_L$ and therefore preserves the custodial symmetry. It is instead broken by g' since only the subgroup corresponding to T^3 of $SU(2)_R$ is gauged. The limit $g' \rightarrow 0$ hence decouples the custodial breaking, implies equal masses for W^\pm and Z and consequently degenerate gauge bosons. As before, masses are generated from the Higgs kinetic term $\mathcal{L}_H = 1/2 \text{Tr} \left((D_\mu \mathcal{H})^\dagger D_\mu \mathcal{H} \right)$ through the covariant derivative

$$D_\mu \mathcal{H} = \partial_\mu \mathcal{H} - ig W_\mu^a T^a \mathcal{H} + ig' \mathcal{H} T^3 B_\mu. \quad (2.13)$$

2.1.2 The non-linear σ -model

The Higgs boson is not necessarily a crucial ingredient for EWSB as we will discuss in this section. In fact, we can decouple h from the complex doublet by increasing its mass and integrating it out. What remains is the field

$$\Phi = e^{i\sigma^a \pi^a / F_\pi}, \quad (2.14)$$

where we replaced v by F_π for later convenience, transforming non-linearly as

$$\Phi \rightarrow U_L \Phi U_R^\dagger, \quad (2.15)$$

under the partially gauged $SU(2)_L \times SU(2)_R$. This Goldstone field has its analogue in QCD where it originates from the breaking of the chiral $SU(2)_L \times SU(2)_R$ symmetry to its diagonal subgroup by the QCD vacuum $\langle \bar{u}u + \bar{d}d \rangle \neq 0$. At the confinement scale Λ_{QCD} , the condensate becomes energetically favourable and breaks the symmetry spontaneously to $SU(2)_{L+R}$. Switching on $SU(2)_L \times U(1)_Y$ gauging implies that also the electroweak symmetry is broken. In the case of QCD, the pion decay constant F_π would have to be identified with the experimentally measured $f_\pi \approx 92$ MeV which would lead to gauge boson masses of ~ 30 MeV. QCD alone is therefore not a viable option for electroweak symmetry breaking, in contrast to a scaled-up version of QCD, which would become strong near the scale of EWSB. Such theories are usually called technicolor,¹ (for a detailed review see for example Ref. [60]). Consider the technifermions $\Psi_L, \Psi_R^1, \Psi_R^2$ transforming as $(N, 2)_0, (N, 1)_1, (N, 1)_{-1}$ under $SU(N)_{TC} \times SU(2)_L \times U(1)_Y$ respectively. At a scale Λ_{TC} , they condense into a vacuum $\langle \bar{\psi}_L^i \psi_R^j \rangle \neq 0$ and break $SU(2)_L \times SU(2)_R / SU(2)_{L+R}$. The pion decay constant is now numerically equal to the Higgs vev of the previous section $F_\pi = v$ and reproduces the correct gauge boson masses.

Since EWSB does not pose any problems, we can construct an effective Lagrangian including a light CP-even scalar particle transforming as a singlet under $SU(2)_L \times SU(2)_R$, which, by some abuse of notation, we call h . This choice of CP is both motivated from the theoretical point of view (it follows for example in minimal composite Higgs theories), and supported by the results on the Higgs couplings obtained by the LHC collaborations. Such a construction does not assume that h is part of an $SU(2)_L$ doublet, nor does it make hypotheses on the strength of its interactions, as long as it is weakly coupled at energies of the order of its mass. It is thus completely general and applies as well to the case where h is a Higgs-like impostor not directly involved in EWSB. The Lagrangian is constructed by expanding in the number of derivatives and classifying the various terms according to the number of h fields. The expression obtained in this way extends the EW chiral Lagrangian [61–63] to include the light state h . At $O(p^2)$ in the derivative expansion, the bosonic part of the effective Lagrangian thus reads [64–67]

$$\mathcal{L} = \frac{1}{2} (\partial_\mu h)^2 - V(h) + \frac{v^2}{4} \text{Tr} \left(D_\mu \Phi^\dagger D^\mu \Phi \right) \left(1 + 2a \frac{h}{v} + b \frac{h^2}{v^2} + b_3 \frac{h^3}{v^3} + \dots \right), \quad (2.16)$$

with the potential for h

$$V(h) = \frac{1}{2} m_h^2 h^2 + d_3 \left(\frac{m_h^2}{2v} \right) h^3 + d_4 \left(\frac{m_h^2}{8v^2} \right) h^4 + \dots, \quad (2.17)$$

and a, b, b_3, d_3, d_4 are arbitrary dimensionless parameters. The dots stand for terms of

¹Technicolor was initially introduced in Refs. [58, 59].

higher order in h . Now we see that the kinetic term for Φ generates the gauge boson masses in eq. (2.8). This is most easily understood in the unitary gauge where $\Phi = 1$ and the covariant derivative is given by eq. (2.13). The fermion masses of eq. (2.10) are reproduced from the fermionic part of the Lagrangian

$$\mathcal{L} = -\frac{v}{\sqrt{2}} \sum_{i,j} \left(\bar{u}_L^{(i)} \bar{d}_L^{(i)} \right) \Phi \left(1 + c \frac{h}{v} + \dots \right) \begin{pmatrix} \lambda_{ij}^u u_R^{(j)} \\ \lambda_{ij}^d d_R^{(j)} \end{pmatrix} + \text{h.c.}, \quad (2.18)$$

with the notation used in eq. (2.9).

The SM Higgs of section 2.1.1 can be reproduced for the parameter choice $a = b = d_3 = d_4 = c = 1$ while all higher-order terms vanish. This corresponds exactly to the Lagrangian obtained by substituting the linear doublet

$$H = \frac{1}{\sqrt{2}} \Phi \begin{pmatrix} 0 \\ v + h \end{pmatrix}, \quad (2.19)$$

into Higgs kinetic term and potential and thus mimics the linear representation of $SU(2)_L \times SU(2)_R$. The dilaton couplings are instead characterised by the relations $a = b^2$, $b_3 = 0$ [68–73].

2.1.3 Implications of experimental evidence

The currently available measurements indicate that the properties of the newly discovered scalar particle are SM-like. In fact, so far no significant deviation from the SM predictions have been found. This has profound implications for NP scenarios. Firstly, potential deviations from the SM in form of higher dimensional operators involving a linear doublet have to be small to be compatible with experiments. Secondly, in the parameterization of a non-linear σ -model, data fixes all free coefficients a, b, d_3, c, \dots to be close to their SM value 1. Concrete relations and constraints among the parameters will be discussed in the following section.

One piece of experimental evidence is particularly interesting in order to compare the linear and non-linear realisations. Figure 2.1 shows the fitted Higgs couplings to the τ, b, W, Z, t versus their respective masses. The dashed black line depicts the SM prediction of these couplings. For leptons and quarks the linear relation between Yukawa coupling and mass can be easily understood from eq. (2.9). Since in the unitary gauge H is simply given by $h + v$, the slope is predicted to be v^{-1} . Analogously, we find the same relation for gauge bosons when plotting the square root of the hVV coupling, $g_{hVV} = 2m_V^2/v$, divided by $2v$, versus the mass. As anticipated the combination on the ordinate axis simplifies to the weak coupling, $g/2$. In conclusion, the linear σ -model permits a precise prediction of the Higgs couplings to fermions and gauge bosons which furthermore agrees with the data within 1σ uncertainty. The non-linear realisation, on the contrary, does

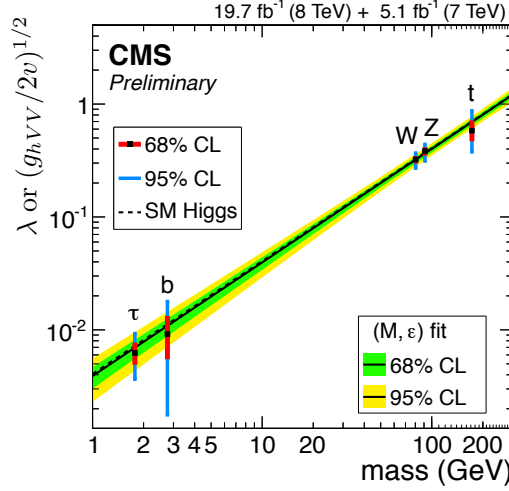


Figure 2.1 – Fitted Higgs couplings presented as the Yukawa couplings $h\bar{f}f$ of τ, b, t and the square root of the hVV coupling, $g_{hVV} = 2m_V^2/v$, divided by $2v$ for W, Z versus the corresponding particle mass are shown. The dashed black line depicts the SM prediction of the couplings in a linear σ -model. The green and yellow bands show the 68% and 95% C.L. bands. The figure is taken from Ref. [9] (for a similar fit see also [74]).

not allow for any prediction. In fact, the ratio of Higgs coupling to the mass depends on the, a priori arbitrary, parameters a and c . Instead of predicting a relation, the best fit to the experimental measurements allows one to fix a and c close to their SM value 1 in which case the two descriptions coincide. Although the non-linear σ -model can not be ruled out, since in some limit it coincides with the linear σ -model, the data clearly points towards the doublet structure of the Higgs and its linear implementation.

2.2 Effective Lagrangian for New Physics effects

While the SM is a renormalizable theory, it is necessary to go to non-renormalizable theories in order to describe physics beyond the SM. This is commonly done by considering the SM as an effective theory. The effect of heavy New Physics can be included in the effective Lagrangian description and parameterized in terms of higher dimensional operators and deviations in the SM couplings. In the following section, we want to discuss the different parameterisations and the relations among them.

2.2.1 Higher dimensional operators

The possible effects of New Physics living at a high mass scale m_* , well above the weak scale m_W , can be parameterized in a general and model independent way. If the New Physics mass scale is parametrically larger than the energy scale at which we want to probe it, like the collider's centre of mass energy, the heavy new states can be integrated

2.2. Effective Lagrangian for New Physics effects

out. This results in an effective Lagrangian expansion in powers of E/m_* which can be organised according to the dimensionality of the operators

$$\mathcal{L}_{\text{eff}} = \mathcal{L}_4 + \mathcal{L}_6 + \mathcal{L}_8 \dots, \quad (2.20)$$

consisting of SM fields and their derivatives only. \mathcal{L}_4 defines the dimension-4 operators of the SM, while \mathcal{L}_6 , \mathcal{L}_8 and higher orders describe BSM effects suppressed by powers of m_*^2 , m_*^4 , etc. respectively. Hence, the higher the dimensionality of the operator, the larger the suppression by inverse powers of m_* and thus, the smaller the NP effect. The dominant NP effects are encoded in \mathcal{L}_6 . The only 5-dimensional operator that can be constructed is of the form $(\bar{L}_L^c H)(L_L H)$, where L denotes the left-handed lepton doublet, and violates lepton number [75]. This operator was introduced by Weinberg [76] to explain a Majorana mass for neutrinos. To comply with current bounds the suppression scale must be $\sim 10^{15}$ GeV giving negligible effects for current collider searches. Similarly, baryon or lepton number violating dimension-6 operators must be suppressed by scales $\sim 10^{16}$ GeV to guarantee bounds from proton decay, making also those operators irrelevant for the LHC.

In general, the low energy effective Lagrangian coming from a heavy NP sector is of the following form

$$\mathcal{L}_{\text{eff}} = \frac{m_*^4}{g_*^2} \mathcal{L} \left(\frac{D_\mu}{m_*}, \frac{g_H H}{m_*}, \frac{g_\Psi \Psi}{m_*^{3/2}} \right), \quad (2.21)$$

where g_* is the typical coupling strength among the states of the new sector which is assumed to lie in the range $g \lesssim g_* < 4\pi$ to ensure the perturbative expansion to hold. The various powers of couplings and the mass cutoff follow from simple dimensional analysis according to the mass and \hbar dimensions given in Table 2.1. H and Ψ are characterised by the couplings g_H and g_Ψ respectively. If g_* is a strong coupling, and $g_H, g_\Psi \sim \mathcal{O}(g_*)$, the particles are strongly coupled and can be interpreted as composite states in a composite Higgs model, while a weak coupling of order g identifies them as elementary states. For all elementary states, the kinetic term violates the power counting since it would assign a smaller coefficient $(g/g_*)^2$ than required. A canonically normalised kinetic term must therefore be added explicitly to eq. (2.21). This is reasonable since the elementary kinetic term does not originate from a strong sector and exists independently. The transverse gauge bosons are always taken as elementary particles coupling weakly to any other state [77]. Experimental measurements have shown that gauge fields and light fermion generations are largely elementary, thus their mixing with the composite sector is extremely small [78, 79]. The Higgs as well as the top quark are often assumed to originate from a strong sector and to couple strongly to its states.

Equation (2.21) generalises the power counting introduced in the SILH Lagrangian in Ref. [80] where H is taken to be composite (i.e. coupling with strength $g_H = g_*$) and all

		dimension
scalar field	ϕ	$[\hbar]^{\frac{1}{2}}[L]^{-1}$
fermion field	ψ	$[\hbar]^{\frac{1}{2}}[L]^{-\frac{3}{2}}$
vector field	A_μ	$[\hbar]^{\frac{1}{2}}[L]^{-1}$
mass	m	$[\hbar]^0[L]^{-1}$
gauge coupling	g	$[\hbar]^{-\frac{1}{2}}[L]^0$
quartic coupling	λ	$[\hbar]^{-1}[L]^0$
Yukawa coupling	y_f	$[\hbar]^{-\frac{1}{2}}[L]^0$

Table 2.1 – Mass (as $[\text{length}]^{-1}$) and \hbar dimensionalities of the classical SM fields and couplings for $c = 1$ but $\hbar \neq 1$. This follows trivially from the dimensionality of the quantum mechanical action $[S] = \hbar$ when \hbar is restored.

fermions elementary ($g_\Psi = g$) from the beginning. If the Higgs is strongly coupled, a simple yet crucial observation is that any additional power of H costs a factor $g_*/m_* \equiv 1/f$ while any additional derivative instead is suppressed by a factor $1/m_*$.² If the light Higgs interacts strongly with the new dynamics, $g_* \gg 1$, then the leading corrections to low-energy observables arise from operators with extra powers of H rather than derivatives. This remark greatly simplifies the list of important operators.

The list of dimension-6 operators has been discussed at length in the literature [81–90], for recent reviews see Refs. [91, 92]. There exist various bases for the dimension-6 operators related by field redefinitions, or equivalently, the classical equations of motion. In the following we will adopt the basis discussed in Refs. [80, 92] which has several advantages. Firstly, it captures the effects of a well motivated set of New Physics models in only a minimal number of operators. Universal theories, for instance, describing those models whose low energy effects can be encoded solely in higher dimensional operators consisting of SM bosons, can be captured by only 14 operators corresponding to the 14 coefficients parametrising all possible NP effects. Composite Higgs models without partial compositeness (as explained in section 3.2) are an example of such models. If the elementary fermions couple to the strong sector, also fermionic operators are induced. Potentially complicated, linear combinations (as would be needed for example in the basis of Ref. [90]) can be avoided. The operators in this basis are furthermore directly related to experimentally measured quantities which simplifies the procedure to set bounds on the coefficients [79]. Secondly, under reasonable assumptions, this basis allows one to distinguish operators arising from tree and loop level diagrams when integrating out the heavy, minimally coupled particles. The dimension-6 operators fall into the following three categories [80, 92].

²Extra powers of the gauge fields are also suppressed by $1/m_*$ as they can only appear through covariant derivatives in minimally coupled theories.

Tree level operators with extra powers of Higgs fields or SM fermions. Operators in this first category are built from products of SM bilinears. They appear by integrating out heavy scalars, fermions or vectors at tree level and contain extra powers of Higgs fields or SM fermions thus contributing additional powers of g_H and g_Ψ . According to the power counting in eq. (2.21) and Table 2.1, these operators can be parameterized by

$$\mathcal{L}_6^1 = \sum_{i_1} g_*^2 \frac{c_{i_1}}{m_*^2} \mathcal{O}_{i_1}, \quad (2.22)$$

where the coefficients c_{i_1} contain only ratios of couplings (e.g. g_H/g_* and g_Ψ/g_*). This implies firstly, that the $1/m_*^2$ suppression is attenuated for composite particles through the strong coupling $g_H, g_\Psi \lesssim 4\pi$ in the numerator. These operators can thus give the largest effects in the strong coupling regime. Secondly, elementary particles coupled by g exhibit an additional suppression $(g_*/m_*)^2 (g/g_*)^2$. It can therefore be concluded that operators of this category are not important for weakly coupled states. In fact, only those operators are included in the first category that are enhanced in the strong coupling limit.

The bosonic operators with additional powers of the Higgs field can be written explicitly as

$$\mathcal{O}_H = \frac{1}{2} (\partial_\mu |H|^2)^2, \quad \mathcal{O}_T = \frac{1}{2} \left(H^\dagger \overleftrightarrow{D}_\mu H \right)^2, \quad \mathcal{O}_6 = \lambda |H|^6, \quad (2.23)$$

where λ is the quartic coupling which appears in front of the marginal operator $(H^\dagger H)^2$. We defined $H^\dagger \overleftrightarrow{D}_\mu H = H^\dagger D_\mu H - (D_\mu H)^\dagger H$ and the covariant derivative is given by eq. (2.6) with $Y = 1/2$. Using the equations of motions for the gauge fields, the seemingly independent operator $\mathcal{O}_r = |H|^2 |D_\mu H|^2$ can be eliminated. In addition to the bosonic operators, there are 30 independent fermionic operators – for each family – listed consistently in Table 2 of Ref. [92]. For future reference, we will report here only those CP-even operators that can be constrained by electroweak precision measurements as discussed in section 2.3. In particular, this implies that we omit to write four-fermion operators that do not affect the precision observables.³ Moreover, we omit CP-odd and dipole (or one-loop) operators which are suppressed by small SM Yukawa couplings under the assumption that the NP sector respects minimal flavour violation (MFV) [94]. The

³Using α_{EM}, m_Z and m_W as SM input parameters and not (as typically done) G_F allows one to study four-fermion operators in complete separation [93].

remaining operators are⁴

$$\begin{aligned}
\mathcal{O}_{y_u} &= y_u |H|^2 \bar{Q}_L \tilde{H} u_R, & \mathcal{O}_{y_d} &= y_d |H|^2 \bar{Q}_L H d_R, \\
\mathcal{O}_{y_e} &= y_e |H|^2 \bar{L}_L H e_R, \\
\mathcal{O}_R^u &= \left(i H^\dagger \overleftrightarrow{D}_\mu H \right) (\bar{u}_R \gamma^\mu u_R), & \mathcal{O}_R^d &= \left(i H^\dagger \overleftrightarrow{D}_\mu H \right) (\bar{d}_R \gamma^\mu d_R), \\
\mathcal{O}_R^e &= \left(i H^\dagger \overleftrightarrow{D}_\mu H \right) (\bar{e}_R \gamma^\mu e_R), \\
\mathcal{O}_L^q &= \left(i H^\dagger \overleftrightarrow{D}_\mu H \right) (\bar{Q}_L \gamma^\mu Q_L), & \mathcal{O}_L^l &= \left(i H^\dagger \overleftrightarrow{D}_\mu H \right) (\bar{L}_L \gamma^\mu L_L), \\
\mathcal{O}_L^{(3)q} &= \left(i H^\dagger \sigma^a \overleftrightarrow{D}_\mu H \right) (\bar{Q}_L \gamma^\mu \sigma^a Q_L), & \mathcal{O}_L^{(3)l} &= \left(i H^\dagger \sigma^a \overleftrightarrow{D}_\mu H \right) (\bar{L}_L \gamma^\mu \sigma^a L_L),
\end{aligned} \tag{2.24}$$

where $\tilde{H} = i\sigma_2 H^*$. The hermitean conjugates of the above operators are understood to be included in the analysis. Since light fermions are typically considered as elementary, these operators are not relevant due to the additional $(g/g_*)^2$ suppression.

Tree level operators with extra derivatives. Analogously to the first category, these operators are generated from tree-level exchanges of heavy particles and consist of products of SM bilinears. However, they also contain additional powers of derivatives or gauge fields. Their suppression is thus $1/m_*^2$. If a canonically normalised gauge field is involved, the suppression is further enhanced by the weak gauge coupling. The general contribution of these operators to the effective Lagrangian is

$$\mathcal{L}_6^2 = \sum_{i_2} \frac{c_{i_2}}{m_*^2} \mathcal{O}_{i_2}. \tag{2.25}$$

The bosonic operators can be written explicitly as

$$\begin{aligned}
\mathcal{O}_W &= \frac{ig}{2} \left(H^\dagger \sigma^a \overleftrightarrow{D}^\mu H \right) D^\nu W_{\mu\nu}^a, & \mathcal{O}_B &= \frac{ig'}{2} \left(H^\dagger \overleftrightarrow{D}^\mu H \right) \partial^\nu B_{\mu\nu}, \\
\mathcal{O}_{2W} &= -\frac{1}{2} (D_\mu W_{\mu\nu}^a)^2, & \mathcal{O}_{2B} &= -\frac{1}{2} (\partial_\mu B_{\mu\nu})^2, \\
\mathcal{O}_{2G} &= -\frac{1}{2} (D_\mu G_{\mu\nu}^A)^2,
\end{aligned} \tag{2.26}$$

where A is the adjoint index of $SU(3)$. There are furthermore six fermionic operators which are all suppressed by two SM Yukawa couplings [92]. The basis is redundant since operators of the first category are related to operators in the second by the equations of

⁴For the complete list see Table 2 of Ref. [92].

motion

$$\begin{aligned}
 D^\nu W_{\mu\nu}^a &= ig H^\dagger \frac{\sigma^a}{2} \overleftrightarrow{D}_\mu H + g \sum_f \bar{f}_L \frac{\sigma^a}{2} \gamma_\mu f_L, \\
 \partial^\nu B_{\mu\nu} &= ig' Y_H H^\dagger \overleftrightarrow{D}_\mu H + g' \sum_f \left(Y_L^f \bar{f}_L \gamma_\mu f_L + Y_R^f \bar{f}_R \gamma_\mu f_R \right).
 \end{aligned}
 \tag{2.27}$$

In particular, \mathcal{O}_B and \mathcal{O}_W can be traded for a combination of operators from the first category. Keeping the redundancy is nonetheless useful at this stage. An appropriate choice can be made for each specific scenario. Consider, for instance, the case of composite Higgs and fermions, where operators from the first category will have a coefficient g_*^2/m_*^2 . By the equations of motion, this can be translated into an enhancement of $c_{B,W} = g_*^2/g^2$ in $\mathcal{O}_{B,W}$ compared to the native expectation of category two. Since composite fermions affect $\mathcal{O}_{B,W}$, it would be convenient to work in a basis with fermionic operators instead of $\mathcal{O}_{B,W}$. For elementary Higgs and fermions, on the contrary, no enhancement is expected and the coefficients $c_{B,W}$ are of order one. Including $\mathcal{O}_{B,W}$ can therefore be convenient.

One-loop operators. Operators in this category arise from one-loop diagrams in renormalizable theories involving heavy fields. Their coefficients are consequently expected to be loop suppressed

$$\mathcal{L}_6^3 = \sum_{i_3} \frac{\kappa_{i_3}}{m_*^2} \mathcal{O}_{i_3}, \tag{2.28}$$

where the prefactor includes the one-loop suppression $\kappa_{i_3} = \frac{g_*^2}{16\pi^2} c_{i_3}$. Explicitly, the CP-even bosonic operators are

$$\begin{aligned}
 \mathcal{O}_{BB} &= g'^2 |H|^2 B_{\mu\nu} B^{\mu\nu}, & \mathcal{O}_{GG} &= g_s^2 |H|^2 G_{\mu\nu}^A G^{A\mu\nu}, \\
 \mathcal{O}_{HW} &= ig (D^\mu H)^\dagger \sigma^a (D^\nu H) W_{\mu\nu}^a, & \mathcal{O}_{HB} &= ig' (D^\mu H)^\dagger (D^\nu H) B_{\mu\nu}, \\
 \mathcal{O}_{3W} &= \frac{1}{3!} g \epsilon_{abc} W_\mu^{a\nu} W_{\nu\rho}^b W^{c\rho\mu}, & \mathcal{O}_{3G} &= \frac{1}{3!} g_s f_{ABC} W_\mu^{A\nu} W_{\nu\rho}^B W^{C\rho\mu} f_{ABC}.
 \end{aligned}
 \tag{2.29}$$

There is an analogous set of six CP-odd operators where one field strength in each operator is replaced by its dual $\tilde{F}_{\mu\nu} = \epsilon_{\mu\nu\rho\sigma} F^{\rho\sigma}/2$. In addition, there are eight fermionic operators in this category which are not only one-loop suppressed but also include a factor of the Yukawa coupling. Since these operators can not be constrained by electroweak measurements, we do not report them here (see Ref. [92] for the full list).

We are thus left with 14 independent bosonic operators shown in eqs. (2.23), (2.26) and (2.29). To complete the basis there are additional 44 operators for each family of SM fermions, some of which are listed in eq. (2.24). The redundancy of the basis lies in

five operators which can be eliminated by the equations of motion of the gauge fields. Therefore five operators, chosen by convenience, can be discarded. Adding, on the other hand, the six CP-odd operators one remains with 59 independent dimension-6 operators encoding NP effects. 20 of them can be severely constrained by electroweak precision test and results from Higgs physics.

There will be an even greater number of dimension-8 operators giving more suppressed contributions to the Higgs couplings. As described in more detail in Appendix C.1, there are only two dimension-8 operators which modify a, b, b_3, d_3 and are of relevance in the following

$$O'_H = \frac{c'_H g_*^4}{2m_*^4} |H|^2 \partial_\mu |H|^2 \partial^\mu |H|^2, \quad O_8 = -\frac{c_8 g_*^4 \lambda}{m_*^4} (H^\dagger H)^4, \quad (2.30)$$

where the coefficients c'_H and c_8 are expected to be of order 1.

2.2.2 Higgs couplings

Some of the $O(1)$ coefficients of the dimension-6 operators, in particular c_H and c_6 , control the Higgs couplings a, b, b_3, d_3 at order $(v/f)^2$. Under the assumption of h being part of a doublet, the Higgs couplings of eq. (2.16) are thus correlated and functions of a smaller set of parameters. To relate the coefficients we need a field redefinition of the form

$$\begin{aligned} h \rightarrow h &+ \frac{h}{8} \frac{v^2}{f^2} \left(-4c_H + (3c_H^2 - 2c'_H) \frac{v^2}{f^2} \right) + \frac{h^2}{2v} \frac{v^2}{f^2} \left(-c_H + (2c_H^2 - c'_H) \frac{v^2}{f^2} \right) \\ &+ \frac{h^3}{12v^2} \frac{v^2}{f^2} \left(-2c_H + (13c_H^2 - 6c'_H) \frac{v^2}{f^2} \right). \end{aligned} \quad (2.31)$$

After canonically normalising the Higgs field, corrections of order $(v/f)^4$ to the Higgs couplings are induced. The expressions for the couplings at $O(v^4/f^4)$ thus read

$$\begin{aligned} a &= 1 - \frac{c_H}{2} \frac{v^2}{f^2} + \left(\frac{3c_H^2}{8} - \frac{c'_H}{4} \right) \frac{v^4}{f^4}, \\ b &= 1 - 2c_H \frac{v^2}{f^2} + \left(3c_H^2 - \frac{3c'_H}{2} \right) \frac{v^4}{f^4}, \\ b_3 &= -\frac{4c_H}{3} \frac{v^2}{f^2} + \left(\frac{14c_H^2}{3} - 2c'_H \right) \frac{v^4}{f^4}, \\ d_3 &= 1 + \left(c_6 - \frac{3c_H}{2} \right) \frac{v^2}{f^2} + \left(\frac{15c_H^2}{8} - \frac{5c'_H}{4} - \frac{c_6 c_H}{2} - \frac{3c_6^2}{2} + 2c_8 \right) \frac{v^4}{f^4}. \end{aligned} \quad (2.32)$$

Any deviation of the couplings a, b, d_3 from their SM values implies the energy growth of some $2 \rightarrow 2$ scattering amplitude whose strength can be parameterized in terms of a “running” coupling $\bar{g}(\sqrt{s})$ at a given center-of-mass (c.o.m.) energy \sqrt{s} . For example, the

2.2. Effective Lagrangian for New Physics effects

couplings a and b control the strength of the interactions in $2 \rightarrow 2$ processes among π 's and h . Under the assumption of $SO(3)$ custodial invariance, the scattering amplitudes read

$$\mathcal{A}(\pi^a \pi^b \rightarrow \pi^c \pi^d) = A(s, t, u) \delta^{ab} \delta^{cd} + A(t, s, u) \delta^{ac} \delta^{bd} + A(u, t, s) \delta^{ad} \delta^{bc}, \quad (2.33)$$

$$\mathcal{A}(\pi^a \pi^b \rightarrow hh) = A_{hh}(s, t, u) \delta^{ab}, \quad (2.34)$$

$$\mathcal{A}(\pi^a \pi^b \rightarrow \pi^c h) = A_{h\pi}(s, t, u) \epsilon^{abc}, \quad (2.35)$$

where s, t, u are the usual Mandelstam variables. As implied by the equivalence theorem [95, 96], at high energy each of the above amplitudes equals one in which each external π is replaced by the corresponding longitudinal vector boson ($\pi^\pm \rightarrow W_L^\pm$, $\pi^0 \rightarrow Z_L$) up to m_W^2/s corrections. From the Lagrangian in eq. (2.16), at leading order in the derivative expansion, it follows $A(s, t, u) = (1 - a^2)s/v^2$ and $A_{hh}(s, t, u) = (a^2 - b)s/v^2$. In both these cases the scattering amplitude defines a coupling strength

$$\mathcal{A}(2 \rightarrow 2) = \delta_{hh} \frac{s}{v^2} \equiv (\bar{g}(\sqrt{s}))^2, \quad (2.36)$$

where we indicate by δ_{hh} both $a^2 - 1$ (for $\pi\pi \rightarrow \pi\pi$) and $a^2 - b$ (for $\pi\pi \rightarrow hh$). A measurement of the $V_L V_L \rightarrow V_L V_L$ and $V_L V_L \rightarrow hh$ ($V = W, Z$) scattering rates at a given centre of mass energy \sqrt{s} thus corresponds to the measurement of an effective coupling $\bar{g}(\sqrt{s})$, characterising the strength of the EWSB dynamics. The effective coupling $\bar{g}(\sqrt{s})$ grows with energy so that perturbativity, and with it the validity of the effective Lagrangian, would be lost at the scale $\sqrt{s_*}$ where $\bar{g}(\sqrt{s_*}) \sim 4\pi$. A reasonable expectation is then that new states will UV complete the effective Lagrangian at a scale $m_* \leq \sqrt{s_*}$. The new states would expectedly saturate the growth of the effective coupling to $g_* \equiv \bar{g}(m_*) \leq 4\pi$.

$2 \rightarrow 2$ scattering processes with an odd number of NGB. In the case of the scattering $\pi\pi \rightarrow \pi h$, Bose and crossing symmetries imply that the function $A_{h\pi}(s, t, u)$ is antisymmetric under the exchange of any two Mandelstam variables. As a consequence, the lowest-order contribution to $A_{h\pi}(s, t, u)$ arises at $O(p^6)$, that is $A_{h\pi} \propto (s - u)(u - t)(t - s)$, in accordance with the fact that there exists no local operator at the level of two and four derivatives giving a vertex with three π 's. The corresponding scattering amplitude, $V_L V_L \rightarrow V_L h$, is expected to be suppressed by a factor $(s/m_*^2)^2$ compared to that of $V_L V_L \rightarrow V_L V_L, hh$, and is thus not a sensitive probe of the Higgs interaction strength at energies below the scale m_* of New Physics. In fact, the absence of an energy growth in the $\pi\pi \rightarrow \pi h$ amplitude could have been anticipated on the basis of a simple symmetry argument. The request of custodial invariance fixes the global coset to be $SO(4)/SO(3)$, which is a symmetric space. The grading of its algebra, under which all broken generators and thus all NG bosons change sign, is an accidental symmetry of the

$O(p^2)$ Lagrangian (2.16) ⁵

$$P_{LR} : \quad \pi^a(x) \rightarrow -\pi^a(x), \quad h(x) \rightarrow h(x). \quad (2.37)$$

Any process with an odd number of π 's, including $\pi\pi \rightarrow \pi h$, must thus vanish at leading derivative order. Furthermore, although P_{LR} is generically broken at $O(p^4)$, it turns out that none of the P_{LR} -odd operators with four derivatives contributes to $2 \rightarrow 2$ processes [97]. In absence of custodial symmetry, on the other hand, the global coset is $SU(2) \times U(1)/U(1)$ rather than $SO(4)/SO(3)$. This is not a symmetric space, and there is no grading symmetry which forbids vertices with three NG bosons at $O(p^2)$. In particular, the operator $[\text{Tr}(\Phi^\dagger D_\mu \Phi \sigma^3)]^2 h$ contains the term $h \partial_\mu \pi^3 (\pi^+ i \overleftrightarrow{\partial}_\mu \pi^-)$, which gives $\mathcal{A}(\pi^+ \pi^- \rightarrow \pi^3 h) \propto (t - u)$. In practice, the experimental results on the Higgs couplings obtained by the LHC collaborations already set tight limits on possible custodial breaking effects [98–100] and thus on the energy growth of $V_L V_L \rightarrow V_L h$. These new constraints are not surprising given the very strong constraint on custodial symmetry breaking provided by electroweak precision tests at LEP/SLC/Tevatron.

One might ask whether the amplitude of the process $V_T V_L \rightarrow V_L h$, with one transversely polarised vector boson, grows with the energy and thus probes the Higgs interaction strength. By virtue of the equivalence theorem, at high energy this coincides with the amplitude of $V_T \pi \rightarrow \pi h$, for which a naive power counting would suggest $\mathcal{A} \sim g\sqrt{s}/v$. A direct calculation, on the other hand, reveals that the energy-growing term cancels after summing all relevant diagrams, thus implying $\mathcal{A}(V_T \pi \rightarrow \pi h) \sim g^3(v/\sqrt{s})$. ⁶ Eventually, the leading contribution to $VV \rightarrow Vh$ comes from the scattering amplitude with *two* transversely polarised vector bosons, $\mathcal{A}(V_T V_T \rightarrow V_L h) \sim g^2$, which makes it clear that this process cannot be used to probe the Higgs interaction strength. Incidentally, notice that there is no analog cancellation in the scatterings with zero or two Higgses and one transverse vector boson, that is: $\mathcal{A}(V_T \pi \rightarrow hh) \sim (a^2 - b)g\sqrt{s}/v$ and $\mathcal{A}(V_T \pi \rightarrow \pi\pi) \sim (a^2 - 1)g\sqrt{s}/v$.

2.3 Electroweak precision tests

2.3.1 Current constraints on higher dimensional operators

Electroweak precision data refers to a set of high precision measurements from LEP I and II, SLC, Tevatron and further low energy experiments that probe SM observables to a very high precision and thus allow one to infer constraints on NP parameters through their indirect effects. Following Ref. [79], we discuss the current constraints on the dimension-6 operators introduced in the previous section. The five redundancies due to the equations

⁵ It coincides with parity up to a spatial inversion: $P = P_0 P_{LR}$, with $P_0 : \{\vec{x} \rightarrow -\vec{x}, t \rightarrow t\}$.

⁶ The cancellation follows from the fact that all the diagrams have the same dependence on the Higgs couplings, namely they are all proportional to a . Since in the SM limit $a = 1$ the amplitude cannot grow with the energy, by continuity this implies that the same holds true for any a .

of motion are used to eliminate the operators $\mathcal{O}_{2W,2B,2G}$ and $\mathcal{O}_L^l, \mathcal{O}_L^{(3)l}$. The constraints can be classified according to their strength.

Z-pole measurements at the per-mille level. Deviations in the weak gauge boson propagators and their couplings to fermions can be constrained at the per-mille level by Z-pole observables from LEP I and SLC [101]. In the leptonic sector, the constraints can be set on $\Gamma(Z \rightarrow \bar{l}_L l_L), \Gamma(Z \rightarrow \bar{l}_R l_R)$ and $\Gamma(Z \rightarrow \bar{\nu} \nu)$. These quantities are modified by the three dimension-6 operators proportional to c_T, c_V^+, c_R^e , where $c_V^\pm = (c_W \pm c_B)/2$. Performing a χ^2 fit (for details see Ref. [79]) sets the following bounds at 95% C.L. on the three coefficients.

$$\begin{aligned} \frac{v^2}{f^2} c_T &\in [-5, 1] \times 10^{-3}, & \frac{m_W^2}{m_*^2} c_V^+ &\in [-6, 0] \times 10^{-3}, \\ \frac{v^2}{f^2} c_R^e &\in [-5, 0] \times 10^{-3}. \end{aligned} \quad (2.38)$$

LEP I can constrain only the combination $c_W + c_B$. The orthogonal combination $c_W - c_B$ thus represents a so-called blind direction of LEP I. It can however be constrained by trilinear gauge coupling measurements, as show in the following.

Bounds on hadronic operators originate from Z-pole measurements and the extraction of G_F from quark-lepton weak interactions at the low energy experiment KLOE and β -decays [102]. In addition, the high energy cross section $\bar{q}q \rightarrow \bar{l}\nu$ accessible at the LHC [103] can be used. Combining this data yields the following bounds

$$\begin{aligned} \frac{v^2}{f^2} c_L^q &\in [-1, 4] \times 10^{-3}, & \frac{v^2}{f^2} c_L^{(3)q} &\in [-7, 4] \times 10^{-3}, \\ \frac{v^2}{f^2} c_R^u &\in [-8, 0] \times 10^{-3}, & \frac{v^2}{f^2} c_R^d &\in [-53, 1] \times 10^{-3}, \\ \frac{v^2}{f^2} c_L^{+q3} &\in [-7, 13] \times 10^{-3}, \end{aligned} \quad (2.39)$$

where $c_L^{+q3} = (c_L^{q3} + c_L^{(3)q3})/2$.

Trilinear gauge coupling measurements at the per-cent level. Trilinear gauge couplings (TGCs) were accessible at LEP II and the Tevatron through di-boson production processes such as $e^+e^- \rightarrow W^+W^-$ and are currently probed at the per-cent level [104]. Although the LHC is not yet competitive, the next run of the LHC should be sensitive and improve the current measurements. In the SM, TGCs arise from the non-abelian structure of the field strength in the gauge kinetic term

$$\mathcal{L}_{\text{kin}} = -\frac{1}{4} W_{\mu\nu}^i W^{\mu\nu i}, \quad W_{\mu\nu}^i = \partial_\mu W_\nu^i - \partial_\nu W_\mu^i + g\epsilon^{ijk} W_\mu^j W_\nu^k. \quad (2.40)$$

Consequently, the TGCs are of the form $g\epsilon^{ijk}\partial_\mu W_\nu^i W^{\mu j} W^{\nu k}$, where the Levi-Civita symbol implies couplings between the W^+ , W^- and a neutral boson Z or γ after EWSB. Interactions between three neutral fields are not present in the SM. The couplings are given by the electric charge e for the $\gamma W^+ W^-$ coupling, and eg/g' for $ZW^+ W^-$. Dimension-6 operators can give corrections to these SM values and are already constrained by current precision measurements of the couplings. The extracted limits are [79, 105]

$$\frac{m_W^2}{m_*^2} (c_V^- + \kappa_{HV}^-) \in [-4.4, 6.6] \times 10^{-2}, \quad \frac{m_W^2}{m_*^2} \kappa_{HV}^+ \in [-5.5, 3.9] \times 10^{-2}, \quad (2.41)$$

where $\kappa_{HV}^\pm = (\kappa_{HW} \pm \kappa_{HB})/2$. The coefficient κ_{HV}^- affects the Higgs branching ratio into $Z\gamma$.

Higgs measurements. Recent LHC measurements of Higgs production and partial decay widths into $b\bar{b}$, $\tau\tau$, $\gamma\gamma$ and $Z\gamma$ can constrain further indirect NP effects

$$\begin{aligned} \frac{m_W^2}{m_*^2} \kappa_{GG} &\in [-0.8, 0.8] \times 10^{-3}, & \frac{m_W^2}{m_*^2} \kappa_{BB} &\in [-1.3, 1.8] \times 10^{-3}, \\ \frac{m_W^2}{m_*^2} \kappa_{Z\gamma} &\in [-6, 12] \times 10^{-3}, \end{aligned} \quad (2.42)$$

while operators such as c_H and c_6 remain unconstrained for the time being. Despite the stringent constraint, the bound on $\kappa_{Z\gamma}$ corresponds to the latest experimental bound on the $h \rightarrow Z\gamma$ branching ratio at 10 times its SM value [106, 107]. This is thus the only process which still allows for large deviations. Considerable improvements are expected with the next run and more precise measurements of the LHC.

2.3.2 Current constraints on the Higgs couplings

The coupling a is indirectly constrained by the precision tests of the EW observables performed at LEP, SLD and Tevatron, and directly measured in single Higgs processes studied at the LHC. However, there is currently no significant constraint on the couplings b and d_3 as these can be measured only through double Higgs processes.

The sensitivity of the EW observables on a arises at the 1-loop level only through the Higgs contribution to vector boson self energies.⁷ This is the leading effect, two-loop corrections are small and thus negligible. Compared to a few years ago, the information that comes from the EW fit has sharpened [108–111]. This is mainly due to the value of the Higgs mass being now precisely known experimentally, so that a global fit can be used to extract the Higgs coupling to vector bosons directly, but also due to the new and more precise measurement of the W mass from Tevatron. For example, compared

⁷The 1-loop Higgs contribution to the $b\bar{b}Z$ vertex is suppressed by y_b^2 and thus negligible.

to the average of Tevatron and LEP measurements $m_W = (80.425 \pm 0.034) \text{ GeV}$ used in the 2006 final report on EW tests at the Z pole [112], the current world average $m_W = (80.385 \pm 0.015) \text{ GeV}$ [101] has an error smaller by more than a factor 2. As a matter of fact, among the various observables sensitive to the Higgs coupling a , m_W is the one which leads to the most precise determination [111]. Focusing on the 1-loop Higgs contribution to the vector boson self energies, the dependence on a can be straightforwardly derived from that on m_H at $a = 1$ [45]: the b -quark forward-backward asymmetry A_{FB}^b prefers values $a < 1$, while the leptonic asymmetries A_l and m_W favour values slightly larger than 1. Overall, the global fit of a is dominated by m_W due to its small uncertainty, with the other observables individually playing a minor role. By using the results from the GFitter collaboration [108], we find that in absence of additional NP contributions to the EW fit, the Higgs coupling is expected to lie in the interval $0.98 \leq a^2 \leq 1.12$ with 95% of probability. A similar result has been recently obtained by Ref. [111]. This is an extremely strong bound which seems to disfavour Higgs compositeness as a natural solution of the little hierarchy problem, in particular its realisations through compact cosets where a is always reduced compared to its SM value (see for example eq. (3.7)).

To better understand this result it is useful to perform a two-dimensional fit in terms of the Peskin–Takeuchi \hat{S} and \hat{T} parameters [113, 114]. It is well known that modifying the Higgs coupling to vector bosons compared to its SM prediction leads to a logarithmically divergent shift in these two parameters, with $\Delta\hat{S} > 0$ and $\Delta\hat{T} < 0$ [45]. For $m_H = 125 \text{ GeV}$ and $a = 1$ the theoretical point lies slightly outside the 68% contour, and by decreasing a it moves further outside the experimentally preferred region, following a trajectory almost orthogonal to the probability isocontours. Thus, small reductions of the coupling a have dramatic impact on the fit. Values $a > 1$ are less constrained but also theoretically less motivated, as they require either non-compact cosets (like for example $SO(4, 1)/SO(4)$), or a sizeable tree-level contribution from a scalar resonance with isospin $I = 2$ [115, 116].⁸ If one excludes these more exotic theoretical scenarios, one concludes that sizeable NP contributions to the EW observables, in particular to the vector boson self energies, are required to accommodate $\sim O(10\%)$ shifts in the Higgs coupling a .

A negative and large $\Delta\hat{S}$ can follow from loops of fermion resonances [117–120]. A sizeable and positive $\Delta\hat{T}$ could also be generated by the 1-loop exchange of composite fermions, in particular the top partners. For example, if both SM top chiralities couple with the same strength to the strong dynamics, one naively expects $\Delta\hat{T} \sim \xi y_t^2 / (16\pi^2)$ (see for example Ref. [80]), which shows that it is possible to obtain $\Delta\hat{T} \sim \text{a few} \times 10^{-3}$ for $\xi \sim O(10\%)$. Corrections of this size would dramatically modify the range of a preferred by the EW fit, especially if accompanied by an additional $\Delta\hat{S} < 0$. For example, by assuming $\Delta\hat{T} = +1.5 \times 10^{-3}$ (with no extra $\Delta\hat{S}$), we find that the 95% interval on the Higgs coupling becomes $0.70 \leq a^2 \leq 0.92$. It is thus interesting to see under what conditions models can accommodate such corrections while satisfying all other constraints,

⁸The latter possibility can be directly tested experimentally, since the $I = 2$ multiplet includes doubly-charged scalars which can be produced and observed at the LHC.

in particular on the $Z\bar{b}b$ vertex, and investigate what their predictions for the production of the top partners are at the LHC. The first analyses that appeared in the literature seemed to indicate a generic difficulty to obtain positive $\Delta\hat{T}$ [45, 121–123]. However, a more detailed exploration of the full parameter space in a broader class of models has shown that there is more freedom in accommodating a positive and sizeable $\Delta\hat{T}$ while keeping corrections to $Z\bar{b}b$ under control [119] (see also Ref. [124]).

One might wonder if a modified value of a can be helpful in relaxing the tension of the b -quark observables A_{FB}^b and R_b .⁹ In fact, as we already pointed out, all the observables, including those related to the b quark, depend on a mainly through the 1-loop contribution of the Higgs to the vector boson self-energies. As a consequence, any NP correction to a cannot lead to an effect restricted to the b -quark sector, but will propagate to all observables. Notice also that excluding A_{FB}^b from the fit pushes a towards larger values, which are even more problematic from the theoretical viewpoint, although the effect is small. It is thus clear that the existence of a tension in the b observables does not lead to any room for relaxing the strong bound on the Higgs coupling a . Yet, the fact that in a fit to the couplings of b_L and b_R to the Z the SM point lies outside the 95% probability contour (see Refs. [110, 111, 126]) might indicate that the contribution from NP states is already at work.

Apart from possible NP effects, the fit of a is strongly sensitive to the value of the W and top quark masses. We have already stressed that m_W dominates over the other observables. Its current experimental measurement is $\sim 1.2\sigma$ larger than the one preferred by the EW fit, if it goes down in the future also the central value of a will diminish. The strong dependence on the top mass originates from the 1-loop correction to the ρ parameter, $\Delta\rho = \Delta\hat{T} \propto m_t^2 G_F$, which we have seen has an important impact on a . In this regard one must notice that the error reported in the current Tevatron average $m_t = (173.18 \pm 0.94) \text{ GeV}$ [127] does not include the theoretical uncertainty on the definition of the parameter extracted from the event kinematics in terms of the \overline{MS} mass. If one instead adopts the larger error $\sigma_t = 2.8 \text{ GeV}$ that follows from measuring the \overline{MS} mass directly from the $t\bar{t}$ cross section [128], one finds that the uncertainty on a increases by a non-negligible amount [111]. While these issues have to be considered to make a precise determination of the Higgs coupling, the overall picture which emerges from the EW fit seems quite robust: $O(10\%)$ decrease in a require sizeable NP contributions to the vector-boson self energies.

2.3.3 Oblique parameters

A particular subset of the electroweak precision data constrains deviations in the vacuum polarisations of the SM gauge bosons, the so called oblique corrections, which were

⁹By including the two-loop calculation of R_b performed by Ref. [125], the pulls of A_{FB}^b and R_b are respectively $+2.7\sigma$ and -2.1σ [111] (see also [108] for similar results).

especially well experimentally accessible at LEP through $2 \rightarrow 2$ fermion scattering. The oblique parameters have been initially introduced in Refs. [113, 117, 129] and were discussed in detail in the literature, see for example Refs. [114, 130, 131]. They can be conveniently quantified in terms of the effective Lagrangian [132]

$$\mathcal{L} = -\frac{1}{2}W_\mu^3\Pi_{33}(p^2)W^{\mu 3} - \frac{1}{2}B_\mu\Pi_{00}(p^2)B^\mu - W_\mu^3\Pi_{30}(p^2)B^\mu - W_\mu^+\Pi_\pm(p^2)W^{\mu-}. \quad (2.43)$$

The various form factors are then expanded in powers of p^2

$$\Pi(p^2) = \Pi(0) + p^2\Pi'(0) + \frac{p^4}{2!}\Pi''(0) + \dots \quad (2.44)$$

From the 12 parameters at $\mathcal{O}(p^4)$, three of them can be absorbed in the definition of the SM parameters

$$v^2|_{\text{exp}} \equiv -4\Pi_\pm(0), \quad \frac{1}{g^2}|_{\text{exp}} \equiv \Pi'_\pm(0), \quad \frac{1}{g'^2}|_{\text{exp}} \equiv \Pi'_{00}(0). \quad (2.45)$$

Two further relations among the zeroth-order coefficients follow from the massless photon: $\Pi_{\gamma\gamma}(0) = \Pi_{\gamma Z} = 0$. We are hence left with seven free oblique parameters

$$\begin{aligned} \hat{S} &= \frac{g}{g'}\Pi'_{30}(0), & \hat{T} &= \frac{\Pi_{33}(0) - \Pi_\pm(0)}{m_W^2}, & Y &= \frac{m_W^2}{2}\Pi''_{00}(0), & W &= \frac{m_W^2}{2}\Pi''_{33}(0), \\ X &= \frac{m_W^2}{2}\Pi''_{30}(0), & -\hat{U} &= \Pi'_{33}(0) - \Pi'_\pm(0), & V &= \frac{m_W^2}{2}(\Pi''_{33}(0) - \Pi''_\pm(0)). \end{aligned} \quad (2.46)$$

The second line consists of the same linear combinations of form factors as the first line with additional derivatives. These oblique parameters are thus associated to dimension-8 and 10 operators whose effects are negligible compared to dimension-6. Since each derivative contributes a suppression factor of $1/m_*$, the second line is suppressed by powers of m_W/m_* with respect to the first and can therefore be neglected. Consequently, we remain with the four oblique parameters given in the first line of eq. (2.46) which constrain NP effects in the gauge boson propagators. Their relation to the S and T parameters introduced in Ref. [113] is simply

$$S = \frac{4s_W^2}{\alpha_{EM}}\hat{S} \approx 119\hat{S}, \quad T = \frac{1}{\alpha_{EM}}\hat{T} \approx 129\hat{T}. \quad (2.47)$$

Note that \hat{T} breaks the custodial symmetry $SU(2)_R \times SU(2)_L$. Generally, \hat{S} and \hat{T} describe NP related to electroweak symmetry breaking involving the Higgs field while Y and W are Higgs independent and related to new structures in the heavy sector, such as additional heavy vectors as we will show explicitly in section 6.2, but also fermions or scalars (see for example Ref. [133]).

In the SM, the leading contributions to \hat{S} and \hat{T} can be computed from the various 1-loop corrections to the gauge boson correlators. Three different loop diagrams, with NGBs, the Higgs and the top running in the loop, contribute to the vacuum polarisations as depicted in Fig. 2.2 [134]. Since \hat{T} is expected to be proportional to the custodial breaking parameter g' , the computation can be performed in the gaugeless limit, $g = 0$, and it suffices to consider diagrams with external NGBs only. It is important to note that this is not an application of the equivalence theorem since we are interested in the form factors at zero momentum. Furthermore, this small number of diagrams is sufficient only in an R_ξ -gauge where the kinetic $B_\mu - \pi^3$ mixing vanishes [135]. Otherwise, more diagrams with explicit mixings would have to be taken into account. In particular, it is most convenient to work in the Landau gauge ($\xi = 0$) where the NGBs are massless. The explicit computation of the NGB and Higgs loops in Fig. 2.2 gives

$$\begin{aligned}\hat{S}_{SM} &= \frac{g^2}{96\pi^2} \log\left(\frac{m_*}{m_W}\right) - \frac{g^2}{96\pi^2} a^2 \log\left(\frac{m_*}{m_h}\right), \\ \hat{T}_{SM} &= -\frac{3g'^2}{32\pi^2} \log\left(\frac{m_*}{m_W}\right) + \frac{3g'^2}{32\pi^2} a^2 \log\left(\frac{m_*}{m_h}\right),\end{aligned}\tag{2.48}$$

where m_* is the cutoff of the loop integrals and can again be associated to the scale of NP. As anticipated \hat{T} is proportional to the custodial breaking parameter g' . Note that we take a possibly modified coupling of the Higgs to vector bosons and NGBs through the parameter a into account. Subleading corrections of order $\mathcal{O}(m_W^2/m_h^2)$ have been neglected in the above expressions. However, they explain the slight bend in the curve describing the effect of the Higgs mass in the (\hat{S}, \hat{T}) plane [134]. The apparent logarithmic divergences in the above equations can be recast into

$$\begin{aligned}\hat{S}_{SM} &= \frac{g^2}{96\pi^2} \log\left(\frac{m_h}{m_W}\right) + \frac{g^2}{96\pi^2} (1 - a^2) \log\left(\frac{m_*}{m_h}\right), \\ \hat{T}_{SM} &= -\frac{3g'^2}{32\pi^2} \log\left(\frac{m_h}{m_W}\right) - \frac{3g'^2}{32\pi^2} (1 - a^2) \log\left(\frac{m_*}{m_h}\right),\end{aligned}\tag{2.49}$$

where now the first term, usually referred to as the IR contributions to the oblique parameters, is finite and the Higgs mass can be interpreted as the cutoff value of the divergent loop integral while the second term involves the factor $1 - a^2$ which vanishes for a SM Higgs boson with $a = 1$. Hence in the SM, the logarithmic divergence cancels between the two diagrams. For modified Higgs couplings this is, however, no longer true and a logarithmic dependence on the cutoff scale arises. Finally, the top gives the leading contribution in the fermion loops as shown in Fig. 2.3

$$\begin{aligned}\hat{S}_{top} &= -\frac{g^2}{48\pi^2} \log\left(\frac{m_t^2}{m_Z^2}\right), \\ \hat{T}_{top} &= \frac{3g^2 m_t^2}{64\pi^2 m_W^2},\end{aligned}\tag{2.50}$$

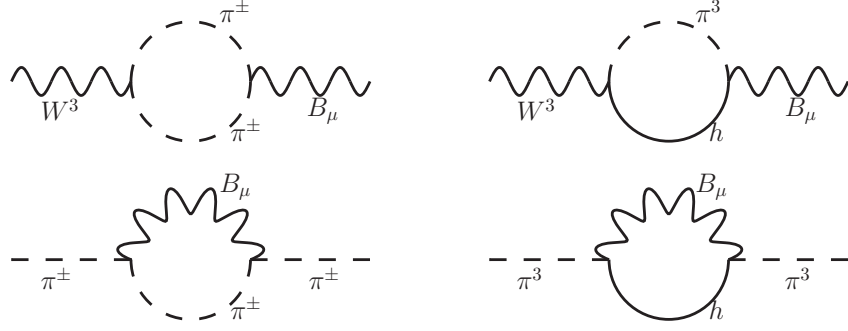


Figure 2.2 – The Goldstone boson and Higgs contribution to \hat{S} (upper row) and \hat{T} (lower row).

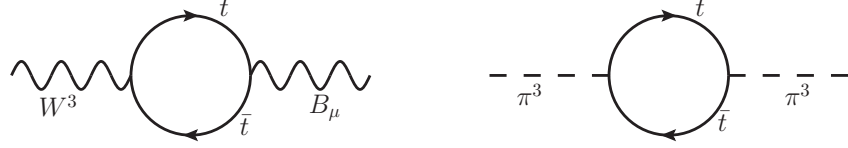


Figure 2.3 – The leading top loop contribution contribution to \hat{S} (left) and \hat{T} (right).

Note that current fits are usually centred around the SM value, i.e. the top and NGB contributions have been subtracted such that only NP effects have to be taken into account. The following contributions to the oblique parameters arise from the dimension-6 operators of the effective Lagrangian

$$\begin{aligned} \hat{S} &= (c_W + c_B) \frac{m_W^2}{m_*^2}, & \hat{T} &= c_T \frac{g_*^2 v^2}{m_*^2}, \\ W &= c_{2W} \frac{m_W^2}{m_*^2}, & Y &= c_{2B} \frac{m_W^2}{m_*^2}. \end{aligned} \quad (2.51)$$

The \hat{S} and \hat{T} parameters have been very precisely constrained in recent fits [108, 111] while W and Y have not been updated [114]. The current constraints are

$$\begin{aligned} \hat{S} &\in [-0.59, 1.09] \times 10^{-3}, & \hat{T} &\in [-0.54, 1.32] \times 10^{-3}, \\ W &\in [-0.7, 9.1] \times 10^{-3}, & Y &\in [-4.7, -0.7] \times 10^{-3}. \end{aligned} \quad (2.52)$$

3 The Minimal Composite Higgs Model

In the past decade a realistic framework has emerged [40–46] in which the Higgs boson arises as a pseudo-Nambu-Goldstone Boson (pNGB) from the spontaneous breaking of a global symmetry G , of a new strongly interacting sector, to a subgroup H . These models have two crucial advantages over plain technicolor models. Firstly, the presence of a light Higgs boson allows the parametric separation between the $G \rightarrow H$ breaking scale f and the electroweak symmetry breaking scale v . This alleviates the tension of technicolor models with electroweak precision tests [136]. Secondly, the flavour problem of technicolor can be greatly improved by the implementation of partial compositeness [137] discussed in more detail in section 3.2.

3.1 The Goldstone and gauge sector: a Higgs as a pNGB

Nambu-Goldstone bosons. The simplest realistic realisation of the composite Higgs idea is represented by $G = SO(5) \times U(1)_X$ and $H = SO(4) \times U(1)_X$. The $U(1)_X$ factor is needed to obtain the correct hypercharge, $Y \equiv T_R^3 + X$, for the SM fermions. This breaking pattern satisfies the two conditions of a viable model. Firstly, the SM gauge bosons gauge a subgroup $SU(2)_L \times U(1)_Y \subset SU(2)_L \times SU(2)_R \sim SO(4)' \subset G$. Secondly, G/H contains one $SU(2)_L$ doublet which can be identified with the Higgs doublet. The coset space of $SO(5) \times U(1)_X / SO(4) \times U(1)_X$ contains a quadruplet of NGBs $h^{\hat{a}} = (\pi^a, h)$ transforming as a **4** of $SO(4)$, three of which are eaten by the SM gauge bosons while the fourth is the physical Higgs boson.¹

Let us outline the symmetry breaking pattern in more detail. The global symmetry G is broken spontaneously to the subgroup H at a scale f . Simultaneously, the couplings of the elementary fields to the strong sector (discussed in section 3.2) break the global symmetry G explicitly and generate a potential for the Higgs which is calculable in specific

¹There are just two custodially symmetric cosets yielding only one complex doublet of Goldstones: $SO(5)/SO(4)$ and $SO(4,1)/SO(4)$.

Chapter 3. The Minimal Composite Higgs Model

models and whose general structure is sketched in section 3.2.2. The potential aligns the non-zero vacuum along a particular direction inside the coset. Four NGBs arise in the breaking and can be encoded in the Goldstone boson matrix

$$U(h) = \exp \left(i \frac{\sqrt{2} h^{\hat{a}} T^{\hat{a}}}{f} \right), \quad (3.1)$$

where $T^{\hat{a}}$ are the broken $SO(5)/SO(4)$ generators (see Appendix A.2 for their explicit expressions). Notice that $U(h)$ is an orthogonal matrix transforming as [138]

$$U(h) \rightarrow g U(h) \hat{h}(g, h)^{-1}, \quad g \in G, \hat{h} \in H. \quad (3.2)$$

$U(h)$ can be used to turn irreducible representations of G into irreducible representations of H . Moreover, we can use $U(h)$ to construct the 5-vector parameterising the NGB fields

$$\Sigma_I(h) = U(h) \Sigma_0 = U_{I5}(h) = \frac{1}{h} \sin \frac{h}{f} \left(h^1, h^2, h^3, h^4, h \cot \frac{h}{f} \right)^T, \quad (3.3)$$

transforming linearly under $SO(5)$, i.e. $\Sigma(h) \rightarrow g \Sigma(h)$. The vacuum configuration is given by $\Sigma_0 = (0, 0, 0, 0, 1)$ and we defined $h = \sqrt{(h^i)^2}$. Σ_0 is the $SO(5)$ vacuum that preserves $SO(4)'$, i.e. the subgroup that embeds the complete SM gauge group $SU(2)_L \times U(1)_Y$. Notice, however, that the true vacuum, given by

$$\Sigma = \left(0, 0, 0, \sin \frac{h}{f}, \cos \frac{h}{f} \right)^T, \quad (3.4)$$

preserves a different $SO(4) \neq SO(4)'$ which overlaps with $SO(4)'$ only in one generator for the electromagnetic subgroup $U(1)_Q$. The true vacuum corresponds to eq. (3.3) in the unitary gauge. The misalignment between the two vacua is parameterized by the angle $\theta = \langle h \rangle / f$ which is determined dynamically in the breaking. We can distinguish two cases. For $\theta = 0$, no vacuum expectation value is generated and the two vacua coincide. This is the case because the partially gauged $SO(4)'$ coincides with the preserved $SO(4)$ and the EW symmetry remains unbroken. The vacua of $SO(4)'$ and $SO(4)$ are only misaligned for $\theta \neq 0$, when the EW symmetry is broken by the dynamically generated non-zero vev $v = f \sin \theta$. Also the gauge group is spontaneously broken at the same time as G/H . To consider the different limits let us also define the parameter²

$$\xi = \frac{v^2}{f^2} = \sin^2 \theta > 0. \quad (3.5)$$

The limit $\xi \rightarrow 0$ corresponds to the SM since NP only comes in at such high energies, $f \rightarrow \infty$, that its effects are negligible. Instead, $\xi \rightarrow 1$ describes the maximally broken, technicolor case where $v = f$. The physical Higgs field decouples at linear order from the

²Note that for $SO(4, 1)/SO(4)$ it would be $\xi = -v^2/f^2 < 0$.

3.1. The Goldstone and gauge sector: a Higgs as a pNGB

electroweak sector as can be seen explicitly from the Higgs couplings in eq. (3.7). In this case, the technicolor vacuum of the remaining NGBs, introduced in section 2.1.2, breaks the electroweak symmetry. A composite Higgs model thus interpolates between the two breaking mechanisms.

The chiral Lagrangian at $\mathcal{O}(p^2)$ can be simply written as

$$\begin{aligned}\mathcal{L}^{(2)} &= \frac{f^2}{2} (D_\mu \Sigma)^T (D^\mu \Sigma) , \\ &= \frac{1}{2} (\partial_\mu h)^2 + \frac{f^2}{4} \text{Tr} (D_\mu \Phi)^\dagger (D^\mu \Phi) \sin^2 \left(\theta + \frac{h}{f} \right) .\end{aligned}\tag{3.6}$$

such that $m_W = gf/2 \sin \theta$. To construct the $\mathcal{O}(p^4)$ chiral Lagrangian, it is most convenient to use the covariant CCWZ variables discussed in appendix A.1. Equation 3.6 reduces to a particular case of eq. (2.16) where

$$a = \sqrt{1 - \xi} , \quad b = 1 - 2\xi , \quad b_3 = -\frac{4}{3}\xi\sqrt{1 - \xi} .\tag{3.7}$$

once the sine is expanded. Further expanding the above relations to $\mathcal{O}(\xi^2)$, eq. (2.32) with $c_H = 1$, $c'_H = 2$ is reproduced. The expression for d_3 depends instead on the form of the Higgs potential, which is model dependent since it requires some explicit breaking of the Goldstone symmetry G . For example, in the minimal composite Higgs models with the elementary fermions embedded in **4** or **5** of $SO(5)$, MCHM4 and MCHM5 of Refs. [41, 43], one has

$$\text{MCHM4: } d_3 = \sqrt{1 - \xi} , \quad \text{MCHM5: } d_3 = \frac{1 - 2\xi}{\sqrt{1 - \xi}} ,\tag{3.8}$$

from which $c_6 = 1$, $c_8 = 5/4$ in the MCHM4 and $c_6 = c_8 = 0$ in the MCHM5 follows.

The fact that at $\mathcal{O}(v^2/f^2)$ the couplings a, b, b_3 are affected by only one operator [80], whose coefficient c_H can always be redefined away by a proper redefinition of f (for example it can be set to 1), has an important consequence.³ Since the predictions of any coset G/H must match those of the SILH Lagrangian at low energy, this implies that the expressions of eq. (2.32) are universal at first order in v^2/f^2 , i.e. they are the same for a pNGB and for a generic scalar. At order v^4/f^4 , instead, the couplings a, b, b_3 are modified by two operators, whose coefficients are thus related by a specific relation for any given coset G/H ; for example, the coset $SO(5)/SO(4)$ implies $c'_H = 2c_H$. One can thus distinguish the case of a generic SILH, where c'_H can have any value, from that of a pNGB Higgs.

³Note that custodial symmetry is crucial for this argument since otherwise two dimension-6 operators would contribute at $\mathcal{O}(v^2/f^2)$.

Gauge bosons. The bosonic sector of the theory comprises not only the Goldstone bosons of the $SO(5)/SO(4)$ coset but also the gauge bosons of the $SU(2)_L \times U(1)_Y$ SM gauge symmetry. We expect the elementary gauge bosons to couple linearly to dimension-3 conserved currents of the strong sector, as discussed below eq. (3.13). Upon integrating out the heavy degrees of freedom of the composite sector these G -breaking interactions will generate an effective Lagrangian for the gauge bosons which can be used to derive the gauge contribution to the Higgs potential. The most general effective action for the SM gauge fields can be derived under the assumption that the full global symmetry of the strong sector G is gauged. Working in Landau gauge, at the quadratic level in momentum space, this $SO(5) \times U(1)_X$ invariant Lagrangian is given by

$$\mathcal{L}_{\text{eff}}^g = \frac{1}{2} P_{\mu\nu}^{(t)} [\Pi_0^X(p) A^{X\mu} A^{X\nu} + \Pi_0(p) \text{Tr}[A^\mu A^\nu] + \Pi_1(p) \Sigma^T A^\mu A^\nu \Sigma] , \quad (3.9)$$

where $P_{\mu\nu}^{(t)} = \eta_{\mu\nu} - p_\mu p_\nu / p^2$ is the transverse projector.⁴ We identify the SM gauge bosons among the $SO(5) \times U(1)_X$ ones according to

$$A_\mu^{aL} = W_\mu^a, \quad A_\mu^{3R} = A_\mu^X = B_\mu, \quad A_\mu^{1R,2R} = A_\mu^{\hat{a}} = 0. \quad (3.10)$$

Using these relations, the effective Lagrangian for the SM gauge fields becomes

$$\mathcal{L}_{\text{eff}}^g = P_{\mu\nu}^{(t)} \left[\frac{1}{2} W^{a\mu} \Pi_{ab} W^{b\nu} + W^{3\mu} \Pi_{30} B^\nu + \frac{1}{2} B^\mu \Pi_{00} B^\nu \right] , \quad (3.11)$$

where the form factors are related to those in eq. (3.9) by

$$\begin{aligned} \Pi_{00} &= \Pi_0 + \Pi_0^X + \frac{s_h^2}{4} \Pi_1, \\ \Pi_{03} &= -\frac{s_h^2}{4} \Pi_1, \\ \Pi_{ab} &= \delta_{ab} \left(\Pi_0 + \frac{s_h^2}{4} \Pi_1 \right). \end{aligned} \quad (3.12)$$

where we used the shorthand notation $s_h \equiv \sin h/f$.

3.2 The fermionic sector: partial compositeness

The degrees of freedom, whose elementary nature is well probed (the light quarks and leptons and the transverse polarisations of the gauge bosons), are external to the strongly interacting sector and they communicate with it only through linear couplings of the form

$$\mathcal{L}_{\text{mix}} = g A_\mu \mathcal{J}^\mu + \lambda q \mathcal{O} + \dots , \quad (3.13)$$

⁴Notice that $\Sigma^T A \Sigma = 0$.

3.2. The fermionic sector: partial compositeness

where \mathcal{J} is a global current of the strong sector which is gauged by the SM vector bosons A_μ and \mathcal{O} is a fermionic operator (assumed to have a scaling mass dimension 5/2) [139]. The couplings of the elementary fields to the strong sector break the global symmetry G explicitly and generate a potential for the Higgs. The largest contribution to the pNGB potential comes typically from the interactions generating the top quark mass. The Yukawa for the top quark arises from the coupling of the elementary q_L and t_R to the strong sector according to the pattern sketched above in eq. (3.13)

$$\mathcal{L}_{\text{mix}} = \lambda_L f q_L \mathcal{O}_L^q + \lambda_R f t_R \mathcal{O}_R^t + \text{h.c.}, \quad (3.14)$$

where f is the sigma model decay constant and \mathcal{O} stands for fermionic resonances of mass m_ψ in the low energy theory (their naive dimension is now 3/2). Dimensional analysis ensures the leading contribution to the top Yukawa to be

$$y_t \sim \frac{\lambda_L \lambda_R}{g_\psi}, \quad (3.15)$$

where $1 < g_\psi \sim m_\psi/f < 4\pi$ is the typical coupling among these fermionic resonances. We wish to distinguish this coupling from the one among the vector resonances, g_ρ . Notice that g_ψ can be naturally smaller than g_ρ due to an approximate chiral symmetry. So far, both couplings were jointly referred to as g_* . The dimensionless parameters $\epsilon_{L,R} \equiv \lambda_{L,R}/g_\psi$ determine the degree of compositeness of the various SM fields ranging from 0 (elementary state) to 1 (composite state). Furthermore, flavour changing neutral currents arising through four fermion interactions (falling in the first category of dimension-6 operators introduced in section 2.2.1) which have been problematic in traditional technicolor are now of the form

$$\frac{\lambda_i \lambda_j \lambda_k \lambda_l}{g_\psi^2 m_\psi^2}, \quad (3.16)$$

and thus strongly suppressed by four powers of the elementary-composite mixing.

Deep insight into the structure of the Higgs potential is obtained by exploiting the symmetry properties of eq. (3.14). As the strong sector obeys a global symmetry G the operators \mathcal{O}^q and \mathcal{O}^t can be classified according to their transformation properties under G .⁵ Furthermore when both interactions in eq. (3.14) and the SM gauge interactions are switched off, the action for the elementary fields is invariant under an independent $SU(2) \times U(1)$ group, with charges corresponding to their SM quantum numbers. The couplings λ_L and λ_R break this large $\mathcal{G} \equiv SU(2) \times U(1) \times G$ to the gauged $SU(2)_L \times U(1)_Y$ vector subgroup. It is however possible to assign spurious transformation properties to

⁵The fact that G is spontaneously broken to a subgroup H does not affect this statement as the Goldstone bosons from $G \rightarrow H$ can be used in the definition of \mathcal{O}^q and \mathcal{O}^t in order to make them transform linearly under G .

Chapter 3. The Minimal Composite Higgs Model

the λ s, promoting them to $\hat{\lambda}$ s, in order to make eq. (3.14) formally invariant under \mathcal{G}

$$\mathcal{L}_{\text{mix}} = f q_L^\alpha (\hat{\lambda}_L)^\alpha_I \mathcal{O}_L^{qI} + f t_R^\alpha (\hat{\lambda}_R)^\alpha_I \mathcal{O}_R^{tI} + \text{h.c.}; \quad (3.17)$$

α and I are irreducible $SU(2) \times U(1)$ and G indices respectively.

When both the strong sector and the high energy fluctuations of the elementary modes are integrated out the resulting effective action will respect the spurious \mathcal{G} symmetry. $SU(2) \times U(1)$ invariance implies that, for instance, at leading order in λ_L only the combination $X_{LI \otimes J} \equiv (\hat{\lambda}_L \hat{\lambda}_L)_{I \otimes J}$ will enter the Higgs potential. The same argument constrains the form of the λ_R contribution.

$X_{L,R}$ transform spuriously as reducible representations of G : $X_{I \otimes J} = \sum_r X_{I_r}^r$. Combining X with the Goldstone matrix U in eq. (3.2) according to their transformation properties we can construct non-linear G invariants, $I_i(h/f)$, which depend non-trivially on the pNGB h . The structure of the potential will thus be [80]

$$\begin{aligned} V(h) &= V^{(1\text{loop})}(h/f) + V^{(2\text{loop})}(h/f) + \dots \\ &= f^2 m_\Psi^2 \left(\frac{g_\psi}{4\pi} \right)^2 \left(\epsilon^2 \mathcal{F}_1^{(1)}(h/f) + \epsilon^4 \mathcal{F}_2^{(1)}(h/f) + \dots \right) \\ &\quad + f^2 m_\Psi^2 \left(\frac{g_\psi}{4\pi} \right)^4 \left(\epsilon^2 \mathcal{F}_1^{(2)}(h/f) + \dots \right) + \dots, \end{aligned} \quad (3.18)$$

where

$$\mathcal{F} = \sum_i c_i I_i \left(\frac{h}{f} \right), \quad (3.19)$$

i.e. each of the functions \mathcal{F} is a sum of the non-trivial G invariants which can be constructed at a given order in ϵ and \hbar . eq. (3.18) allows us to determine how EWSB occurs. Generically we expect the one-loop, leading order $\mathcal{F}_1^{(1)}$ contribution to be dominant. As the various \mathcal{F} are expected to be $O(1)$ functions of their argument, some degree of cancellation among the c_i is necessary to obtain a small enough ratio $\xi = (v/f)^2$ which is crucial for a realistic phenomenology. In the absence of other cancellations, this irreducible tuning of a composite Higgs model can be quantified by ξ itself.

For certain choices of the operators $\mathcal{O}^{q,t}$, the leading contribution to the Higgs potential, $\mathcal{F}_1^{(1)}$, contains a single invariant at $O(\epsilon^2)$. This happens for instance in the simplest case in which both \mathcal{O}^q and \mathcal{O}^t transform as a **5** of $SO(5)$ where

$$\epsilon^2 \mathcal{F}_1^{(1)} = c_1 \epsilon^2 s_h^2, \quad (3.20)$$

with $s_h \equiv \sin h/f$, and only a discrete set of values is available for ξ . In order to be able to tune $\xi \ll 1$, it is necessary to suppress the coefficient of the leading order term in eq. (3.20) to be of the same order as the $O(\epsilon^4)$ subleading contribution which will

contribute with the new independent functions of h/f

$$\epsilon^4 \mathcal{F}_2^{(1)} = (c_2 \epsilon^2) \epsilon^2 s_h^2 (1 - s_h^2). \quad (3.21)$$

In other words we need $c_1 \approx c_2 \epsilon^2$ and the tuning is worsened to $\xi \times \epsilon^2$. The simplest situation that avoids this peculiar behaviour corresponds to the \mathcal{O}^q being the **14** dimensional (symmetric and traceless) representation of $SO(5)$ and \mathcal{O}^t being a singlet. This choice defines the MCHM₁₄ [48]. In the MCHM₁₄, already $\mathcal{F}_1^{(1)}$ contains two invariants and a viable EWSB can be achieved with the minimal amount of tuning.

To study the consequences of this model beyond simple dimensional analysis the calculability of the Higgs potential is a crucial property. A 4D realisation of the MCHM₁₄ has been obtained in Ref. [48] using Weinberg's sum rules to ensure calculability.⁶ Collective breaking, used in Ref. [47], led to the same result. In this section, we follow the original approach of Ref. [41] studying a holographic realisation of the MCHM₁₄ where calculability is related to locality in an extra dimension. The only difference between our approach and the original holographic approach to composite Higgs models is the 5D metric, that we choose to be flat and not AdS₅.

The remainder of this section is organised as follows. In section 3.2.1 and 3.2.2, we clarify the role of symmetries and dimensional analysis in the structure of the Higgs potential of the MCHM₁₄. We recall the general features of holographic composite Higgs models in section 3.3 and describe the setup leading to the MCHM₁₄ in detail. In section 3.4, we compute the Higgs potential and study the dependence of ξ and m_h on the parameters of the 5D model. Here we study the spectrum of the fermionic resonances, their relations with the Higgs mass and the tuning of the holographic implementation. In section 3.5 we summarise and conclude, sketching some possible phenomenological implications of the model.

3.2.1 A composite Higgs with $q_L \in \mathbf{14}$ and $t_R \in \mathbf{1}$

We assume the existence of fermionic operators $\mathcal{O}_L^q \in \mathbf{14}_{2/3}$ and $\mathcal{O}_R^t \in \mathbf{1}_{2/3}$. The subscript refers to the $U(1)_X$ charge.⁷ According to partial compositeness these operators couple to the elementary fermions through linear mixings

$$\mathcal{L}_{\text{mix}} = \lambda_L f q_L^\alpha \text{Tr} [P_L^\alpha \mathcal{O}_L^q] + \lambda_R f t_R^\alpha P_R^\alpha \mathcal{O}_R^t + \text{h.c.} . \quad (3.22)$$

⁶For an extensive discussion of the use of generalised Weinberg's sum rules in general composite Higgs models see Ref. [49].

⁷Notice that our choice of the representations of the composite operators mixing with the top sector do not generate dangerous corrections to the $Z b_L b_L$ coupling thanks to a P_{LR} symmetry [140, 141]. In this section we do not discuss the implementation of SM fermion masses apart from the top quark since their effect on the Higgs potential is subleading. However, the model can be extended in order to generate a mass for the b -quark without introducing large corrections to the $Z b_L b_L$ and $Z b_R b_R$ couplings. These will be generically proportional to the mixing angles in the bottom sector which can be small consistently with the generation of the small b mass.

Chapter 3. The Minimal Composite Higgs Model

To make contact with eq. (3.17), we define $\hat{\lambda}_L = \lambda_L P_L$ and analogously $\hat{\lambda}_R = \lambda_R P_R$ where λ_L and λ_R are numerical coefficients describing the mixing strength between the elementary states and the composite sector. Both P_L^α and \mathcal{O}_q are taken to be 5×5 matrices transforming as

$$\mathcal{O}_q \rightarrow g^{-1} \mathcal{O}_q g, \quad P_L^\alpha \rightarrow g^{-1} P_L^\alpha g, \quad g \in SO(5). \quad (3.23)$$

α is an elementary $SU(2)$ index. eq. (3.22) is formally invariant under a spurious symmetry group $\mathcal{G} \equiv SU(2) \times U(1) \times SO(5) \times U(1)_X$ if one assumes

$$\begin{aligned} q_L &\equiv (\mathbf{2}, 2/3, \mathbf{1}, 0), & \mathcal{O}_q &\equiv (\mathbf{1}, 0, \mathbf{14}, 2/3), & P_L &\equiv (\mathbf{2}, -2/3, \mathbf{14}, -2/3), \\ t_R &\equiv (\mathbf{1}, 2/3, \mathbf{1}, 0), & \mathcal{O}_t &\equiv (\mathbf{1}, 0, \mathbf{1}, 2/3), & P_R &\equiv (\mathbf{1}, -2/3, \mathbf{1}, -2/3). \end{aligned} \quad (3.24)$$

The spurion P_L^α is given by

$$P_L^\alpha = \frac{1}{2} \left(\begin{array}{c|c} & \vec{v}^\alpha \\ \hline \vec{v}^{\alpha T} & \end{array} \right), \quad (3.25)$$

with

$$\vec{v}^{1T} = (0, 0, i, -1), \quad \vec{v}^{2T} = (i, -1, 0, 0), \quad (3.26)$$

while $P_R = 1$. The explicit expression for the matrix $\psi_q \equiv q_L^\alpha P_L^\alpha$ is thus

$$\psi_q = \frac{1}{2} \left(\begin{array}{cccc|c} & & & & ib_L \\ & & & & -b_L \\ & & & & it_L \\ & & & & -t_L \\ \hline ib_L & -b_L & it_L & -t_L & \end{array} \right). \quad (3.27)$$

Once the strong sector is integrated out the resulting effective Lagrangian for the light degrees of freedom has to respect the full spurionic symmetry which implies that q_L and t_R will only enter through the combinations ψ_q and $\psi_t \equiv t_R$. The relevant terms in the most general effective Lagrangian are thus

$$\begin{aligned} \mathcal{L}_{\text{eff}} &= \Pi_0^q \text{Tr} [\bar{\psi}_q \not{p} \psi_q] + \Pi_0^t \bar{\psi}_t \not{p} \psi_t \\ &\quad + 4\Pi_1^q \Sigma^T \bar{\psi}_q \not{p} \psi_q \Sigma + \Pi_2^q (\Sigma^T \bar{\psi}_q \Sigma) \not{p} (\Sigma^T \psi_q \Sigma) \\ &\quad + M_1^t \bar{\psi}_t \Sigma^T \psi_q \Sigma + \text{h.c.}, \end{aligned} \quad (3.28)$$

where $\Pi_0^q, \Pi_0^t, \Pi_1^q, \Pi_2^q, M_1^t$ are p^2 -dependent form factors that we will determine in the complete 5D theory in section 3.3 (the explicit form in 5D can be found in Appendix

A.3.2). In terms of t_L , b_L and t_R the Lagrangian in eq. (3.28) becomes

$$\mathcal{L}_{\text{eff}}^f = \Pi^{b_L} \bar{b}_L \not{p} b_L + \Pi^{t_L} \bar{t}_L \not{p} t_L + \Pi^{t_R} \bar{t}_R \not{p} t_R - (\Pi^{t_L t_R} \bar{t}_L t_R + \text{h.c.}) , \quad (3.29)$$

where the form factors are related by

$$\begin{aligned} \Pi^{b_L} &= \Pi_0^q + 2\Pi_1^q c_h^2, \\ \Pi^{t_L} &= \Pi_0^q + \Pi_1^q (1 + c_h^2) + \Pi_2^q s_h^2 c_h^2, \\ \Pi^{t_R} &= \Pi_0^t, \\ \Pi^{t_L t_R} &= M_1^t s_h c_h, \end{aligned} \quad (3.30)$$

with $s_h \equiv \sin h/f$ and $c_h \equiv \cos h/f$.

eq. (3.29) is sufficient to extract the top quark mass:

$$m_t^2 = \frac{|M_1^t|^2 s_h^2 c_h^2}{\Pi_0^t (\Pi_0^q + \Pi_1^q (1 + c_h^2) + \Pi_2^q s_h^2 c_h^2)} \approx \xi \frac{|M_1^t|^2}{\Pi_0^t \Pi_0^q}. \quad (3.31)$$

Here the form factors are evaluated at $p = 0$ which neglects effects of order m_t^2/m_T^2 where m_T is the mass of the fermionic resonances in the strong sector. In the last equality we assumed the existence of a hierarchy $\Pi_1^q, \Pi_2^q \ll \Pi_0^q$. As we will explain below this assumption is guaranteed by partial compositeness.

3.2.2 The Higgs potential

As the couplings of the elementary fermions and gauge bosons break the global symmetry of the strong sector, integrating out their high energy modes at 1-loop or higher order will generate a non-vanishing potential for the Higgs boson. At 1-loop the calculation is the one of Coleman and Weinberg in Ref. [142]. The gauge contribution to the Higgs potential is obtained starting from eq. (3.9). After rotation of the form factors to Euclidean space we obtain

$$V_g(h) = \frac{3}{2} \int \frac{d^4 p_E}{(2\pi)^4} \left[2 \log \left(1 + \frac{s_h^2}{4} \frac{\Pi_1}{\Pi_0} \right) + \log \left(1 + \frac{s_h^2}{4} \frac{\Pi_1}{\Pi_0} \frac{2\Pi_0 + \Pi_0^X}{\Pi_0 + \Pi_0^X} \right) \right], \quad (3.32)$$

where $p_E^2 = -p^2$ is the Euclidean momentum. The explicit expression of the form factors in a 5D model is obtained in section 3.3. Similarly, the fermionic contribution to the Higgs potential follows from eq. (3.29)

$$V_{\text{top}}(h) = -2N_c \int \frac{d^4 p_E}{(2\pi)^4} \left[\log \left(\Pi^{b_L} \right) + \log \left(p_E^2 \Pi^{t_L} \Pi^{t_R} + |\Pi^{t_L t_R}|^2 \right) \right], \quad (3.33)$$

where again all form factors are functions of the Euclidean momentum p_E . The convergence of the integrals in eq. (3.32) and eq. (3.33) depends on the details of the model. In the holographic case the form factors turn out to be exponentially decreasing functions of p_E , while the convergence is only power-like in discretised models.

Chapter 3. The Minimal Composite Higgs Model

To extract the structure of the Higgs potential we use again the relations $\Pi_1 \ll \Pi_0$ and $\Pi_1^q, \Pi_2^q \ll \Pi_0^q$ that allow us to expand the logarithms and write the non-constant part of the potential as

$$V(h) = \alpha c_h^2 + \beta s_h^2 c_h^2 = (\beta - \alpha) s_h^2 - \beta s_h^4. \quad (3.34)$$

The coefficients α and β are given by

$$\alpha = -\frac{3}{4} \int \frac{d^4 p_E}{(2\pi)^4} \frac{\Pi_1}{\Pi_0} \left(1 + \frac{2\Pi_0 + \Pi_0^X}{2(\Pi_0 + \Pi_0^X)} \right) - 6N_c \int \frac{d^4 p_E}{(2\pi)^4} \frac{\Pi_1^q}{\Pi_0^q}, \quad (3.35a)$$

$$\beta = -2N_c \int \frac{d^4 p_E}{(2\pi)^4} \left(\frac{\Pi_2^q}{\Pi_0^q} - \frac{|M_1^t|^2}{p_E^2 \Pi_0^q \Pi_0^t} \right). \quad (3.35b)$$

The potential in eq. (3.34) has a minimum for

$$\frac{v^2}{f^2} \equiv \xi = \sin^2 \left(\frac{\langle h \rangle}{f} \right) = \frac{\beta - \alpha}{2\beta}, \quad (3.36)$$

corresponding to a physical Higgs mass

$$m_h^2 = 2 \frac{\alpha^2 - \beta^2}{\beta f^2} = -\frac{8\beta}{f^2} \xi(1 - \xi). \quad (3.37)$$

Assuming the gauge contribution to be subleading we can estimate the expected size of α and β using spurionic symmetries and dimensional analysis [141]. The Lagrangian in eq. (3.22) is formally invariant under the spurious symmetry group \mathcal{G} described in the Introduction. As the composite sector and the high energy fluctuations of the SM fields are integrated out, the Higgs potential has to satisfy the spurionic symmetry \mathcal{G} with its $SO(5)$ subgroup being non-linearly realised. Since no non-trivial invariants can be build out of $\lambda_R P_R$ which does not break $SO(5)$, this structure will not enter the potential. For $\lambda_L P_L^\alpha$ there are two possibilities

$$\begin{aligned} I_1 &\equiv (U^\dagger P_L^\alpha P_{L\alpha}^\dagger U)_{55} = \Sigma^T P_L^\alpha P_{L\alpha}^\dagger \Sigma = 1 - \frac{3}{4} s_h^2, \\ I_2 &\equiv (U^\dagger P_L^\alpha U)_{55} (U^\dagger P_{L\alpha}^\dagger U)_{55} = (\Sigma^T P_L^\alpha \Sigma) (\Sigma^T P_{L\alpha}^\dagger \Sigma) = s_h^2 c_h^2. \end{aligned} \quad (3.38)$$

Both invariants can be generated at 1-loop order and are proportional to λ_L^2 . The leading contribution to the potential will thus be of the form

$$V(h) \approx N_C \frac{m_\psi^4}{16\pi^2} \frac{\lambda_L^2}{g_\psi^2} (a_1 I_1 + a_2 I_2), \quad (3.39)$$

where a_1, a_2 are coefficients of order 1, and $m_\psi \equiv g_\psi f$ is the typical mass of the fermionic resonances cutting off the UV divergences in $V(h)$. As a_1 is naturally of the same order as a_2 , a given value of ξ requires a cancellation of order ξ among the parameters. The

Higgs mass, on the other hand, is given by

$$m_h^2 \sim N_C \frac{g_\psi^2}{2\pi^2} \frac{g_\psi^2}{\lambda_R^2} y_t^2 v^2 |a_2| (1 - \xi) \approx (380 \text{ GeV})^2 \frac{1}{\epsilon_R^2} \left(\frac{g_\psi}{4} \right)^2 |a_2|. \quad (3.40)$$

This implies that, to obtain the measured value of the Higgs mass in a natural way, we need $\epsilon_R \approx 1$ (in which case t_R would be a fully composite state), a small g_ψ and $|a_2| \sim O(1)$ or a suppressed quartic coupling $|a_2| \lesssim 1$. This second possibility will increase the tuning from ξ to $\xi \times |a_2|$ if it is obtained through cancellations between the two pieces in the expression of β in eq. (3.35). These considerations must be taken with a grain of salt. While the parametric behaviour of m_h as a function of the various parameters is a solid prediction, the overall normalisation of eq. (3.40) is only an educated guess. In a specific model, numerical factors of order 1 can conspire to make $|a_2|$ somewhat larger or smaller than 1 in a completely natural way. In the former case the tuning needed to obtain a light Higgs boson would be enhanced while in the latter it would be reduced. We will show an effect of this kind in our specific example in section 3.4.

3.3 The 5D construction

In order to make quantitative predictions from our setup we need a framework where the Higgs potential is calculable. In this section we follow the holographic approach where finiteness is ensured by locality in an extra dimension. This follows from the AdS/CFT correspondence [143], where a strongly coupled 4D theory can be related to a weakly coupled theory in a slice of 5D anti de-Sitter (AdS) space (for detailed reviews see [144, 145]). For simplicity, and as justified in the next paragraph, we define our theory in a compact extra dimension $\mathbb{R}^4 \times [0, L]$ with a flat metric

$$ds^2 = \eta_{\mu\nu} dx^\mu dx^\nu - dz^2, \quad (3.41)$$

and with $L^{-1} = O(\text{TeV})$. To compute the effective action for the light degrees of freedom we follow the holographic prescription as described in Ref. [146] where the fields at one boundary are separated from the bulk degrees of freedom. The bulk obeys an enlarged gauge symmetry $SO(5) \times U(1)_X$ and is broken to the SM gauge group at the UV brane and $SO(4) \times U(1)_X$ at the IR brane. Elementary fields are mostly localised in the UV while composite particles, including the Higgs boson and right-handed top quark, live on the IR brane. By integrating out the bulk, an effective holographic Lagrangian for the boundary fields can be obtained. Form factors are computed in terms of boundary to boundary 5D propagators. The scalar degrees of freedom arise as the fifth gauge field component in so called gauge-Higgs unification models [40, 147]. In this case, the scalars correspond to pNGBs of the 4D theory. For a detailed analysis of the holographic techniques and gauge-Higgs unification in a flat extra dimension see Ref. [148].

One may question the use of the flat metric in our construction: extra dimensional models

require warping in order to properly address the hierarchy problem. It is known however that it is possible to mimic the low energy behaviour of a theory in warped space (AdS₅ in particular) by a theory formulated in a flat extra dimension with suitable terms added to its action [149–151]. This is enough to implement features like partial compositeness in flat space. In a warped theory these properties would follow automatically from the dual 4D interpretation.

In Appendix A.3 we give all the formulas which are necessary to implement our model also on an AdS₅ background.

3.3.1 Gauge degrees of freedom

The bulk theory obeys a gauged $SO(5) \times U(1)_X$ symmetry⁸ corresponding to the action

$$S_{5D}^g = - \int d^4x \int_0^L \frac{dz}{L} \left[\frac{1}{4g_5^2} \text{Tr}[F_{MN}^2] + \frac{1}{4g_X^2} (F_{MN}^X)^2 \right]. \quad (3.42)$$

The gauge symmetry is broken to $SU(2)_L \times U(1)_Y$ in the UV ($z = 0$) and to $SO(4) \times U(1)_X$ in the IR ($z = L$) by the boundary conditions [150]

$$\begin{aligned} F_{\mu 5}^{aL} = F_{\mu 5}^{aR} = F_{\mu 5}^X = 0, & \quad A_{\mu}^{\hat{a}} = 0, & \quad z = L, \\ A_{\mu}^{aL} = W_{\mu}^a, \quad A_{\mu}^{3R} = A_{\mu}^X = B_{\mu}, & \quad A_{\mu}^{1R,2R} = A_{\mu}^{\hat{a}} = 0, & \quad z = 0. \end{aligned} \quad (3.43)$$

The $z = 0$ values of the 5D fields are used as interpolating fields (holographic fields) in the low energy theory.

The bulk gauge symmetry has to be gauge fixed. A useful gauge to adopt is the one in which A_5 vanishes along the extra dimension. This is reached by a rotation of the gauge fields by the Wilson line

$$\bar{g}(x, z) = P \left[\exp \left(i \int_0^z dz' A_5^a(x, z') T^a \right) \right], \quad (3.44)$$

where ‘P’ stands for path ordered exponential and T^a are the $SO(5)$ generators. The issue with \bar{g} is that it does not reduce to an element of $SO(4)$ on the IR boundary. This problem can be bypassed by enlarging the gauge group at $z = L$ through the explicit introduction of Goldstone bosons. The IR boundary conditions in eq. (3.43) are therefore redefined in terms of the rotated field

$$A_M^{(U)} \equiv U(A_M + i\partial_M)U^\dagger, \quad (3.45)$$

⁸The gauged symmetry includes colour $SU(3)$ which we do not write explicitly.

where U is the matrix in eq. (3.1) and

$$\left(A^{(U)}\right)_{\mu}^{\hat{a}}(x, L) = 0, \quad \left(F^{(U)}\right)_{\mu 5}^{\hat{a}}(x, L) = 0. \quad (3.46)$$

This corresponds to an $SO(5)$ gauge transformation by the matrix U . Thanks to the transformation properties of U the IR boundary conditions are now invariant under the full $SO(5)$ group and eq. (3.44) can be used to reach the $A_5 = 0$ gauge. It is important to keep in mind that no new degree of freedom has been introduced in the theory. This is clear since the new scalars in U can be gauge fixed to zero by an appropriate gauge transformation on the IR boundary. The dependence of the IR action on U can be removed through a constant bulk gauge transformation $A \rightarrow A^{(U^\dagger)}$. As the bulk action is $SO(5)$ invariant, the effect is merely to move the dependence on U to the UV boundary conditions which become

$$A_\mu(x, 0) = a_\mu^{(U)}. \quad (3.47)$$

This rotation will affect all the fields in the theory according to their $SO(5)$ representations and determine how the Higgs boson enters the theory.

Localised terms consistent with the reduced gauge symmetry can be added on both boundaries. For the gauge fields we add kinetic terms for the holographic sources

$$S_{\text{UV}}^g = - \int d^4x \left[\frac{1}{4g_2^2} (W_{\mu\nu}^a)^2 - \frac{1}{4g_1^2} (B_{\mu\nu})^2 \right]. \quad (3.48)$$

Following Ref. [146] we obtain the effective action for the holographic degrees of freedom. We solve the classical equations of motion for the bulk fields with the boundary conditions specified in eq. (3.43) and we get

$$S_{\text{eff}}^g = S_{\text{UV}}^g - \int d^4x \left[\frac{1}{2g_5^2 L} \text{Tr}[A_\mu \partial_5 A^\mu] + \frac{1}{2g_X^2 L} A_\mu^X \partial_5 A^{X\mu} \right]. \quad (3.49)$$

The gauge fields can be split into their longitudinal and transverse parts $A_\mu = A_\mu^{(l)} + A_\mu^{(t)}$. It is easy to show that the solution of the equation of motion for the longitudinal part is

$$A^{\hat{a}(l)}(z) = A^{\hat{a}(l)}(0) \left(1 - \frac{z}{L}\right), \quad A^{a(l)}(z) = 0. \quad (3.50)$$

The $A_5 = 0$ gauge is reached by rotating the UV boundary values of the gauge fields as in eq. (3.47). The residual gauge freedom can be fixed by going to the Landau gauge $B_\mu^{(l)} = W_\mu^{a(l)} = 0$. Now the terms in eq. (3.49) corresponding to the longitudinal part of the broken $SO(5)/SO(4)$ gauge fields deliver the kinetic term for the Goldstone bosons

$$\mathcal{L}_{\text{kin}} = -\frac{1}{2g_5^2 L^2} \text{Tr}[(U^\dagger \partial_\mu U)^2]. \quad (3.51)$$

Chapter 3. The Minimal Composite Higgs Model

Matching its normalisation to eq. (3.6) implies the relation

$$f^2 = \frac{2}{L^2} \frac{1}{g_5^2}. \quad (3.52)$$

From the remaining part of eq. (3.49) one obtains the form factors appearing in eq. (3.12)

$$\begin{aligned} \Pi_0^X &= \frac{p^2}{g_1^2} - \frac{p^2}{g_2^2} + \frac{\Pi(p)_V}{g_X^2 L}, \\ \Pi_0 &= \frac{p^2}{g_2^2} + \frac{\Pi(p)_V}{g_5^2 L}, \\ \Pi_1 &= 2 \frac{\hat{\Pi}_V(p) - \Pi_V(p)}{g_5^2 L}, \end{aligned} \quad (3.53)$$

where $\Pi_V(p) = p \tan pL$ and $\hat{\Pi}_V(p) = -p \cot pL$. Using eqs. (3.12) and (3.53) we obtain for the gauge couplings

$$\frac{1}{g^2} = \frac{1}{g_2^2} + \frac{1}{g_5^2} \left(1 - \frac{\xi}{3}\right) \approx \frac{1}{g_2^2}, \quad \frac{1}{g'^2} = \frac{1}{g_1^2} + \frac{1}{g_X^2} + \frac{1}{g_5^2} \left(1 - \frac{\xi}{3}\right) \approx \frac{1}{g_1^2}, \quad (3.54)$$

which also imply $g_1 \approx g'$, $g_2 \approx g$ and therefore $g_1 = g_2 t_W$ with t_W the tangent of the weak mixing angle. The first zero of Π_{ab} in eq. (3.9) corresponds to the W mass. In the limit $g_2 \ll g_5$ this is given by

$$m_W^2 \approx \frac{1}{L^2} \frac{g_2^2 \xi}{2g_5^2}. \quad (3.55)$$

The masses of the Kaluza-Klein resonances can be obtained from the zeros of the form factors. The first KK partner of the W has a mass, before EWSB, given by

$$M_{KK} = \frac{\pi}{2L} + O\left(\frac{g_2^2}{Lg_5^2}\right). \quad (3.56)$$

Also the \hat{S} parameter is readily computed from eq. (3.9)

$$\hat{S} \equiv g^2 \Pi'_{30}(0) = \frac{\xi}{3(1 + g_5^2/g_2^2) - \xi} \approx \frac{g_2^2 \xi}{3g_5^2}. \quad (3.57)$$

One can interpret \hat{S} as originating from the tree level exchange of the massive KK vectors

$$\hat{S} \sim \frac{m_W^2}{M_{KK}^2}. \quad (3.58)$$

Notice the factor of π^2 mismatch between eqs. (3.57) and (3.58) when eq. (3.56) is used.

This is due to the sum over the whole KK tower ($M_{KK}^{(n)} \sim n\pi/L$) since $\sum 1/n^2 = \pi^2/6$.

Substituting the form factors in eqs. (3.12) and (3.53) into the potential of eq. (3.32) and assuming $g_2 \ll g_5$, $g_1 \ll g_X$ and $g_5 \approx g_X$ we can perform the integral explicitly to get

$$V_g(s_h) = -\frac{1}{L^4} \frac{63\zeta(3)}{256\pi^2} \left(1 + \frac{t_W^2}{3}\right) \frac{g_2^2}{g_5^2} c_h^2. \quad (3.59)$$

Notice that the gauge contribution to the potential gives a positive mass term for the Higgs and therefore does not break electroweak symmetry [152, 153].

Let us now discuss the role of the UV localised kinetic terms for the gauge fields in a flat extra dimension [151]. As shown in eq. (3.54), in the absence of these contributions the kinetic terms of the gauge bosons would come only from the strong sector $1/g^2 \approx 1/g_5^2$. In this case we would expect no difference between the electroweak bosons and the other vector resonances of the theory: this is exemplified by the value of \hat{S} which is of order one without UV localised kinetic terms. Such a scenario is clearly not viable. The inclusion of large kinetic terms on the UV boundary is required to ensure that the SM W and Z are sufficiently weakly coupled to the strong sector. The parameter g/g_5 can be understood as the degree of mixing between the elementary gauge fields and the composite resonances of the strong dynamics.

When the theory is formulated in AdS_5 space the suppression of the mixing between the elementary and the composite sector is guaranteed by the curvature of the metric without the necessity to add localised kinetic terms (see Appendix A.3). The reason for this is the presence of a warping which makes a clear distinction between the UV localised (elementary) and IR localised (composite) states: the small overlap of their wave functions automatically ensures a suppression of their mixing.

3.3.2 Fermionic degrees of freedom

We introduce two bulk Dirac fermions in $SO(5) \times U(1)_X$ representations: $\Psi_q = \mathbf{14}_{2/3} = \mathbf{1}_{2/3} \oplus \mathbf{4}_{2/3} \oplus \mathbf{9}_{2/3}$ and $\Psi_t = \mathbf{1}_{2/3}$. We work in the massless b quark limit. To properly account for the b quark mass two further multiplets embedding a q_L and a b_R with $X = -1/3$ have to be introduced with appropriate boundary conditions. There is some degree of arbitrariness in the definition of the boundary conditions for the various

Chapter 3. The Minimal Composite Higgs Model

fermionic components. Our choice is the following⁹

$$\Psi_t = (\psi_{tL}(-+) \quad \psi_{tR}(+-)) , \quad (3.60)$$

$$\Psi_q \supset \begin{cases} \psi_{qL}^{(1)}(-) & \psi_{qR}^{(1)}(+) \\ \psi_{qL}^{(4)} = \begin{pmatrix} q_L'(-+) \\ q_L(++) \end{pmatrix} & \psi_{qR}^{(4)} = \begin{pmatrix} q_R'(+-) \\ q_R(--) \end{pmatrix} \\ \psi_{qL}^{(9)}(-+) & \psi_{qR}^{(9)}(+-) \end{cases} \quad (3.61)$$

where we take the UV boundary values of the $T_R^3 = -1/2$ components of $\psi_{qL}^{(4)}$ and of ψ_{tR} as holographic fields. Notice that the boundary conditions on the IR brane commute with the unbroken $SO(4)$ symmetry. The two multiplets are assigned the bulk masses M_{Ψ_t} and M_{Ψ_q} respectively so that the bulk action is given by

$$S_{5D}^f = \int d^4x \int_0^L \frac{dz}{L} \text{Tr}[\bar{\Psi}_q (i\mathcal{D} + M_{\Psi_q}) \Psi_q] + \Psi_t (i\mathcal{D} + M_{\Psi_t}) \Psi_t , \quad (3.62)$$

where the factor $1/L$ has been introduced to ensure the dimensionality of the 5D fermions to be equivalent to the canonically normalised 4D fields. At this level the only zero modes are a left-handed $SU(2)_L$ doublet, q_L , and a right-handed $SU(2)_L$ singlet, $\psi_{qR}^{(1)}$, both coming from Ψ_q .

The IR boundary terms allowed by the unbroken $SO(4) \times U(1)_X$ symmetry at $x = L$ are given by the sum of four different kinetic terms for the four $SO(4)$ representations plus a mass mixing between the two $SO(4)$ singlets:

$$S_{\text{IR}}^f = \int d^4x \int_0^L dz \left[\left(k_1^t \bar{\psi}_{tL} i\mathcal{D} \psi_{tL} + k_1^q \bar{\psi}_{qR}^{(1)} i\mathcal{D} \psi_{qR}^{(1)} + k_4^q \bar{\psi}_{qL}^{(4)} i\mathcal{D} \psi_{qL}^{(4)} + k_9^q \bar{\psi}_{qL}^{(9)} i\mathcal{D} \psi_{qL}^{(9)} \right) + \left(m_{11} \bar{\psi}_{qR}^{(1)} \psi_{tL} + \text{h.c.} \right) \right] \delta(z - L) . \quad (3.63)$$

The parameter m_{11} has the dimension of a mass and controls the mixing between the right-handed component of the singlet inside Ψ_q and the left-handed component of Ψ_t . This mixing ensures that the holographic source for ψ_{tR} has a non vanishing Yukawa overlap with the right-handed zero mode living in Ψ_q . This is crucial because the top Yukawa coupling arises from the kinetic term of Ψ_q after EWSB.¹⁰ The parameters k_i are dimensionless

⁹For the decomposition of the $\mathbf{14}_{2/3}$ representation in terms of SM quantum numbers see Appendix A.3.2.

¹⁰Notice that we could have exchanged the boundary conditions of Ψ_t with those of $\psi_{qR}^{(1)}$ with little change in the physics. Another possibility could have been to dispose of the 5D singlet and to use the UV boundary value of $\psi_{qR}^{(1)}$ as the holographic field. In a model implemented in AdS_5 space this possibility requires both the t_L and the t_R to couple to the same operator in the strong sector thus implying $\lambda_L \sim \lambda_R \sim \sqrt{y_t g_\psi}$. This is problematic for two reasons: firstly it does not allow us to reach the limit in which the t_R is fully composite thus disfavouring a light Higgs boson; secondly it creates

and control the magnitude of the IR localised kinetic terms for the four different $SO(4)$ representations. Notice that k_1^t and the combination $k_1^q = k_4^q = k_9^q$ are $SO(5)$ invariants. To simplify the discussion and without losing any qualitative effect we set $k_1^t = k_1^q = 0$. Non vanishing values for k_4^q and k_9^q are thus needed to break $SO(5)$ on the IR boundary. Moreover a non vanishing difference $k_4^q - k_9^q$ is required to break an $SU(9+4) = SU(13)$ accidental global symmetry of the bulk theory under which the fields in the **9** and those in the **4** rotate as a single multiplet. In the absence of such a breaking the Π_1^q form factor would vanish: the only contribution to α in eq. (3.34) would then come from the gauge sector.

As discussed in the previous section for the gauge sector, realising partial compositeness in a flat extra dimension requires the introduction of UV localised kinetic terms. We introduce the UV boundary action

$$S_{\text{UV}}^f = \int d^4x \int_0^L dz \left[Z_q \bar{q}_L i \not{D} q_L + Z_t \bar{q}_R i \not{D} q_R \right] \delta(z), \quad (3.64)$$

which contributes to the form factors in eq. (3.30) as

$$\Delta \Pi_0^q = Z_q, \quad \Delta \Pi_0^t = Z_t. \quad (3.65)$$

Assuming $Z_q \gg 1$ implies a hierarchy $\tilde{\Pi}_0^q \gg \Pi_1^q, \Pi_2^q$ which is the one invoked in eq. (3.31) and above eq. (3.34).¹¹ All interactions of the elementary fields with the strong sector get suppressed by a factor $Z_{q,t}^{-1/2}$ which can be interpreted as the mixing $\epsilon_{L,R} \equiv \lambda_{L,R}/g_\psi$ between elementary and composite fields (see Introduction). In view of eq. (3.40), to obtain a composite top right ($\epsilon_R \approx 1$) we take $Z_t = 0$.¹²

3.3.3 The spectrum of fermionic resonances

In this paragraph we review how the spectrum of fermionic resonances is encoded in the holographic action for the boundary degrees of freedom. Using the holographic procedure one can obtain the effective Lagrangian in Fourier space for a fermionic bulk field Ψ

$$\bar{\Psi}(p) \not{p} \Pi(p) \Psi(-p). \quad (3.66)$$

a tension with EWPT, in particular with the \hat{T} parameter, which scales like $\hat{T} \sim \frac{g_\psi^2}{(4\pi)^2} \frac{\lambda_L^4}{g_\psi^4} \xi$. Although there is more freedom in flat space, we discard this possibility to make the comparison with AdS_5 more transparent.

¹¹In flat space we will use the notation $\tilde{\Pi}_0^q = Z_q + \Pi_0^q$, $\tilde{\Pi}_0^t = Z_t + \Pi_0^t$ as we do in Appendix A.3.2 to distinguish the form factors with and without the localised kinetic terms. Notice that $\tilde{\Pi}_0^q$ and $\tilde{\Pi}_0^q$ enter in the Coleman-Weinberg potential of eq. (3.33).

¹²Other UV and IR boundary terms are needed to ensure that the total variation of the 5D action vanishes [147]. These terms play a crucial role in the calculation of the 4D effective action and are listed in Appendix A.3.2.

Chapter 3. The Minimal Composite Higgs Model

The function $\Pi(p)$ contains all the information about the masses of the physical states in the theory. If the source Ψ is not dynamical (Dirichlet BC in the UV), holography relates $\not{p}\Pi(p)$ with the two-point function $\langle \bar{\mathcal{O}}_\Psi(p) \mathcal{O}_\Psi(-p) \rangle$ of the operator \mathcal{O}_Ψ associated to Ψ in the dual 4D picture. This implies that the masses of the physical states are associated with the poles of $\not{p}\Pi(p)$ (the poles in the two point functions of \mathcal{O}_Ψ). If on the other hand the source Ψ is dynamical, it mixes with the bound states interpolated by \mathcal{O}_Ψ and the masses of the physical states are given by the zeros of $\not{p}\Pi(p)$. In the following we will have to deal with cases where Ψ is a vector and Π a matrix. Here three possibilities occur. If all the sources in Ψ are non dynamical it is sufficient to consider the poles of any of the entries in $\not{p}\Pi(p)$ as all the states with the same quantum numbers in the strong sector are mixed. If all the sources are instead dynamical one has to find the zeros of the various eigenvalues of $\not{p}\Pi(p)$, that is the zeros of their determinant. Finally, in the intermediate situation in which only a subset of sources is dynamical, it is enough to find the zero eigenvalues of the sub-matrix corresponding to these fields.

For the model presented in this section, the resonance spectrum before EWSB consists of various towers labeled by their $SU(2)_L \times U(1)_Y$ quantum numbers:

- a $\mathbf{1}_{2/3}$ tower with masses given by the zeros of $\not{p}\tilde{\Pi}_0^t$;
- a $\mathbf{2}_{1/6}$ tower with masses given by the zeros of $\not{p}(\tilde{\Pi}_0^q + 2\Pi_1^q)$;
- a $\mathbf{2}_{7/6}$ tower with masses given by the poles of $\not{p}(\Pi_0^q + 2\Pi_1^q)$;
- a $\mathbf{9}_{2/3}$ tower under $SO(4)$, decomposing as $\mathbf{3}_{5/3} \oplus \mathbf{3}_{2/3} \oplus \mathbf{3}_{-1/3}$ under $SU(2)_L \times U(1)_Y$ with masses given by the poles of $\not{p}\Pi_0^q$.

After EWSB the physical states are organised according to their electric charge:

- a charge 2/3 tower with masses given by the zeroes of

$$p^2 \tilde{\Pi}_0^t \left(\tilde{\Pi}_0^q + \Pi_1^q (1 + c_h^2) + \Pi_2^q c_h^2 s_h^2 \right) - |M_1^t|^2 s_h^2 c_h^2,$$

where the first zero corresponds to the top quark mass;

- a charge -1/3 tower with masses given by the zeros of $\not{p}(\tilde{\Pi}_0^q + 2\Pi_1^q c_h^2)$, where the massless pole corresponds to the bottom quark;
- a charge 5/3 tower with masses given by the poles of $\not{p}(\Pi_0^q + 2\Pi_1^q c_h^2)$;
- charge 8/3 and -4/3 towers with masses given by the poles of $\not{p}\Pi_0^q$.

All the form factors appearing in these expressions are given in Appendix [A.3.2](#).

Before closing this section it is important to discuss a crucial feature of holographic

composite Higgs models, which pertains the relation between the two couplings g_ρ and g_ψ described in the Introduction. They can be defined schematically by their relation to the masses of bosonic and fermionic resonances of the theory: $m_\rho \equiv g_\rho f$ and $m_\psi \equiv g_\psi f$. While these two couplings can be split in generic 4D constructions [154–156], in a 5D theory the Kaluza-Klein masses are all set by a single mass scale, L^{-1} . For the coupling among vectors, using eq. (3.56) for the mass of the first KK state and eq. (3.52), one gets

$$g_\rho \equiv \frac{\pi}{2\sqrt{2}} g_5. \quad (3.67)$$

The fermionic spectrum and thus the coupling g_ψ are more model dependent. Considering a 5D bulk fermion with $M_\Psi = 0$ whose right-handed component has $(+, -)$ BC we find again

$$g_\psi \equiv \frac{\pi}{2\sqrt{2}} g_5. \quad (3.68)$$

Thus in general

$$g_\rho = g_\psi = g_5. \quad (3.69)$$

This has an important consequence in view of eq. (3.40) since g_ψ is now identified with g_ρ . Barring accidental cancellations in the quartic coupling of the Higgs and assuming the most favourable situation of a composite t_R ($\epsilon_R \sim 1$), g_ρ has to be small to accommodate the observed value of m_h . This generates a tension with the value of the \hat{S} parameter (see eq. (3.57))

$$\hat{S} \approx \xi \frac{g^2}{3g_\rho^2} \approx 10^{-3} \left(\frac{\xi}{0.1} \right) \left(\frac{4}{g_\rho} \right)^2. \quad (3.70)$$

We will come back to this issue in the next section.

3.4 Numerical analysis

In this section we present a numerical analysis of the model focusing on the Higgs potential and on the fermionic spectrum. We begin by discussing the parametric behaviour of the various observables we are interested in and later present our numerical procedure.

As we are mainly interested in the composite t_R case we first describe the ideal situation in which $Z_q \gg 1$ and $\tilde{\Pi}_0^q \approx Z_q$. The parameters of the 5D model can be related using the expressions for the weak coupling g , the W , top and Higgs masses. The Higgs potential has the following parametric behaviour

$$V(h) = \frac{1}{L^4} \frac{N_C}{(4\pi)^2 Z_q} V_h(\{p_i\}; \xi) + V_g(h), \quad (3.71)$$

Chapter 3. The Minimal Composite Higgs Model

where $V_g(h)$ is the gauge contribution given in eq. (3.59). p_i is the set of dimensionless parameters $M_q L$, $M_t L$, $m_{11} L$, k_1^t , k_1^q , k_4^q , k_9^q . If we can neglect V_g (that is if g_5 is sufficiently large) the value of ξ can be determined as soon as the p_i are fixed. In the limit $g_5 \gg g^{13}$ the W mass is given by eq. (3.55). The top mass can be read off eq. (3.31) and, in the large Z_q limit, can be written as

$$m_t^2 = \frac{1}{L^2} \frac{\xi}{Z_q} F_t(\{p_i\}), \quad (3.72)$$

where F_t is a dimensionless function of the various p_i . Our final input, the Higgs mass, follows from eq. (3.71)

$$m_h^2 = \frac{1}{L^2} \frac{N_C g_5^2}{(4\pi)^2} \frac{\xi}{Z_q} F_h(\{p_i\}). \quad (3.73)$$

For a given set of p_i it is then possible to fix g_5 , Z_q and L to reproduce the three input values m_W , m_t and m_h .

In order to include the effect of a non vanishing gauge potential and to allow for smaller values of Z_q we scan randomly and uniformly over the parameters p_i and over both g_5 and Z_q . For each point we evaluate ξ and compute the ratios m_t/m_W and m_h/m_W . We discard points which do not fall into the interval defined by

$$\begin{aligned} m_W &= 81 \text{ GeV}, \\ 148 \text{ GeV} \leq m_t &\leq 154 \text{ GeV}^{14}, \\ 120 \text{ GeV} \leq m_h &\leq 130 \text{ GeV}. \end{aligned} \quad (3.74)$$

We choose the following range for the parameters p_i

$$\begin{aligned} M_q L, M_t L &: (-2 \div 2), \\ m_{11} L &: (0.3 \div 2), \\ k_4^q, k_9^q &: (0 \div 2), \\ \sqrt{Z_q} &: (0 \div 10), \\ g_5 &: (1 \div 9). \end{aligned} \quad (3.75)$$

To simplify the scan we fix $k_1^t, k_1^q = 0$ since these parameters are not expected to modify the qualitative picture as we explained in section 3.3.2. We furthermore restrict m_{11} to positive values as it only enters through the combination $|m_{11}|^2$.

In order to conform to the general discussion at the end of section 3.2.2 it is necessary to understand the typical size of the coefficient a_2 defined in eq. (3.39). To do so we scan over the range defined by eq. (3.75) and calculate a_2 without imposing any additional

¹³These various relations hold with good accuracy as long as $g_5 \gtrsim 1.5$.

¹⁴The central value corresponds to the top quark mass renormalized at the scale $\mu = 1 \text{ TeV}$, $m_t = 150.7 \pm 3.4 \text{ GeV}$.

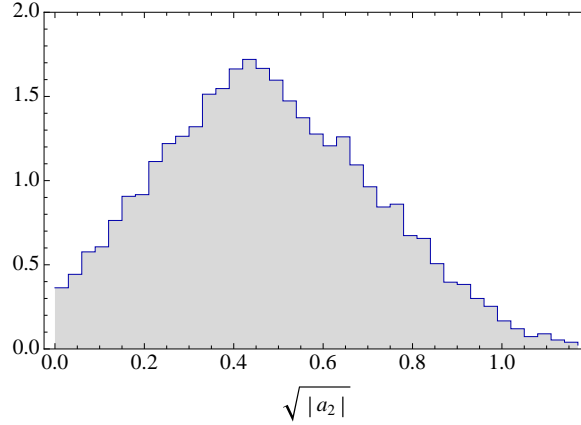


Figure 3.1 – Distribution of the values of $\sqrt{|a_2|}$ as defined in eq. (3.40). The parameter range is the one defined in eq. (3.75). We only keep points with negative a_2 .

requirement. This will give the correct normalisation of eq. (3.39) within our model. The results are shown in Fig. (3.1). We selected only points in which a_2 is negative (the distribution is basically symmetric around 0). The distribution is quite broad but clearly peaks around $\sqrt{|a_2|} \sim 0.4$.¹⁵ Thus, it is more appropriate to rewrite the NDA estimate of the Higgs mass in eq. (3.40) by factoring out the normalisation of a_2

$$m_h^2 \approx (150 \text{ GeV})^2 \frac{1}{\epsilon_R^2} \left(\frac{g_\psi}{4} \right)^2 |\tilde{a}_2|, \quad (3.76)$$

where now $\sqrt{|\tilde{a}_2|} \sim 1$. If the constraints that we impose on the parameter space to obtain the correct values for ξ and the top mass do not push a_2 to the right tail of its distribution, it is clear that the tension of the model with the \hat{S} parameter will be substantially relieved compared to the naive expectation.

3.4.1 Results

In the left panel of Fig. (3.2) we show the distribution of points passing the various cuts in eq. (3.74) as a function of g_ρ . The grey histogram includes all points for which $m_h < 400 \text{ GeV}$, while the red distribution requires m_h to fall inside the interval $120 \div 130 \text{ GeV}$. As expected from the scaling of m_h (see eqs. (3.40) and (3.76)), g_ρ cannot be too large and its distribution is peaked between 3 and 4. In the right panel of Fig. (3.2) we show the distribution of the parameter $\sqrt{|\tilde{a}_2|}$ as defined in eq. (3.76) and compare it with the one already shown in Fig. (3.1), taking into account the new normalisation of $|\tilde{a}_2|$. The scan thus selects values with $\tilde{a}_2 \sim 1$, that is in its natural range.

¹⁵ $|a_1|$ has a similar distribution. We have also checked the suppression in the potential does not correlate with the presence of anomalously light fermionic resonances in the spectrum [157]. This could happen if this suppression was due to the presence of light top partners cutting of the quadratic divergences of the Higgs potential at a lower scale.

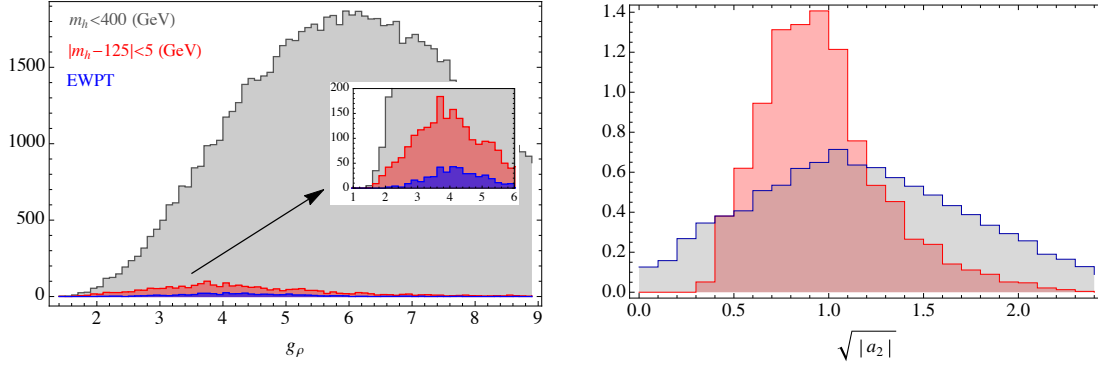


Figure 3.2 – Left panel: distribution of points coming from the scan with parameter ranges given by eq. (3.75) as a function of g_ρ . Grey: points with $115 \text{ GeV} < m_h < 400 \text{ GeV}$; red: points with $120 \text{ GeV} < m_h < 130 \text{ GeV}$; blue: points with $120 \text{ GeV} < m_h < 130 \text{ GeV}$ which are consistent with the electroweak fit at 99% C.L. assuming a 10^{-3} positive contribution to \hat{T} . Right panel: distribution of the values of $\sqrt{a_2}$ as defined in eq. (3.39) and eq. (3.76).

We estimate the tuning of the model as follows. Among all points in which the experimental inputs are reproduced, we pick those satisfying the experimental constraint from the EWPT. These points represent a fraction of the total, and this fraction is what we denote as the tuning of the model. This definition measures the size of the region in parameter space (according to the measure defined by eq. (3.75)) which is left after the various experimental constraints are imposed. In this way we automatically take into account that unnatural conspiracies among parameters, which are needed to satisfy the experimental constraints, occur rarely [158].

Our measure of the tuning differs from the one in Ref. [47] where the more common definition in terms of the logarithmic derivative of m_Z^2 with respect to the various parameters was used [159].¹⁶

Requiring the points satisfying eq. (3.74) to be consistent with the LEP electroweak fit at 99% C.L., we remain with the fractions shown in Table 3.1. In this subset, the value of ξ is always below 0.04, corresponding to $f > 1.2 \text{ TeV}$. Notice that the fraction of points remaining ($\sim 5\%$) is consistent with a measure of the tuning given just by ξ . This is the

¹⁶The relation between the two criteria is particularly transparent in Supersymmetry [160]. Here one can write a simple relation between the soft parameters at the scale at which they are generated and m_Z :

$$m_Z^2 = aM^2 + bm^2 - c|\mu|^2.$$

M and m are the common gaugino and scalar masses at the high scale and $a, b, c > 0$. The log-derivative tuning associated to M is given by $\Delta = aM^2/m_Z^2$. Notice that in the $(x \equiv \frac{M^2}{|\mu|^2}, y \equiv \frac{m^2}{|\mu|^2})$ plane this can be interpreted by saying that for a fixed lower bound on Δ_{exp} (implied for instance by an experimental lower bound M_{exp} on the gluino mass), the only allowed region of the (x, y) plane is the one bounded by the two lines $ax + by - c = 0$ (on which m_Z vanishes) and $ax + by - c = ax/\Delta_{\text{exp}}$. For $a \gtrsim b$ this slice covers a fraction of order $b/(a\Delta_{\text{exp}})$ of the whole plane. If we randomly scan the (x, y) plane fixing μ to reproduce the Z mass, a fraction $b/(a\Delta_{\text{exp}})$ of points will satisfy the experimental bound $M > M_{\text{exp}}$. This relates the criterion we adopt to the one using the local logarithmic derivative estimate.

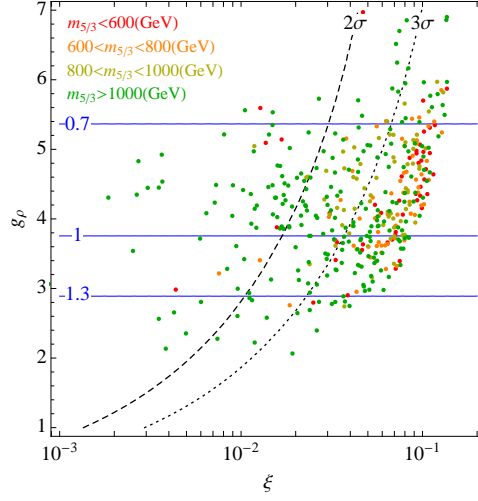


Figure 3.3 – Scatter plot in the (ξ, g_ρ) plane for those points that can be made consistent with the EWPT at 99% C.L. assuming a $\Delta\hat{T} = 10^{-3}$. The black lines are the 2σ and 3σ contours from the LEP EW fit. Blue lines indicate the suppression in $\sqrt{a_2}$ which is necessary to achieve $m_h = 125$ GeV according to the NDA estimate of the Higgs boson mass of eq. (3.76). The colour of the points indicates the mass of the lightest charge 5/3 top partner in the spectrum (see figure).

	EWPT	EWPT ($+\Delta\hat{T} = 10^{-3}$)
%	4.5 ± 0.4	18 ± 1

Table 3.1 – Fraction of points where the experimental inputs in eq. (3.74) are reproduced which are allowed at 99% C.L. by the EW fit as described in the text.

case because as discussed above we do not need any additional suppression in the Higgs quartic coupling in order to get a light Higgs mass and to cope with the constraints on the \hat{S} parameter.

Before moving on we notice that by artificially adding an additional positive contribution to $\hat{T} = 10^{-3}$ the fraction of allowed points grows from 5% to roughly 18% (see the blue histogram in the left panel of Fig. (3.2)). This contribution to \hat{T} , corresponding to one tenth of the top contribution in the SM, is an optimistic estimate of the corrections coming from loops of heavy top partners.¹⁷

Figure 3.3 shows the distribution of points in the (ξ, g_ρ) plane. We included all points that can be made consistent with EWPT at the 99% C.L. with the assumption of an additional contribution $\Delta\hat{T} = 10^{-3}$. Red and orange points have a spectrum which contains a charge 5/3 top partner which is lighter than 800 GeV. Any detailed study of the experimental status of these points is beyond the scope of this work, nevertheless we believe that they should be severely constrained by the available experimental searches

¹⁷These contributions are finite and computable in our model. See Ref. [42] for a discussion.

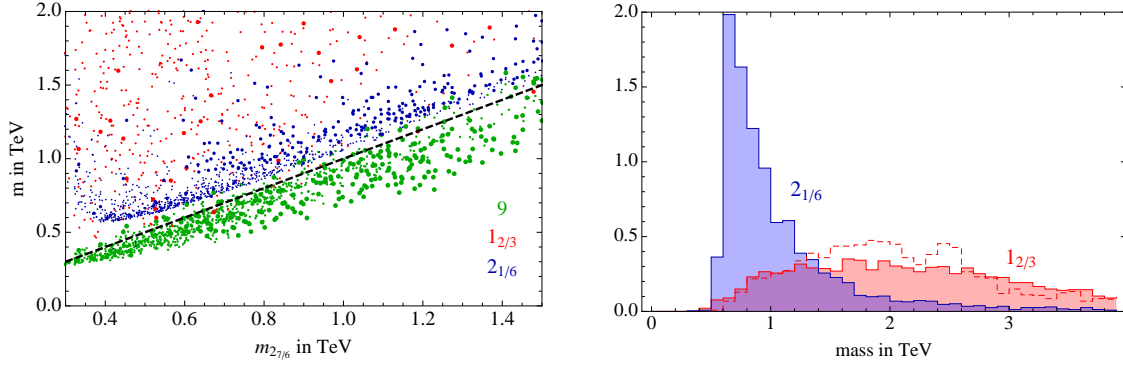


Figure 3.4 – Left panel: Distribution of fermionic resonance masses before EWSB according to their quantum numbers: $\mathbf{9}$ in green, $\mathbf{2}_{1/6}$ in blue and $\mathbf{1}_{2/3}$ in red. Thicker points are those passing the EWPT constraint. Right panel: mass distributions for the $\mathbf{2}_{1/6}$ (blue) and $\mathbf{1}_{2/3}$ (red) $SO(4)$ representations without considering EWPT. The red dashed histograms is the expected mass distribution from the NDA scaling $m_\psi = g_\rho f$.

[161, 162]. The blue contours show the necessary suppression in $\sqrt{a_2}$ according to the NDA estimate of the Higgs boson mass. Fig. (3.3) is puzzling. If we believe the NDA formula $m_\psi \sim g_\rho f$ we should expect a much heavier spectrum than what we find in Fig. 3.3, as $g_\rho = 4$ and $\xi = 0.1$ give $m_\psi = 3$ TeV!

The solution of this puzzle is shown in Fig. (3.4). In the left panel we show the fermionic spectrum before EWSB of all points that reproduce the experimental inputs (thicker dots are for points also satisfying EWPT). A definite hierarchy $m_{\mathbf{9}} < m_{\mathbf{2}_{7/6}} < m_{\mathbf{2}_{1/6}} \ll m_{\mathbf{1}_{2/3}}$ emerges from the figure. In the right panel of the same figure we compare the mass distribution of the $SO(4)$ representations $\mathbf{1}_{2/3}$ (shaded red) and $\mathbf{2}_{1/6}$ (shaded blue) before requiring EWPT. The red-dashed histogram shows the distribution of masses obtained from the NDA estimate $m_\psi \sim g_\rho f$. It is clear that, while the singlet matches reasonably well with the expectations, the other three $SO(4)$ representations are much lighter.

To understand this behaviour it is necessary to inspect how the top mass is obtained in terms of the model parameters. Using the approximation in eq. (3.31) and the form factors in eqs. (A.36), one finds that for large positive M_{Ψ_q} the top mass is exponentially suppressed, while for $M_{\Psi_q} < 0$

$$\frac{m_t^2}{m_W^2} = \frac{g_5^2}{g_2^2} \frac{5|M_{\Psi_q}L|}{Z_q + e^{2|M_{\Psi_q}L|}k_9^q}. \quad (3.77)$$

Reproducing the correct m_t/m_W ratio thus fixes $M_{\Psi_q} \lesssim -1$. Next, in the limit of large Z_q and vanishing Z_t, k_4^q, k_9^q , the KK masses of the $\mathbf{9}$, $\mathbf{2}_{7/6}$ and $\mathbf{2}_{1/6}$ towers are all given by the zeros of $M_{\Psi_q} + \omega_q \cot \omega_q L$ while those of the $\mathbf{1}_{2/3}$ tower are given by the zeros of $M_{\Psi_t} + \omega_t \cot \omega_t L$. The approximate expression for the first KK mode mass can be

written as

$$\begin{aligned} p &\sim 2|M_{\Psi_i}|e^{-|M_{\Psi_i}|L}, & M_{\Psi_i}L &\lesssim 0, \\ \sqrt{\frac{\pi^2}{4L^2} + M_{\Psi_i}^2} < p < \sqrt{\frac{\pi^2}{L^2} + M_{\Psi_i}^2}, & M_{\Psi_i}L &\gtrsim 0. \end{aligned} \quad (3.78)$$

We see that since M_{Ψ_q} should be large and negative to reproduce the correct top mass (see eq. (3.77)) we expect the masses of the first resonances in the **9**, **2**_{7/6}, **2**_{1/6} towers to be parametrically (exponentially) suppressed with respect to the mass of the first KK mode in the **1**_{2/3} tower, whose corresponding bulk mass M_{Ψ_t} is unconstrained.

We now explain the smaller splittings giving $m_{\mathbf{9}} < m_{\mathbf{2}_{7/6}} < m_{\mathbf{2}_{1/6}}$. First of all, the splitting between the **9** and the **2**_{7/6} is proportional to the difference $(k_4^q - k_9^q)$. Expanding the relevant form factors around the point $k_4^q - k_9^q = 0$ explicitly shows that $m_{\mathbf{9}} - m_{\mathbf{2}_{7/6}}$ is positive when $k_4^q - k_9^q$ is positive. Next we rewrite the Higgs potential in eq. (3.34) separating the fermionic and gauge contributions to α and β :

$$V(h) = (-\alpha_f - \alpha_g + \beta_f)s_h^2 - \beta_f s_h^4. \quad (3.79)$$

The coefficient α_g is negative, β_f is always negative in the region we consider, while α_f can have both signs depending on $k_4 - k_9$. A viable electroweak symmetry breaking requires the coefficient of the s_h^2 term to be negative. The Higgs mass input needs a small g_5 which enhances the electroweak symmetry preserving gauge contribution. As the size of β is basically fixed by the top and Higgs mass measurements, EWSB typically requires an extra positive contribution to α (see the minus sign in eq. (3.79)), favouring $k_4 < k_9$ and thus $m_{\mathbf{9}} < m_{\mathbf{2}_{7/6}}$.

The mass difference between the **2**_{7/6} and the **2**_{1/6} towers is due to the different UV boundary conditions for these fields. The zeros of $\tilde{\Pi}_0^q$ give the masses of the **2**_{1/6} while the poles of Π_0^q give the masses of the **2**_{7/6}. It is clear that in the large Z_q limit the masses will coincide. In particular, from the explicit form of $\tilde{\Pi}_0^q$ for $k_9^q = 0$ (see Appendix A.3.2),

$$\tilde{\Pi}_0^q = Z_q + \frac{1}{M_{\Psi_q}L + \omega_q L \cot \omega_q L}, \quad (3.80)$$

it follows that the states in the **2**_{7/6} are always heavier than those in the **2**_{1/6}. A summary of the mass distributions of the fermionic resonances before (red) and after (blue) requiring the electroweak fit at 99% C.L. (with an additional positive contribution $\Delta T = 10^{-3}$) is given in Figure 3.5. We show the distributions for the different $SO(4)$ representations **1**_{2/3} (top left), **9** (top right), **2**_{1/6} (bottom left) and **2**_{7/6} (bottom right).

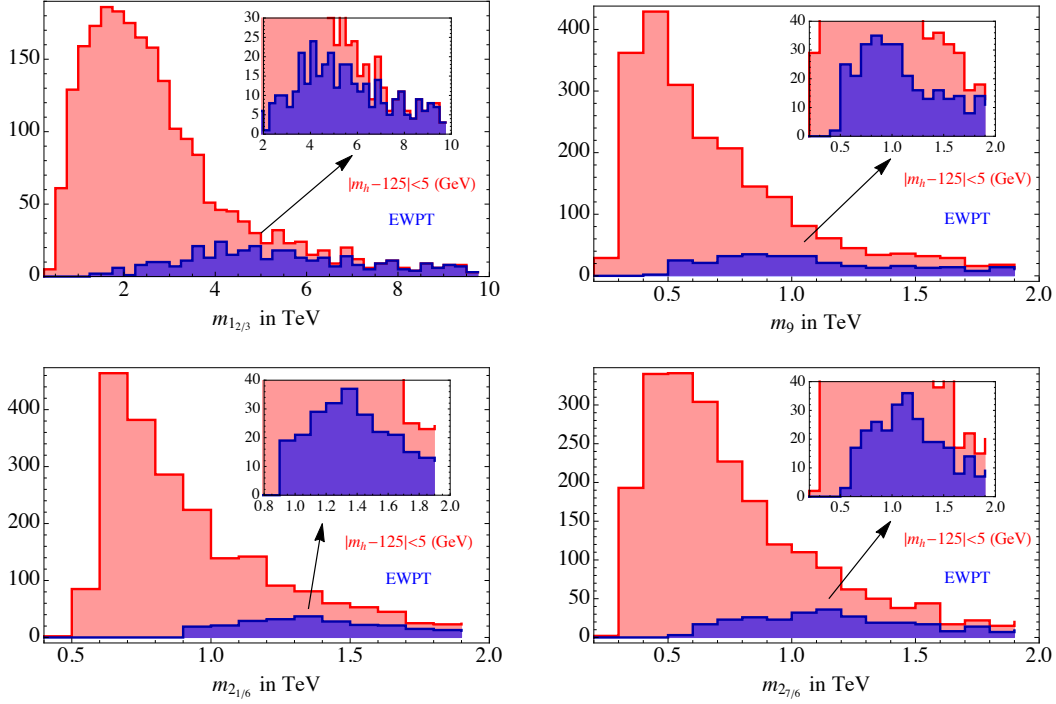


Figure 3.5 – Mass distributions of the $\mathbf{1}_{2/3}$ (top left), $\mathbf{9}$ (top right), $\mathbf{2}_{1/6}$ (bottom left) and $\mathbf{2}_{7/6}$ (bottom right) obtained from the scan with parameter ranges given by eq. (3.75). Red: points with $120 \text{ GeV} < m_h < 130 \text{ GeV}$; blue: points with $120 \text{ GeV} < m_h < 130 \text{ GeV}$ which are consistent with the electroweak fit at 99% C.L. assuming a 10^{-3} positive contribution to \hat{T} .

3.5 Conclusions

The main challenge of composite Higgs models to naturally describe electroweak symmetry breaking are the constraints coming from precision electroweak physics. The tension of these theories with electroweak precision tests is the one of old fashioned Technicolor models and is due to the unavoidable existence of heavy spin-1 states mixing with the SM gauge bosons. This mixing corrects the \hat{S} parameter by an amount

$$\Delta\hat{S} \sim \frac{m_W^2}{m_\rho^2}, \quad (3.81)$$

requiring $m_\rho \gtrsim 2.6 \text{ TeV}$.

The masses of the spin-1 resonances $m_\rho \sim g_\rho f$ are controlled by two parameters, their coupling g_ρ and the decay constant f determining the non-linear interactions of the composite Higgs. As we described in the text, pushing f to large values implies an upper bound on the tuning of the model of order $\xi \equiv v^2/f^2$. Before Higgs discovery, electroweak physics was pointing towards a strongly coupled theory, $g_\rho \sim 4\pi$, and $\xi \lesssim 0.1$ was needed to regulate the infrared contributions of the composite Higgs to electroweak observables.

The measurement of the Higgs boson mass, $m_h \approx 125$ GeV, adds extra information to this picture. The generic expectation of the Higgs boson mass in composite Higgs models can be given in terms of the mass of the fermionic resonances which regulate the UV divergence of the Higgs potential:

$$m_h \sim 125 \text{ GeV} \left(\frac{m_\psi}{1.0 \text{ TeV}} \right) \sqrt{\frac{\xi}{0.1}} \sqrt{\tilde{a}_2}. \quad (3.82)$$

The parameter a_2 is naturally expected to be of order 1. In order not to worsen the tuning of the model it is thus important to have light enough fermionic top partners.

In this section we presented the 5D implementation of a specific class of composite Higgs models with a (pseudo-)Goldstone boson Higgs from the $SO(5)/SO(4)$ coset. Our starting point is the observation, already present in Refs. [47, 48], that in order for ξ to be a good measure of fine tuning and not to underestimate it, the Higgs potential must be the sum of at least two independent periodic functions of the Higgs field h which are generated at the same order in the elementary-composite mixing expansion. This fact constrains the fermionic content of the model. The simplest way to satisfy this requirement is to couple the left-handed top quark to a symmetric representation of $SO(5)$, a **14**, and the right-handed top quark to an $SO(5)$ singlet.

Models in 5D are expected to be more constrained and to face a more severe fine tuning problem with respect to more general composite Higgs models. The reason for this are eqs. (3.81) and (3.82) and the fact that the masses of the fermionic and bosonic resonances are predicted to be parametrically the same, fixed by the size L of the extra dimension. This implies that, once $m_\psi \sim m_\rho$ is fixed to comply with the bound on \hat{S} , an additional suppression of either ξ or a_2 is needed to obtain the right Higgs mass.

We discussed these issues in our model finding that the NDA estimate in eq. (3.82) may be too pessimistic. In our model this occurs because of an additional, fortuitous, overall suppression of the estimate in eq. (3.82) by a factor $\sim 0.4 \div 0.5$. The existence of such a suppression implies a somewhat heavier spectrum of the top partners can be obtained without worsening the fine tuning. Our model is somewhat peculiar in this respect because the requirement of a heavy enough top implies that some of the $SU(2)_L$ representations, into which the **14** decomposes, have to be anomalously light. The existence of light, exotic charged, top-partners is probably the most important prediction of the class of composite Higgs models we have been discussing. Their experimental search is to be considered one of the most important avenues to either verify or falsify the composite Higgs idea.

A thorough discussion of the phenomenology of the fermionic sector of our model is presented in more detail in sections 6.3. Here we would just like to point out that in our model, and in all constructions where the Higgs is a PGB from $SO(5)/SO(4)$, the fermionic resonances fill degenerate $SO(4)$ multiplets before EWSB and in the

Chapter 3. The Minimal Composite Higgs Model

absence of elementary-composite mixing. In our model the lightest among these $SO(4)$ representations is a **9** which decomposes under $SU(2)_L \times U(1)_Y$ as $\mathbf{3}_{5/3} \oplus \mathbf{3}_{2/3} \oplus \mathbf{3}_{-1/3}$. This $SO(4)$ multiplet contains, in particular, two charge 5/3 and a charge 8/3 quarks.

Finally, as in every composite Higgs model, the Higgs couplings to SM gauge bosons and fermions are modified. From this point of view our model is indistinguishable from other known composite Higgs models as the one described in [42]. Deviations from the SM are controlled by a single parameter, ξ . Bounds on ξ coming from Higgs coupling measurements are currently mild, requiring $\xi < 0.3 \div 0.4$ [163].

4 Indirect Probes of NP at the LHC

4.1 Introduction

After the discovery of a Higgs-like scalar particle, an important program has been launched to measure the Higgs couplings to known elementary particles of the Standard Model (SM). The goal is not so much to determine a few further unknown parameters of the SM but to understand the underlying structures of the laws of physics at high energy: if the SM were to be valid up to the scale of quantum gravity, the couplings of the Higgs boson would be uniquely fixed in terms of other already known and well-measured quantities. On the contrary, any deviation in these couplings, for instance of the order of 20%, would unambiguously signal new physics at a scale below 5 TeV.

The study of the LHC sensitivity on the Higgs couplings has been initiated in Refs. [164–167]. Upon the first and still incomplete measurements reported by both ATLAS and CMS as well as by the Tevatron experiments, a simple methodology inspired by a chiral effective Lagrangian approach has been developed in Refs. [168–170] in order to quantify to which extent the Higgs boson is really fulfilling the role it has been devoted to in the SM, namely the screening of scattering amplitudes involving massive bosons and fermions at high energy.

At the LHC, the main production channel of the Higgs boson as well as its cleanest decay mode proceed through purely quantum mechanical processes and rely on couplings to massless gluons and photons that are vanishing in the Born approximation. This results in an ambiguity in the value of the tree-level Higgs couplings since the coupling likelihood function exhibits several and almost degenerate minima (see e.g. Refs. [167, 169, 170]). Indeed, the degeneracy can be found in the current combined data of the 7 and 8 TeV run in Refs. [9, 171]. As was emphasised [170, 172] the degeneracies remained even after the whole 8 TeV dataset was analysed. Measuring processes involving real top quarks in the final state will bring invaluable information. With the largest rate, the Higgs production in association with a top pair is a golden channel and has received great attention by the

experimental [173, 174] as well as theoretical [175–179] communities.

In this chapter we argue that, even though subleading, Higgs boson production in association with a single top quark can also bring valuable information, in particular regarding the *sign* of the top Yukawa coupling.¹ This is because an almost totally destructive interference between two large contributions, one where the Higgs couples to a space-like W boson and the other where it couples to the top quark, takes place in the SM. This fact can be exploited to probe deviations in the Higgs coupling structure, which will inevitably jeopardise perturbative unitarity at high energy and lead to a striking enhancement of the cross section compared to the SM. We discuss how this enhancement can be used to extract information on the sign of the top Yukawa coupling and we show that th production can be used to lift the degeneracy plaguing the Higgs coupling fit of the LHC data. While a moderate integrated luminosity at 14 TeV should allow us to make a conclusive statement, we point out that already with the full 2012 luminosity, corresponding to $\sim 25 \text{ fb}^{-1}$ per experiment, an interesting sensitivity on the sign of the top Yukawa could be reached.

In our study we focus on the decay of the Higgs into $b\bar{b}$, updating the early analysis of Ref. [180] (see also Refs. [181, 182]). This choice leads to an experimental signature (lepton + missing energy + multijets, among which ≥ 3 are b -jets) which is very similar to the one ATLAS and CMS have already analysed in their searches for $t\bar{t}h$ production [173, 174]. In this respect we believe that the experimental collaborations could easily perform the analysis we propose here in the very near future, thus adding new important information to the challenge of identifying the true nature of the recently discovered particle. Single top production in association with a Higgs boson has also been studied in Refs. [183, 184] focussing on the $h \rightarrow \gamma\gamma$, $h \rightarrow WW^*$ and $h \rightarrow \tau\tau$ decay channels.

The large enhancement of the th cross section for nonstandard Higgs couplings is associated to the growth of the scattering amplitude at high energy, which in turn implies that perturbative unitarity is lost at some UV scale Λ . We estimate Λ , which acts as the cutoff of our effective theory, to be at least of $\mathcal{O}(10)$ TeV and thus above the energy scales that the LHC will be able to probe. In fact, the th invariant mass distribution in LHC collisions essentially vanishes above 1 TeV, therefore we can safely conclude that our analysis remains insensitive to UV physics above the cutoff scale.

This chapter is structured as follows: we start by introducing the general features of the th process and discussing its implications, including an estimate of the scale where perturbative unitarity is lost, in section 4.2. We proceed in section 4.3 to the analysis of the signal and of the main backgrounds at the LHC, performing a parton-level simulation. In section 4.4, we discuss the implications on the determination of the Higgs parameters. Finally, we conclude in section 5.6. Unless otherwise specified, the Higgs mass is assumed

¹The sign of the top Yukawa coupling is not physical by itself, but the relative sign compared to the Higgs coupling to gauge bosons (we take the latter to be positive) is physical.

4.2. Single top and Higgs associated production

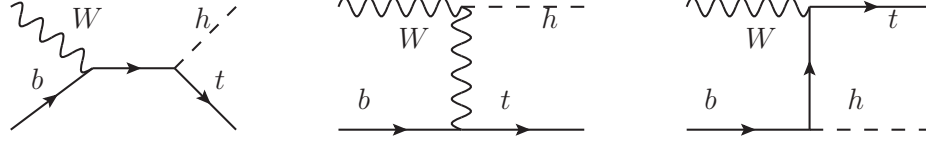


Figure 4.1 – Feynman diagrams contributing to the partonic process $Wb \rightarrow th$.

to be $m_h = 125 \text{ GeV}$ throughout this work. For the top mass we take $m_t = 173 \text{ GeV}$. Finally, the shorthand th is always understood to include also the charge-conjugated case where t is replaced by \bar{t} . Therefore all our cross sections include both t and \bar{t} production.

4.2 Single top and Higgs associated production

The Feynman diagrams contributing to the core process $Wb \rightarrow th$ are shown in Fig. 4.1. The diagram where the Higgs is emitted from a b leg is suppressed by the bottom Yukawa, and will be consistently neglected in our study. In the th production process at the LHC the initial W is radiated from a quark in the proton, and is thus spacelike. However, at high energy the effective W approximation [185, 186] holds, which allows us to factorize the process into the emission of an approximately on-shell W from the quark times its hard scattering with a bottom. Thus it makes sense to discuss the amplitude for $Wb \rightarrow th$ at high energies assuming the initial W to be on-shell, in order to gain an approximate understanding of the full picture.

In the high-energy, hard-scattering regime, where $s, -t, -u \gg m_t^2, m_W^2, m_h^2$, the amplitude for $W_L b \rightarrow th$ (the longitudinal polarisation dominates at large s) reads²

$$\begin{aligned} \mathcal{A} = & \frac{g}{\sqrt{2}} \left[(c_F - c_V) \frac{m_t \sqrt{s}}{m_W v} A\left(\frac{t}{s}, \varphi; \xi_t, \xi_b\right) \right. \\ & \left. + \left(c_V \frac{2m_W s}{v} \frac{1}{t} + (2c_F - c_V) \frac{m_t^2}{m_W v} \right) B\left(\frac{t}{s}, \varphi; \xi_t, \xi_b\right) \right], \end{aligned} \quad (4.1)$$

where we have omitted terms that vanish in the high-energy limit and, for simplicity, also neglected the Higgs mass in addition to setting $m_b = 0$. The generalised couplings of the Higgs are defined as $c_V \equiv g_{hWW}/g_{hWW}^{SM}$ and $c_F \equiv g_{ht\bar{t}}/g_{ht\bar{t}}^{SM}$. The functions A, B are

²We take final momenta outgoing, and define $s = (p_W + p_b)^2$, $t = (p_W - p_h)^2$. φ is the azimuthal angle around the z axis, which is taken parallel to the direction of motion of the incoming W .

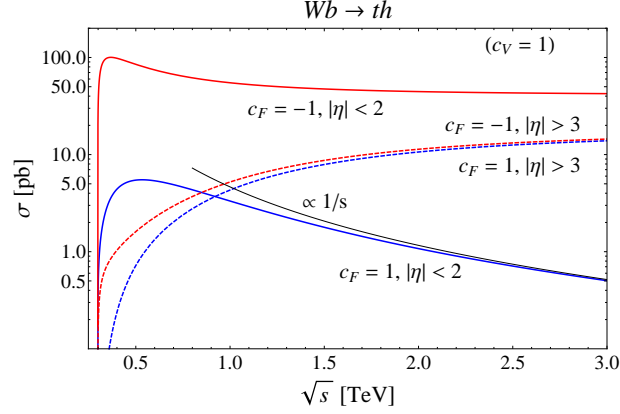


Figure 4.2 – Partonic cross sections for the process $Wb \rightarrow th$ as a function of the center of mass energy \sqrt{s} . The parameter c_V is set to 1. The hard scattering cross section is defined by a cut $|\eta| < 2$: the large enhancement obtained for $c_F = -c_V$ with respect to the SM case is evident. The forward cross section, defined by a cut $|\eta| > 3$, is also shown (dashed curves).

given by

$$A(t/s, \varphi; \xi_t, \xi_b) = \xi_t^\dagger \begin{pmatrix} -t/s & 0 \\ -e^{i\varphi} \sqrt{-\frac{t}{s}(1+\frac{t}{s})} & 0 \end{pmatrix} \xi_b \longrightarrow \begin{pmatrix} 0 & 0 \\ -e^{i\varphi} \sqrt{-t/s} & 0 \end{pmatrix}, \quad (4.2)$$

$$B(t/s, \varphi; \xi_t, \xi_b) = \xi_t^\dagger \begin{pmatrix} 1+t/s & 0 \\ e^{i\varphi} \sqrt{-\frac{t}{s}(1+\frac{t}{s})} & 0 \end{pmatrix} \xi_b \longrightarrow \begin{pmatrix} e^{i\varphi} \sqrt{1+t/s} & 0 \\ 0 & 0 \end{pmatrix}, \quad (4.3)$$

where in the rightmost term of each line we have chosen a specific basis for the spinors, namely

$$\xi_b^L = \begin{pmatrix} 1 \\ 0 \end{pmatrix}, \quad \xi_b^R = \begin{pmatrix} 0 \\ 1 \end{pmatrix}; \quad \xi_t^L = \begin{pmatrix} e^{-i\varphi} \sqrt{1+t/s} \\ \sqrt{-t/s} \end{pmatrix}, \quad \xi_t^R = \begin{pmatrix} -e^{-i\varphi} \sqrt{-t/s} \\ \sqrt{1+t/s} \end{pmatrix}, \quad (4.4)$$

which correspond to the chiral states $\{F_L, F_R\}$ ($F = b, t$) in the $m_F \rightarrow 0$ limit³. The amplitudes involving the helicity state ξ_b^R , which is identified with a right-handed bottom since we are assuming $m_b = 0$, exactly vanish due to the $V - A$ structure of the couplings of the W to fermions. From eq. (4.1) we see that when $c_V \neq c_F$ the amplitude grows with energy like \sqrt{s} and is enhanced compared to the case $c_V = c_F$ (which includes the SM), where the amplitude is constant in the large s limit. The non-cancellation of the terms in the amplitude growing with energy is at the origin of the striking enhancement of the cross section when $c_V \neq c_F$.

³However, note that the limit $m_t \rightarrow 0$ does not interest us here.

4.2. Single top and Higgs associated production

The cross section for $Wb \rightarrow th$ is shown as a function of the center of mass energy in Fig. 4.2. The large enhancement of the hard scattering cross section (defined by a centrality cut $|\eta| < 2$) for $c_F = -c_V$ is evident.⁴ At large energies, the amplitude is constant for $c_V = c_F$ and thus the cross section vanishes as $\sim 1/s$. On the other hand, when $c_F \neq c_V$ the amplitude grows with energy like \sqrt{s} and as a consequence the cross section tends to a constant for large s . It is easy to compute this asymptotic value of the cross section: squaring the leading term of the amplitude in eq. (4.1), summing and averaging over polarisations and integrating over t we find

$$\sigma(|\eta| < \tilde{\eta}, s \rightarrow \infty) \simeq \frac{g^2(c_F - c_V)^2 m_t^2}{384\pi m_W^2 v^2} \tanh \tilde{\eta}. \quad (4.5)$$

This simple formula gives accurate results: for example for $\sqrt{s} = 5$ TeV, $c_V = -c_F = 1$ and a centrality cut⁵ $|\eta| < 2$ we find that the cross section computed without any approximations is $\sigma_{\text{full}}(|\eta| < 2) = 41.3$ pb, whereas $\sigma(|\eta| < 2, s \rightarrow \infty) = 40.7$ pb.

Since for $c_V \neq c_F$ the hard scattering amplitude grows with energy, perturbative unitarity will be lost at some cutoff scale Λ , which we now estimate. In the spinor basis of eq. (4.4), only one s -wave amplitude is non-vanishing

$$a_0 = \frac{1}{16\pi\sqrt{2}\sqrt{s}}(c_F - c_V) \frac{gm_t}{m_W v} \int_{-s}^0 A(t/s, \varphi; \xi_t^R, \xi_b^L) = -\frac{1}{24\sqrt{2}\pi}(c_F - c_V) \frac{gm_t\sqrt{s}}{m_W v} e^{i\varphi} \quad (4.6)$$

from which, imposing the condition $|a_0| < 1$, we find that perturbative unitarity is violated at a scale $\sqrt{s} \simeq \Lambda$ with

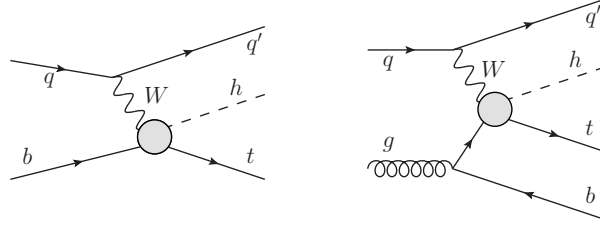
$$\Lambda = 12\sqrt{2}\pi \frac{v^2}{m_t |c_F - c_V|}. \quad (4.7)$$

For example, for $c_V = -c_F = 1$ the cutoff is $\Lambda \simeq 9.3$ TeV. One may worry about other processes involving top quarks, in which perturbative unitarity could be lost at a scale lower than the one in eq. (4.7) for $c_F < 0$. A relevant and often mentioned process is $W_L^+ W_L^- \rightarrow t\bar{t}$, for which we find $\Lambda = 16\pi v^2/(m_t |1 - c_V c_F|)$. For $c_V = -c_F = 1$ this formula yields 8.8 TeV, essentially the same cutoff scale we found for $W_L b \rightarrow th$. For previous discussions of perturbative unitarity breakdown in processes with external fermions, see Refs. [187, 188].

Having analysed the behaviour of the partonic cross section, we can now turn our attention

⁴Incidentally, we note that the cross section shows another feature, a Coulomb enhancement at small $|t|$ due to the diagram with a W exchange in the t -channel. As can be read off Fig. 4.2 the forward cross section tends to a constant limit for large s , which can be computed in a simple way in terms of the parameter c_V alone and is insensitive to the value of c_F . A short discussion of the forward cross section is contained in Appendix B.1.

⁵Note that for the expression in eq. (4.5) to be reliable, $\tilde{\eta}$ cannot be too large. In fact, as already mentioned, in the forward region the cross section has a Coulomb enhancement which is not captured by the approximations we made here. See also Appendix B.1.


 Figure 4.3 – Feynman diagrams for the processes $pp \rightarrow thj$ and $pp \rightarrow thjb$.

	$\sigma^{\text{LO}}(pp \rightarrow thj)$ [fb]		$\sigma^{\text{LO}}(pp \rightarrow thjb)$ [fb]	
	$c_F = 1$	$c_F = -1$	$c_F = 1$	$c_F = -1$
8 TeV	17.4	252.7	5.4	79.2
14 TeV	80.4	1042	26.9	363.5

 Table 4.1 – Leading-order cross sections for the processes $pp \rightarrow thj$ and $pp \rightarrow thjb$ (with $p_T^b > 25$ GeV and $|\eta^b| < 2.5$) at the LHC. The parameter c_V has been set to 1.

to single top and Higgs associated production in hadron collisions. At the LHC, t -channel single top production goes through an initial-state gluon splitting into a $b\bar{b}$ pair. Such a process can be efficiently described by a 5-flavor scheme where b 's are in the initial state and described by a perturbative b PDF, Fig. 4.3(a). In this scheme, the non-collinearly enhanced contribution, where the spectator b (i.e. the one not struck by the W boson) is central and at high p_T (see Fig. 4.3(b)), is moved to the next-to-leading order term. This contribution, which we indicate with $pp \rightarrow thjb$, is finite and can be easily calculated at tree-level, contributing to a final state signature with an extra b -jet, a useful handle to suppress the background. In Table 4.1 we present the rates for th production in the 5-flavor scheme, fully inclusive as well as with the requirement of the extra b to be in the tagging region, for 8 and 14 TeV, in the $c_V = 1, c_F \pm 1$ cases. Our analysis in section 4.3 will consider both processes, which lead to final states containing 3 and 4 b -jets respectively, once the decay of the Higgs to $b\bar{b}$ is taken into account. The cross sections in Table 4.1 were computed using MADGRAPH 5[189] with CTEQ6L1 PDFs [190], setting the factorisation and renormalization scales to the default event-by-event MADGRAPH 5 value. As an estimate of the theoretical uncertainty on the signal, we have computed the fully inclusive cross sections at NLO in QCD, in the 5-flavor scheme, using AMC@NLO [191–193] and CTEQ6M PDFs [190]. The results are reported in Table 4.2, where the uncertainties correspond to variations of the factorisation and renormalization scales with $\mu_F = \mu_R$ around $\mu = (m_t + m_h)/2$ from $\mu/2$ to 2μ . The NLO cross sections appear to be extremely stable under radiative corrections and therefore we deem the theory uncertainty of the signal rates in our analysis negligible.

The striking enhancement of the hadronic cross section for $c_F \neq c_V$ is shown in Fig. 4.4, where $\sigma(pp \rightarrow thj)$ for an LHC energy of 14 TeV, normalised to its SM value, is displayed as a function of c_F for three different choices of c_V (very similar plots are obtained

4.2. Single top and Higgs associated production

	$\sigma^{\text{NLO}}(pp \rightarrow thj) \text{ [fb]}$	
	$c_F = 1$	$c_F = -1$
8 TeV	$18.28^{+0.42}_{-0.38}$	$233.8^{+4.6}_{-0.}$
14 TeV	$88.2^{+1.7}_{-0.}$	982^{+28}_{-0}

Table 4.2 – Cross sections at NLO in QCD for the process $pp \rightarrow thj$ at the LHC. The parameter c_V has been set to 1.

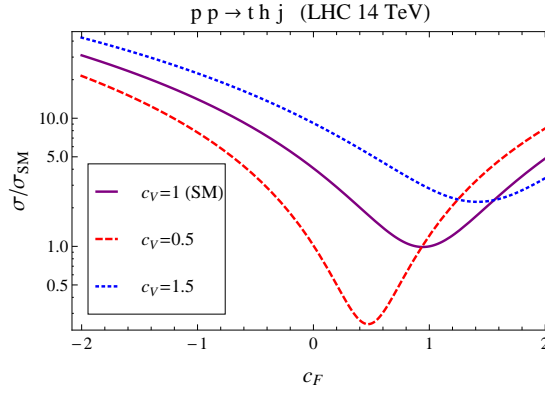


Figure 4.4 – Cross section for $pp \rightarrow thj$ at 14 TeV normalised to the SM one, as a function of c_F for three choices of c_V . Solid, dashed and dotted lines correspond to $c_V = 1, 0.5$ and 1.5 respectively.

considering 8 TeV and/or the $pp \rightarrow thjb$ process). For example, for a standard hWW coupling, i.e. $c_V = 1$, a top Yukawa with equal magnitude and opposite sign with respect to the standard one ($c_F = -1$) yields an enhancement of the cross section of more than a factor 10.

As noted above, perturbative unitarity in $Wb \rightarrow th$ scattering is lost at a scale $\Lambda \gtrsim 10$ TeV for $c_V, c_F \sim \mathcal{O}(1)$. Figure 4.5 clearly shows that after convolution with the PDFs the contribution of the region $\sqrt{\hat{s}} \gtrsim 1$ TeV, where $\sqrt{\hat{s}}$ is the center of mass energy of the th system, to the hadronic cross section is negligible. This implies that our perturbative computations can be fully trusted. Indeed Fig. 4.5 demonstrates that the relative contribution to the cross section from large values of $\sqrt{\hat{s}}$ is more sizeable in the SM than for $c_F \neq c_V$. This is compatible with the different behaviours of the partonic cross section in the two cases, shown in Fig. 4.2.

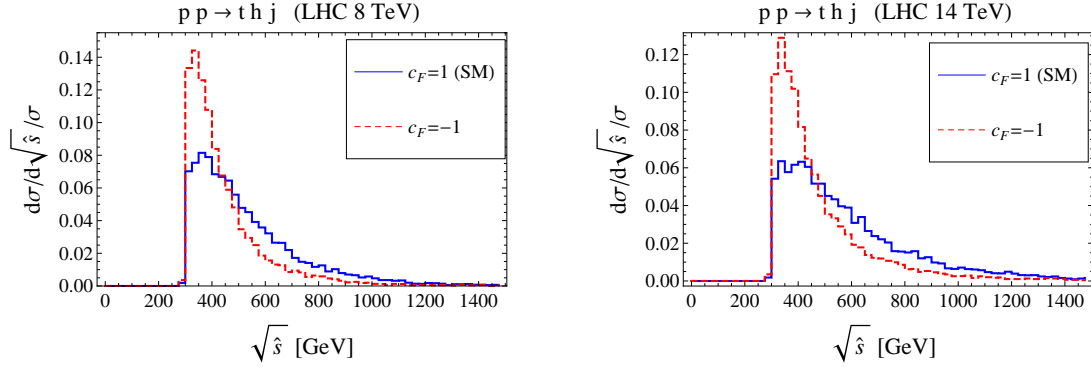


Figure 4.5 – Histograms of normalised $pp \rightarrow thj$ cross section as a function of the center of mass energy of the hard scattering process $Wb \rightarrow th$. The left panel is for 8 TeV, the right one for 14 TeV.

4.3 Signal and background study

4.3.1 Parton-level simulation

Signal and background events have been generated at the parton level using MADGRAPH 5 with CTEQ6L1 PDFs, setting the factorisation and renormalization scales to the default event-by-event MADGRAPH 5 value. Jets are defined at the parton level. In order to take showering, hadronization, detector and reconstruction effects minimally into account, we smear the p_T of the jets uniformly in η using a jet energy resolution defined by

$$\frac{\sigma(p_T)}{p_T} = \frac{a}{p_T} \oplus \frac{b}{\sqrt{p_T}} \oplus c, \quad (4.8)$$

where the parameters are taken to be $a = 2$, $b = 0.7$ and $c = 0.06$. With these choices, eq. (4.8) is compatible with the results of the ATLAS jet energy resolution study of Ref. [194] (see Fig. 9 there). The jet 4-momentum is then rescaled by a factor p_T^{smear}/p_T . The acceptance cuts reported in Table 4.3, chosen following the ATLAS $t\bar{t}h$ analysis [173], are applied on the physical objects. We do not require any acceptance cut on the missing transverse energy.

Cut	$p_T^b >$	$p_T^\ell >$	$p_T^j >$	$ \eta^{b,\ell} <$	$ \eta^j <$	$\Delta R_{ij} >$
Value	25 GeV	25 GeV	30 GeV	2.5	5	0.4

Table 4.3 – Acceptance cuts applied to the signal and backgrounds at the reconstructed level. The ΔR requirement applies to all objects.

An object is considered to be missed if it does not pass one of the acceptance cuts. If, in particular, two jets are collinear with $\Delta R < 0.4$ we merge them by summing their

4-momenta and we consider them as a single jet when applying further cuts.⁶ Additionally we require the lepton to be isolated from any jet in the event, including those that do not pass acceptance cuts and therefore are missed.

In all the signal and background processes we consider in this section, a semileptonically decaying top is present. We assume a 100% efficiency for the reconstruction of this top, which implies an unambiguous identification of the b originating from its decay. This assumption is of course idealised, however the use of a more realistic semileptonic top reconstruction efficiency will only affect the overall normalisation of both signal and background, and not their relative values.

Concerning b -tagging, we assume the following performance: efficiency $\epsilon_b = 0.7$, charm mistag probability $\epsilon_c = 0.2$ and light jet mistag probability $\epsilon_j \approx 0.008$ [173]. Finally we assume a lepton reconstruction efficiency $\epsilon_\ell = 0.9$.

4.3.2 Final state with 3 b -tags

We start by discussing the 3 b -jet final state, which arises from $pp \rightarrow thj$ after selecting the Higgs decay into $b\bar{b}$. Requiring the top to decay semileptonically ($t \rightarrow b\ell^+\nu$) gives the signature

$$3b + 1 \text{ forward jet} + \ell^\pm + E_T^{\text{miss}}. \quad (4.9)$$

We can now turn our attention to the most relevant backgrounds:⁷

- tZj , $Z \rightarrow b\bar{b}$: an irreducible background where a Z boson mimics the Higgs in decaying to $b\bar{b}$.
- $t\bar{t}b\bar{b}j$: an irreducible QCD background.
- $t\bar{t}$, $\bar{t} \rightarrow \bar{b}\bar{c}s$: a reducible background where either the c or s are mis-tagged.
- $t\bar{t}j$, $\bar{t} \rightarrow \bar{b}\bar{c}s$: also in this case, either the c or s are mis-tagged while the other is missed.

As can be seen in Table 4.4 for 8 TeV and in Table 4.5 for 14 TeV, after acceptance cuts and efficiencies the last two backgrounds are extremely large. In particular, their values are larger than those quoted in Ref. [180], mainly due to a larger charm mistag rate considered here (we use $\epsilon_c = 0.2$, whereas Ref. [180] adopted $\epsilon_c = 0.1$) and to the fact that we increased the p_T threshold for jets, which results in a larger probability of missing a

⁶The exception to this procedure is the case where the b coming from a semileptonic top decay is collinear to another jet. Since we are assuming ideal semileptonic top reconstruction (see below), we simply reject the event in this case.

⁷For the sake of readability we do not write the top decay $t \rightarrow b\ell^+\nu$ explicitly, as it is the same for all processes.

Cuts	Signal		Backgrounds				
	$c_F = 1$	$c_F = -1$	Total	tZj	$t\bar{b}\bar{b}j$	$t\bar{t}$	$t\bar{t}j$
Acceptance Cuts + ϵ	0.18	2.88	600.81	0.61	1.01	456.40	142.80
$ m_{bb} - m_h < 15 \text{ GeV}$	0.15	2.55	245.95	0.02	0.11	184.2	61.65
$m_{bbj} > 270 \text{ GeV}$	0.10	2.02	31.78	0.01	0.08	0.	30.68
$ \eta^j > 1.7$	0.08	1.70	17.98	0.01	0.06	0.	17.24
Events at 25 fb^{-1}	1.9	42.5	449.4				

Table 4.4 – Cross sections in fb for the 3 b -tag case at 8 TeV. In the event line backgrounds are summed.

jet from $t\bar{t}j$. The dominance of backgrounds where a c is mistagged suggests that it may be sensible to prefer a b -tagging performance with smaller efficiency but higher rejection against charm. However, for definiteness we stick to the numbers reported in section 4.3.1, taken from Ref. [173].

After acceptance cuts and efficiencies, the signal is overwhelmed by the $t\bar{t}$ background not only for the standard case $c_F = 1$, but even considering the enhanced case $c_F = -1$ (we set $c_V = 1$). Thus, we require a set of additional cuts in order to isolate the signal. These cuts are listed in Tables 4.4-4.5, together with the cross sections obtained after their application. The value of each cut is chosen by optimising the Poisson exclusion limit in the $c_F = -1$ case. We remark that since we are assuming ideal top reconstruction, the b coming from the semileptonic top is always assumed to be unambiguously identified, therefore no cut on it is applied beyond the detector ones, neither for the signal nor for the backgrounds.

The first cut we apply requires the $b\bar{b}$ pair to have an invariant mass around m_h , which of course helps to eliminate the tZj background. The second cut selects large values for the bbj invariant mass and is effective against the reducible backgrounds, in particular it suppresses enormously $t\bar{t}$, where the jet and 2 b 's are decay products of a top and therefore we expect their invariant mass to be close to m_t . The last cut singles out a forward jet, which is a distinctive feature of the signal. However, after all cuts the background cross section, completely dominated by $t\bar{t}j$, is still one order of magnitude larger than the signal for $c_F = -1$.

In the last line of Tables 4.4 and 4.5, we present the number of signal and total background events expected after 25 fb^{-1} of integrated luminosity. At 8 TeV, the Poisson exclusion is at 97.4% CL or 2.2σ (by abuse of notation, we are expressing the probability in terms of number of σ 's, e.g. 2σ approximately corresponds to the 95% CL), while at 14 TeV it reaches $\sim 4\sigma$.

4.3. Signal and background study

	Signal		Backgrounds				
Cuts	$c_F = 1$	$c_F = -1$	Total	tZj	$t\bar{b}\bar{b}j$	$t\bar{t}$	$t\bar{t}j$
Acceptance Cuts + ϵ	0.71	11.55	2448.18	2.29	3.72	1773.35	668.83
$ m_{bb} - m_h < 15 \text{ GeV}$	0.63	10.23	1020.4	0.07	0.38	737.23	282.76
$m_{bbj} > 280 \text{ GeV}$	0.46	8.59	153.10	0.05	0.31	0.	152.74
$ \eta^j > 2$	0.34	7.12	79.26	0.03	0.24	0.	79.00
Events at 25 fb^{-1}	8.4	178.0	1981.5				

Table 4.5 – Cross sections in fb for the 3 b -tag case at 14 TeV. In the event line backgrounds are summed.

4.3.3 Final state with 4 b -tags

As suggested in Ref. [180], a way to enhance the sensitivity on the th signal is to require an extra b , coming from the splitting of an initial gluon: the process of interest is thus $pp \rightarrow thjb$. Requiring a semileptonic top and the decay $h \rightarrow b\bar{b}$ leads to the signature

$$4b + 1 \text{ forward jet} + \ell^\pm + E_T^{\text{miss}}. \quad (4.10)$$

Here the main backgrounds are:

- $tZ\bar{b}j$, $Z \rightarrow b\bar{b}$: an irreducible background where the Z mimics the Higgs.
- $t\bar{b}\bar{b}j$: similarly to the 3 b case, an irreducible QCD background.
- $t\bar{t}\bar{b}\bar{b}$, $\bar{t} \rightarrow \bar{b}jj$: a reducible background where one of the two jets, originating from a hadronically decaying W , is missed.
- $t\bar{t}\bar{b}\bar{b}$, $\bar{t} \rightarrow \bar{b}\bar{c}s$ (one mistag): here the c or the s is mis-tagged, while either the other one is missed (and one b is not tagged) or one of the b 's is missed.
- $t\bar{t}j$, $\bar{t} \rightarrow \bar{b}\bar{c}s$ (two mistags): in this case both c and s are mistagged.

Looking at Tables 4.6 and 4.7, we see that requiring 4 b -jets allows us to obtain a much larger signal to background ratio after acceptance cuts compared to the 3 b case. On the other hand, the overall rates are obviously smaller. Analogously to what was done in the 3 b case, a set of additional cuts are imposed to enhance the signal. The cuts are listed in Tables 4.6-4.7, together with the cross sections obtained after their application. The value of each cut is again chosen by optimising the Poisson exclusion limit in the $c_F = -1$ case.

The first cut requires the invariant mass of one of the 3 $b\bar{b}$ pairs (we recall that ideal reconstruction of the semileptonic top is assumed) to be inside a window around m_h . This helps again to eliminate the $tZ\bar{b}j$ background. The second cut demands all $b\bar{b}$ invariant masses to be higher than about 100 GeV, and is most effective on $t\bar{t}j$, where the

Chapter 4. Indirect Probes of NP at the LHC

Cuts	Signal		Backgrounds					
	$c_F = 1$	$c_F = -1$	Total	$tZ\bar{b}j$	$t\bar{b}b\bar{b}j$	$t\bar{t}b\bar{b}$	$t\bar{t}b\bar{b} \text{ (mis)}$	$t\bar{t}j$
Acceptance Cuts + ϵ	0.043	0.63	7.81	0.11	0.26	2.66 (0.48)	2.25	2.54
$ m_{bb} - m_h < 15 \text{ GeV}$	0.039	0.58	4.06	0.03	0.08	0.94 (0.40)	1.29	1.71
min $m_{bb} > 110 \text{ GeV}$	0.023	0.30	0.67	0.002	0.015	0.20 (0.18)	0.44	0.
min $m_{bj} > 180 \text{ GeV}$	0.008	0.15	0.014	0.	0.007	0.002 (0.001)	0.004	0.
Events at 25 fb^{-1}	0.2	3.8	0.4					

Table 4.6 – Cross sections in fb for the 4 b -tag case at 8 TeV. In the event line backgrounds are summed. For $t\bar{t}b\bar{b}$, the contribution of $t\bar{t}h$ is shown in parentheses.

Cuts	Signal		Backgrounds					
	$c_F = 1$	$c_F = -1$	Total	$tZ\bar{b}j$	$t\bar{b}b\bar{b}j$	$t\bar{t}b\bar{b}$	$t\bar{t}b\bar{b} \text{ (mis)}$	$t\bar{t}j$
Acceptance Cuts + ϵ	0.19	2.85	39.14	0.46	1.07	14.40 (1.94)	11.53	11.69
$ m_{bb} - m_h < 15 \text{ GeV}$	0.17	2.61	19.78	0.12	0.32	4.88 (1.63)	6.52	7.93
min $m_{bb} > 90 \text{ GeV}$	0.13	1.82	5.97	0.05	0.09	1.68 (1.04)	3.54	0.61
min $m_{bj} > 170 \text{ GeV}$	0.07	1.20	0.35	0.02	0.06	0.03 (0.03)	0.05	0.19
Events at 25 fb^{-1}	1.7	30.1	8.7					

Table 4.7 – Cross sections in fb for the 4 b -tag case at 14 TeV. In the event line backgrounds are summed. For $t\bar{t}b\bar{b}$, the contribution of $t\bar{t}h$ is shown in parentheses.

mis-tagged c and s , coming from a W decay, have an invariant mass around m_W . The last cut requires all 3 bj pairs to have a large invariant mass. This efficiently suppresses the $t\bar{t}b\bar{b}$ backgrounds, for which in most cases at least one bj pair comes from a top decay and thus has an invariant mass $m_{bj} \lesssim \sqrt{m_t^2 - m_W^2} \sim 150 \text{ GeV}$.

The exclusion limits obtained for $c_F = -1$, assuming 25 fb^{-1} of data, are 2.4σ and $\sim 6\sigma$ at 8 and 14 TeV respectively. The sensitivity at 8 TeV is comparable to the one obtained in the 3 b case, while at 14 TeV requiring an extra b -jet improves the result significantly.

Before discussing the implications of our results, we wish to comment here on the sensitivity of the proposed analysis to the $t\bar{t}h$ process. As can be read from Tables 4.6 and 4.7, this process makes up a sizeable fraction of the $t\bar{t}b\bar{b}$ cross section after the cuts. Moreover, after the first three cuts, the rate for $t\bar{t}h$ is comparable to the th signal for $c_F = -1$. Being insensitive to the sign of the top Yukawa, $t\bar{t}h$ can be considered as a background process in our analysis. It is, however, quite useful to observe that the simple search strategy we propose in the 4 b channel would be sensitive to both single and pair top production in association with a Higgs boson. In this respect, a key role is played by the cut on m_{bj} that was designed to suppress processes with a $t\bar{t}$ pair in the final state, as discussed above. The relative contribution of $t\bar{t}h$ to the $t\bar{t}b\bar{b}$ background with one mistag, on the other hand, is small, approximately 5%.

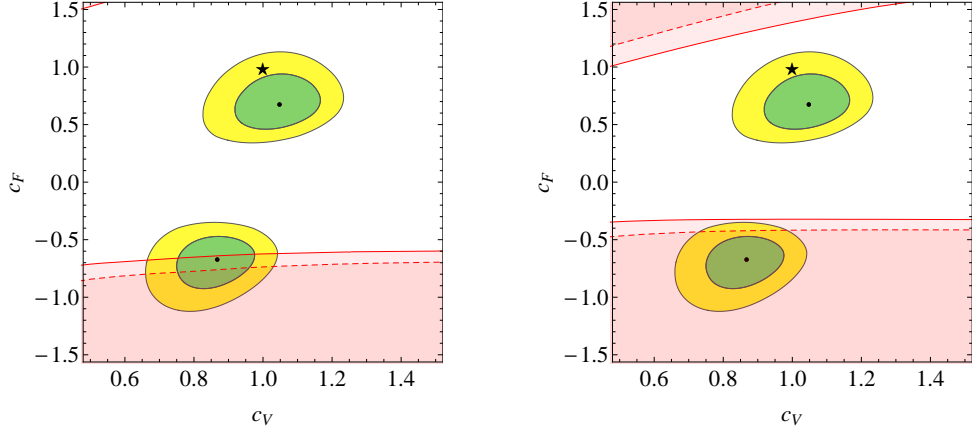


Figure 4.6 – Regions of the (c_V, c_F) plane excluded at 95% CL by our analysis of $th \rightarrow hbb$ (3 and 4 b final states combined), at 8 TeV (left) and 14 TeV (right), assuming an integrated luminosity of 25 fb^{-1} and 50 fb^{-1} (dashed and solid respectively). The 68% and 95% CL contours of a fit to current Higgs data are also shown, in green and yellow respectively. A universal rescaling by c_F of the Higgs coupling to fermions is assumed. The Higgs coupling fit is based on the data reported by ATLAS, CMS and Tevatron after ICHEP 2012 and collected in Ref. [195].

4.4 Implications on Higgs couplings

We are now able to study the implications of our results on the general parameter space of Higgs couplings. To do so we combine the two analyses that we discussed in section 4.3, i.e. 3 and 4 b -tags, to exploit the full LHC sensitivity in $th \rightarrow tb\bar{b}$ production. Note that in the combination we consider the $3b$ and $4b$ samples as independent. While this is an approximation (which can be easily lifted in a more realistic analysis by defining fully exclusive samples), in practice it has a small effect as the $4b$ sample is significantly smaller than the $3b$ one. In Fig. 4.6 we present the results of our analysis in the (c_V, c_F) plane, where a universal rescaling of the Higgs couplings to fermions $c_t = c_b = c_\tau = c_c = c_F$ is assumed. The regions that can be excluded (at 95% CL) by th production with an integrated luminosity of 25 and 50 fb^{-1} are presented, along with the regions currently favoured by a fit to Higgs data. As can be seen, already at 8 TeV parts of the preferred region with $c_F < 0$ can be excluded. The current best fit point with $c_F < 0$ is excluded at 2.1σ with 50 fb^{-1} . On the other hand, a moderate luminosity at 14 TeV can conclusively remove the degeneracy between the two regions that are at the present time preferred by Higgs data, for example reaching a 5.8σ exclusion of the best fit point with $c_F < 0$ after 50 fb^{-1} . Notice that in addition to the th production cross section (recall Fig. 4.4), also the branching ratio of the Higgs into $b\bar{b}$ depends on the parameters (c_V, c_F) .

It is also possible to relax the assumption of universal couplings of the Higgs to fermions and consider the case where only the htt coupling c_t has a rescaled value compared to the

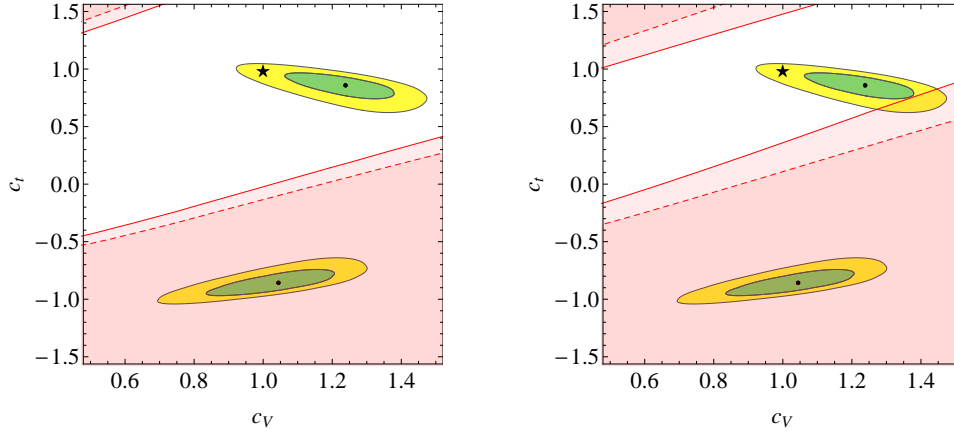


Figure 4.7 – Regions of the (c_V, c_t) plane excluded at 95% CL by our analysis of $th \rightarrow hb\bar{b}$ (3 and 4 b final states combined), at 8 TeV (left) and 14 TeV (right), assuming an integrated luminosity of 25 fb^{-1} and 50 fb^{-1} (dashed and solid respectively). The 68% and 95% CL contours of a fit to current Higgs data are also shown, in green and yellow respectively. The top Yukawa is assumed to be rescaled by c_t , while we have set $c_b = c_\tau = c_c = 1$. The Higgs coupling fit is based on the data reported by ATLAS, CMS and Tevatron after ICHEP 2012 and collected in Ref. [195].

SM while $c_b = c_\tau = c_c = 1$, so in particular $\Gamma(h \rightarrow b\bar{b})$ is equal to its SM value. In this case, the $th \rightarrow tb\bar{b}$ rate is essentially fixed by the dependence on c_V, c_t of the production cross section (a mild sensitivity to c_V, c_t through the Higgs total width is also present). The results are shown in the (c_V, c_t) plane in Fig. 4.7. Excluded regions at 95% C.L. are displayed for 25 fb^{-1} and 50 fb^{-1} integrated luminosity. Superimposed are the regions currently favoured by Higgs data. The most striking feature is, that the best fit region with $c_t < 0$ can already be completely excluded at 8 TeV with 25 fb^{-1} (reaching a 4.0σ exclusion of the best fit point with negative c_t).

4.5 Conclusions

After the time of discovery comes the need for measurements. The couplings of the putative Higgs boson are of prime importance since they control the behaviour of the whole theory at high energy. The dominant processes involving the Higgs boson that are currently investigated at the LHC do not allow us to determine all its couplings unambiguously. An important task now is therefore to systematically identify additional processes that could complement the first LHC information and lift degeneracies appearing in Higgs coupling fits.

In this chapter, we studied single top production in association with a Higgs boson, focusing on the Higgs decay into $b\bar{b}$. We discussed the form of the amplitude of the hard scattering process $Wb \rightarrow th$, showing that for nonstandard couplings of the Higgs to the

W boson and/or to the top quark a striking enhancement of the cross section can be obtained. The enhancement is due to the non-cancellation of terms that grow with energy in the amplitude and lead to violation of perturbative unitarity at some UV scale. We estimate the new physics scale to be at most 10 TeV, concluding that corrections to our computation of the cross section from physics above the cutoff are always negligible.

We have performed a parton-level study of the LHC signal processes $pp \rightarrow thj$ and $pp \rightarrow thjb$, and of the corresponding irreducible and some of the most relevant reducible backgrounds. The combination of the two final states, containing 3 and 4 b -jets respectively, shows that if a universal rescaling c_F of the fermion couplings is assumed, already at 8 TeV parts of the preferred region with $c_F < 0$ can be excluded. On the other hand, a moderate luminosity of 50 fb^{-1} at 14 TeV can conclusively remove the degeneracy between the two regions that are at the present time preferred by Higgs data, reaching a 5.8σ exclusion of the best fit point with negative c_F . In addition, we investigated the case where only the $ht\bar{t}$ coupling differs from its SM value while the other Yukawa couplings are standard. Here, the best fit region with negative top Yukawa coupling can be completely excluded at 8 TeV with 25 fb^{-1} , reaching a 4.0σ exclusion of the best fit point with $c_t < 0$.

Our results, along with similar studies [183, 184], have already motivated the experiments to investigate single top and Higgs associated production in the $H \rightarrow \gamma\gamma$ channel. CMS quotes to be sensitive to 4.1 times the expected cross section for $c_F = -1$ at 95% C.L. [196], while ATLAS [197] reports the 95% C.L. intervals of c_F to be $[-1.3, 7.9]$. As expected from our analysis, the 8 TeV dataset is not yet conclusive. Experimental analyses in $H \rightarrow \bar{b}b$ are currently underway. Besides the experimental analyses, our results also motivate an improvement in the accuracy of the theoretical predictions. It would be certainly interesting to evaluate the (possibly significant) impact of NLO QCD corrections to signal and irreducible backgrounds, i.e., thj and tZj , a task that can now be accomplished in a fully automatic way [177, 191, 192, 198].

Further information on the Higgs couplings to heavy quarks could also come from other processes at the LHC. One example is double Higgs production, $gg \rightarrow hh$. This process proceeds through a triangle and a box diagram, which, again, interfere destructively in the SM and therefore result in a sensitive probe of the Higgs-heavy quarks interactions, see, e.g., Refs. [199–201]. Finally we remark that complementary information could a priori also come from the observation of $B_s \rightarrow \mu^+\mu^-$ recently reported by LHCb [202]. The measured value of $\text{BR}(B_s \rightarrow \mu^+\mu^-)$ agrees well with the SM prediction [203]. The SM contribution is actually dominated by the interactions associated to the top Yukawa coupling and therefore this measurement could be naively expected to provide a good probe of any deviation of the top Yukawa itself. However, only the Yukawa interactions between the Goldstone bosons and the quarks contribute to this process. What we have proposed to probe via th production is rather the interaction of the physical Higgs boson with the top quark, i.e. the one controlled by the parameter c_t . Actually, if the deviations from $c_t = 1$ originate from pure Higgs non-linearities as in composite Higgs models, for

instance via a higher dimensional operator like $|H|^2 \bar{Q}_L H^\dagger t_R$, then it is easy to see that the prediction for $\text{BR}(B_s \rightarrow \mu^+ \mu^-)$ remains unaffected.

5 Indirect Probes of NP at Future Colliders

5.1 Introduction

With the discovery of the Higgs boson [12, 13] and with the absence, thus far, of any clear evidence for New Physics, a basic feature of the dynamics underlying electroweak symmetry breaking has begun to materialise: the new states associated with that dynamics do not seem to be as light as naturalness considerations would have recommended. That this might be the case has been suggested for quite some time by considerations based on precision electroweak and flavor data, but the LHC results have made this picture more concrete. Of course, we may just sit at the edge of New Physics and evidence may plentifully show up in the next run of the LHC. However, once a bit of un-naturalness is accepted, it is *natural* to expect, or fear, that history may repeat itself at 13 TeV. For instance, keeping the composite Higgs scenario in mind [33–39], a plausible situation is one where, at the end of its program, the LHC will have only measured inconclusive $O(10\%)$ deviations from the Standard Model in the Higgs couplings. In a definitely more optimistic situation these small deviations would appear along with some new states, but without a clear indication for their role in the EWSB dynamics. Under the above circumstances, the next experimental project would be more one of exploration and discovery than one of refinement and consolidation. With this in mind, a high-energy hadron machine like the LHC at $\sqrt{s} = 33$ TeV [204–206] would superficially seem better suited than a cleaner but less powerful leptonic machine like the ILC [50] or CLIC [51, 207, 208]. However, given the criticality of the decisions we may face in the coming years, it is important to carefully assess the potential of each machine in each plausible NP scenario. It is the goal of this chapter to provide one such assessment: by focussing on a high-energy lepton machine such as CLIC, we shall explore its potential in the exploration of the composite Higgs scenario.

Single Higgs production at a linear collider, even at 500 GeV, is known to be a very sensitive probe of compositeness [209], even though an indirect one. In the case where resonances are still out of reach, a more direct probe on compositeness is offered by the study of the

interactions of longitudinally polarised electroweak vector bosons and the Higgs. The relevant processes are $VV \rightarrow VV$ and $VV \rightarrow hh$ ($V = W, Z$), whose cross sections grow like E^2 . There exist several studies of $VV \rightarrow VV$ at hadron machines [64, 210–219] but just a few of $VV \rightarrow hh$ [64, 80]. The study of these processes in hadron collisions is not an easy task. $VV \rightarrow VV$ offers final states with leptons that stand out well against the QCD background. However, the genuine SM contribution to $VV \rightarrow VV$ happens to be numerically so large that the effects of compositeness dominate only at very high energy, where LHC parton luminosities are small [64]. The result is a poor reach on the scale of compositeness. In the case of $VV \rightarrow hh$ the genuine SM contribution is numerically small, so that in principle this would be a good probe of compositeness. However the final states and branching ratios of Higgs decay are not favourable in a hadronic environment. The reach on compositeness from this process at the LHC is thus also not very good. Instead, as we will show in this chapter, a machine like CLIC offers the right combination of a clean environment and center-of-mass energy to significantly probe the composite Higgs scenario. The improvement compared to hadron machines is particularly stark for $VV \rightarrow hh$. Our main result is that $VV \rightarrow hh$ at CLIC offers about half the reach on the scale of compositeness as single Higgs production at a 500 GeV ILC. However the observation of a cross section for hh production that grows with energy would be a more direct and convincing evidence of the strongly coupled nature of NP. It also turns out that in the presence of a signal in $VV \rightarrow hh$ one may in principle be able to make more refined statements about the nature of h . First of all, via a comparison with single h processes, one can nicely and directly confirm that h is part of a doublet. Moreover one can in principle test whether h is a pseudo Nambu–Goldstone boson (pNGB) living in a coset space [33–39] or whether it is a generic composite scalar. A way in which this could also be done is by studying triple Higgs production: $VV \rightarrow hhh$. This process could be marginally observable in the case of a generic composite h , while in the case of a pNGB non-trivial selection rules suppress its rate below observability.

This chapter is organised as follows. In section 2.2.2, we review the general parameterization of the Higgs couplings and the relative importance of energy-growing $2 \rightarrow 2$ scattering processes. Current constraints on the couplings, especially from electroweak precision tests, and their consequences on the scale of NP are discussed in detail in section 5.2. In sections 5.3 and 5.4, we study the information contained in single, double and triple Higgs production on the structure of the underlying theory. A quantitative analysis of the ILC and CLIC sensitivities on the anomalous couplings and their reach in the parameter space is given in section 5.5. We present our conclusions and outlook in section 5.6.

5.2 Current constraints on the Higgs couplings

Past and current experiments set important constraints on the Higgs couplings and on the scale of New Physics m_* . For a detailed discussion of EW precision observables see section 5.2.

5.2.1 Direct coupling measurements

The precision currently reached at the LHC on the direct measurement of the Higgs couplings to vector bosons and to fermions is limited. The exact value depends on the assumptions one makes to extract the couplings. For example, one can make a two-dimensional fit of a and c , where the latter parameterises a common rescaling of all the Yukawa couplings. Even neglecting the second solution at $c < 0$, the uncertainty in the official fits of the ATLAS and CMS collaborations is of the order of $\sim 20\%$ on a and even larger on c [99, 100]. In particular, while ATLAS prefers values $a > 1$, the best fit value of CMS is for $a < 1$. A naive combination of these results leads to a smaller uncertainty [74, 79, 163, 220–222], but more data are definitely required to form a clearer picture. Preliminary studies indicate that eventually a precision of $\sim 5\%$ on a should be reached at the 14 TeV LHC with an integrated luminosity of 300 fb^{-1} [223, 224].

5.2.2 Resonance searches

Searches for direct production of resonances at the LHC also set important constraints on the mass scale m_ρ of a new strongly-interacting sector. Here we consider the case of a generic $SO(5)/SO(4)$ composite Higgs theory as a benchmark scenario, although the actual bounds will depend on the details of the strong dynamics and on how it couples to the SM fermions. For illustrative purposes we focus on the lightest spin-1 resonance of the strong sector, which we denote by ρ , and assume that it transforms as a $(3, 1)$ under $SU(2)_L \times SU(2)_R \sim SO(4)$ (for recent studies in this direction see for example [97, 225–227]). The dominant production is via Drell–Yan processes (see for example Ref. [228]). A class of theories motivated both theoretically and experimentally is one in which the spin-1 resonance couples to light fermions only through its mixing to the SM gauge fields [229] (see Ref. [230] for alternative possibilities). In this case the Drell–Yan production cross section scales as $1/g_\rho^2$, since couplings of the resonances to the SM fermions are suppressed by $1/g_\rho$. The strongest exclusion limits are currently set by the LHC searches performed at 8 TeV with 20 fb^{-1} in final states with one lepton and missing transverse energy [231, 232] or dileptons [233, 234], looking for charged and neutral spin-1 resonances respectively. For values of ξ of order 1, searches for resonances decaying into WZ , in particular those with three leptons in the final state [235, 236], give slightly stronger bounds.¹ Assuming the ρ to be a $(\mathbf{3}, \mathbf{1})$ of $SU(2)_L \times SU(2)_R$, we translated the bounds on $(\sigma \times BR)$ set by the experimental collaborations into a combined exclusion region in the (ξ, m_ρ) plane.

The situation of direct and also indirect constraints is summarised in Fig. 5.1 for the case of a generic $SO(5)/SO(4)$ composite Higgs theory. We fix $a_\rho \equiv m_\rho/(g_\rho f) = 1$, where we define g_ρ as the physical coupling strength between three ρ resonances. The fundamental

¹We find that the more recent searches for spin-1 resonances decaying to pairs of vector bosons with boosted decay products [237–239] give less strong constraints.

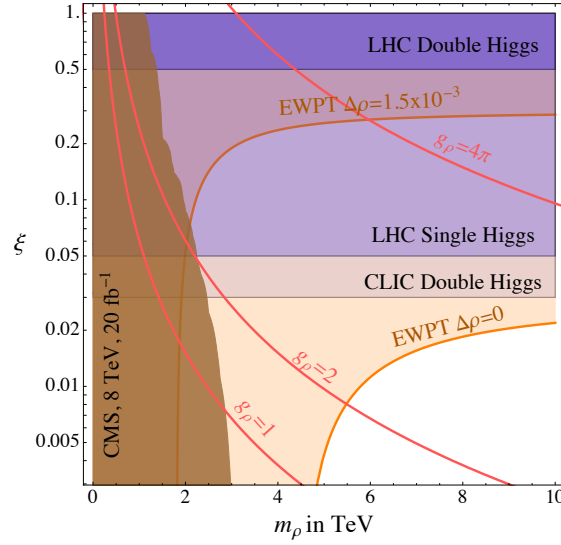


Figure 5.1 – Summary of current constraints (orange curves and brown region) and expected sensitivities at CLIC and the LHC (horizontal regions) on $\xi = (v/f)^2$ and the mass of the lightest spin-1 resonance m_ρ for $SO(5)/SO(4)$ composite Higgs theories. See text.

free parameters of the new dynamics are then the mass of the spin-1 resonance, m_ρ , and the strengths of the Higgs interactions parameterized by $\xi = (v^2/f^2)$. The dark brown region on the left shows the current 95% combined limit from direct production of the charged ρ^\pm at the LHC decaying to $l\nu$ and $WZ \rightarrow 3l\nu$ final states. A similar exclusion region follows from the limits on the production of the neutral ρ^0 . The dark (medium light) horizontal purple bands of Fig. 5.1 indicate instead the sensitivity on ξ expected at the LHC from double (single) Higgs production with 300 fb^{-1} of integrated luminosity (see footnote 12 for the definition of sensitivity adopted in this chapter). The value shown for the case of double Higgs production is based on a naive (and perhaps optimistic) extrapolation of the study of Ref. [64]; a more precise determination requires an updated analysis for $m_h = 125 \text{ GeV}$. As we will discuss in section 5.5, the study of double Higgs processes alone at CLIC is expected to lead to a precision on ξ larger than what obtainable at the LHC through single Higgs studies. In the plot of Fig. 5.1 this is illustrated by the lowest horizontal band. The possibility of directly testing such small values of ξ at CLIC has to be compared with the indirect bounds set by the EW precision data. By including only the tree-level contribution $\Delta\hat{S} = m_W^2/m_\rho^2$ from the ρ exchange [97] and the 1-loop IR effect from the modified Higgs couplings, we find that the region above the lower orange band is excluded at 95%. For $m_\rho \rightarrow \infty$ the upper limit on ξ tends to ~ 0.02 , as previously reported in the discussion of the EW fit. In the absence of other contributions to the oblique parameters, masses $m_\rho \lesssim 5 \text{ TeV}$ are already excluded even for very small ξ . Lowering the value of a_ρ makes the bound on m_ρ weaker, but does not change much that on ξ . The allowed region instead opens up in presence of an additional contribution to \hat{T} : for $0 < \Delta\hat{T} \leq +1.5 \times 10^{-3}$ the 95% exclusion boundary varies between the upper and lower orange lines and masses as low as $m_\rho \sim 2 \text{ TeV}$ can still be viable.

5.3. What can be learned from single and double Higgs production?

The domain of validity of our predictions, $g_\rho < 4\pi$, is below the upper red line.

5.3 What can be learned from single and double Higgs production?

In this section we discuss what could be learned directly, or indirectly, from a program of precise Higgs measurements at CLIC. For definiteness we can imagine a scenario where the LHC did not measure deviations from the SM larger than $O(20\%)$ in single Higgs production, and also no clear indications emerged on what the underlying theory may be (new particles may have been discovered but not with a clear role, i.e. no supersymmetric particles). There are various broad questions one can in principle address with these measurements. One question is whether the scalar h is elementary or composite. Other questions concern the nature of h , whether or not it fits into an $SU(2)$ doublet (an explicit, if not well motivated, example of a non-doublet Higgs-like scalar is a dilaton [68–73]) or whether or not it is a pNGB. To some extent the information will be indirect, so it is worth illustrating the logic in some detail.

Consider the issue of compositeness first. Of course, in order to directly answer this question, it would be necessary to explore the energy scale associated with the new states and observe the onset of a novel UV regime, perhaps described by a strongly coupled CFT. That would be the analogue of observing the hadron to parton transition in QCD processes. However, the measurement of low-energy quantities can already give an appraisal of the strength of the underlying interactions, thus favouring or disfavouring a composite scenario. Indeed for an $SU(2)$ Higgs doublet, a heavy particle with mass m_ρ and coupling to the Higgs g_ρ modifies the low-energy couplings by a relative amount of order $(g_\rho v/m_\rho)^2$.² For instance, massive fermions with a vectorlike mass m_ρ and a Yukawa interaction to the Higgs of strength g_ρ affect the coupling of h to two gluons and two photons by a relative amount $\sim (g_\rho v/m_\rho)^2$ (for recent work in the context of composite Higgs models see e.g. Ref. [241–243]). Similarly, a heavy singlet scalar S coupled to the Higgs doublet via a trilinear term $g_\rho m_\rho S|H|^2$ mixes by an angle $\theta \sim g_\rho v/m_\rho$ with h , implying shifts in its couplings of order $\theta^2 \sim (g_\rho v/m_\rho)^2$.³ In the absence of new states below a certain scale M , the observation of deviations of order δ_h^{exp} in single Higgs production would then imply a qualitative lower bound on the coupling

$$g_\rho > \sqrt{\delta_h^{exp}} \frac{M}{v}. \quad (5.1)$$

Sizeable deviations δ_h^{exp} in the absence of new states would suggest a strong coupling and, indirectly, h compositeness. A more direct measurement of the strength of the underlying

²Notice that a light Higgs mass $m_h = 125$ GeV disfavors maximal values $g_\rho \sim 4\pi$ unless some (additional) tuning is present in the Higgs potential. See for example Refs. [1, 47, 240].

³One could also consider a potential $V = -m_\rho^2|S|^2 + g_\rho^2|S|^2|H|^2 + g_\rho^2|S|^4$, by which $\langle S \rangle \sim m_\rho/g_\rho \equiv f$, and reach the same conclusion.

interaction is obtained by a study of the processes $WW \rightarrow WW$ and $WW \rightarrow hh$. As discussed in section 2.2.2, a deviation from $a = b = 1$ leads to a cross section that grows with s . The $2 \rightarrow 2$ amplitude can be taken as a measure of a “running” coupling $\bar{g}(\sqrt{s})$, see eq. (2.36). The measurement of an enhancement, quantified by δ_{hh}^{exp} , in these processes at an energy \sqrt{s} , corresponds directly, though qualitatively, to a lower bound on the strength of the interaction

$$g_\rho > \bar{g}(\sqrt{s}) \sim \sqrt{\delta_{hh}^{exp}} \frac{\sqrt{s}}{v}. \quad (5.2)$$

Equations (5.1) and (5.2) look similar, and not by chance. Notice, however, that the second equation corresponds to a direct measurement of the coupling, and is thus a more robust estimate. Indeed, at a precise machine such as CLIC a detailed study of $2 \rightarrow 2$ processes would allow even stronger conclusions. The point is that eq. (2.36) is only the leading term in a derivative expansion, the subleading corrections being of relative size s/m_ρ^2 :

$$\mathcal{A}(2 \rightarrow 2) = \delta_{hh} \frac{s}{v^2} \left(1 + O\left(\frac{s}{m_\rho^2}\right) \right). \quad (5.3)$$

In principle at CLIC one could measure the leading $O(s)$ contribution and set an upper bound ϵ_{hh} on the relative size of the $O(s^2)$ term. That would indirectly suggest that there are no new states below a mass $M \sim \sqrt{s}/\sqrt{\epsilon_{hh}}$ and that the amplitude will keep rising at least until that scale. That would amount to a stronger indirect bound

$$g_\rho > \bar{g}(M) \sim \sqrt{\frac{\delta_{hh}^{exp}}{\epsilon_{hh}}} \frac{\sqrt{s}}{v}. \quad (5.4)$$

We clearly see here the value of being able to measure $2 \rightarrow 2$ processes with high precision below the threshold of New Physics. Of course another possibility is that of directly observing, rather than setting limits on, the $O(s^2)$ effects from the tails of heavy resonances. In this case detailed information on the strong dynamics, such as the quantum numbers of its resonances, can come from the comparison of different scattering channels, see for example Refs. [97, 244–246].⁴

Consider now the properties of h from the standpoint of symmetries. In the case of the SILH, in which h fits into a doublet of $SU(2)$ arising from some unspecified dynamics at the scale m_ρ , the bosonic couplings a, b, b_3 are predicted in terms of just one parameter at $O(v^2/f^2)$, as illustrated by eq. (2.32). In particular, by defining $\Delta a^2 \equiv a^2 - 1$ and $\Delta b \equiv b - 1$ one has

$$\Delta b = 2\Delta a^2 (1 + O(\Delta a^2)), \quad (5.5)$$

⁴The effects from the tails of spin-1 resonances can also be studied through the process $e^+e^- \rightarrow VV$, see for example Refs. [247–252].

5.3. What can be learned from single and double Higgs production?

where the higher-order corrections are determined by the tower of higher-dimensional operators with two derivatives and $2n$ H fields using the SILH power counting. Furthermore, in the very special case where H is a pNGB the whole tower of operators and the resulting WWh^n couplings are all fixed in terms of a single parameter ξ . Equation (3.7) reports for example the predictions of the minimal $SO(5)/SO(4)$ and $SO(4,1)/SO(4)$ theories. In both cases eq. (5.5) becomes exactly

$$\Delta b = 2\Delta a^2. \quad (5.6)$$

From single Higgs production one would be able to measure Δa^2 with an error $\sim 10^{-2}$, maybe of a few per mille [50, 209, 253–256]. The measurement of $WW \rightarrow hh$, as we will discuss in the next sections, allows one in principle to measure Δb with an error of order 10^{-2} . Equations (5.5) and (5.6) can then be tested at the percent level. For instance, in the case of a SILH not embedded in a coset one could imagine finding $\Delta a^2, \Delta b \gtrsim 0.1$ and to be compatible with eq. (5.5) but violating eq. (5.6) by an amount bigger than the expected percent accuracy. On the other hand, for $\Delta a^2, \Delta b < 0.1$, it would not be possible to distinguish between a SILH and a pNGB. Finally, down to $\Delta a^2, \Delta b \sim 10^{-2}$ one could find that eq. (5.5) is not respected, indirectly speaking against the embedding of h in a doublet. It should however be pointed out that such a scenario, normally associated with a fully composite h , would more probably imply Δ 's of order 1, which are already excluded by the current LHC results. It should also be remarked that the only case of this type with some mild motivation is the one of a light dilaton, corresponding to

$$\Delta b = \Delta a^2, \quad (5.7)$$

implying a vanishing contribution to $WW \rightarrow hh$ at leading order in the energy expansion [64].

We should finally point out the potential role of the rates for $h \rightarrow gg$ and $h \rightarrow \gamma\gamma$ in distinguishing a pseudo Nambu–Goldstone h from a generic composite scalar. The basic remark [80] is that there are two classes of corrections to these rates. One correction originates from the modification of the coupling of h to WW and to $\bar{t}t$ and affects the on-shell $h \rightarrow gg$, $h \rightarrow \gamma\gamma$ amplitudes via the W and t loop contribution. In a sense this contribution is long distance. A second correction is the genuine short-distance contribution to the Wilson coefficient of the operators

$$\mathcal{O}_{gg} = hG_{\mu\nu}G^{\mu\nu}, \quad \mathcal{O}_{\gamma\gamma} = hF_{\mu\nu}F^{\mu\nu}, \quad (5.8)$$

that arises from loops of heavy states. In the case of a pNGB this second class of effects is suppressed with respect to the first by a factor $(g_{\mathcal{G}}/g_\rho)^2$, where by $g_{\mathcal{G}}$ we indicate a weak spurion coupling which breaks the Goldstone symmetry. This suppression is a consequence of the Goldstone symmetry selection rules and would be absent in the case of a generic composite scalar, like for instance the dilaton. In the limit where $g_{\mathcal{G}}/g_\rho \ll 1$, the

rates $h \rightarrow gg$, $h \rightarrow \gamma\gamma$ are fully controlled by a and c_t (c_t measures the deviations of the top Yukawa coupling [80]), a result that can in principle be tested. However, one should keep in mind that the measured value of m_h prefers a scenario where the top partners are somewhat lighter than the rest and only moderately strongly coupled [1, 47–49, 157]. In that situation the correlation between $h \rightarrow gg$, $h \rightarrow \gamma\gamma$ and the parameters a, c_t may receive important corrections.

5.4 What can be learned from triple Higgs production?

In this section we discuss the relevance of the process $VV \rightarrow hhh$ in distinguishing between a generic SILH and a pNGB (for an earlier study of this process at a linear collider, see Ref. [257], while a study at the LHC has been recently carried out in Ref. [258] and triple Higgs production by gluon fusion has also been studied in Ref. [259]). We will show that this process is suppressed in the pNGB case as a consequence of a Z_2 invariance of the Lagrangian under which the NG bosons are odd. A priori, any three-body final state involving the Higgs and gauge bosons could be a further probe of the nature of the Higgs. In practice, however, $VV \rightarrow hhh$ is the only process that adds new information, thanks to its sensitivity to b_3 . Studying further final states like hhV , hVV and VVV merely gives a complementary probe of the relation between a^2 and b .

5.4.1 Symmetry structure

In a symmetric coset like $SO(5)/SO(4)$ there exists a Z_2 invariance of the algebra (grading) under which the broken generators $T^{\hat{a}}$ change sign while the unbroken generators T^a do not: $T^a \rightarrow +T^a$, $T^{\hat{a}} \rightarrow -T^{\hat{a}}$. At the field level this corresponds to a parity R under which all NG bosons are odd

$$R: \quad \pi^{\hat{a}}(x) \rightarrow -\pi^{\hat{a}}(x). \quad (5.9)$$

In general, R is an accidental invariance of the Lagrangian at the two-derivative level and is violated at higher orders. This is for example the case of $SO(4)/SO(3)$, where R coincides with the P_{LR} parity of eq. (2.37). It may happen however, as for example in the case of $SO(5)/SO(4)$, that R is an element of G , in which case it remains unbroken to all orders in the derivative expansion of the strong dynamics. In fact, this is true for any coset G/H involving only doublets under some $SU(2)' \subset \mathcal{H}$.⁵ In particular this property is shared by the simplest cosets involving just one scalar doublet, whether custodially symmetric ($SO(5)/SO(4)$ or $SO(4,1)/SO(4)$) or not ($SU(3)/SU(2) \times U(1)$). Consequently, when the Higgs doublet is the only pNGB multiplet from some strong dynamics, processes with an odd number of pseudo-NG bosons are forbidden to all orders

⁵Such a coset is obviously symmetric, as the commutator of any element in G/H cannot be a doublet, and must therefore belong to \mathcal{H} . Moreover the residual $SU(2)'$ will forbid odd powers of the NG-bosons at any order in the derivative expansion.

5.4. What can be learned from triple Higgs production?

Polarisation	Amplitude for	
	pNGB	SILH
$V_L V_L \rightarrow hhh$	$g^2 v / f^2$	$\hat{s} v / f^4$
$V_L V_T \rightarrow hhh$	$\sqrt{\hat{s}} g / f^2$	
$V_T V_T \rightarrow hhh$	$g^2 v / f^2$	

Table 5.1 – Naive high-energy and large-angles behaviour of partonic $VV \rightarrow hhh$ amplitudes for a pNGB Higgs (first column) and a generic SILH scalar (second column).

in the strong dynamics and only arise as a weak effect of the SM couplings.

The above argument implies that, although by a naive counting one would expect the $V_L V_L \rightarrow hhh$ cross section to grow with \hat{s}^2 ,⁶ this does not happen for a pNGB Higgs. In practice R is weakly broken by the gauging, so that this process is not strictly zero but only suppressed by g . The expected energy behaviour of the amplitude at the parton level can be estimated by power counting and is shown in Table 5.1. Longitudinal modes interact with coupling strength $\bar{g}(\sqrt{\hat{s}}) \sim \sqrt{\hat{s}}/f$, while transverse modes have weak coupling strength g . Measuring the cross section of triple Higgs production can thus give important indications on the nature of the Higgs boson and distinguish the case of a pNGB from that of a generic SILH. Indeed, as it will become more clear in a moment, the grading symmetry R is reflected in some non-trivial correlations among the coefficients of operators of different dimensionality in the expansion of the effective Lagrangian in powers of the Higgs doublet H .

5.4.2 Quantitative analysis of $VV \rightarrow hhh$

We checked that the expected cancellation of the energy-growing term of the $V_L V_L \rightarrow hhh$ scattering amplitude takes place by performing an explicit computation in the gaugeless limit $g = g' = 0$. By the equivalence theorem, the leading energy behaviour of $V_L V_L \rightarrow hhh$ is captured by the NG boson scattering $\chi\chi \rightarrow hhh$. From the Lagrangian of eq. (2.16) we find three distinct diagrams, depicted in Fig. 5.2, plus their crossings, which contribute to the amplitude. At leading order in \hat{s} we find⁷

$$\mathcal{A}(\chi\chi \rightarrow hhh) = \frac{i\hat{s}}{v^3} (4ab - 4a^3 - 3b_3) . \quad (5.10)$$

⁶From here on we will indicate the partonic c.o.m. energy with \hat{s} , while s will denote the collider energy.

⁷Note that, similarly to the process $VV \rightarrow hh$, anomalous Higgs self-interactions parameterized by d_3 and d_4 modify the amplitude of triple Higgs production near threshold but do not affect the asymptotic behaviour at large partonic energy. Their contribution is thus subleading and will be neglected in the following.

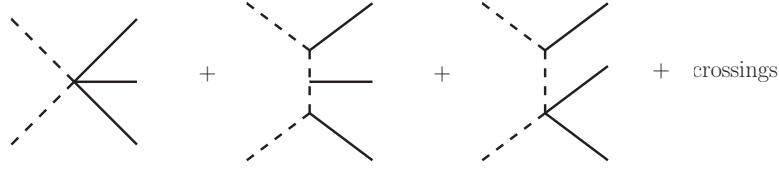


Figure 5.2 – Leading diagrams contributing to the $\chi\chi \rightarrow hhh$ amplitude. Dashed lines represent the NG bosons χ , while solid lines denote the Higgs boson h . The sum of these diagrams with their crossings cancels out exactly in the gaugeless limit for a symmetric coset and at the $O(p^2)$ level for any coset. See text.

σ [ab]	ξ						
	0	0.05	0.1	0.2	0.3	0.5	0.99
pNGB	0.32	0.46	0.71	1.47	2.41	4.13	0.30
SILH	0.32	0.71	0.87	7.56	42.89	407.9	7808

Table 5.2 – Cross section for the process $e^+e^- \rightarrow \nu\bar{\nu}hhh$ for $m_h = 125$ GeV at $\sqrt{s} = 3$ TeV. The first line shows the cross sections obtained in the symmetric $SO(5)/SO(4)$ coset for various values of ξ . The cross sections in the second line are for a SILH with $c_H = 1$ and $c'_H = 0$ and vanishing higher-order operators.

In the case of $SO(5)/SO(4)$ the values of the couplings a, b and b_3 are given by eq. (3.7) and the coefficient of the term growing with \hat{s} in the amplitude vanishes identically. In the case of a generic Higgs doublet the cancellation works at the $O(v^2/f^2)$ level, as due to the universality of the SILH Lagrangian, but it fails at higher orders. By substituting the relations of eq. (2.32) into eq. (5.10) we find

$$\mathcal{A}(\chi\chi \rightarrow hhh) = 2i (c'_H - 2c_H^2) \frac{\hat{s}}{v^3} \left(\frac{v^4}{f^4} \right). \quad (5.11)$$

As expected, the coefficient of the energy-growing term is of order v^4/f^4 and proportional to the linear combination $(c'_H - 2c_H^2)$. This latter must vanish if the Higgs lives on a symmetric coset \mathcal{G}/\mathcal{H} .⁸

At CLIC, triple Higgs production proceeds through the process $e^+e^- \rightarrow \nu\bar{\nu}VV \rightarrow \nu\bar{\nu}hhh$, where $V = W^\pm, Z$. Some typical values of the cross section are shown in Table 5.2 for the case of a pNGB and a SILH with $c_H = 1$ and $c'_H = 0$ (and vanishing higher-order operators). While the cross section for a pNGB is in the range of a few ab, in the case of a generic SILH it can be much bigger and grows like ξ^4 , with the dominant contribution coming from the subprocess $V_L V_L \rightarrow hhh$. A careful analysis of the sensitivity of a linear collider to the anomalous couplings involved in triple Higgs production is beyond the scope of this work. A very conservative approach is to decay every Higgs to $b\bar{b}$ and to require the identification of at least 5 b -jets. The branching ratio of three Higgses into 3 $b\bar{b}$ pairs is 20%. Assuming an 80% b -tagging probability, the efficiency to reconstruct at

⁸This shows that the relation $c'_H = 2c_H^2$ holds true in any symmetric coset, and not only in $SO(5)/SO(4)$.

5.4. What can be learned from triple Higgs production?

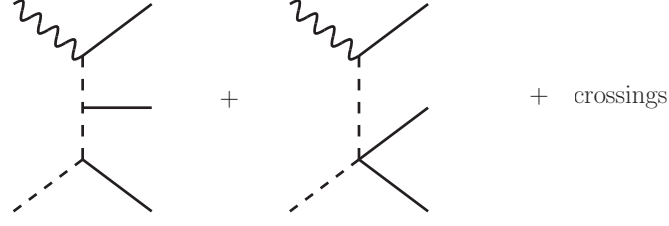


Figure 5.3 – Diagrams giving the dominant contribution to the $V_T\chi \rightarrow hhh$ cross-section. Continuous, dashed and wiggly lines denote a Higgs boson h , the NG bosons χ , and a transverse gauge boson V_T respectively.

least 5 b -jets out of the available 6 in the final state is 66%. Including an additional factor 3 reduction due to identification cuts to be performed on the final state jets one obtains an overall efficiency on the signal which is roughly 5%. Requiring the identification of $O(10)$ triple Higgs events implies the possibility to detect this process with an integrated luminosity of 1 ab^{-1} as soon as $\xi \gtrsim 0.3$ for a generic SILH.

The dominant contribution to triple Higgs production in the case of a pNGB Higgs comes from the subprocess $W_L^\pm W_T^\mp \rightarrow hhh$, whose cross section is expected to grow as $\hat{s} \log \hat{s}$. The leading logarithmic behaviour can be extracted by using the equivalence theorem and arises from the subset of diagrams shown in Fig. 5.3. In the limit in which the intermediate pNGB line is nearly on-shell, the total cross section factorizes into the product of a collinear $W_T \rightarrow \chi h$ splitting times the cross section of a hard $\chi^\pm \chi^\mp \rightarrow hh$ scattering

$$\sigma(W_T^\pm \chi^\mp \rightarrow hhh) = \int dx dp_T^2 f(x, p_T) \sigma(\chi^\pm \chi^\mp \rightarrow hh)(x\hat{s}). \quad (5.12)$$

Here x is the fraction of the W energy carried by the emitted χ , p_T is its transverse momentum and \hat{s} is the total center-of-mass energy of the $W_T\chi \rightarrow hhh$ process. The splitting function $f(x, p_T)$ can be calculated using eq. (2.16) and is given by

$$f(x, p_T) = \frac{1}{p_T^4} \frac{x(1-x)}{8\pi^2} |\mathcal{A}(W_T \rightarrow \chi h)|^2 = \frac{x(1-x)}{p_T^2} \frac{a^2 g^2}{32\pi^2}, \quad (5.13)$$

where we have neglected the masses of the gauge and Higgs bosons. Notice that the amplitude of the splitting $\mathcal{A}(W_T \rightarrow \chi h)$ vanishes in the forward direction as required by angular momentum conservation. At leading order in \hat{s} , the cross section of the hard $\chi\chi \rightarrow hh$ scattering does not depend on p_T , and reads

$$\sigma(\chi^\pm \chi^\mp \rightarrow hh)(\hat{s}) = \frac{\hat{s}(b - a^2)^2}{32\pi v^4}. \quad (5.14)$$

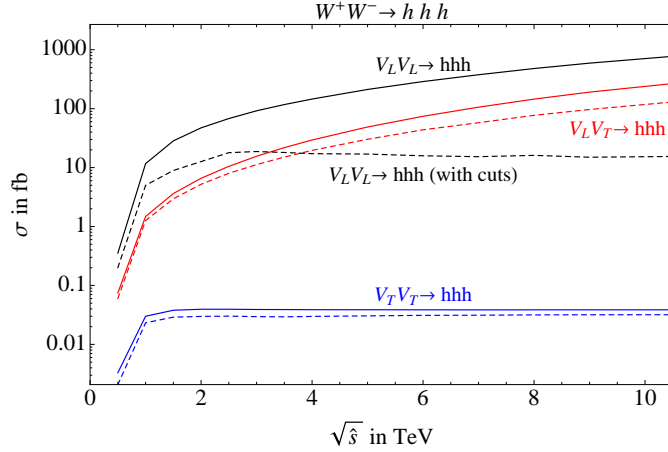


Figure 5.4 – Partonic cross-sections of the processes $V_L V_L \rightarrow hhh$ (black), $V_L V_T \rightarrow hhh$ (red) and $V_T V_T \rightarrow hhh$ (blue) as a function of $\sqrt{\hat{s}}$ for a pNGB Higgs with $\xi = 0.1$ and $m_h = 125$ GeV. The dashed line shows the partonic cross section after applying the cuts $p_T > 0.05\sqrt{\hat{s}}$ for each Higgs and $m_{hh} > 0.1\sqrt{\hat{s}}$ for all Higgs pairs.

We thus obtain

$$\sigma(W_T^\pm \chi^\mp \rightarrow hhh) = \frac{g^2}{12288 \pi^3} \frac{(ab - a^3)^2}{v^4} \hat{s} \log \frac{\hat{s}}{m_W^2}. \quad (5.15)$$

The factor $\log(\hat{s}/m_W^2)$ originates from the logarithmic divergence of the integral over p_T , which is cut off in the infrared at $p_T^2 \sim m_W^2$ once the W mass dependence is properly taken into account.

Although this calculation captures the exact asymptotic behaviour of the $W_T^\pm W_L^\mp \rightarrow hhh$ process, it turns out that the subleading contribution proportional to \hat{s} is numerically large, so that the logarithmically enhanced term starts to dominate only at very high center-of-mass energies. The energy dependence of the process $VV \rightarrow hhh$ ($V = W, Z$) in the various polarisation channels is shown in Fig. 5.4. We assume that the Higgs boson is a pNGB living on the coset $SO(5)/SO(4)$, so that the selection rules discussed at the beginning of this section apply. The expectation for the various $2 \rightarrow 3$ amplitudes is reported in Table 5.1. Notice that for a three-body process the product of the flux factor and phase space is dimensionless. The naive high-energy behaviour of the various cross sections is then obtained by squaring the entries of Table 5.1. The total cross section is expected to follow this naive energy behaviour only if the phase space integral does not get any particular enhancement from singular kinematic configurations. As explained above, the LT polarisation channel indeed gets a logarithmic enhancement from the kinematical region where one of the final Higgs bosons is collinear with the incoming transverse vector. As Fig. 5.4 shows, the TT channel cross section is constant at high energy, in agreement with the naive expectation $\sigma(V_T V_T \rightarrow hhh) \sim (g^4/(4\pi)^3)(v^2/f^4)$. On the other hand the inclusive $V_L V_L \rightarrow hhh$ cross section grows like \hat{s} at high energy, faster than what is

expected from Table 5.1. This is due to the Coulomb singularity that some of the diagrams have in the limit in which one of the final Higgs bosons is collinear to the incoming beam. The amplitude of those diagrams goes as $\mathcal{A}(V_L V_L \rightarrow hhh) \sim (g^2 v / f^2)(\hat{s} / \hat{t})$, where \hat{t} is the squared difference of one of the initial momenta and the momentum of the collinear Higgs boson. The integral over \hat{t} is dominated by the singular region $t \simeq t_{min} \sim -m_W^2$, so that the total cross section gets enhanced by a factor (\hat{s} / m_W^2) . Such an enhancement can be removed by suitable kinematic cuts to avoid all collinear configurations. For example, the dashed curves of Fig. 5.4 show the energy dependence of the cross sections after requiring $p_T > 0.05\sqrt{\hat{s}}$ on each of the Higgs final momenta. As expected, the TT and LT channels are only slightly suppressed by the cuts, while the Coulomb singularity of the LL channel is removed and its cross section is constant at high energies.

5.5 Quantitative analysis of $VV \rightarrow VV$ and $VV \rightarrow hh$

In this section we study the sensitivity of a linear e^+e^- collider to the anomalous Higgs couplings a , b and d_3 through vector boson scattering and double Higgs production. In section 5.5.2 we discuss $V_L V_L \rightarrow V_L V_L$ scattering at low-energy (ILC) and high-energy (CLIC) linear colliders; in sections 5.5.3 and 5.5.4 we focus on double Higgs production. We show that, while CLIC can provide a precise determination of the anomalous couplings through the study of the vector boson fusion process $e^+e^- \rightarrow hh\nu\bar{\nu}$, a lower-energy machine like the ILC has to rely on the double Higgs-strahlung process $e^+e^- \rightarrow hhZ$. Previous analyses of $VV \rightarrow VV$ and $VV \rightarrow hh$ at high-energy linear colliders appeared in Refs. [260–262] and [209, 263, 264] respectively.⁹

5.5.1 Identification cuts

In the following we set $m_h = 125$ GeV and focus on final states where W , Z and h decay hadronically, with the only exception of double Higgs-strahlung where we include leptonic decays of the Z . Our analysis is at the parton level and does not include corrections due to QCD radiation. Final-state partons are passed through a simple algorithm to obtain a crude though sufficiently accurate approximation of jet-reconstruction and detector effects of a real experiment. We perform a simple Gaussian smearing of the parton energies assuming a constant resolution $\Delta E/E = 5\%$ [51, 207, 208]. Two partons with

$$\Delta R_{jj} < 0.4 \tag{5.16}$$

are merged together by summing their 4-momenta. The algorithm is applied recursively until it converges to a list of final partons. A parton thus obtained which satisfies the

⁹See also Ref. [265] for a study of the process $\gamma\gamma \rightarrow VV$ ($V = W, Z$) to extract the anomalous Higgs couplings.

cuts

$$E_j > 20 \text{ GeV}, \quad |\eta_j| < 2 \quad (5.17)$$

is identified with a reconstructed jet. The rapidity cut, in particular, excludes reconstructed jets which fall within 15° of the collision axis. Leptons (muons and electrons) are identified if they satisfy the following cuts:

$$E_\ell > 5 \text{ GeV}, \quad |\eta_\ell| < 2. \quad (5.18)$$

We furthermore require a separation $\Delta R_{j\ell} > 0.4$ between reconstructed jets and leptons.

In events with two Higgs bosons (like those coming from WW fusion or double Higgs-strahlung) we require at least 3 b -tags with a b -tagging efficiency of 80% assumed throughout the analysis. According to Ref. [51, 207, 208], this is associated with mistag rates of $\sim 10\%$ and $\sim 1\%$ for c -jets and light jets respectively. With this assumption the probability of tagging at least 3 b -jets out of 4 is 82%.

All our event samples are generated with MADGRAPH5 [189], except for the background to $VV \rightarrow VV$ scattering which has been generated with WHIZARD [266]. We do not include parton showering and hadronization.

5.5.2 $VV \rightarrow VV$ scattering

All the channels $e^+e^- \rightarrow VV\ell\bar{\ell}$, where ℓ is either an electron or a neutrino, provide a framework for studying vector boson scattering at a linear collider. VV scattering processes with electrons in the final state are initiated by a neutral current splitting $e^\pm \rightarrow \gamma e^\pm$ or $e^\pm \rightarrow Ze^\pm$. While the first always contributes as a large background to the signal we are interested in, the second splitting is a factor of 2 smaller than the charged current splitting $e \rightarrow W\nu$. We will focus therefore on $VV\nu\bar{\nu}$ final states and neglect VVe^+e^- for simplicity. We will consider hadronically decaying vector bosons and, to avoid possible experimental issues related to energy resolution and W/Z separation, we will be inclusive and sum over final states with W 's or Z 's.

The cross section for the process $e^+e^- \rightarrow VV\nu\bar{\nu}$ can be parameterized in terms of the coupling shift Δa^2 as

$$\sigma(\Delta a^2) = \sigma_{SM} (1 + A \Delta a^2 + B (\Delta a^2)^2), \quad (5.19)$$

where σ_{SM} is the SM cross section and A, B are two dimensionless coefficients. Notice

that $\Delta a^2 = \xi$ in the MCHM. For $\sqrt{s} = 3$ TeV we find, before any cut,

$$\sigma_{SM} = 184 \text{ fb}, \quad \{A, B\} = \{0.01, 0.15\} \quad \left[\begin{array}{c} e^+e^- \rightarrow VV\nu\bar{\nu} \\ \text{before any cut} \end{array} \quad \sqrt{s} = 3 \text{ TeV} \right]. \quad (5.20)$$

It is clear that at this level the cross section is largely dominated by the SM term. One reason is the “accidental” numerical enhancement, discussed in Ref. [64], of the partonic $V_T V_T \rightarrow V_T V_T$ cross section compared to $V_L V_L \rightarrow V_L V_L$. Another reason is that the total cross section displayed here is dominated by threshold production and does not really probe the highest energies.

The situation is worsened by the presence of backgrounds. The largest contribution arises from the process $e^+e^- \rightarrow W^+W^-e^+e^-$, which goes through a $\gamma\gamma \rightarrow W^+W^-$ hard scattering, where the final electron and positron escape the detector. A similar though smaller background comes from $e^+e^- \rightarrow W^\pm Z e^\mp \nu$. Before cuts, the cross section of these background processes is of the order of hundreds of pico-barns.

We focus on hadronic decays of the W and Z bosons and select events with at least four reconstructed jets, where jet reconstruction is done according to the procedure discussed in section 5.5.1. The two V candidates are defined by considering the four most energetic jets in each event, $j_{1,\dots,4}$, and by identifying the pairing $(j_1 j_2, j_3 j_4)$ which minimises the χ^2 function

$$(m_{j_1 j_2} - m_V)^2 + (m_{j_3 j_4} - m_V)^2, \quad (5.21)$$

where $m_V \equiv (m_W + m_Z)/2$. We use the average mass m_V in the χ^2 function since we do not know a priori if the V candidate is a W or a Z . The algorithm is however quite effective to identify real vector bosons, and the percentage of fake pairings is negligible. After their reconstruction, we impose the following cut on the invariant mass of each of the two V candidates:

$$|m_{jj} - m_V| < 15 \text{ GeV}. \quad (5.22)$$

Events where such requirement is not satisfied are discarded. The overall efficiency of the identification cuts in eqs. (5.17) and (5.22) is roughly 30% for both signal and background. After imposing the identification cuts and including the hadronic branching ratios of the W and Z bosons, we find that the signal rate $r = \sigma(e^+e^- \rightarrow VV\nu\bar{\nu}) \times BR(VV \rightarrow 4j)$ is parameterized by

$$r(\Delta a^2) = r_{SM} (1 + A_r \Delta a^2 + B_r (\Delta a^2)^2), \quad (5.23)$$

with

$$r_{SM} = 28.7 \text{ fb}, \quad \{A_r, B_r\} = \{0.04, 0.16\} \quad \left[\begin{array}{c} e^+e^- \rightarrow 4j\nu\bar{\nu} \\ \text{after identification cuts} \end{array} \quad \sqrt{s} = 3 \text{ TeV} \right]. \quad (5.24)$$

In order to enhance the signal and reduce the backgrounds we apply the following additional set of cuts

$$\begin{aligned}
m_{V_1 V_2} &> 500 \text{ GeV}, \\
\min p_T(V_i) &> 100 \text{ GeV}, \\
\max |\eta_{V_i}| &< 1.1, \\
m_{\nu\nu} &> 150 \text{ GeV},
\end{aligned} \tag{5.25}$$

where $V_{1,2}$ denote the two V candidates. The cut on the invariant mass of the two neutrinos, in particular, eliminates those backgrounds, like $e^+e^- \rightarrow VVZ$ (with $Z \rightarrow \nu\bar{\nu}$), where the missing energy arises from the invisible decay of an on-shell Z boson. Finally, we require

$$p_T(V_1 V_2) > 75 \text{ GeV}. \tag{5.26}$$

This latter cut on the transverse momentum of the VV system is applied to further reduce the $e^+e^- \rightarrow W^+W^-e^+e^-$ and $e^+e^- \rightarrow W^\pm Z e^\mp \nu$ backgrounds: if the final electrons are so forward to be lost in the beam-pipe it is reasonable to expect the total p_T of the recoiling vectors to be small. After all these cuts, the signal rate is parameterized by

$$r_{SM} = 1.7 \text{ fb}, \quad \{A_r, B_r\} = \{0.04, 0.7\} \quad \left[\begin{array}{c} e^+e^- \rightarrow 4j\nu\bar{\nu} \quad \sqrt{s} = 3 \text{ TeV} \\ \text{after analysis cuts} \end{array} \right]. \tag{5.27}$$

The background rate from $e^+e^- \rightarrow W^+W^-e^+e^-$ and $e^+e^- \rightarrow W^\pm Z e^\mp \nu$ processes amounts to roughly $r_b = 2.5 \text{ fb}$ after the cuts. The calculation has been performed using WHIZARD [266] by requiring the electrons in the final state to be undetected ($\eta(e^\pm) > 2.5$).¹⁰

We thus proceed to estimate the expected sensitivity on Δa^2 . We follow a Bayesian approach and construct a posterior probability for the total event rate r_{tot}

$$p(r_{tot}|N_{obs}) \propto \mathcal{L}(N_{obs}|r_{tot}L)\pi(r_{tot}), \tag{5.28}$$

where N_{obs} is the assumed number of observed events and L is the integrated luminosity. We denote with $\pi(r_{tot})$ the prior distribution and with $\mathcal{L}(N_{obs}|r_{tot}L)$ the likelihood function, which we take to be a Poisson distribution

$$\mathcal{L}(N_{obs}|r_{tot}L) = \frac{e^{-r_{tot}L} (r_{tot}L)^{N_{obs}}}{N_{obs}!}. \tag{5.29}$$

For a given true value $\Delta \bar{a}^2$ of the coupling shift, we assume the number of observed

¹⁰We found significant numerical instabilities in the MC computation of the cross section, with variations in the final result up to 30 – 50%. As explained below, we took into account such uncertainty in our analysis by rescaling the final background rate by a factor 1.5.

5.5. Quantitative analysis of $VV \rightarrow VV$ and $VV \rightarrow hh$

$\Delta\bar{a}^2 = \bar{\xi}$	Δa^2	$\xi^{(68)}$	$\xi^{(95)}$
0	(-0.21, 0.17)	(0, 0.17)	(0, 0.29)
0.05	(-0.22, 0.17)	(0, 0.18)	(0, 0.29)
0.1	(-0.23, 0.18)	(0, 0.19)	(0, 0.30)
0.2	$(-0.34, -0.1) \cup (0.04, 0.28)$	(0.06, 0.28)	(0.0, 0.34)
0.3	$(-0.45, -0.22) \cup (0.17, 0.39)$	(0.17, 0.39)	(0.0, 0.45)
0.5	$(-0.62, -0.49) \cup (0.45, 0.56)$	(0.43, 0.56)	(0.36, 0.61)

Table 5.3 – Expected 68% probability intervals on Δa^2 (second column) and ξ (third column) and 95% probability intervals on ξ (fourth column) for different true values $\Delta\bar{a}^2 = \bar{\xi}$ measured at CLIC 3 TeV through $VV \rightarrow VV$ scattering. The limits on ξ have been derived by taking into account that only values in the range $\xi \in [0, 1]$ are theoretically allowed. See the text for details on the statistical analysis.

events to be $N_{obs} = (r(\Delta\bar{a}^2) + r_b)L$, while the total rate is $r_{tot} = r(\Delta a^2) + r_b$. As we do not explicitly introduce additional uncertainties (theoretical or systematic) on the estimate of the background in our statistical analysis,¹¹ we have conservatively rescaled the background rate r_b by a factor 1.5 compared to the MC prediction.

By assuming a flat prior on Δa^2 and setting the integrated luminosity to $L = 1 \text{ ab}^{-1}$, we obtain the 68% probability intervals shown in Table 5.3 (second column) for different true values $\Delta\bar{a}^2$. We find that for large $\Delta\bar{a}^2$, the term proportional to $(\Delta a^2)^2$ dominates the rate and a second peak of the likelihood appears at negative values of the coupling shift. The 68% interval in these cases consists of two disconnected parts. We also considered the $SO(5)/SO(4)$ models MCHM where the coupling shift is $\Delta a^2 = \xi$, see eq. (3.7). In this case we have imposed a prior on ξ which is flat in the theoretically allowed range $[0, 1]$ and vanishing outside. The corresponding 68% probability intervals on ξ are reported in the third column of Table 5.3 for different true values $\bar{\xi}$. With our set of cuts, a 3 TeV linear collider is sensitive to values of Δa^2 (ξ) bigger than ~ 0.2 through WW scattering.¹² We do not find any significant gain in resolution by applying a harder cut on the VV invariant mass.

A similar analysis can be carried out for a lower energy machine. We considered for example the case of a 500 GeV linear collider. Parameterizing the signal cross section as in eq. (5.19), before cuts we find

$$\sigma_{SM} = 5.12 \text{ fb}, \quad \{A, B\} = \{-0.03, 0.06\} \quad \left[\begin{array}{c} e^+e^- \rightarrow VV\nu\bar{\nu} \quad \sqrt{s} = 500 \text{ GeV} \\ \text{before any cut} \end{array} \right]. \quad (5.30)$$

¹¹This would require introducing one or more corresponding nuisance parameters in the likelihood function, which is beyond the scope of our simple statistical analysis.

¹²Here and in the following, by sensitivity/precision on some anomalous Higgs coupling we mean the 68% error on its measured value for injected SM signal.

At this stage the background processes have very large cross sections, of the order of 100 fb. However, all backgrounds can be reduced to a negligible level by applying the identification cuts of eqs. (5.17) and (5.22), the additional cuts $p_T(V_1 V_2) > 40 \text{ GeV}$, $m_{\nu\nu} > 100 \text{ GeV}$ and requiring all electrons in the final states to escape detection, $\eta(e^\pm) > 2.4$. After these cuts, and including the hadronic branching ratio of W and Z , the signal rate is parameterized as in eq. (5.23) with:

$$r_{SM} = 0.5 \text{ fb}, \quad \{A_r, B_r\} = \{-0.03, 0.15\} \quad \left[\begin{array}{c} e^+ e^- \rightarrow 4j\nu\bar{\nu} \quad \sqrt{s} = 500 \text{ GeV} \\ \text{after analysis cuts} \end{array} \right]. \quad (5.31)$$

By repeating the previous statistical analysis, we find that with an integrated luminosity $L = 1 \text{ ab}^{-1}$ the effect of a non-vanishing hVV anomalous coupling can be resolved in $e^+ e^- \rightarrow VV\nu\bar{\nu}$ only for large values of $\Delta a^2(\xi)$, of the order $0.5 - 0.6$.

5.5.3 $VV \rightarrow hh$ scattering

The scattering amplitude for $V_L V_L \rightarrow hh$ depends on a , b and d_3 and can be conveniently written as $\mathcal{A} = a^2 (\mathcal{A}_{SM} + \mathcal{A}_1 \delta_b + \mathcal{A}_2 \delta_{d_3})$, where \mathcal{A}_{SM} is the value predicted by the SM and ¹³

$$\delta_b \equiv 1 - \frac{b}{a^2}, \quad \delta_{d_3} \equiv 1 - \frac{d_3}{a}. \quad (5.32)$$

At large partonic center-of-mass energies, $E \gg m_V$, \mathcal{A}_1 grows like E^2 , while \mathcal{A}_2 and \mathcal{A}_{SM} are constant. The parameter δ_b thus controls the high-energy behaviour of the amplitude and gives a genuine “strong coupling” signature. On the contrary, δ_{d_3} determines the value of the cross section at threshold [64]. In an $e^+ e^-$ collider, $V_L V_L \rightarrow hh$ scatterings can be studied via the processes $e^+ e^- \rightarrow \nu\bar{\nu}hh$ and $e^+ e^- \rightarrow e^+ e^- hh$. The latter, initiated by a partonic ZZ state, has a cross section which is roughly one order of magnitude smaller than the former. This is due in particular to the fact that the $e^\pm \rightarrow Ze^\pm$ splitting function is roughly a factor of 2 smaller than $e^\pm \rightarrow W^\pm \nu$. For this reason we neglect $e^+ e^- \rightarrow e^+ e^- hh$ in the following. The $e^+ e^- \rightarrow \nu\bar{\nu}hh$ cross section can be written as

$$\sigma = a^4 \sigma_{SM} (1 + A \delta_b + B \delta_{d_3} + C \delta_b \delta_{d_3} + D \delta_b^2 + E \delta_{d_3}^2), \quad (5.33)$$

where σ_{SM} denotes its SM value. Notice that a enters only as an overall factor. Without applying any kinematic cut on the Higgs decay products (nor including the branching fraction of Higgs decays) we find, for $\sqrt{s} = 3 \text{ TeV}$,

$$\sigma_{SM} = 0.83 \text{ fb}, \quad \{A, B, C, D, E\} = \{3.83, 0.64, 3.41, 15.6, 0.48\} \quad \left[\begin{array}{c} \sqrt{s} = 3 \text{ TeV} \\ \text{before any cut} \end{array} \right].$$

¹³In the MCHM4 $\delta_b = \xi/(1-\xi)$, $\delta_{d_3} = 0$, while in the MCHM5 $\delta_b = \delta_{d_3} = \xi/(1-\xi)$. See eqs. (3.7), (3.8)

$$(5.34)$$

Notice that although the SM cross section σ_{SM} of the processes $VV \rightarrow VV$ and $VV \rightarrow hh$ differs by more than two orders of magnitude, the energy-growing contributions (given by $\sigma_{SM}B = 27.6 \text{ fb}$ for $VV \rightarrow VV$, see eqs. (5.19) and (5.20), and $\sigma_{SM}D = 12.9 \text{ fb}$ for $VV \rightarrow hh$, see eqs. (5.33) and (5.34)) are of the same size, as required by the $SO(4)$ invariance.

In contrast to $VV \rightarrow VV$ scattering, in the case of double Higgs production simple acceptance and reconstruction cuts keep the background at a negligible level. For our analysis we focus on events where both Higgs bosons in the signal decay to $b\bar{b}$, and select events with four or more jets and at least three b -tags. The most important processes which can fake the signal are then $e^+e^- \rightarrow \nu\bar{\nu}hZ$, $e^+e^- \rightarrow \nu\bar{\nu}ZZ$ and $e^+e^- \rightarrow e^+e^-ZZ$. In all cases the Z boson must decay to a $b\bar{b}$ pair, and in the latter process both electrons have to be missed in the beam pipe. Before cuts we find

$$\begin{aligned}\sigma(e^+e^- \rightarrow hZ\nu\bar{\nu} \rightarrow b\bar{b}b\bar{b}\nu\bar{\nu}) &= 0.88 \text{ fb}, \\ \sigma(e^+e^- \rightarrow ZZ\nu\bar{\nu} \rightarrow b\bar{b}b\bar{b}\nu\bar{\nu}) &= 1.26 \text{ fb}, \\ \sigma(e^+e^- \rightarrow ZZe^+e^- \rightarrow b\bar{b}b\bar{b}e^+e^-) &= 0.58 \text{ fb},\end{aligned}\tag{5.35}$$

which can be compared to the signal cross section in eq. (5.34) after multiplying this latter by the Higgs pair branching fraction $BR(hh \rightarrow b\bar{b}b\bar{b}) \simeq BR(hh \rightarrow b\bar{b}b\bar{b})_{SM} = 0.34$. Further backgrounds, like for example $t\bar{t} \rightarrow b\bar{b}W^+W^- \rightarrow b\bar{b}jjl\nu$, can fake our signal only if one or more light jets are mistagged as b -jets and if extra charged leptons escape into the beam pipe. This is enough suppression to safely ignore them. The backgrounds in eq. (5.35), on the other hand, are largely suppressed, and thus negligible, if the jet energy resolution of the detector is sufficiently good to accurately distinguish a Z from a Higgs boson. This seems to be a valid assumption according to Ref. [51, 207, 208], and in the following we will consequently assume the backgrounds to be negligible.

A simple-minded approach to the extraction of the two parameters δ_b and δ_{d_3} is the following. Let us consider a kinematical variable \mathcal{O} whose value increases with the c.o.m. energy of the $W^+W^- \rightarrow hh$ subprocess. The invariant mass of the two Higgses, m_{hh} , and the sum of their transverse momenta, H_T , are two valid examples for \mathcal{O} . We can divide the set of $e^+e^- \rightarrow \nu\bar{\nu}hh$ events into two categories according to whether $\mathcal{O} < \bar{\mathcal{O}}$ or $\mathcal{O} > \bar{\mathcal{O}}$, where $\bar{\mathcal{O}}$ is some fixed value. The number of observed events in these two categories can be fitted to $\sigma_{<}(\delta_b, \delta_{d_3})$ and $\sigma_{>}(\delta_b, \delta_{d_3})$. Notice that thanks to the cut on \mathcal{O} , $\sigma_{>}(\delta_b, \delta_{d_3})$ will have an enhanced sensitivity to δ_b while $\sigma_{<}(\delta_b, \delta_{d_3})$ is more sensitive to δ_{d_3} .

We thus adopt the above strategy and proceed as follows. We start by selecting events with four or more reconstructed jets. The Higgs candidates are identified from the list of

the four most energetic jets, $j_{1,\dots,4}$, by selecting the pairing $(j_1 j_2, j_3 j_4)$ which minimises the χ^2 function

$$(m_{j_1 j_2} - m_h)^2 + (m_{j_3 j_4} - m_h)^2. \quad (5.36)$$

We impose the following cut on the invariant mass of each of the two Higgs candidates

$$|m_{jj} - m_h| < 15 \text{ GeV}, \quad (5.37)$$

and require that at least three of the jets $j_{1,\dots,4}$ are b -tagged. Events where these requirements are not fulfilled are discarded. We find that the overall efficiency of the identification cuts of eqs. (5.16), (5.17) and (5.37) varies from 20% to roughly 35% when δ_b ranges in the interval $0 - 0.5$, while it is only marginally sensitive to δ_{d_3} . In particular, the energy cut on the jets has an almost constant efficiency (roughly 80%) over the whole parameter space. The variation in the total efficiency comes mainly from the cuts on pseudorapidity and on ΔR . The cut on η disfavours small values of δ_b , since these typically lead to more forward Higgses and consequently more forward b -jets, which in turn have a smaller probability to pass the η cut. The cut on minimum ΔR , eq. (5.16), on the other hand, disfavours large values of δ_b , since these lead to more boosted Higgses and thus more collimated decay products. Finally, the cut in eq. (5.37) has an almost unit efficiency in our parton-level analysis with our assumed energy resolution.

Figure 5.5 shows the distributions of m_{hh} and H_T for some fixed values of the parameters δ_b and δ_{d_3} after the identification cuts. While a single cut on either of these two kinematic variables is sufficient to extract the dependence on δ_b and δ_{d_3} , we found that using both m_{hh} and H_T gives a slightly better sensitivity. We thus consider the four independent kinematical regions

$$\begin{aligned} \text{I : } & m_{hh} > 700 \text{ GeV and } H_T > 400 \text{ GeV}, \\ \text{II : } & m_{hh} > 700 \text{ GeV and } H_T < 400 \text{ GeV}, \\ \text{III : } & m_{hh} < 700 \text{ GeV and } H_T > 400 \text{ GeV}, \\ \text{IV : } & m_{hh} < 700 \text{ GeV and } H_T < 400 \text{ GeV}. \end{aligned} \quad (5.38)$$

Our final results do not crucially depend on the specific choice of the cuts on m_{hh} and H_T . One could in principle optimise them to obtain the best sensitivity on the parameters. We checked, however, that reasonable variations around the values adopted in eq. (5.38) result in small variations of the final results. For each of the kinematic regions (5.38), the signal rate $r \equiv \sigma(e^+ e^- \rightarrow \nu \bar{\nu} hh) \times BR(hh \rightarrow b\bar{b}b\bar{b})$ can be parameterized as follows

$$r = r_{SM} a^4 \left(\frac{BR(b\bar{b})}{BR(b\bar{b})_{SM}} \right)^2 (1 + A_r \delta_b + B_r \delta_{d_3} + C_r \delta_b \delta_{d_3} + D_r \delta_b^2 + E_r \delta_{d_3}^2), \quad (5.39)$$

5.5. Quantitative analysis of $VV \rightarrow VV$ and $VV \rightarrow hh$

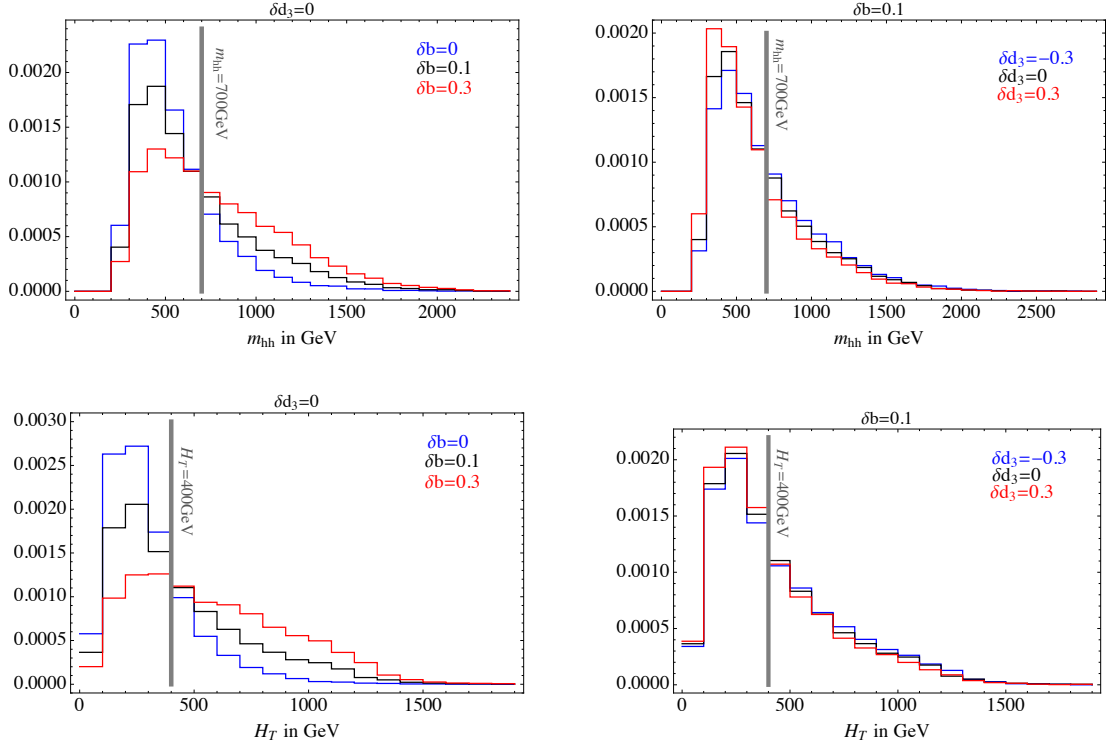


Figure 5.5 – Normalised differential cross sections $d\sigma/dm_{hh}$ and $d\sigma/dH_T$ for $e^+e^- \rightarrow \nu\bar{\nu}hh$ at CLIC with $\sqrt{s} = 3$ TeV after the identification cuts of eqs. (5.17) and (5.37), for several values of δ_b and δ_{d_3} .

where r_{SM} is the SM rate and $BR(b\bar{b})$ is the Higgs branching fraction to $b\bar{b}$. The values of the coefficients A_r, B_r, C_r, D_r, E_r and of r_{SM} are reported in Table 5.4. Figure 5.6 shows the curves of constant rate in the plane (δ_b, δ_{d_3}) for three choices of cuts: only the identification cuts of eqs. (5.17) and (5.37), identification cuts + region I, identification cuts + region IV.

In order to derive the expected sensitivity on δ_b and δ_{d_3} , we construct a Poisson likelihood function (see eq. (5.29)) for each of the kinematical regions of eq. (5.38), and a global likelihood as the product of the individual ones. We assumed a flat prior on δ_b and δ_{d_3} . Since a and the branching ratio $BR(b\bar{b})$ appear in eq. (5.39) as overall factors, they can be conveniently absorbed by rescaling the integrated luminosity L (note that, by the time the study of $VV \rightarrow hh$ will be feasible, both a and $BR(b\bar{b})$ will be known precisely enough through single Higgs processes). The sensitivity on δ_b (δ_{d_3}) is obtained by marginalising the posterior probability over δ_{d_3} (δ_b) and using the resulting single-parameter function to find the 68% probability interval on δ_b (δ_{d_3}).

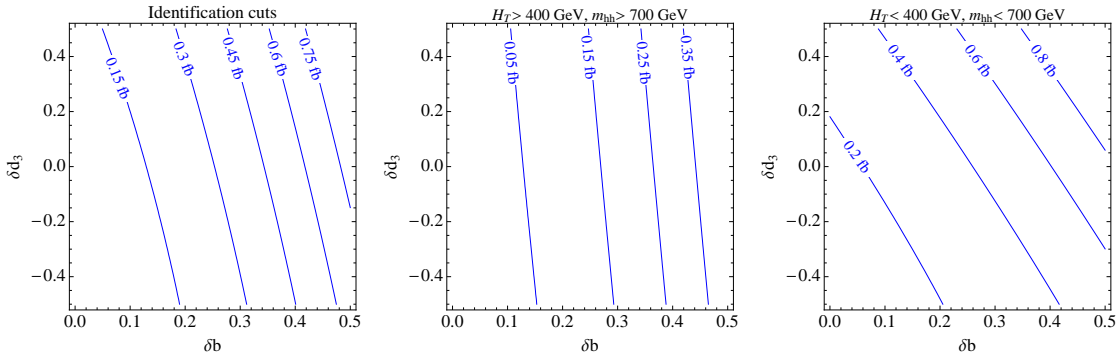
The results for a 3 TeV linear collider with $L = 1 \text{ ab}^{-1}/(a^2 BR(b\bar{b})/BR(b\bar{b})_{SM})^2$ are shown in Tables 5.5 and 5.6.¹⁴ For injected (true) values $(\bar{\delta}_b, \bar{\delta}_{d_3}) = (0, 0)$ we find that the

¹⁴Notice that for small δ_b and large and negative δ_{d_3} , the central value of the measured parameter

Chapter 5. Indirect Probes of NP at Future Colliders

	r_{SM} [ab]	A_r	B_r	C_r	D_r	E_r
I	8.8	15.6	0.88	14.5	164	0.07
II	4.5	3.87	0.30	0.92	4.44	-0.08
III	6.5	9.89	1.25	17.1	55.4	1.54
IV	44	3.95	1.23	5.09	7.3	1.10

Table 5.4 – Fit of the $e^+e^- \rightarrow hh(\rightarrow b\bar{b}b\bar{b})\nu\bar{\nu}$ rate (see eq. (5.39)) at CLIC with $\sqrt{s} = 3$ TeV in the various kinematical regions defined in eq. (5.38).



5.5. Quantitative analysis of $VV \rightarrow VV$ and $VV \rightarrow hh$

measured δ_{d_3}	$\bar{\delta}_{d_3}$						
	-0.5	-0.3	-0.1	0	0.1	0.3	0.5
0	$-0.50^{+0.35}_{-0.25}$	$-0.25^{+0.20}_{-0.50}$	$0.00^{+0.25}_{-0.40}$	$0.05^{+0.30}_{-0.30}$	$0.10^{+0.25}_{-0.20}$	$0.30^{+0.20}_{-0.15}$	$0.50^{+0.15}_{-0.15}$
0.01	$-0.45^{+0.35}_{-0.30}$	$-0.20^{+0.30}_{-0.55}$	$-0.05^{+0.30}_{-0.30}$	$0.00^{+0.25}_{-0.25}$	$0.10^{+0.20}_{-0.20}$	$0.30^{+0.15}_{-0.15}$	$0.50^{+0.15}_{-0.15}$
$\bar{\delta}_b$ 0.02	$-0.35^{+0.30}_{-0.35}$	$-0.25^{+0.25}_{-0.60}$	$-0.10^{+0.25}_{-0.30}$	$0.00^{+0.20}_{-0.25}$	$0.10^{+0.15}_{-0.20}$	$0.30^{+0.15}_{-0.15}$	$0.50^{+0.15}_{-0.15}$
0.03	$-0.40^{+0.30}_{-0.35}$	$-0.25^{+0.20}_{-0.70}$	$-0.10^{+0.20}_{-0.25}$	$0.00^{+0.15}_{-0.20}$	$0.10^{+0.15}_{-0.20}$	$0.30^{+0.15}_{-0.15}$	$0.50^{+0.15}_{-0.15}$
0.05	$-0.55^{+0.30}_{-0.40}$	$-0.30^{+0.20}_{-0.30}$	$-0.10^{+0.20}_{-0.20}$	$0.00^{+0.15}_{-0.20}$	$0.10^{+0.15}_{-0.15}$	$0.30^{+0.15}_{-0.15}$	$0.50^{+0.10}_{-0.10}$
0.1	$-0.50^{+0.15}_{-0.25}$	$-0.30^{+0.15}_{-0.20}$	$-0.10^{+0.20}_{-0.20}$	$0.00^{+0.15}_{-0.15}$	$0.10^{+0.15}_{-0.15}$	$0.30^{+0.10}_{-0.10}$	$0.50^{+0.10}_{-0.10}$
0.3	$-0.50^{+0.15}_{-0.15}$	$-0.30^{+0.15}_{-0.15}$	$-0.10^{+0.10}_{-0.10}$	$0.00^{+0.10}_{-0.10}$	$0.10^{+0.10}_{-0.10}$	$0.30^{+0.10}_{-0.10}$	$0.50^{+0.10}_{-0.10}$
0.5	$-0.50^{+0.15}_{-0.10}$	$-0.30^{+0.10}_{-0.10}$	$-0.10^{+0.10}_{-0.10}$	$0.00^{+0.10}_{-0.10}$	$0.10^{+0.10}_{-0.10}$	$0.30^{+0.10}_{-0.10}$	$0.50^{+0.10}_{-0.10}$

Table 5.6 – Expected precision on δ_{d_3} for different true values $\bar{\delta}_b$ and $\bar{\delta}_{d_3}$ obtained at CLIC with $\sqrt{s} = 3 \text{ TeV}$ and $L = 1 \text{ ab}^{-1}/(a^2 BR(b\bar{b})/BR(b\bar{b})_{SM})^2$ through $VV \rightarrow hh$ scattering.

68% error on δ_{d_3} is equal to ~ 0.3 (see Table 5.6), which means that a measurement of the Higgs trilinear coupling in the SM should be possible with a precision of $\sim 30\%$ with $L = 1 \text{ ab}^{-1}$. This has to be compared with the 16% and 20% precisions reported respectively in Ref. [253] and in the third paper of Ref. [51, 207, 208] for 2 ab^{-1} of integrated luminosity and unpolarised beams. For injected $(\bar{\delta}_b, \bar{\delta}_{d_3}) = (0, 0)$ we also find that the precision attainable on δ_b with $L = 1 \text{ ab}^{-1}$ is $\sim 5\%$ (see Table 5.5), which is compatible with the 3% recently reported for $L = 2 \text{ ab}^{-1}$ by Ref. [253].

The results of Tables 5.5 and 5.6 have been obtained by considering a , b and d_3 as independent parameters. Alternatively, by assuming them to be related as in eqs. (3.7) and (3.8) for the $SO(5)/SO(4)$ model MCHM4 (where $BR(b\bar{b}) = BR(b\bar{b})_{SM}$), one can optimise the analysis to extract ξ . We do so by applying, besides the identification cuts of eqs. (5.17) and (5.37), a single cut on H_T to isolate the energy growing behaviour. Since we need to fit a single parameter, we select events with $H_T > 400 \text{ GeV}$. The corresponding efficiencies are reported in Table 5.7. Larger values of ξ give larger efficiencies for the identification cuts, as mainly due to the stronger boost of the Higgses, as previously discussed. The signal rate can be parameterized in this case as follows

$$r(\xi) = r_{SM} (1 + A_r \xi + B_r \xi^2) . \quad (5.40)$$

The SM rate r_{SM} and the coefficients A_r , B_r are reported in Table 5.8. In order to estimate the sensitivity on ξ that can be reached at CLIC, for any given true value ξ we construct a posterior probability (see eqs. (5.28) and (5.29)) by assuming a prior on ξ which is flat in the theoretically allowed range $[0, 1]$ and vanishing outside. The results

sometimes does not coincide with the true value. This is because in this limit, for our choice of integrated luminosity, the 2D likelihood can be largely non-gaussian and its marginalization over one parameter can lead to a shift of the central value of the second one.

	All $\times[H_T > 400 \text{ GeV}]$	No $\eta\times[H_T > 400 \text{ GeV}]$	No $\Delta R\times[H_T > 400 \text{ GeV}]$
$\xi = 0$	0.07=0.28 \times 0.24	0.10=0.90 \times 0.11	0.08=0.30 \times 0.26
$\xi = 0.1$	0.15=0.35 \times 0.44	0.20=0.89 \times 0.23	0.18=0.39 \times 0.46
$\xi = 0.5$	0.42=0.55 \times 0.77	0.50=0.81 \times 0.62	0.54=0.65 \times 0.83

Table 5.7 – Efficiencies of the kinematic cuts imposed on the $e^+e^- \rightarrow \nu\bar{\nu}hh$ signal events to extract the parameter ξ at CLIC with $\sqrt{s} = 3 \text{ TeV}$. The format is $A = B \times C$, where B is the efficiency for the identification cuts of eqs. (5.17) and (5.37), and C is the efficiency of the cut $H_T > 400 \text{ GeV}$ on the reconstructed Higgses.

	$r_{SM} \text{ [ab]}$	A_r	B_r
All cuts	15	11	106
No H_T	63	4.1	28.3
No η	23	10.5	76.9
No ΔR	17	11	118

Table 5.8 – Fit of the $e^+e^- \rightarrow hh(\rightarrow b\bar{b}b\bar{b})\nu\bar{\nu}$ in the MCHM4 (see eq. (5.40)) at CLIC with $\sqrt{s} = 3 \text{ TeV}$. The numbers in the second row have been obtained by applying the whole set of kinematic cuts described in the text (eqs. (5.17), (5.37) and the cut on H_T), while each of the last three rows is obtained by removing one the cuts.

are shown in Table 5.9 for $L = 1 \text{ ab}^{-1}$.

The results obtained in this section can be translated into an estimate of the sensitivity of CLIC on the scale of compositeness. In the presence of a shift in the Higgs couplings, $\delta_h \sim (v/f)^2$, the low-energy theory becomes strongly coupled at the scale $\Lambda = 4\pi f \sim 4\pi v/\sqrt{\delta_h}$ unless New Physics states set in at a scale $m_\rho < \Lambda$, expectedly freezing the growth of the coupling at $g_\rho \sim m_\rho/f < 4\pi$. From Tables 5.5 and 5.9 we conclude that the study of double-Higgs production at CLIC with 3 TeV can lead to a sensitivity on Λ of the order of $\sim 15 - 20 \text{ TeV}$ with an accumulated luminosity of 1 ab^{-1} . This has to be compared with sensitivities of the order of $\sim 10 \text{ TeV}$ and $\sim 30 - 40 \text{ TeV}$ expected from the study of single-Higgs processes respectively at the 14 TeV LHC with 300 fb^{-1} [223, 224] and at the ILC with 250 fb^{-1} of luminosity accumulated at $\sqrt{s} = 250 \text{ GeV}$ plus another 500 fb^{-1} at $\sqrt{s} = 500 \text{ GeV}$ [50, 254–256]. Table 5.13 summarises the reach on the compositeness scale at various experiments from the study of single and double Higgs processes.

5.5.4 Double Higgs-strahlung

The cross section for double Higgs production through WW fusion drops as the energy of the collider is lowered: in the SM it goes from 1 fb for $\sqrt{s} = 3 \text{ TeV}$ down to 0.01 fb for $\sqrt{s} = 500 \text{ GeV}$. At such low energies one has to resort to other processes in order to measure the anomalous Higgs couplings δ_b and δ_{d_3} . One possibility is double Higgs-

5.5. Quantitative analysis of $VV \rightarrow VV$ and $VV \rightarrow hh$

	$\bar{\xi}$					
	0	0.02	0.05	0.1	0.2	0.5
All cuts (68%)	$0_{-0}^{+0.020}$	$0.02_{-0.015}^{+0.015}$	$0.05_{-0.015}^{+0.015}$	$0.1_{-0.015}^{+0.015}$	$0.2_{-0.015}^{+0.015}$	$0.5_{-0.015}^{+0.010}$
No H_T	$0_{-0}^{+0.025}$	$0.02_{-0.020}^{+0.015}$	$0.05_{-0.020}^{+0.020}$	$0.1_{-0.015}^{+0.015}$	$0.2_{-0.015}^{+0.015}$	$0.5_{-0.015}^{+0.010}$
No η	$0_{-0}^{+0.015}$	$0.02_{-0.015}^{+0.015}$	$0.05_{-0.015}^{+0.015}$	$0.1_{-0.015}^{+0.015}$	$0.2_{-0.015}^{+0.010}$	$0.5_{-0.010}^{+0.010}$
No ΔR	$0_{-0}^{+0.020}$	$0.02_{-0.015}^{+0.015}$	$0.05_{-0.015}^{+0.015}$	$0.1_{-0.015}^{+0.015}$	$0.2_{-0.010}^{+0.010}$	$0.5_{-0.010}^{+0.010}$
All cuts (95%)	$0_{-0}^{+0.040}$	$0.02_{-0.02}^{+0.03}$	$0.05_{-0.03}^{+0.03}$	$0.1_{-0.03}^{+0.03}$	$0.2_{-0.03}^{+0.03}$	$0.5_{-0.03}^{+0.02}$

Table 5.9 – Expected 68% (first four lines) and 95% (last line) probability intervals on ξ for different true values $\bar{\xi}$ obtained at CLIC with $\sqrt{s} = 3$ TeV and $L = 1 \text{ ab}^{-1}$ through $VV \rightarrow hh$ scattering.

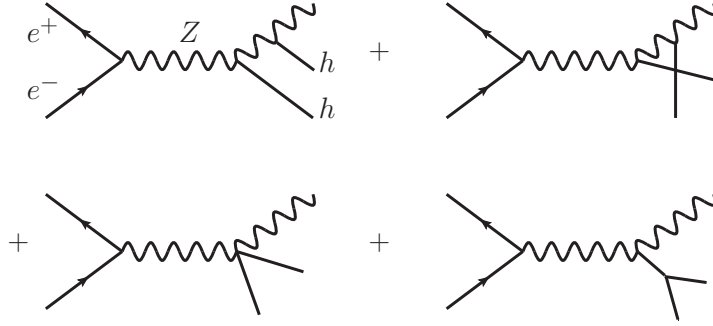


Figure 5.7 – Diagrams contributing to double Higgs-strahlung at an e^+e^- collider. The two diagrams in the upper row are proportional to a^2 , while the first and second diagrams in the lower row are proportional respectively to b and ad_3 .

strahlung (DHS), $e^+e^- \rightarrow hhZ$ [267–271]. The relevant Feynman diagrams are shown in Fig. 5.7, and the analytic expression of the differential cross section is known (see Appendix C.2). Figure 5.8 shows the value of the total cross section as a function of the e^+e^- center-of-mass energy for some values of δ_b and δ_{d_3} . For $\delta_b = 0$ the cross section drops as $1/s$ at high energy, while it asymptotically approaches a constant value for $\delta_b \neq 0$. This different high-energy behaviour is due to the $e^+e^- \rightarrow hhZ_L$ amplitude and can be easily derived by using the equivalence theorem (see Appendix C.2). Notice that for $m_h = 125 \text{ GeV}$ the cross section is maximal between 500 GeV and 1 TeV.

Before decaying the Higgs bosons, the DHS total cross section can also be parameterized as in eq. (5.33). By using the analytic expressions given in Appendix C.2, we find the coefficients reported in Table 5.10. In Fig. 5.9 we compare the invariant mass distributions of the two Higgses at $\sqrt{s} = 500 \text{ GeV}$ and $\sqrt{s} = 1 \text{ TeV}$ for various values of the parameters. ¹⁵

¹⁵ The enhancement of the cross section at $m_{hh} \sim \sqrt{s}$ is due to the infrared singularity associated with

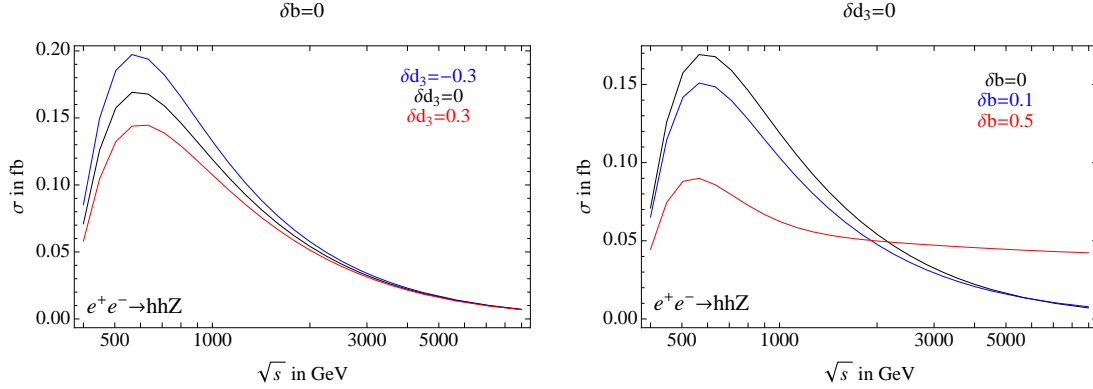


Figure 5.8 – Total cross section of double Higgs-strahlung, $e^+e^- \rightarrow hhZ$, as a function of the c.o.m energy for several values of the parameters δ_b and δ_{d_3} .

$e^+e^- \rightarrow hhZ$	σ_{SM} [fb]	A	B	C	D	E
500 GeV	0.16	-1.02	-0.56	0.31	0.28	0.10
1 TeV	0.12	-1.42	-0.35	0.48	0.93	0.91
1 TeV ($m_{hh} < 500$)	0.03	-2.45	-1.02	1.42	1.85	0.33
1 TeV ($m_{hh} > 500$)	0.09	-3.15	-0.36	0.48	1.83	0.03

Table 5.10 – Parameterization of the double Higgsstrahlung $e^+e^- \rightarrow hhZ$ cross section (see eq. (5.33)) for various center-of-mass energies and cuts on the invariant mass of the two Higgses. The coefficients in the Table have been computed by using the analytic expressions given in Appendix C.2. Decay branching fractions and reconstruction efficiencies are not included.

Our strategy to extract the anomalous couplings in this section differs in part from the one employed to analyse WW scattering. In the case of DHS, at the energies we are interested in, the efficiency of the identification and reconstruction cuts is practically insensitive to the value of the Higgs couplings. The final rate can then be obtained by starting from the analytical expression of the cross section in terms of the parameters δ_b and δ_{d_3} given in eq. (5.33) and Table 5.10, and rescaling the value of σ_{SM} by an overall efficiency factor to include the decay branching fractions and the effect of kinematic cuts. We extracted such efficiency factor by generating a single sample of events corresponding to the SM choice of parameters. Such simplified approach fully exploits the analytic expression of the DHS cross section and greatly reduces the complexity of the Monte Carlo simulation.

The analysis of DHS turns out to be more difficult than the one of double Higgs production via WW fusion due to the presence of non-negligible background processes. We focus on final states where both Higgses decay to $b\bar{b}$ and the Z decays either hadronically or to a pair of charged leptons. We thus select events with 6 or more jets (and no

the soft emission of a transversely-polarised Z in the diagrams in the first row of Fig. 5.7. The energy of the Z boson, E_3 , is related to the invariant mass of the two Higgses by the formula $m_{hh}^2/s = 1 - 2E_3/\sqrt{s} + m_Z^2/s$. In the limit $E_3 \rightarrow 0$ it then follows $m_{hh} \rightarrow \sqrt{s}(1 + O(m_Z^2/s))$. See Appendix C.2 for more details.

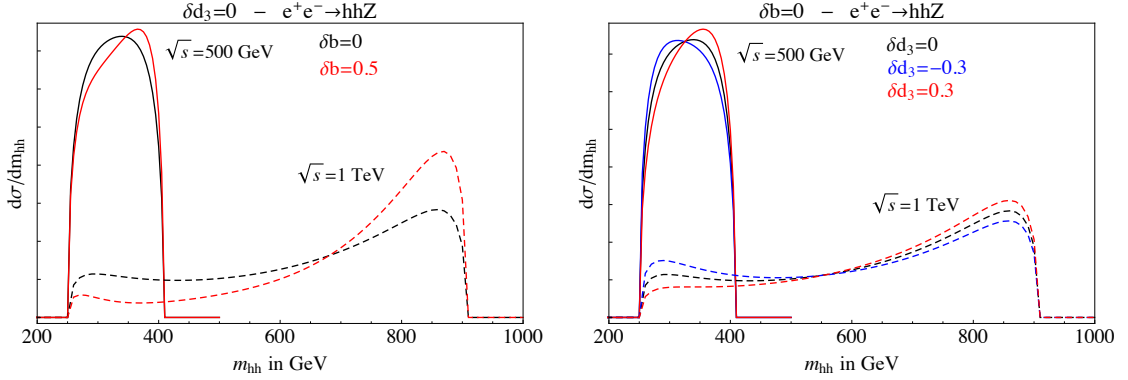


Figure 5.9 – Differential cross section $d\sigma/dm_{hh}$ of double Higgsstrahlung at a linear collider with $\sqrt{s} = 500$ GeV (solid lines) and $\sqrt{s} = 1$ TeV (dashed lines), for several values of δ_b and δ_{d_3} . All distributions have been normalized to unit area.

lepton), or with 4 or more jets plus 2 opposite-charge leptons (electrons or muons). Jets and leptons are reconstructed according to the criteria defined in eqs. (5.17) and (5.18). Our selection ensures a full reconstruction of the momentum of the Z boson in signal events and consequently a substantial reduction of background contamination. As a final discrimination we require at least 3 of the jets in the event to be b -tagged.

The reconstruction of the Higgs and Z candidates proceeds as follows. In the case of events with 4 or more jets and 2 leptons, the Z is reconstructed from the lepton pair, while the two Higgs candidates are identified as done in the case of $WW \rightarrow hh$, see section 5.5.3. We impose the following cut on the invariant mass of the lepton pair

$$|m_{ll} - m_Z| < 10 \text{ GeV}, \quad (5.41)$$

while the invariant masses of the Higgs candidates are required to satisfy eq. (5.37). Events which do not satisfy these cuts are rejected. In the case of fully hadronic events, the Higgs and Z candidates are reconstructed from the six most energetic jets, $j_{1,\dots,6}$, by identifying the pairing (j_1j_2, j_3j_4, j_5j_6) that minimises the χ^2 function

$$(m_{j_1j_2} - m_h)^2 + (m_{j_3j_4} - m_h)^2 + (m_{j_5j_6} - m_Z)^2. \quad (5.42)$$

We focus only on pairings where at least three among the four jets $j_{1\dots 4}$ are b -tagged, discarding the other pairings. This implies the presence of at least 3 b -tags in the decay products of the two reconstructed Higgs bosons. After the Higgs $(j_1j_2$ and $j_3j_4)$ and Z (j_5j_6) candidates have been reconstructed, we impose a cut

$$|m_{j_5j_6} - m_Z| < 10 \text{ GeV} \quad (5.43)$$

on the invariant mass of the Z candidate, and the cut of eq. (5.37) on the invariant mass of each of the two Higgs candidates. Events where these requirements are not fulfilled are rejected. This algorithm has a fake rate (i.e. the rate at which it reconstructs fake

	Energy	Efficiency	r_{SM} [ab]
$hhZ \rightarrow b\bar{b}b\bar{b}jj$	500 GeV	0.56	21
	1 TeV-I	0.50	3.5
	1 TeV-II	0.50	10.2
$hhZ \rightarrow b\bar{b}b\bar{b}\ell\ell$	500 GeV	0.58	2.2
	1 TeV-I	0.56	0.34
	1 TeV-II	0.56	1.0

Table 5.11 – Efficiencies for the identification of the Higgs and Z candidates in the DHS signal at 500 GeV and 1 TeV (for both regions I and II of eq. (5.44)) for the two final states discussed in the analysis. The variation of the efficiency with the parameters δ_b and δ_{d_3} is negligible. The last column reports the SM rate after the identification cuts, r_{SM} , as defined in eq. (5.39).

Higgs or Z candidates) always below 5% in the case of fully-hadronic events, and even smaller in the case of events with two leptons. The identification efficiencies on the signal at $\sqrt{s} = 500$ GeV and 1 TeV are given in Table 5.11 for each of the two final states under consideration. They are to a large extent constant upon variations of δ_b and δ_{d_3} . The signal rate $r(\delta_b, \delta_{d_3})$ can be thus parameterized as in eq. (5.39) with coefficients A_r, B_r, C_r, D_r, E_r equal to the A, B, C, D, E given in Table 5.10, and an overall factor r_{SM} fully subsuming the reconstruction efficiency and the decay branching fraction.

At a center-of-mass energy of 500 GeV, the signal rate is mostly dominated by events at the kinematical threshold. Disentangling the effect of δ_b from that of δ_{d_3} by means of kinematic cuts does not seem possible (at least for reasonable values of integrated luminosity). A measurement of the total cross section gives nevertheless the possibility to constrain a combination of the two relevant parameters δ_b and δ_{d_3} . At the higher center-of-mass energy $\sqrt{s} = 1$ TeV, a better determination of both parameters is possible by cutting on the invariant mass of the two Higgs bosons. We define the two kinematical regions

$$\begin{aligned} \text{I : } & m_{hh} > 500 \text{ GeV}, \\ \text{II : } & m_{hh} < 500 \text{ GeV}. \end{aligned} \tag{5.44}$$

The signal rate in each region and for each of the two final states (leptonic and fully hadronic) is obtained by multiplying the cross section by the decay branching fraction and an overall reconstruction efficiency.¹⁶ The value of the SM rate r_{SM} for each of the event categories at $\sqrt{s} = 500$ GeV and 1 TeV is reported in Table 5.11.

As previously mentioned, a crucial difference between DHS and double Higgs production

¹⁶Notice that in order for this procedure to be accurate it is crucial that the fake-rate of our algorithm for the reconstruction of the Higgs and Z candidates is very small. If this was not the case, the measured invariant mass distribution of the Higgs pair could be affected by the reconstruction and this would invalidate our procedure.

5.5. Quantitative analysis of $VV \rightarrow VV$ and $VV \rightarrow hh$

	scaling with a	Rate		
		500 GeV	1 TeV-I	1 TeV-II
$b\bar{b}b\bar{b}jj$	a^0	$r_b^{(0)} = 20 \text{ ab}$	$r_b^{(0)} = 1.4 \text{ ab}$	$r_b^{(0)} = 3.1 \text{ ab}$
$hb\bar{b}jj$	a^2	$r_b^{(1)} = 5.5 \text{ ab}$	$r_b^{(1)} = 0.4 \text{ ab}$	$r_b^{(1)} = 0.3 \text{ ab}$
$b\bar{b}b\bar{b}\ell\ell$	a^0	$r_b^{(0)} = 0.2 \text{ ab}$	$r_b^{(0)} = 0.05 \text{ ab}$	$r_b^{(0)} = 0.01 \text{ ab}$

Table 5.12 – Rates after identification and reconstruction cuts for the backgrounds included in our double Higgs-strahlung analysis at $\sqrt{s} = 500 \text{ GeV}$ and 1 TeV (for both regions I and II of eq. (5.44)). The leptonic background $hb\bar{b}\ell\ell$ is negligible.

via vector boson fusion is the presence of background processes that cannot be neglected. They can be classified according to their scaling with the parameter a , which sets the strength of the hVV coupling. The powers of a thus control the number of external Higgs boson legs. Notice that up to effects of order Γ/m the interference between amplitudes with a different number of on-shell Higgs boson legs is negligible. Under this assumption, each factor a^2 is accompanied by one power of the Higgs decay branching ratio to $b\bar{b}$. The total rate can thus be parameterized as follows:

$$r_{tot}(\delta_b, \delta_{d_3}) = r_b^{(0)} + a^2 \frac{BR(b\bar{b})}{BR(b\bar{b})_{SM}} r_b^{(1)} + a^4 \left(\frac{BR(b\bar{b})}{BR(b\bar{b})_{SM}} \right)^2 r(\delta_b, \delta_{d_3}), \quad (5.45)$$

where $r^{(0)}$ and $r^{(1)}$ are the rates for background processes respectively with 0 and 1 Higgs boson. Simple inspection of eq. (5.45) shows that in this case our results will depend in a non-trivial way on three quantities: $a^2(BR(b\bar{b})/BR(b\bar{b})_{SM})$, δ_b and δ_{d_3} . The backgrounds included in our analysis are listed in Table 5.12, together with their rate after applying the same reconstruction algorithm adopted for the signal.

We derive the expected sensitivity on δ_b and δ_{d_3} by assuming a flat prior on these coupling shifts and constructing a Poissonian likelihood function for each event category: two categories for a $\sqrt{s} = 500 \text{ GeV}$ collider (the leptonic and fully hadronic final states); four categories for a $\sqrt{s} = 1 \text{ TeV}$ collider (two kinematic regions for each of the two final states). In each case, the total likelihood is obtained by taking the product of the individual ones. In general, we find that the fully hadronic final states lead to a better sensitivity on the couplings than the leptonic ones. As a way to effectively take into account the systematic and theoretical uncertainties on the estimate of the background in our statistical analysis, we have rescaled all the background rates by a factor 1.5 compared to the MC predictions reported in Table 5.12.

Figure 5.10 shows the regions of 68% probability obtained in the plane (δ_b, δ_{d_3}) with $L = 1 \text{ ab}^{-1}$ by setting $a^2(BR(b\bar{b})/BR(b\bar{b})_{SM}) = 0.81$ (left plot) and $a^2(BR(b\bar{b})/BR(b\bar{b})_{SM}) = 1$ (right plot). The various contours are relative to the following two benchmark points: $(\delta_b, \delta_{d_3}) = (0, 0)$ (in blue), and $(\delta_b, \delta_{d_3}) = (0.25, 0.25)$ (in red). The latter point is obtained

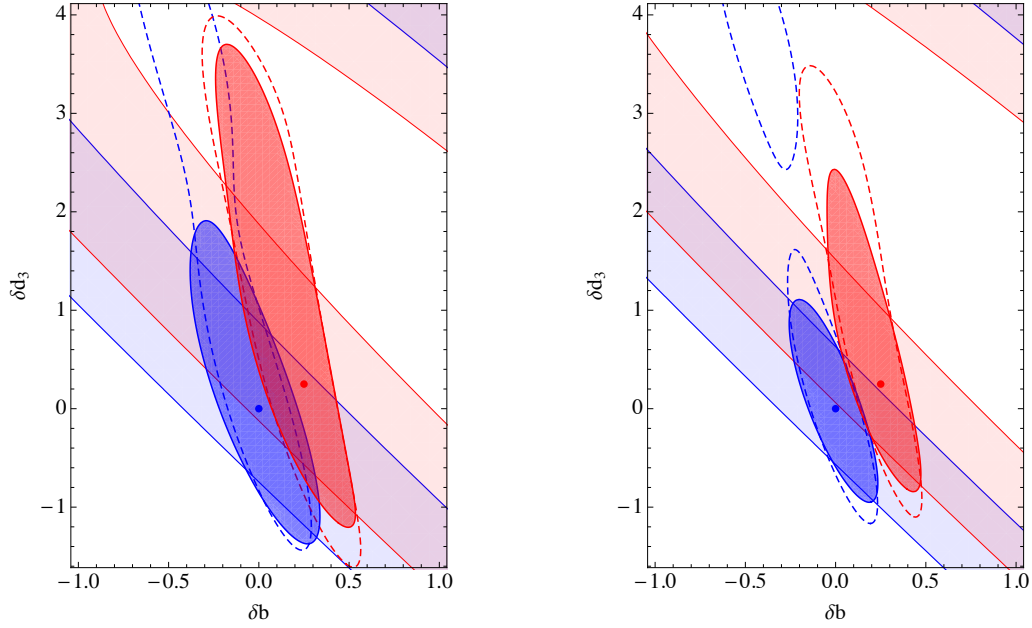


Figure 5.10 – Regions of 68% probability in the plane (δ_b, δ_{d_3}) obtained from the analysis of double Higgs-strahlung at various collider energies. Blue (red) shapes and contours are relative to the case of injected values $\bar{\delta}_b = 0$, $\bar{\delta}_{d_3} = 0$ ($\bar{\delta}_b = 0.25$, $\bar{\delta}_{d_3} = 0.25$). Lighter shaded bands: 500 GeV; Dashed contours: 1 TeV; Darker shaded regions: 500 GeV + 1 TeV. The plots have been obtained by assuming an integrated luminosity $L = 1 \text{ ab}^{-1}$ and setting $a^2(BR(b\bar{b})/BR(b\bar{b})_{SM}) = 0.81$ (left plot) and $a^2(BR(b\bar{b})/BR(b\bar{b})_{SM}) = 1$ (right plot).

in the $SO(4)/SO(5)$ MCHM5 for $\xi = 0.2$, see eqs. (3.7), (3.8). The bands in light (red and blue) colour indicate the result obtainable by measuring just the total cross section at a 500 GeV collider. The red and blue dashed curves show instead the precision achievable at a linear collider with 1 TeV c.o.m. energy by exploiting the cut on m_{hh} . If measurements at both 500 GeV and 1 TeV c.o.m. energies are possible (each with an integrated luminosity $L = 1 \text{ ab}^{-1}$), an even more accurate precision on the couplings can be reached. The corresponding 68% regions are shown in darker (red and blue) colour in Fig. 5.10.

An estimate of the precision attainable on the Higgs trilinear coupling at the ILC has been recently derived in Ref. [50] assuming $a = 1$, $b = 1$. It is found that for $\sqrt{s} = 500 \text{ GeV}$ and with an integrated luminosity $L = 500 \text{ fb}^{-1}$, d_3 can be measured with a precision of 104% through DHS. At $\sqrt{s} = 1 \text{ TeV}$ with $L = 1 \text{ ab}^{-1}$, Ref. [50] cites a precision of 28% through $VV \rightarrow hh$ scattering, while DHS is found to be less powerful. This suggests that a substantial improvement of our results can be obtained by including double Higgs production via vector boson fusion at $\sqrt{s} = 1 \text{ TeV}$ into the analysis. Another recent study appeared in Ref. [272] whose approach is more similar to the one presented in this chapter. The couplings b and d_3 are extracted through the measurement of the total DHS cross section at 500 GeV and 1 TeV (with no cut on m_{hh} applied), and on double Higgs production through VV fusion at 1 TeV. In the case of DHS, all the final states $Z \rightarrow \ell\ell, \nu\bar{\nu}, jj$ were included. We find that, although we did not include $VV \rightarrow hh$ and

the $\nu\bar{\nu}$ final state in DHS, our analysis gives a better precision on the couplings d_3 and b for those benchmark points where a comparison can be performed.

5.6 Conclusions

The observation of a resonance with a mass around 125 GeV and properties remarkably compatible with those of the Standard Model Higgs boson makes the questions about the dynamics at the origin of electroweak symmetry breaking more pressing. The most relevant and urgent issue now facing us concerns the structure of the newly discovered (Higgs) scalar. Are there additional states accompanying it? Is it elementary or is it composite? Could this really be the first elementary scalar observed in Nature, or could it just be a bound state arising from some novel strong dynamics, like a π or η in QCD? The answer to these questions will have profound implications on our picture of fundamental physics. That is because of the hierarchy problem. Establishing, to the best of our experimental capability, that the Higgs boson is elementary, weakly coupled and solitary, would surely be shocking, but it may well start a revolution in the basic concepts of quantum mechanics and space-time. If instead deviations from the SM will emerge in the dynamics of the Higgs, we will have to use them as a diagnostic tool of the underlying dynamics. A crucial part of this program is the identification of the smoking guns of compositeness in Higgs dynamics. Moreover, along this basic question there are more specific ones we can ask, related to the symmetry properties of the new state. For instance, it will be essential to establish whether the new scalar is indeed “a Higgs” fitting into an $SU(2)$ doublet and not some exotic impostor, like for instance a pseudo-dilaton. Although there is really no strong theoretical motivation for such an alternative, and so far the data disfavour it, it remains a logical possibility that can be tested and possibly ruled out. A perhaps more interesting question is whether the Higgs particle is just an ordinary composite, like a σ , or whether it is a pseudo-Nambu–Goldstone boson, like the π . The answer to this question will give us important clues on the UV completion of the electroweak breaking dynamics.

It is well known that in a fully natural theory of electroweak symmetry breaking the Higgs couplings must deviate, even in a significant way, from the predictions of the Standard Model. Note, however, that past and current experiments already put stringent constraints on these deviations, specifically on the single-Higgs hVV coupling a , while the quadratic h^2VV coupling b and the Higgs cubic self-coupling d_3 so far remain unconstrained. Thanks to finally precise knowledge of the Higgs mass and to a more accurate measurement of the W mass, the Higgs coupling a is now constrained to lie with 95% probability in the interval $0.98 \leq a^2 \leq 1.12$ under the assumption of no further contribution from New Physics. The tension with the theoretically motivated range $a < 1$ can be slightly lifted by including an extra positive contribution to $\Delta\hat{T}$ in the electroweak fit, as it can arise in explicit models. Assuming $\Delta\hat{T} = +1.5 \times 10^{-3}$ leads to an interval $0.70 \leq a^2 \leq 0.92$. Important constraints are also set by direct searches for spin-1 resonances at the LHC,

which start to exclude interesting portions of the parameter space. Direct Higgs coupling measurements at the LHC, on the other hand, still have a limited precision but they are expected to reach a $\sim 5\%$ resolution on a at the 14 TeV LHC.

In this chapter we laid down a strategy to infer information about the scale and the nature of the dynamics behind EWSB through a precise measurement of the Higgs couplings. Observing a shift in the Higgs couplings of order δ_h in single-Higgs processes, together with the absence of any other new degree of freedom below a scale M , puts a qualitative lower bound on the strength of the interaction within the New Physics sector, $g_\rho > \sqrt{\delta_h} \times M/v$. This could provide a first indirect evidence for strong dynamics at the origin of EWSB and a hint towards a composite nature of the Higgs boson. For instance, $O(10\%)$ deviations without any new states below 2 TeV, would already correspond to a coupling exceeding all the SM interactions in strength. Qualitatively, an analogous lower bound on g_ρ can be obtained from the observation of an enhanced amplitude for the scattering of massive gauge bosons. Indeed, as we point out in section 5.3, at an electron-positron collider, the precision of the measurements could in principle allow us to estimate the size of subleading terms in the growth of the amplitude, thus providing a stronger indirect bound on the strength of the coupling.

Multi-Higgs production can bring additional valuable information to characterise the strong sector, even if it does not provide stronger bounds on its coupling strength or its scale. Double Higgs production by vector boson fusion gives access to the linear and quadratic couplings of the Higgs to the electroweak gauge bosons. We established a *universal* relation among these couplings, valid at order v^2/f^2 (where the scale f is defined by $f = m_\rho/g_\rho$ for a generic composite state and corresponds to the decay constant for a pNGB), that follows when the Higgs boson is part of an electroweak doublet. This is because a single operator of dimension-6 controls the leading corrections to both scattering amplitudes and single Higgs couplings. Furthermore, we studied the corrections to this relation that arise at order v^4/f^4 from dimension-8 operators and we demonstrated that they can distinguish scenarios with a pNGB Higgs from those where the discovered boson is a generic light scalar resonance of the strong dynamics. The reason for this non-trivial result, is that, in the case of a pNGB Higgs, the non-linearly realised symmetry relates operators of different dimension.

We also emphasised the importance of a precise and energetic lepton collider such as CLIC to study the rare process of triple Higgs production through vector boson fusion, $VV \rightarrow hhh$. For a generic composite Higgs, the leading expected growing behaviour of the cross section below the scale of the resonances is $\sim v^2 s^2/f^8$ and could in principle be observed provided $v^2/f^2 \sim 0.1$. However we pointed out that for a pNGB Higgs based on cosets involving only doublets, in particular in the simplest cases of $SO(5)/SO(4)$ or $SO(4,1)/SO(4)$, this leading term exactly cancels. This cancellation is a simple consequence of the homogeneity and of the grading symmetry of such cosets, but in the effective Lagrangian it corresponds to a more obscure correlation among the coefficients

of operators of dimension 6 and dimension 8. This is the same correlation we mentioned before. The observation, or lack thereof, of a visible rate for $VV \rightarrow hhh$ could then play a relevant role in the reconstruction of the underlying theory.

We presented a quantitative analysis of vector boson scattering and double Higgs production, both through vector boson fusion and double Higgs-strahlung, at the ILC and CLIC for two different center-of-mass energies. Focusing on $VV \rightarrow VV$ scattering processes and using a simple cut-and-count analysis, we found that a $\sqrt{s} = 500$ GeV linear collider with an integrated luminosity of 1 ab^{-1} is only sensitive to large deviations of the coupling a from its SM value, $\Delta a^2 \sim 0.5$ (see footnote 12 for the definition of sensitivity used in this chapter). A 3 TeV linear collider with the same luminosity, on the other hand, is sensitive to shifts in a^2 larger than ~ 0.2 . Double Higgs production depends both on a and on the couplings b and d_3 . Its cross section can be conveniently expressed in terms of the two shifts $\delta_b \equiv 1 - b/a^2$ and $\delta_{d_3} \equiv 1 - d_3/a$, while the parameter a enters as a simple overall rescaling which can be absorbed in the value of the luminosity (note that, at the time of the studies we are proposing, a will be known with good accuracy thanks to single Higgs processes, hence δ_b and δ_{d_3} will really measure the deviations in the b and d_3 couplings). As it emerges clearly throughout our study, δ_b offers a more sensitive probe into the Higgs structure than the trilinear δ_{d_3} . In the case of a 3 TeV CLIC machine with $L = 1 \text{ ab}^{-1}$, the study of $VV \rightarrow hh$ offers a sensitivity of about 0.05 on δ_b while that on δ_{d_3} is hardly better than 0.3. In a specific model like the Minimal Composite Higgs model the couplings a , b and d_3 depend on the single parameter $\xi = (v/f)^2$. Through the study of $e^+e^- \rightarrow hh\nu\bar{\nu}$, a machine like CLIC with $\sqrt{s} = 3 \text{ TeV}$ and $L = 1 \text{ ab}^{-1}$ can reach a sensitivity as small as 0.02 on ξ . These sensitivities can be translated into an indirect reach on the cutoff scale $\Lambda \equiv 4\pi f$, that is the mass scale of the resonances for the case where the underlying dynamics is maximally strong. We find a reach $\Lambda \sim 15 - 20 \text{ TeV}$, which should be compared with the reach $\Lambda \sim 30 - 40 \text{ TeV}$ expected through single-Higgs processes at the ILC with 250 fb^{-1} of luminosity accumulated at $\sqrt{s} = 250 \text{ GeV}$ plus another 500 fb^{-1} at $\sqrt{s} = 500 \text{ GeV}$ [50, 254–256]. Table 5.13 summarises the values of Λ which can be probed at various experiments through the study of single and double Higgs processes. Though the reach on Λ seems remarkable, one should not forget that the measured value of the Higgs mass disfavors a maximally strong coupling [1]: new states are therefore expected significantly below Λ with a mass around $m_\rho \sim \Lambda \times g_\rho/(4\pi)$. Still, even in the case of a moderately strong sector $g_\rho \sim 3$, direct production of resonances at a high-energy hadron collider like the LHC with $\sqrt{s} = 33 \text{ TeV}$ may not become competitive. Of course one must beware of these qualitative arguments, as the model's details often matter.

At lower energies the $e^+e^- \rightarrow hh\nu\bar{\nu}$ process is not effective to measure the couplings b , d_3 , and one has to resort to double Higgs-strahlung, $e^+e^- \rightarrow hhZ$. At 500 GeV center-of-mass energy, only a linear combination of the two couplings δ_b and δ_{d_3} can be extracted from a measurement of the total cross section. For $\sqrt{s} = 1 \text{ TeV}$, on the other hand, it is possible to exploit the kinematical distribution of the final state to extract both couplings

			$\xi = (v/f)^2$	$\Lambda = 4\pi f$
LHC	14 TeV	$L = 300 \text{ fb}^{-1}$	0.5 (double Higgs [64, 80])	4.5 TeV
			0.1 (single Higgs [223, 224])	10 TeV
ILC	250 GeV	$L = 250 \text{ fb}^{-1}$	$0.6\text{-}1.2 \times 10^{-2}$ (single Higgs [50, 254–256])	30-40 TeV
	+ 500 GeV	$L = 500 \text{ fb}^{-1}$		
CLIC	3 TeV	$L = 1 \text{ ab}^{-1}$	$2\text{-}5 \times 10^{-2}$ (double Higgs [this work])	15-20 TeV
CLIC	350 GeV	$L = 500 \text{ fb}^{-1}$	$1.1\text{-}2.4 \times 10^{-3}$ (single Higgs [253])	60-90 TeV
	+ 1.4 TeV	$L = 1.5 \text{ ab}^{-1}$		
	+ 3.0 TeV	$L = 2 \text{ ab}^{-1}$		

Table 5.13 – Summary of the precision on ξ (as defined in footnote 12) and the corresponding reach on the compositeness scale at various experiments from the study of single and double Higgs processes.

independently, even though with large uncertainties. The combined measurement of double Higgs-strahlung at both 500 GeV and 1 TeV allows us to obtain the sensitivity contours shown in Figure 5.10, which again indicate that δ_b can be measured more precisely than δ_{d_3} . For all those interested in the structure of the Higgs the message is then very clear. The parameter b not only encodes more robust information than d_3 about the nature of h , whether an impostor, a composite or a pNGB, but it also affords better sensitivity.

In the absence of direct production of new particles at the LHC, precision measurements in the sector of the newly discovered Higgs boson can play a key role in the search for New Physics. The time has come to establish a clear strategy to extract the information on the origin of electroweak symmetry breaking encoded in the Higgs measurements and to pave the way for a future experimental program.

6 Direct Probes of NP

6.1 Introduction

While the problem of comparing data to theory is probably too hard to be tackled in full generality, progress can be made if we restrict our attention to direct experimental manifestations of New Physics which consist of the production of reasonably narrow new particles. In this case one can conveniently adopt the so-called “Simplified Model” strategy [53] which has by now become a standard method in supersymmetry searches and starts to be developed also in non-supersymmetric frameworks [240, 273–285]. The point is that resonant searches are typically not sensitive to all the details and the free parameters of the underlying model, but only to those parameters or combinations of parameters that control the mass of the resonance and the interactions involved in its production and decay. Therefore one can employ a simplified description of the resonance defined by a phenomenological Lagrangian where only the relevant couplings and mass parameters are retained. Aside from symmetry constraints, the Simplified Model Lagrangian does not need to fulfil any particular theoretical requirement. Its sole goal is to provide a phenomenological parameterization of a broad enough set of explicit models and should thus contain all and only those terms which are present in the explicit constructions. The experimental results should be presented in the parameter space of the phenomenological Lagrangian, expressed by confidence level curves or, if possible, in terms of a likelihood function. In this way they could be easily translated into any specific model where the phenomenological parameters can be computed explicitly. The advantage of this two-step approach is that the phenomenological parameters can always be expressed analytically in terms of those of the “fundamental” theory. No matter how complicated the model is, the comparison with the data will always be performed analytically rather than with numerical simulations, in a way that furthermore does not require any knowledge of the experimental details of the analysis.

The procedure is conveniently depicted as a two-span bridge, shown in Figure 6.1, where the Simplified Model constitutes the central pillar and the two spans represent the

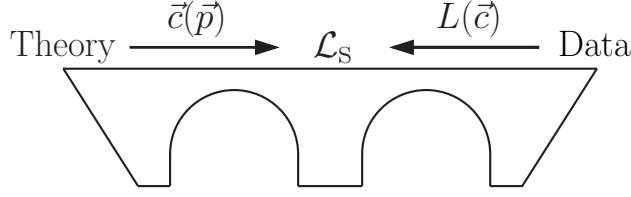


Figure 6.1 – Pictorial view of the Bridge Method.

fundamental/phenomenological parameter relations and the comparison of the Simplified Model with the data respectively. In the Figure, we denote collectively as \vec{c} the parameters of the phenomenological Lagrangian and as $L(\vec{c})$ the likelihood function, or the CL curves, as extracted from the experimental data. Notice that $L(\vec{c})$ could very well be the result of a combination of different analyses, which can be performed directly on the Simplified Model parameter space. Once the likelihood or the CL limits are known, the experimental information is immediately translated into the free parameters \vec{p} of any explicit model by computing the phenomenological/explicit parameter relations $\vec{c}(\vec{p})$.

When comparing the Simplified Model with the data, some care is required. The crucial point is that the Simplified Model, differently for instance from the SM or the MSSM, is not supposed to be a complete theory and attention must be paid not to use it outside its realm of validity. Namely, the Simplified Model is constructed to describe only the *on-shell* resonance production and decay. A good experimental search should thus be only sensitive to the on-shell process and insensitive to the off-shell effects. The simplest example of this situation, which we will discuss in detail, is the Drell-Yan (DY) process where the invariant mass distribution of the final state is studied. Aside from the resonant peak, the distribution is characterised by a low mass tail which can become prominent, because of the rapidly-falling parton distribution functions, when the resonance approaches the kinematical production threshold or when a large interference with the SM background is present. Many different New Physics effects, not included in the Simplified Model, might contribute to the tail and radically change the Simplified Model prediction. This could come, for instance, from extra contact interactions or from heavier resonances produced in the same channel. Around the peak, and only in this region, these effects are negligible and the Simplified Model prediction is trustable. Indeed the peak shape is well described, through the Breit-Wigner (BW) formula, in terms of purely on-shell quantities such as the production rate times the Branching Ratio (BR) to the relevant final state, $\sigma \times \text{BR}$, and by the resonance total decay width. Experimental searches should focus on the peak and avoid contamination from the other regions as much as possible. More in general, any resonance search relies on the measurement of a given observable, either the number of events or a distribution, restricted by suitable identification and selection cuts. Only “on-shell” observables, which are exclusively sensitive to the resonance formation and decay, should be employed in Simplified Model searches. Notice that whether an experimental observable is on-shell or not can crucially depend on the cuts and must be

checked case by case.

Aside from addressing the conceptual issues previously outlined, the usage of on-shell observables is also an important practical simplification. Because of factorisation of the production cross-section and the decay BR, on-shell observables are “easy” to predict within the Simplified Model since they do not depend on all the parameters of the phenomenological Lagrangian in a complicated way but only on few combinations that describe the on-shell resonance. In the example of the invariant mass distribution, a search performed at the peak can be turned into limits on $\sigma \times \text{BR}$ as a function of the resonance mass and possibly of its width. The width and BRs are simple analytical functions of the Simplified Model parameters and also the total production rate can be expressed semi-analytically in terms of the parton luminosities at each mass point. The mass- and width- dependent limits can thus be mapped *analytically* into the phenomenological parameter space. Obviously, taking the experimental efficiencies properly into account is essential. This is typically rather easy because, as in the examples discussed in the following, the efficiencies only depend on the resonance mass and can be extracted from a few benchmark simulations. The tail of the invariant mass distribution, instead, has a more complicated dependence on the model parameters and can not be predicted analytically. Therefore a search which is sensitive to the tail can not be cast into a limit on $\sigma \times \text{BR}$ and it can be interpreted within the model only by scanning the parameter space with long and demanding simulations.

The aim of the following chapter is to illustrate these general concepts in detail by focusing on the simple but well-motivated example of electroweak-charged spin one resonances which are a common prediction of many New Physics scenarios. The latter can be weakly coupled, like for instance Z' [276, 286–296] or W' [277, 278, 280, 281, 297–301] models, or strongly coupled constructions such as Composite Higgs models [97, 302–307] and some variants of Technicolor [225, 226, 228, 244, 308–312]. The experimental searches for these particles, performed by ATLAS [161, 234, 236, 313–319] and CMS [231, 233, 235, 237–239, 320–323], provide theoretical interpretations of the results in terms of an extremely small subset of the possible models and moreover restrict to limited benchmark regions of the parameter space. This strategy does not provide a sufficient coverage of the theoretical possibilities and furthermore it precludes reinterpretation in other models. Here we will show that a great improvement can be achieved with the Bridge method.

The chapter is organised as follows. In section 6.2 we introduce the Simplified Model Lagrangian and discuss some basic aspects of its phenomenology. We also show how the resonance production cross-section in the two relevant channels, DY and Vector Boson Fusion (VFB), can be parameterized semi-analytically in a way that, as previously described, allows for an efficient comparison of the model with the experimental results. We restrict, for definiteness, to the case of an $SU(2)_L$ iso-triplet of resonances. The extension to other representations should be straightforward and is left to future work. Section 6.2.3 is a survey of the present experimental situation where, based on the

	$SU(3)_C$	$SU(2)_L$	$U(1)_Y$
Q	3	2	1/6
u	$\bar{\mathbf{3}}$	1	-2/3
d	3	1	1/3
L	1	2	-1/2
e	1	1	1
H	1	2	1/2

	$SU(3)_C$	$SU(2)_L$	$U(1)_Y$
\mathcal{B}_μ	1	1	0
\mathcal{B}_μ^1	1	1	1
\mathcal{L}_μ	1	2	-3/2
V_μ	1	3	0
V_μ^1	1	3	1

Table 6.1 – Left table: Standard Model matter content. Right table: Colour singlet vectors transforming under irreducible representations of \mathcal{G}_{SM} that admit linear, dimension 4 couplings with the SM particles. All spinors are left-handed Weyl spinors.

present experimental limits, we derive 95% CL exclusion bounds in the Simplified Model parameter space. This is done by taking the experimental results at face value, *i.e.* by assuming that the limits are properly set on $\sigma \times \text{BR}$ as a function of the resonance mass as presented by the experimental collaborations. However this might not be completely correct, since important effects associated with the finite resonance width could affect the $\sigma \times \text{BR}$ currently extracted by the experiments, which would result in an incorrect definition of the quantity on which the limit is set. In section 6.2.3.3 we will illustrate these effects in detail by focusing on the examples of di-lepton and lepton-neutrino searches. In section 6.2.4 we relate the Simplified Model to explicit constructions. Two examples are considered as representatives of weakly and strongly coupled theories, showing that the Simplified Model is general enough to describe both cases in different regions of the parameter space. The examples are the extension of the SM gauge group described in Ref. [286] and the effective description of Composite Higgs models vectors of Ref. [97]. In section 6.4 we present our Conclusions. Our Simplified Model is implemented in a series of tools described in Appendix D.3 and available at the webpage [324]. Section 6.3 is devoted to a brief summary of recent progress in the simplified model description of fermionic resonances and highlights differences with respect to the vector triplet. Since their effective description is bound to be more model-dependent, we restrict ourselves to a discussion of the strongly coupled top partners, especially of the charge-8/3 resonance introduced in the minimally tuned model in section 3.3. We discuss current experimental searches and bounds.

6.2 A Simple Simplified Model for a Heavy Vector Triplet

We assume the existence of a multiplet of vector bosons transforming linearly as some irreducible representation of the SM gauge group. Since we require couplings of one vector to two fermions and gauge bosons, we are limited to colour singlet representations only. The possible quantum numbers are summarised in Table 6.1. In the following we consider a real vector V_μ^a , $a = 1, 2, 3$, in the adjoint representation of $SU(2)_L$ and with vanishing hypercharge in addition to the SM fields and interactions. It captures a large fraction of

6.2. A Simple Simplified Model for a Heavy Vector Triplet

the interesting features of a spin one resonance. V_μ^a describes one charged and one neutral heavy spin-one particle with the charge eigenstate fields defined by the familiar relations

$$V_\mu^\pm = \frac{V_\mu^1 \mp iV_\mu^2}{\sqrt{2}}, \quad V_\mu^0 = V_\mu^3. \quad (6.1)$$

Similarly to Ref. [282], we describe the dynamics of the new vector by a simple phenomenological Lagrangian

$$\begin{aligned} \mathcal{L}_V = & -\frac{1}{4}D_{[\mu}V_{\nu]}^a D^{[\mu}V^{\nu]}{}^a + \frac{m_V^2}{2}V_\mu^a V^{\mu a} \\ & + i g_V c_H V_\mu^a H^\dagger \tau^a \overleftrightarrow{D}^\mu H + \frac{g^2}{g_V} c_F V_\mu^a J_F^{\mu a} \\ & + \frac{g_V}{2} c_{VVV} \epsilon_{abc} V_\mu^a V_\nu^b D^{[\mu}V^{\nu]}{}^c + g_V^2 c_{VVHH} V_\mu^a V^{\mu a} H^\dagger H - \frac{g}{2} c_{VW} \epsilon_{abc} W^{\mu\nu a} V_\mu^b V_\nu^c. \end{aligned} \quad (6.2)$$

The first line of the above equation contains the V kinetic and mass term, plus trilinear and quadrilinear interactions with the vector bosons from the covariant derivatives

$$D_{[\mu}V_{\nu]}^a = D_\mu V_\nu^a - D_\nu V_\mu^a, \quad D_\mu V_\nu^a = \partial_\mu V_\nu^a + g \epsilon^{abc} W_\mu^b V_\nu^c, \quad (6.3)$$

where g denotes the $SU(2)_L$ gauge coupling. Notice that the V_μ^a fields are not mass eigenstates as they mix with the W_μ^a after EWSB and the mass parameter m_V does not coincide with the physical mass of the resonances.

The second line contains direct interactions of V with the Higgs current

$$i H^\dagger \tau^a \overleftrightarrow{D}^\mu H = i H^\dagger \tau^a D^\mu H - i D^\mu H^\dagger \tau^a H, \quad (6.4)$$

and with the SM left-handed fermionic currents

$$J_F^{\mu a} = \sum_f \bar{f}_L \gamma^\mu \tau^a f_L, \quad (6.5)$$

where $\tau^a = \sigma^a/2$. The Higgs current term c_H leads to vertices involving the physical Higgs field and the three unphysical Goldstone bosons. By the Equivalence Theorem [95], the Goldstones represent the longitudinally polarised SM vector bosons W and Z in the high-energy regime which is relevant for the resonance production and decay. Thus c_H controls the V interactions with the SM vectors and with the Higgs, and in particular its decays into bosonic channels. Similarly, c_F describes the direct interaction with fermions, which is responsible for both the resonance production by DY and for its fermionic decays. In eq. (6.2) we reported, for shortness, a universal coupling of V to fermions, but in our analysis we will consider a more general situation with different couplings to leptons, light quarks and the third quark family. The interaction in eq. (6.2) should thus be generalised

to

$$c_F V \cdot J_F \rightarrow c_l V \cdot J_l + c_q V \cdot J_q + c_3 V \cdot J_3. \quad (6.6)$$

Given the strong constraints on additional sources of lepton and light quark flavor violation further generalisations seem unnecessary. The proliferation of fermionic parameters is a complication, but the effects of c_l , c_q , and c_3 can be easily disentangled by combining searches in different decay channels including third family quarks.

Finally, the third line of eq. (6.2) contains 3 new operators and free parameters, c_{VVV} , c_{VVHH} and c_{VW} . None of them, however, contains vertices of one V with light SM fields, thus they do not contribute directly to V decays¹ and single production processes which are the only relevant for LHC phenomenology. As we will discuss in the following section, they do affect the above processes only through the mixing of V with the W , but since the mixing is typically small their effect is marginal. Therefore to a first approximation the operators in the third line can be disregarded and the phenomenology described entirely by the four parameters c_H , c_l , c_q and c_3 , plus the mass term m_V .

In eq. (6.2) we adopted a rather peculiar parameterization of the interaction terms, with a coupling g_V weighting extra insertions of V , of H and of the fermionic fields. Similarly, the insertions of W in the last line is weighted by the $SU(2)_L$ coupling g . We take g_V to represent the typical strength of V interactions while the dimensionless coefficients “ c ” parameterise the departures from the typical size. The parameterization of the fermion couplings is an exception to this rule. In this case one extra factor of g^2/g_V^2 has been introduced. This is convenient because in all the explicit models we will be interested in, both of weakly- and strongly-coupled origin, this factor is indeed present and the c_F ’s, as defined in eq. (6.2), are of order one. The other c ’s are typically of order one, except for c_H which is of order one in the strongly-coupled scenario but can be reduced in the weakly coupled case as described in section 6.2.4. In all cases, the c ’s are never parametrically larger than one, with the notable exception of the third family coupling c_3 , which could be enhanced in strongly-coupled scenarios where the top quark mass is realised by the mechanism of Partial Compositeness, see for instance [80]. The coupling g_V can easily vary over one order of magnitude in different scenarios, ranging from $g_V \sim g \sim 1$ in the “typical” weakly-coupled case up to $g_V \simeq 4\pi$ in the extreme strong limit. Therefore it is useful to factor it out of the operator estimate. Notice that there is no sharp separation between the weak and strong coupling regimes as nothing forbids to consider theories with a “weak” UV origin but with large g_V , of the order of a few, and “strong” models where g_V is reduced by the large number of colours of the strong sector, $g_V = 4\pi/\sqrt{N_c}$. This provides one additional motivation for our approach which interpolates between the two cases.

Our parameterization of the operators is useful at the theoretical level but obviously

¹A priori, they could contribute to cascade decays. However, as we will see below, the mass splitting between the neutral and the charged state is very small and cascade decays are extremely suppressed.

6.2. A Simple Simplified Model for a Heavy Vector Triplet

redundant as g_V could be reabsorbed in the c 's and is not a genuine new parameter of the model. For instance, one could resolve the redundancy by setting $c_{VVV} = 1$ and thus define g_V as the V self-interaction strength. However for practical purposes, and in particular for presenting the experimental limits of the model, it could be easier to treat $g_V c_H$ and $g^2/g_V c_F$, the combinations that enter in the vertices, as fundamental parameters.

In the Bridge approach, as discussed in the Introduction, the Simplified Model does not need to fulfil any particular theoretical requirement and its only goal is to be simple enough while still capable to reproduce a large set of explicit models. Therefore a complete justification of our phenomenological Lagrangian has to be postponed to section 6.2.4 where the matching with explicit constructions will be discussed. However we can already appreciate the general validity of the description by noticing that eq. (6.2) is the most general Lagrangian compatible with the SM gauge invariance and with the CP symmetry restricted to operators of energy dimension below or equal to 4. Assuming CP , which we take to act on V as on the SM W

$$V^a(\vec{x}, t) \rightarrow -(-)^{\delta_{a2}} V^a(-\vec{x}, t) \Leftrightarrow \begin{cases} V^\pm(\vec{x}, t) \rightarrow -V^\mp(-\vec{x}, t) \\ V^0(\vec{x}, t) \rightarrow -V^0(-\vec{x}, t) \end{cases}, \quad (6.7)$$

is very convenient as it avoids the proliferation of operators constructed with the Levi-Civita tensor. Furthermore, it leads to a unique coupling of V to the Higgs parameterized by only one real coefficient c_H . CP is often also a good symmetry of explicit models so that it is not a too restrictive assumption. It is important to note that the Lagrangian with the imposed CP symmetry is also accidentally invariant under the custodial group $SO(4) = SU(2)_L \times SU(2)_R$, with V in the $(\mathbf{3}, \mathbf{1})$ representation. The custodial symmetry is of course broken, but only by the gauging of the hypercharge. This makes our setup very efficient in reproducing strongly-coupled scenarios where custodial symmetry is imposed by construction.

One invariant low-dimensional operator, the W - V kinetic mixing

$$D_{[\mu} V_{\nu]}^a W^{\mu\nu a}, \quad (6.8)$$

is not reported in eq. (6.2) because, following Ref. [325], it can be eliminated from the Lagrangian by a field redefinition of the form

$$\begin{cases} W_\mu^a \rightarrow W_\mu^a + \alpha V_\mu^a \\ V_\mu^a \rightarrow \beta V_\mu^a \end{cases}. \quad (6.9)$$

More details on this can be found in Appendix D.1. We also ignored dimension four quadrilinear V interactions because they are irrelevant for the LHC phenomenology.

The choice of restricting to low-dimensional operators is clearly well-justified in the weakly-

coupled case where the underlying model is a renormalizable theory, but it is questionable in the strongly-coupled one where higher-dimensional operators are potentially relevant. However in all strongly-coupled scenarios that obey the SILH paradigm [80] we do have a reason to stop at $d = 4$. In the SILH power-counting the most relevant higher dimensional operators are those involving extra powers of the Higgs or the V field which are weighted by the Goldstone-Boson-Higgs decay constant f . Their effects are generically suppressed by the parameter

$$\xi = \frac{v^2}{f^2},$$

where $v \simeq 246$ GeV is the EWSB scale. Since ξ controls the departures from the Standard Higgs model, compatibility with the ElectroWeak Precision Tests (EWPT) and the LHC Higgs coupling measurements [3, 111] requires $\xi \lesssim 0.2$. If the higher dimensional operators do not induce any qualitatively new effect and only give relative corrections of order ξ to the vertices, they can be safely ignored given the limited accuracy of the LHC direct searches. This will be confirmed by the analysis of section 6.2.4.²

There exist however other scenarios where higher dimensional operators are unsuppressed and the parameterization of eq. (6.2) is insufficient. These are technicolor-like models where the strong sector condensate breaks the EW symmetry directly and the observed Higgs boson is a light composite particle with couplings compatible with the SM expectations. This might occur by accident or in hypothetical scenarios with a light Higgs-like dilaton [72, 73]. In spite of the tension with EWPT and with the Higgs data it would be interesting to generalise our framework in order to test also these ideas.

6.2.1 Basic phenomenology

Masses and Mixings

Having introduced our Simplified Model in eq. (6.2), let us discuss its phenomenology starting from the mass spectrum. After EWSB, the only massless state is the photon which can be identified as the gauge field associated with the unbroken $U(1)_{\text{em}}$. It is given by the SM-like expression³

$$A_\mu = \cos \theta_W B_\mu + \sin \theta_W W_\mu^3, \quad \text{where} \quad \tan \theta_W = \frac{g'}{g}. \quad (6.10)$$

The orthogonal combination, the Z field, instead acquires a mass and a mixing with V^0 . Notice that since the photon is given by the canonical SM expression, its couplings are

²Notice that this does not need to be the case a priori. There are plenty of examples concerning for instance the LHC phenomenology of Composite Higgs Top Partners [154, 157, 240] where the Higgs non-linearities can not be ignored.

³This only holds in the field basis where the W - V mixing of eq. (6.8) is set to zero, otherwise the photon acquires a component along V^0 .

6.2. A Simple Simplified Model for a Heavy Vector Triplet

also canonical. The electric charge in our model is therefore simply given by

$$e = \frac{gg'}{\sqrt{g^2 + g'^2}}, \Rightarrow \begin{cases} g = e/\sin \theta_W \\ g' = e/\cos \theta_W \end{cases}. \quad (6.11)$$

In what follows we will trade g and g' for e and $\sin \theta_W$, taking e as an input parameter and setting it to the experimental value $e \approx \sqrt{4\pi/137}$.

The two other neutral mass eigenstates are the SM Z boson and one heavy vector of mass M_0 which are obtained by diagonalising the mass matrix of the (Z, V^0) system by a rotation

$$\begin{pmatrix} Z \\ V^0 \end{pmatrix} \rightarrow \begin{pmatrix} \cos \theta_N & \sin \theta_N \\ -\sin \theta_N & \cos \theta_N \end{pmatrix} \begin{pmatrix} Z \\ V^0 \end{pmatrix}. \quad (6.12)$$

The mass matrix is

$$\mathcal{M}_N^2 = \begin{pmatrix} \hat{m}_Z^2 & c_H \zeta \hat{m}_Z \hat{m}_V \\ c_H \zeta \hat{m}_Z \hat{m}_V & \hat{m}_V^2 \end{pmatrix}, \quad \text{where} \quad \begin{cases} \hat{m}_Z = \frac{e}{2 \sin \theta_W \cos \theta_W} \hat{v} \\ \hat{m}_V^2 = m_V^2 + g_V^2 c_{VVHH} \hat{v}^2 \\ \zeta = \frac{g_V \hat{v}}{2 \hat{m}_V} \end{cases}. \quad (6.13)$$

In the above equations \hat{v} denotes the Higgs field Vacuum Expectation Value (VEV) defined by $\langle H^\dagger H \rangle = \hat{v}^2/2$, which in our model can differ significantly from the physical EWSB scale $v = 246$ GeV. The mass eigenvalues and the rotation angles are easily obtained by inverting the relations

$$\begin{aligned} \text{Tr} [\mathcal{M}_N^2] &= \hat{m}_Z^2 + \hat{m}_V^2 = m_Z^2 + M_0^2, \\ \text{Det} [\mathcal{M}_N^2] &= \hat{m}_Z^2 \hat{m}_V^2 (1 - c_H^2 \zeta^2) = m_Z^2 M_0^2, \\ \tan 2\theta_N &= \frac{2 c_H \zeta \hat{m}_Z \hat{m}_V}{\hat{m}_V^2 - \hat{m}_Z^2}. \end{aligned} \quad (6.14)$$

Notice that the tangent can be uniquely inverted because the angle θ_N is in the range $[-\pi/4, \pi/4]$ in the parameter region we will be interested in, where $\hat{m}_Z < \hat{m}_V$.

The situation is similar in the charged sector where the mass matrix of the (W^\pm, V^\pm) system reads

$$\mathcal{M}_C^2 = \begin{pmatrix} \hat{m}_W^2 & c_H \zeta \hat{m}_W \hat{m}_V \\ c_H \zeta \hat{m}_W \hat{m}_V & \hat{m}_V^2 \end{pmatrix}, \quad \text{where} \quad \hat{m}_W = \frac{e}{2 \sin \theta_W} \hat{v} = \cos \theta_W \hat{m}_Z, \quad (6.15)$$

and it is diagonalised by

$$\begin{aligned}\text{Tr} [\mathcal{M}_C^2] &= \hat{m}_W^2 + \hat{m}_V^2 = m_W^2 + M_+^2, \\ \text{Det} [\mathcal{M}_N^2] &= \hat{m}_W^2 \hat{m}_V^2 (1 - c_H^2 \zeta^2) = m_W^2 M_+^2, \\ \tan 2\theta_C &= \frac{2 c_H \zeta \hat{m}_W \hat{m}_V}{\hat{m}_V^2 - \hat{m}_W^2}.\end{aligned}\tag{6.16}$$

The charged and neutral mass matrices are connected by custodial symmetry, which can be shown in full generality to imply

$$\mathcal{M}_C^2 = \begin{pmatrix} \cos \theta_W & 0 \\ 0 & 1 \end{pmatrix} \mathcal{M}_N^2 \begin{pmatrix} \cos \theta_W & 0 \\ 0 & 1 \end{pmatrix}.\tag{6.17}$$

By taking the determinant of the above equation, or equivalently by comparing the charged and neutral determinants in eq. (6.14) and eq. (6.16), we obtain a generalized custodial relation among the physical masses

$$m_W^2 M_+^2 = \cos^2 \theta_W m_Z^2 M_0^2.\tag{6.18}$$

From the simple formulas above we can already derive interesting features of our model. First of all, we can identify the physically “reasonable” region of its parameter space. We aim at describing new vectors with masses at or above the TeV scale, but of course we also want the SM masses $m_{W,Z} \sim 100$ GeV to be reproduced. Therefore we require a hierarchy in the spectrum, which can only occur, barring unnatural cancellations in the determinant of the mass matrices, if $\hat{m}_{W,Z}$ and \hat{m}_V are hierarchical, *i.e.*

$$\frac{\hat{m}_{W,Z}}{\hat{m}_V} \sim \frac{m_{W,Z}}{M_{+,0}} \lesssim 10^{-1} \ll 1.\tag{6.19}$$

The parameter ζ , instead, can be either very small or of order one. Both cases are realised in explicit models. While $\zeta \ll 1$ is the most common situation, $\zeta \sim 1$ only occurs in strongly coupled scenarios at very large g_V .

In the limit of eq. (6.19) we obtain simple approximate expressions for m_W and m_Z

$$\begin{aligned}m_Z^2 &= \hat{m}_Z^2 (1 - c_H^2 \zeta^2) (1 + \mathcal{O}(\hat{m}_Z^2/\hat{m}_V^2)), \\ m_W^2 &= \hat{m}_W^2 (1 - c_H^2 \zeta^2) (1 + \mathcal{O}(\hat{m}_W^2/\hat{m}_V^2)).\end{aligned}$$

Since $\hat{m}_W = \cos \theta_W \hat{m}_Z$, the W - Z mass ratio is thus given, to percent accuracy, by

$$\frac{m_W^2}{m_Z^2} \simeq \cos^2 \theta_W.\tag{6.20}$$

In order to reproduce the observed ratio, which satisfies the $\rho = 1$ SM tree-level relation

to $\sim 1\%$, we need ⁴

$$\cos^2 \theta_W \approx (\cos^2 \theta_W)_{\text{exp}} = 1 - 0.23. \quad (6.21)$$

Similarly to the electric charge, also the weak angle parameter θ_W defined by eq. (6.11), and therefore in turn the couplings g and g' , has to be close to the SM tree-level value. eq. (6.20) also has one important implication on the masses of the new vectors. When combined with the custodial relation (6.18), it tells us that the charged and neutral V s are practically degenerate

$$M_+^2 = M_0^2 (1 + \mathcal{O}(\%)) , \quad (6.22)$$

and therefore they are expected to have comparable production rates at the LHC. Combining experimental searches of charged and neutral states could thus considerably improve the reach, as discussed in Ref. [282]. Furthermore, the small mass splitting implies a phase-space suppression of cascade decays, which can be safely ignored. In the following, when working at the leading order in the limit (6.19), we will ignore the mass splitting and denote the mass of the charged and the neutral states collectively as M_V . It is easy to check that in that limit $M_V = \hat{m}_V$.

Because of the hierarchy in the mass matrices, the mixing angles are naturally small. By looking at eqs. (6.14) and (6.16) we estimate

$$\theta_{N,C} \simeq c_H \zeta \frac{\hat{m}_{W,Z}}{\hat{m}_V} \lesssim 10^{-1}. \quad (6.23)$$

The couplings of the physical states are thus approximately those of the original Lagrangian before the rotation. In particular, the W and Z couplings to fermions and among themselves mainly come from the SM Lagrangian and thus are automatically close to the SM prediction thanks to the hierarchy (6.19) and to the parameter choice (6.21). Obviously this is not enough to ensure the compatibility of the model with observations. The W and Z couplings are very precisely measured, and the deviations due to new physics are constrained at the per mil level. These measurements translate into limits on the so-called EWPT observables [113, 114, 132], which we will compute in Appendix D.2. This will allow us to quantify the additional restrictions on the parameter space, besides eq. (6.19).⁵

⁴The reader might be confused by the fact that $m_Z^2/(\cos^2 \theta_W m_W^2)$ is not strictly equal to one at tree-level in our model, as eq. (6.20) shows, in spite of custodial symmetry. The reason is that custodial symmetry provides a relation, reported in eq. (6.17), among the charged and neutral mass matrices and it does not directly imply a relation among the W and Z mass eigenvalues appearing in eq. (6.20). Moreover, θ_W defined by Eq. (6.11) does not correspond to the physical one. Custodial Symmetry also implies that the \hat{T} parameter of EWPT, defined in terms of zero-momentum correlators and not of the pole masses, vanishes. This fact is explicitly verified to hold in our model in Appendix D.2.

⁵In the following we will not ask EWPT to be strictly satisfied since this would be in contrast with

Decay Widths

Let us now turn to the resonance decays. The relevant channels are di-lepton, di-quark and di-boson. The latter category includes final states with W s, Z s and the Higgs boson. Decay into $W\gamma$ is also possible, but always with a tiny BR, as we will show below.

After rotating to the mass basis, the couplings of the neutral and charged resonances to left- and right-handed fermion chiralities can be written in a compact form⁶

$$\begin{cases} g_L^N = \frac{g^2}{g_V} \frac{c_F}{2} \cos \theta_C + (g_L^Z)_{SM} \sin \theta_N \simeq \frac{g^2}{g_V} \frac{c_F}{2} , \\ g_R^N = (g_R^Z)_{SM} \sin \theta_N \simeq 0 \\ g_L^C = \frac{g^2}{g_V} \frac{c_F}{\sqrt{2}} \cos \theta_C + (g_L^W)_{SM} \sin \theta_C \simeq \frac{g^2}{g_V} \frac{c_F}{\sqrt{2}} , \\ g_R^C = 0 \end{cases} \quad (6.24)$$

for each fermion species $F = \{l, q, 3\}$. In the above equation, $(g_{L,R}^{W,Z})_{SM}$ denotes the ordinary SM W and Z couplings (with the normalisation given by $g_L^W = g/\sqrt{2}$) that originate from the fermion covariant derivatives and contribute to the V interactions because of the rotation. Given that the rotation angles are small, the couplings further simplify, as also shown in the equation. We see that the V s interact mainly with left-handed chiralities and that all the couplings for each fermion species are controlled by the parameter combination $g^2/g_V c_F$. This gives tight correlations among different channels

$$\Gamma_{V_{\pm} \rightarrow f\bar{f}'} \simeq 2\Gamma_{V_0 \rightarrow f\bar{f}} \simeq N_c[f] \left(\frac{g^2 c_F}{g_V} \right)^2 \frac{M_V}{48\pi} , \quad (6.25)$$

where $N_c[f]$ is the number of colours and is equal to 3 for the di-quark and to 1 for the di-lepton decays. The parameters $c_F = \{c_l, c_q, c_3\}$ control the relative BRs to leptons, light quarks and the third family. Furthermore through the partial width to $q\bar{q}$, c_q controls the DY production rate, as we will discuss in the following section.

The analysis is more subtle in the case of di-bosons. Obviously it is straightforward to compute the V couplings to W , Z and Higgs in the Unitary Gauge, after rotating to the mass eigenstates, and to obtain exact analytical formulas for the widths. We will not report the resulting expressions because they are rather involved and not particularly informative. It is instead useful to derive approximate decay widths in the limit of eq. (6.19), but the Unitary Gauge is not suited for this purpose. In the Unitary Gauge there are no direct couplings of V to the SM vectors, these interactions only emerge

the spirit of the Simplified Model approach adopted in this chapter. We will take care of additional contributions to EWPT, not calculable within the Simplified Model, by considering bounds looser than the strict 95% CL limits.

⁶Because of quark mixings, the charged vector couplings should actually be multiplied by the appropriate CKM matrix elements.

6.2. A Simple Simplified Model for a Heavy Vector Triplet

from the mixing and are thus suppressed by the small mixing angles $\theta_{N,C} \lesssim 10^{-1}$. On this basis, one would naively expect small di-boson widths and negligible BR. While this conclusion is correct for the processes involving transversely polarised SM vectors, the decay to zero-helicity longitudinal states is actually unsuppressed and potentially dominant. This is because the longitudinal polarisation vectors grow with the energy of the process and even a tiny Unitary Gauge coupling can have a large effect in a high-energy reaction such as the decay of V . Rather than in the Unitary Gauge, one could work in an “Equivalent Gauge” [96] where the growth of the polarisation vectors is avoided and the decay to longitudinals is straightforwardly estimated. However for the present analysis, it is sufficient to rely on a well-known result, the “Equivalence Theorem” [95], according to which the longitudinal W and Z are equivalent to the corresponding Goldstone Bosons in the high energy limit. Namely, the theorem states that if we parameterise the Higgs doublet as

$$H = \begin{pmatrix} \frac{\pi_2 + i\pi_1}{\sqrt{2}} \\ \frac{\hat{v} + h - i\pi_3}{\sqrt{2}} \end{pmatrix} \equiv \begin{pmatrix} i\pi_+ \\ \frac{\hat{v} + h - i\pi_0}{\sqrt{2}} \end{pmatrix}, \quad (6.26)$$

the longitudinal W s and Z s will be described by π_+ and π_0 , respectively, with h being the physical Higgs boson. The vector fields W_μ and Z_μ can be safely ignored, and the terms in the Lagrangian (6.2) which are relevant for the decay process are only

$$\begin{aligned} \mathcal{L}_\pi = & -\frac{1}{4}\partial_{[\mu}V_{\nu]}^a\partial^{[\mu}V^{\nu]}{}^a + \frac{M_V^2}{2}V_\mu^aV^{\mu a} - c_H\zeta M_V V_\mu^a\partial^\mu\pi^a \\ & + \frac{g_V c_H}{2}V_\mu^a\left(\partial^\mu h\pi^a - h\partial^\mu\pi^a + \epsilon^{abc}\pi^b\partial^\mu\pi^c\right) \\ & + 2g_V c_{VVHH}\zeta M_V h V_\mu^a V^{\mu a} + \frac{g_V}{2}c_{VVV}\epsilon_{abc}V_\mu^a V_\nu^b\partial^{[\mu}V^{\nu]}{}^c. \end{aligned} \quad (6.27)$$

We omitted the kinetic term of the massless Goldstones and of the physical Higgs for shortness and we used $\hat{m}_V \equiv M_V \approx M_{\pm,0}$.

We now see clearly why the longitudinal decays are unsuppressed. The second line of the Lagrangian (6.27) contains a direct interaction of the resonance with the Goldstones. This term gives a universal contribution to di-boson decays of the charged and neutral resonances, which are all controlled by the same parameter combination $g_V c_H$. If it dominates, all the relative BRs in these channels are fixed and uniquely predicted. This is indeed what happens in most of the parameter space of our model where, as discussed in the previous section, ζ is small. When instead ζ is of order one, the widths receive additional contributions because the V - π mixing in the first line of eq. (6.27) can not be ignored and must be eliminated by a field redefinition before reading the physical couplings. The redefinition is performed in two steps, first we shift

$$V_\mu^a \rightarrow V_\mu^a + \frac{c_H\zeta}{M_V}\partial_\mu\pi^a, \quad (6.28)$$

and we cancel the mixing from the variation of the mass term. Second, in order to restore the canonical normalisation of the π kinetic term we rescale

$$\pi^a \rightarrow \frac{1}{\sqrt{1 - c_H^2 \zeta^2}} \pi^a. \quad (6.29)$$

Notice that $1 - c_H^2 \zeta^2$ is necessarily positive to avoid negative-defined mass matrices, see eqs. (6.14) and (6.16).

After these redefinitions, the relevant interactions become⁷

$$\begin{aligned} & \frac{g_V c_H}{2(1 - c_H^2 \zeta^2)} [1 + c_H c_{VVV} \zeta^2] \epsilon^{abc} V_\mu^a \pi^b \partial^\mu \pi^c \\ & - \frac{g_V c_H}{\sqrt{1 - c_H^2 \zeta^2}} [1 - 4c_{VVHH} \zeta^2] h V_\mu^a \partial^\mu \pi^a, \end{aligned} \quad (6.30)$$

and the partial widths are immediately computed

$$\begin{aligned} \Gamma_{V_0 \rightarrow W_L^+ W_L^-} &\simeq \Gamma_{V_\pm \rightarrow W_L^\pm Z_L} \simeq \frac{g_V^2 c_H^2 M_V}{192\pi} \frac{(1 + c_H c_{VVV} \zeta^2)^2}{(1 - c_H^2 \zeta^2)^2} = \frac{g_V^2 c_H^2 M_V}{192\pi} [1 + \mathcal{O}(\zeta^2)], \\ \Gamma_{V_0 \rightarrow Z_L h} &\simeq \Gamma_{V_\pm \rightarrow W_L^\pm h} \simeq \frac{g_V^2 c_H^2 M_V}{192\pi} \frac{(1 - 4c_{VVHH} \zeta^2)^2}{1 - c_H^2 \zeta^2} = \frac{g_V^2 c_H^2 M_V}{192\pi} [1 + \mathcal{O}(\zeta^2)]. \end{aligned} \quad (6.31)$$

We checked that these expressions reproduce the exact widths up to $\mathcal{O}(\hat{m}_{W,Z}^2/\hat{m}_V^2)$ corrections, as expected. The channels which are not reported in the above equations are either forbidden, like hh and $\gamma\gamma$ decays, or suppressed like the decays to transverse polarisations which follow the estimate based on the Unitary Gauge and experience mixing angle suppressions. In particular, the $W\gamma$ final state is generically suppressed, and exactly vanishes in the explicit models described in section 6.2.4 that obey Minimal Coupling [278]. Notice that the dominance of the longitudinal polarisations in the di-boson decays is an important simplification for the interpretation of experimental searches. Indeed, the boosted vector boson reconstruction could slightly depend on the helicity because different helicities would lead to different kinematical distributions of the final decay products. In our case one can safely restrict to the longitudinal case when computing the efficiencies and ignore the transverse.

From the analysis of the present section a very simple picture emerges. At small ζ , all the decay widths are fixed, for a given resonance mass, by the couplings $g^2 c_F/g_V$ and $g_V c_H$, which therefore control the BRs in all the relevant channels. Furthermore, since the dominant processes are $2 \rightarrow 1$ reactions and can be parameterized, as we will do in the following section, in terms of the corresponding decay widths, the two parameters

⁷To obtain the equations that follow we also made use of the V equations of motion or, equivalently, of further field redefinitions.

6.2. A Simple Simplified Model for a Heavy Vector Triplet

$g^2 c_F/g_V$ and $g_V c_H$ also control the production rate. Therefore the phenomenology of the model is entirely described, to a good approximation, in terms of the two couplings $g^2 c_F/g_V$ and $g_V c_H$ and the mass M_V , making, as anticipated in section 6.2.1, c_{VVV} , c_{VVHH} and c_{VVW} basically irrelevant. When studying our model at the LHC the latter parameters can be safely ignored, or set to benchmark values inspired by explicit models, and the limits can be presented in terms of the relevant couplings. Additional plausible assumptions, like the universality of lepton and quark couplings, could further simplify the analysis.

Now that the general picture is clear, we can get an idea of the expected widths and BRs by studying explicit models. We consider two benchmark models, A and B, which correspond to two explicit models describing the heavy vectors, namely those in Refs. [286] and [97], respectively. As discussed in detail in section 6.2.4, all the c 's are fixed to specific values in these models and the only free parameters are the resonance coupling g_V and its mass M_V .⁸ We refer to the benchmark points at fixed $g_V = \bar{g}_V$ with the notation $A_{g_V=\bar{g}_V}$ and $B_{g_V=\bar{g}_V}$. Moreover, since models A and B are inspired, respectively, by weakly coupled extensions of the SM gauge group and strongly coupled scenarios of EWSB, *i.e.* Composite Higgs models, we will consider them in different regions of g_V , relatively small, $g_V \lesssim 3$, and relatively large, $g_V \gtrsim 3$, respectively.

In Figure 6.2 we show the BRs (upper panels) and the total widths (bottom panels) as functions of the mass in models A (left panels) and B (right panels) for different values of g_V . As expected from the discussion above, model $A_{g_V=1}$, which predicts

$$g_V c_H \simeq g^2 c_F/g_V \simeq g^2/g_V, \quad (6.32)$$

has comparable BRs into fermions and bosons, with a factor of two difference coming from a numerical factor in the amplitude squared (cfr. eq. (6.31) with eq. (6.25)). The difference between the BRs into leptons and quarks is due to the colour factor, since c_F is universal both in A and B. The total width in model A decreases with increasing g_V because of the overall suppression g^2/g_V in eq. (6.32). In model B, on the contrary, c_H is unsuppressed

$$g_V c_H \simeq -g_V, \quad g^2 c_F/g_V \simeq g^2/g_V. \quad (6.33)$$

Therefore, for model $B_{g_V=3}$ the dominant BRs are into di-bosons and the fermionic decays are extremely suppressed, of the order of one percent to one per mil. Moreover, the total width increases with increasing g_V since it is dominated by the di-boson width which grows with g_V as expected from eq. (6.33). Finally, in model B we see that a very large coupling g_V (the case of $g_V = 8$ is shown in the Figure) leads to an extremely broad resonance, with $\Gamma/M \gg 0.1$, for which the experimental searches for a narrow resonance

⁸ Actually the model of Ref. [97] has an additional freedom in the choice of c_H , which depends on the additional parameter $a_\rho = m_\rho/(g_\rho f)$ as in eq. (6.60), we define the benchmark model B by setting $a_\rho = 1$.

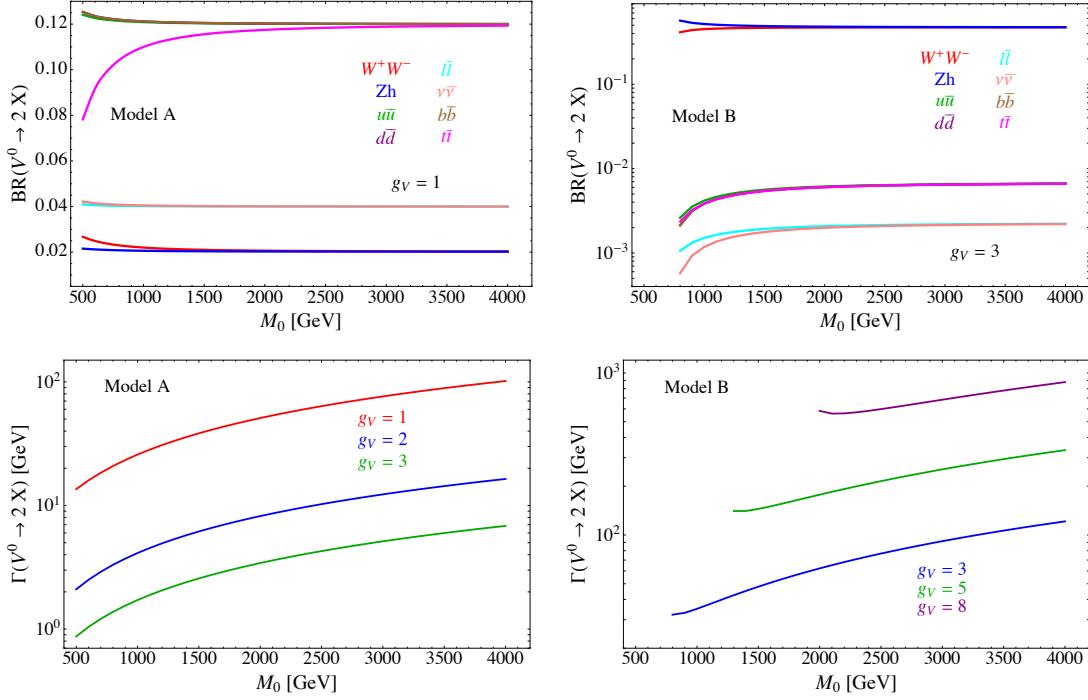


Figure 6.2 – Upper panel: Branching Ratios for the two body decays of the neutral vector V^0 for the benchmarks $A_{g_V=1}$ (left) and $B_{g_V=3}$ (right). Lower panel: Total widths corresponding to different values of the coupling g_V in the models A (left) and B (right).

are no longer motivated. For this reason we expect, if no further suppression is present in the parameter c_H , to be able to constrain heavy vector models from direct searches only up to g_V of the order 6 – 7. For larger couplings different searches become important, like for instance those for four fermion contact interactions.

6.2.2 Production rates parameterized

The two main production mechanisms of the new vectors are DY and VBF.⁹ They are both $2 \rightarrow 1$ processes, therefore their cross-section can be expressed as

$$\sigma(pp \rightarrow V + X) = \sum_{i,j \in p} \frac{\Gamma_{V \rightarrow ij}}{M_V} \frac{16\pi^2(2J+1)}{(2S_i+1)(2S_j+1)} \frac{C}{C_i C_j} \frac{dL_{ij}}{d\hat{s}} \bigg|_{\hat{s}=M_V^2}, \quad (6.34)$$

in terms of the partial widths $\Gamma_{V \rightarrow ij}$ of the inverse decay process $V \rightarrow ij$. In the equation, $i, j = \{q, \bar{q}, W, Z\}$ denote the colliding partons in the two protons, and $dL_{ij}/d\hat{s}|_{\hat{s}=M_V^2}$ is the corresponding parton luminosity evaluated at the resonance mass. The factor J is the spin of the resonance and C its colour factor, $S_{i,j}$ and $C_{i,j}$ are the same quantities

⁹We ignore the production in association with a gauge boson because it is always negligible for V masses and couplings in the interesting region.

6.2. A Simple Simplified Model for a Heavy Vector Triplet

for the initial states. If needed, the cross-section above could be corrected by a k -factor taking into account higher order QCD corrections. It is important to remark that the only terms in the above equation that carry some dependence on the model parameters are the partial widths $\Gamma_{V \rightarrow ij}$, while the parton luminosities are completely model-independent factors that can be encoded in universal fitted functions. Since the widths are analytical functions of the parameters, this allows us to compute the production rates analytically, making the exploration of different regions of the parameter space extremely fast as we will do in the following section. Simple approximated expressions of the partial widths are reported in eqs. (6.25) and (6.31), however in the following we will make use of the exact expressions embedded in a MATHEMATICA code and available through a web interface in [324].

While the meaning of eq. (6.34) is completely obvious for DY, and the corresponding luminosities are immediately computed by convoluting the quark and anti-quark Parton Distribution Functions (PDF), the case of VBF requires additional comments. In eq. (6.34) we are regarding the W and Z bosons as “partons”, or constituents of the proton, relying on the validity of the Effective W Approximation (EWA) [185]. By the EWA, the vector bosons’ PDFs and in turn the corresponding luminosities are obtained by convoluting those of the initial quarks with appropriate splitting functions. More details can be found, for instance, in Ref. [326]. A priori, all the W and Z polarisations should be taken into account, as well as photons. However we saw above that the only sizeable partial widths are those with longitudinal vectors, thus we can safely restrict to the $W_L^+ W_L^-$ and $W_L^\pm Z_L$ initial states for the production of the neutral and the charged V , respectively. It is also important to remark that the EWA has a limited range of validity and it is not expected to reproduce the full partonic process $pp \rightarrow Vjj$ in all possible regimes [327]. It might fail if the W collision is not sufficiently hard, which however is never the case for $M_V \gtrsim 1$ TeV, or if other kinematically enhanced configurations exist, besides the standard VBF ones with forward energetic jets, and contribute to the partonic process. Also this second issue does not arise in our case. Finally, it might happen that other processes give a sizeable contribution to the Vjj final state. This occurs in our case when the V coupling to fermions is much larger than the one to vector bosons. In this case the Vjj final state could arise, for instance, by dressing the DY process with QCD initial state emissions. However when this happens the ordinary DY, without extra parton-level jets, is necessarily the dominant production mechanism and the failure of the EWA is irrelevant at the practical level. We checked that the partonic cross-section is extremely well reproduced by eq. (6.34) in all regions of parameter space, where the VBF rate is not completely negligible, up to order 1% of the DY one.

The parton luminosities for the various production processes are shown in Figure 6.3. The VBF luminosity is obviously much smaller than the DY one because of the α_{EW} suppression in the vector boson PDFs. Therefore VBF only has a chance of being comparable to DY if the widths in $q\bar{q}$ are much smaller than those in di-bosons. We see from eqs. (6.25) and (6.31) that this can happen only at large g_V , and in the strongly

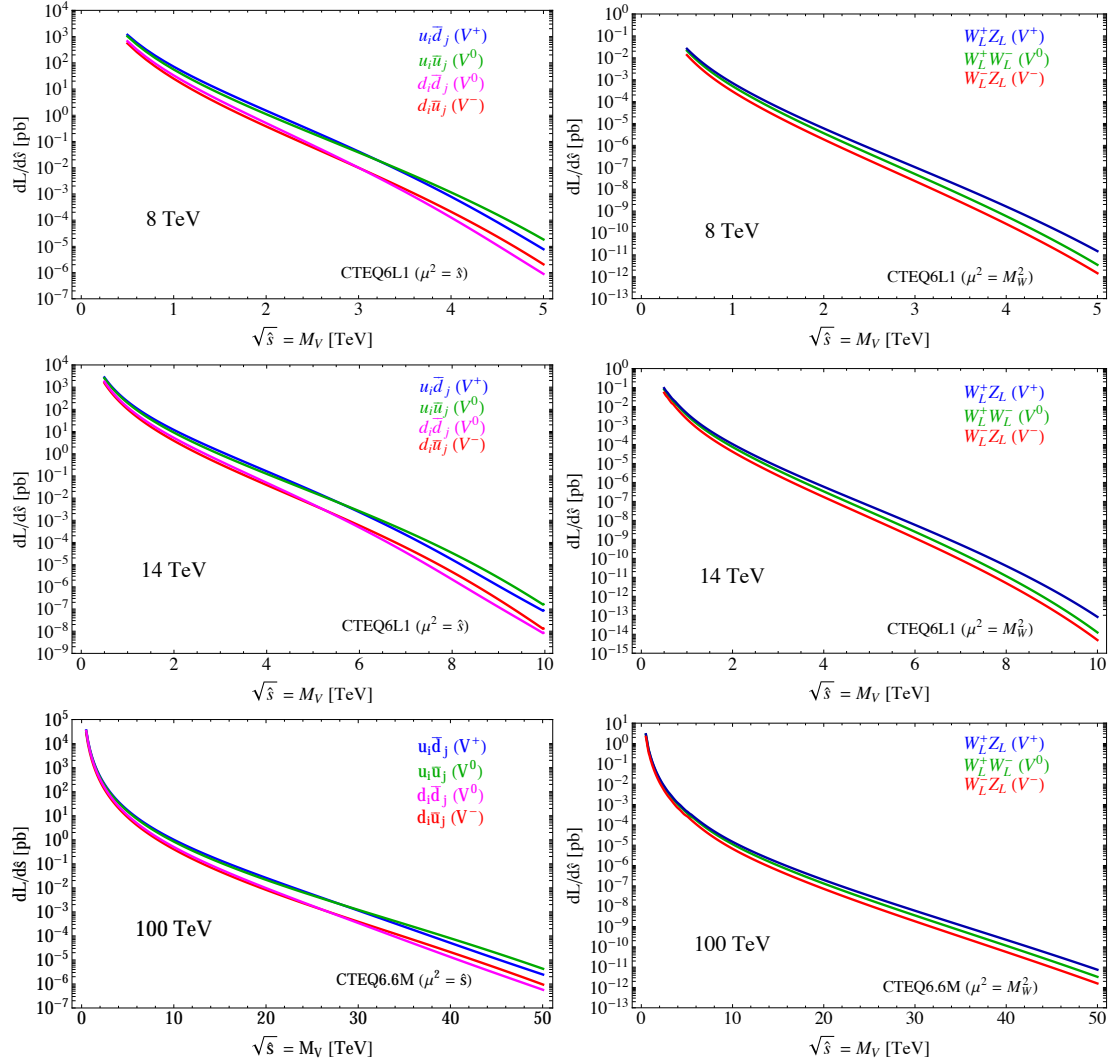


Figure 6.3 – Value of the dL/ds for quark initial states (left plots) and longitudinal vector boson initial states (right plots) for 8 TeV (first row) and 14 TeV (second row) LHC and for a hypothetical 100 TeV pp collider.

coupled scenario, *i.e.* model B, where c_H is not suppressed. In the left panel of Figure 6.4 we show the ratio of the production cross-section by DY and VBF (for the V^+ for illustration) as a function of the c_F/c_H ratio, for different masses at the LHC at 8 TeV and 14 TeV and at a hypothetical 100 TeV pp collider¹⁰. Since, as shown by eq. (6.34) the production cross-section only depends on the corresponding partial widths, we expect the ratio of the cross-sections to depend only on c_F/c_H , up to small corrections of order ζ^2 . The overall normalisation of the c_H, c_F parameters has been set to $c_F = 0.1$. This is necessary because for large g_V , which is the case of interest, when the ratio c_F/c_H becomes small, a c_F of order one would imply a large c_H , which would lead to an unacceptably

¹⁰Studies of new vector resonances at future hadron collider were done in the context of the Snowmass 2013, see Refs. [328–330].

6.2. A Simple Simplified Model for a Heavy Vector Triplet

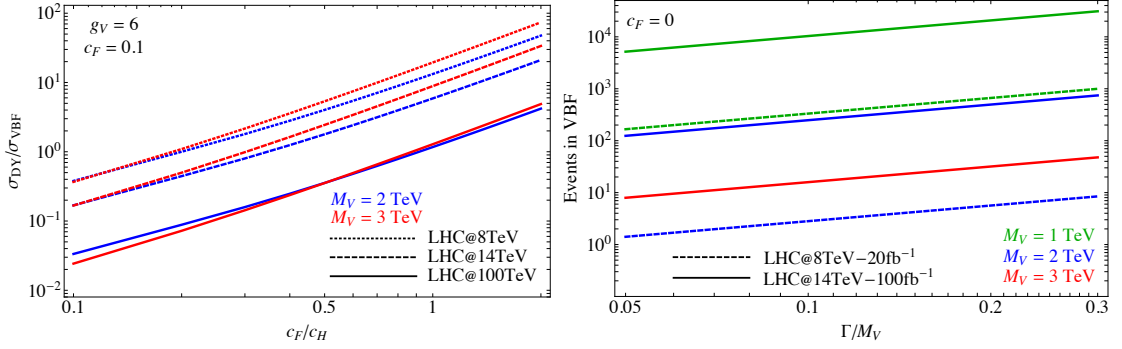


Figure 6.4 – Left panel: ratio of DY over VBF production cross-section for different masses and collider energies. Right panel: expected number of events from VBF production for different masses, collider energies and integrated luminosities, assuming $c_F = 0$. For illustration we consider only V^+ .

large total width. The left panel of Figure 6.4 shows that even for a large coupling $g_V = 6$, a ratio of the order of 3(5) at 14(8) TeV is needed for VBF to become comparable with DY. This ratio can be regarded as the needed suppression in c_F with c_H still being of order one. This further suppression is not expected in general in explicit models, making VBF typically less relevant than DY. For this reason we will ignore VBF in the analysis of the following section and consider only DY production. For the 100 TeV option the situation is different, since for $c_F \approx c_H$ the DY and VBF production cross-sections are comparable for resonances with masses in the few TeV region. Obviously, for higher masses in the range of a few tens of TeV, close to the reach of the 100 TeV collider, we expect VBF to be again subleading with respect to DY.

If the coupling to fermions is suppressed for some reason, $c_F \approx 0$, VBF becomes the dominant production mechanism and it is worth asking ourselves what the mass reach of the LHC would be in this case. In order to answer, we notice that for $c_F \approx 0$ the fermionic decays are suppressed and thus the total resonance width Γ is simply twice the di-boson one which controls, by eq. (6.34), the production rate. Therefore, for a given mass, the expected number of produced vectors (again V^+ for illustration) can be expressed as a function of the Γ/M_V ratio as shown in the right plot of Figure 6.4 for different masses, collider energies and integrated luminosities. The Γ/M_V ratio is an important parameter, as it quantifies to what extent the resonance can be reasonably regarded as a particle. By requiring, for instance, $\Gamma/M_V \lesssim 0.3$ we can obtain an upper bound on the expected signal. We see that at the 8 TeV LHC with 20 fb⁻¹ a reasonable number of events can be obtained only for very low masses, around 1 TeV, where however we expect the resonance to be excluded already by EWPT. At the LHC at 14 TeV with 100 fb⁻¹, a sizeable number of events for a narrow resonance ($\Gamma/M \lesssim 0.1$) seems possible even for relatively high masses, up to around 2.5 TeV. This makes VBF more interesting at the LHC at 14 TeV, at least to explore specific scenarios where the coupling to fermions is suppressed.

Experiment	Channel	Reference
ATLAS	l^+l^-	[234]
CMS		[233]
CMS	$l\nu$	[231]
ATLAS		[232]
ATLAS	$\tau\tau$	[317]
ATLAS	$WZ \rightarrow 3l\nu$	[236]
CMS		[235]
CMS	$qW, qZ, WW/WZ/ZZ \rightarrow jj$	[239]
CMS	$WW \rightarrow l\nu jj$	[237]
ATLAS	jj	[315]
CMS		[322]
CMS	$b\bar{b}, bg$	[321]
ATLAS	$t\bar{t}$	[318]
CMS		[320]
ATLAS	$t\bar{b}$	[319]
CMS		[323]

Table 6.2 – Summary of experimental searches relevant for heavy vector resonances. We have not mentioned the searches of Refs. [238, 316] in the ZZ final state, since this channel is not present in our Simplified Model. The grey entries will not be used when showing bounds in Figure 6.5 since the acceptances for a heavy vector are not reported in the experimental analyses.

6.2.3 Data and Bounds

The ATLAS and CMS collaborations have performed a number of searches for heavy resonances, not only spin-1, decaying into different final states both at the 7 and 8 TeV LHC. A summary of the relevant searches for the study of a heavy vector boson, either charged or neutral, is given in Table 6.2. Most of those analyses present limits on the production cross-section times BR, $\sigma \times \text{BR}$, as a function of the resonance mass.¹¹ If taken at face value, these results are thus very easy to interpret because, as explained in the previous section, both σ and BR can be expressed in analytical form. This allows us to draw exclusion contours in the parameter space of our model in a very efficient way, as we will show in section 6.2.3.2. However, an important message, on which we will elaborate in section 6.2.3.3, is that in some cases the experimental limits, depending on the details of the analysis, are not properly set on $\sigma \times \text{BR}$ because of the effects of the finite resonance width. This problem is particularly acute in strongly coupled scenarios, where the resonance is broader and should be more carefully investigated by the experimental collaborations.

6.2.3.1 A first look at the LHC bounds

Before starting a detailed analysis, let us try to get an idea of the present experimental bounds by discussing two illustrative examples. We consider the benchmark models $A_{g_V=1}$, $B_{g_V=3}$ and $B_{g_V=6}$ described in the previous section as representatives of the “typical” weakly coupled (A) and strongly coupled (B) models with intermediate ($g_V = 3$) and rather strong coupling ($g_V = 6$). In the benchmarks, all the parameters of the model are fixed except for the resonance mass, so they can be very easily compared with the data by looking at Figure 6.5 where we report the bounds on the production cross-sections obtained by rescaling the experimental bounds on $\sigma \times \text{BR}$ by the corresponding BRs and superimpose the theoretical predictions for the production of the positively charged and neutral states. Let us discuss the results separately for the two cases.

Weakly coupled heavy vector

This case is depicted in the upper plots of Figure 6.5. A weakly coupled vector resonance, arising for example as a new gauge boson from an extension of the SM gauge group, is excluded for masses below around 3 TeV for $g_V = 1$. The limit deteriorates for larger coupling because the DY rate is reduced according to eq. (6.25). For this reason, much weaker bounds will be obtained in the strongly-coupled case described below. The bound is dominated by searches into di-lepton and lepton neutrino final states. The searches in di-bosons, *i.e.* namely in hadronic and semileptonic WW and hadronic and fully leptonic WZ are less constraining, but still able to set a bound around 1 – 2 TeV. Also relevant is the search of ATLAS into the $\tau\tau$ final state which sets a bound around 2 TeV. Definitely less constraining are the searches involving the top quark in the final state, like $t\bar{t}$ and $t\bar{b}$.

Using the ratio of the parton luminosities shown in Figure 6.3 we can obtain a naive estimate of the mass reach of the 14 TeV LHC and of a hypothetical 100 TeV pp collider. The exclusion in the weakly coupled region $M_V \sim 3$ TeV for 20 fb^{-1} corresponds to a parton luminosity $\sim 4 \cdot 10^{-2} \text{ pb}$ (see Figure 6.3). Using this number and rescaling to a luminosity of 300 fb^{-1} at the LHC at 14 TeV and to 1 ab^{-1} at the 100 TeV collider we naively find a sensitivity up to $M_V \sim 6$ TeV and $M_V \sim 30$ TeV respectively.

Strongly coupled heavy vector

This case is depicted in the middle and lower plots of Figure 6.5 for an intermediate, $g_V = 3$, and rather stronger, $g_V = 6$, coupling. A strongly coupled vector resonance like a new composite vector boson, analogous to the ρ in QCD, arising for example in Composite Higgs models is excluded up to $\sim 1.5 - 2$ TeV for intermediate coupling of the strong sector and almost unconstrained for large enough coupling ($g_V \gtrsim 5$). The most

¹¹We will not consider the ATLAS and CMS di-jet searches [315, 322] because the limits are given in terms of an acceptance factor. Furthermore the sensitivity of the latter channels is rather reduced.

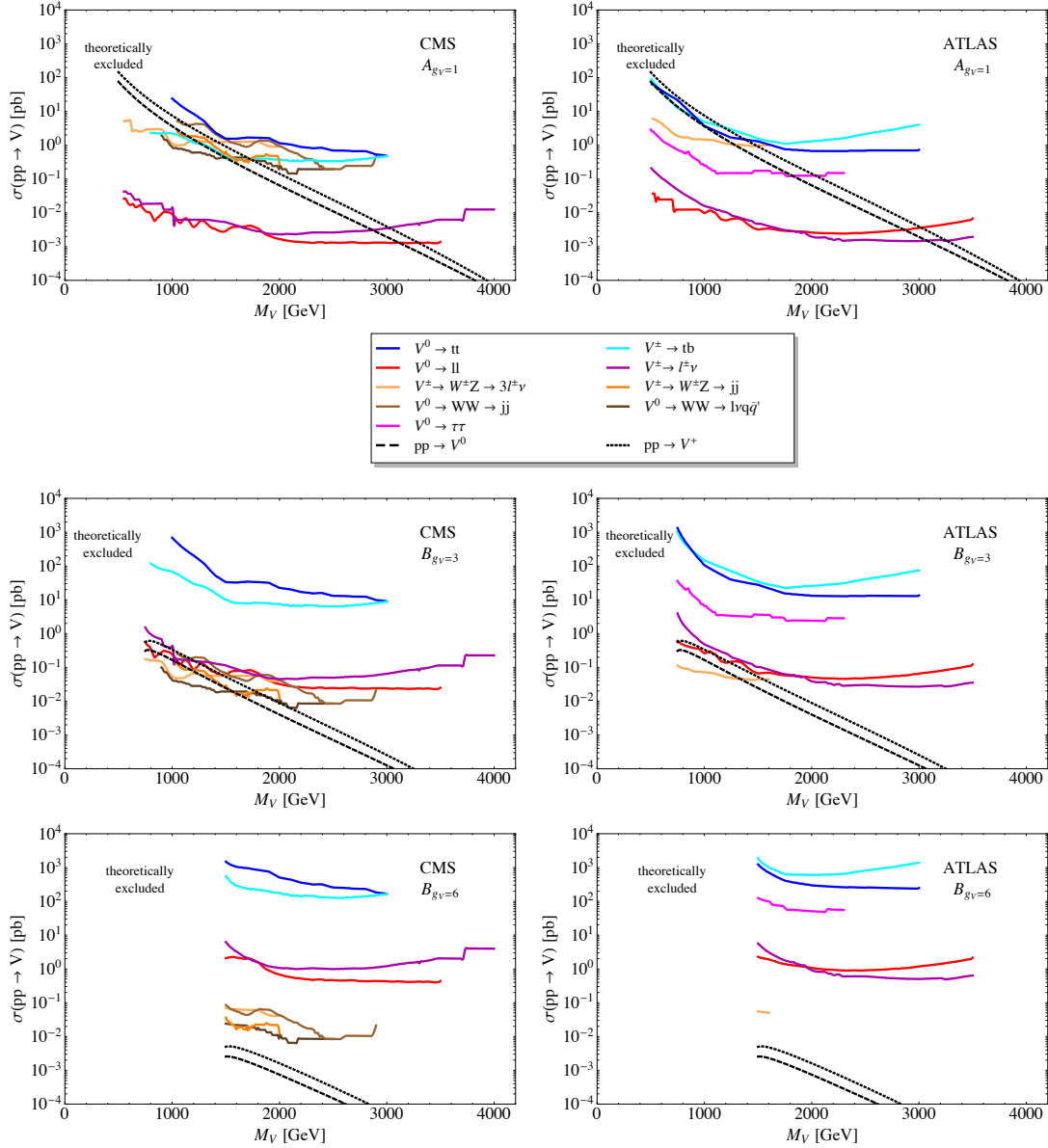


Figure 6.5 – Bounds on the production cross-section for some of the searches listed in Table 6.2 (except for the ones in grey) for the models $A_{g_V}=1$ (upper plots), $B_{g_V}=3$ (middle plots) and $B_{g_V}=6$ (lower plots) for the CMS (left) and ATLAS (right) collaborations.

constraining searches are those into di-boson final states because, as described above, the BRs into vector bosons are much larger than those into fermions. $t\bar{t}$ and tb searches are not particularly sensitive. Notice, however, that we are working under the assumption of a universal coupling to fermions. In potentially realistic strongly coupled scenarios the parameter c_3 is actually expected to be enhanced, improving the sensitivity of third family searches. A careful assessment of this interesting effect is left to future work. Notice that a large portion of the mass range is theoretically excluded, as shown in the plots. This

6.2. A Simple Simplified Model for a Heavy Vector Triplet

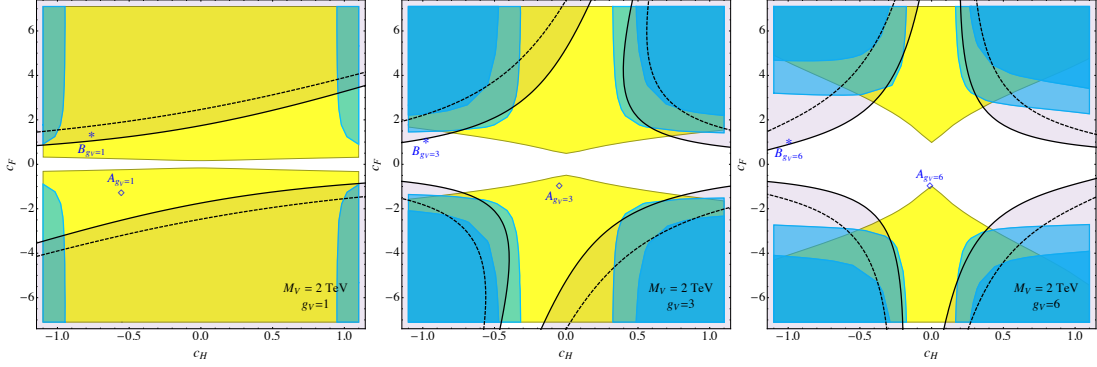


Figure 6.6 – Current experimental constraints in the (c_H, c_F) plane for the four benchmark points at 2 TeV. The yellow region shows the exclusion from $V \rightarrow l\nu$ searches [231] while in blue are regions excluded by $V \rightarrow WZ$ searches with $WZ \rightarrow jj$ [239] in light blue and $WZ \rightarrow 3l\nu$ [235] in dark blue. The solid black lines depict constraints from EWPT at 95% CL and the dashed black line twice this limit. The points corresponding to models A and B for the different values of g_V are also shown.

corresponds to regions where it is not possible to reproduce the SM input parameters α_{EW} , G_F and M_Z for such a small physical mass and large g_V coupling.

Assuming a rather weak strong coupling $g_V = 3$, the same naive rescaling made for the weakly coupled vector gives a naive reach of $M_V \sim 3 - 4$ TeV and $M_V \sim 15 - 20$ TeV at the LHC at 14 TeV with 300 fb^{-1} and the 100 TeV collider with 1 ab^{-1} respectively.

6.2.3.2 Limits on the Simplified Model parameters

The experimental limits on $\sigma \times \text{BR}$ can be simply converted into limits on the relevant parameters of the Simplified Model. In section 6.2 we showed that the most relevant parameters are the mass of the resonance, the overall scale of its couplings g_V and the parameters c_F and c_H describing the interactions with SM fermions and bosons respectively. In order to give an idea of the bounds coming from present analyses we make the simple choice $c_F = c_q = c_l = c_3$ and show the bounds, for given mass and coupling, in the two-dimensional (c_H, c_F) plane. The results, as expected from the discussion of section 6.2, are very weakly sensitive to the other parameters c_{VVW} , c_{VVV} and c_{VVHH} . In the plots we fixed the latter to their values in model A (see section 6.2.4.1) and checked explicitly that the results do not change significantly by setting them to model B.

In Figure 6.6 we show the allowed and excluded regions in the (c_H, c_F) plane for fixed M_V and $g_V = 1, 3, 6$ corresponding, respectively, to weak, intermediate and strong coupling. As an illustrative example we chose $M_V = 2$ TeV as an intermediate mass scale where the experimental constraints are neither too strong nor too weak and thus more interesting. For simplicity, we did not report all the relevant limits in the plots, but only the ones from charged vector searches. The neutral ones could be easily added but would just give

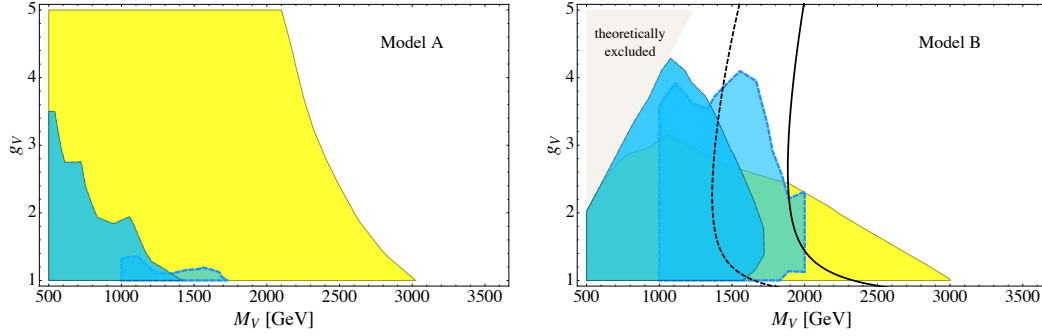


Figure 6.7 – Current experimental constraints in the (M_V, g_V) plane in models A and B. The notation is the same as in Figure 6.6.

comparable constraints and not change the result significantly. Obviously, the situation could have changed if we had performed a statistical combination of the limits in the different channels rather than a superposition of the corresponding excluded regions. However, we think that correlations among the different channels should be taken into account by the experimental collaborations. In the plots, the yellow region represents the exclusion from the CMS $l^+\nu$ analysis of Ref. [233], while the dark and light blue ones show the limits from CMS $WZ \rightarrow 3l\nu$ [235] and $WZ \rightarrow jj$ with W/Z tagged jets [239] respectively.¹² The black curves represent constraints coming from EWPT, *i.e.* from the \hat{S} parameter, which we computed in Appendix D.2. The black solid curve corresponds to the strict 95% C.L. bound on \hat{S} of Ref. [111]¹³, while the dashed line is obtained by artificially enlarging the latter bound by a factor of two. This second line is a more realistic quantification of the constraints than the strict limits because the EWPT observables are eminently off-shell observables and thus not calculable within the Simplified Model. Extra contributions, of the same order as the ones coming from the resonance exchange, can easily arise in the underlying complete model. By enlarging the bound on \hat{S} we take these contributions into account and obtain a conservative exclusion limit.

Any given explicit model corresponds to one point in the plots of Figure 6.6. The two points indicated by *A* and *B* correspond to the prediction of the two benchmark models for the assumed values of g_V and M_V . For small g_V the lepton-neutrino search dominates the exclusion (first plot) and only a narrow band around $-1 \lesssim c_F \lesssim 1$ remains allowed. Here EWPT are not competitive with direct searches and the di-boson searches are almost irrelevant due to the relatively small di-boson BR (see the discussion at the end of section 6.2.1). Moreover, for small g_V both our benchmark models are excluded. As g_V increases we notice four main features: the constraints from EWPT become comparable to the direct searches into di-bosons, di-boson searches become more and more relevant due to

¹²For recent theoretical developments in the search for vector resonances using boosted techniques see, for instance, in Refs. [331–333].

¹³The bound quoted in Ref. [111] is $S = 0.04 \pm 0.10$ obtained from an STU fit.

6.2. A Simple Simplified Model for a Heavy Vector Triplet

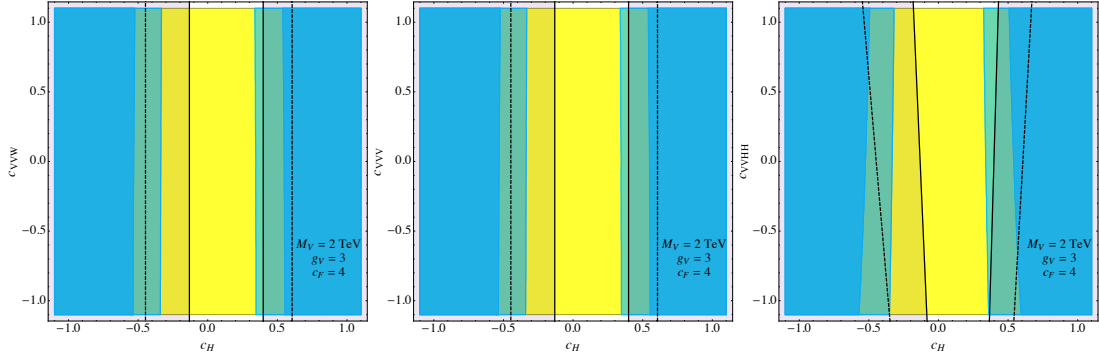


Figure 6.8 – Current experimental constraints in the (c_H, c_{VVW}) , (c_H, c_{VVV}) and (c_H, c_{VVHH}) planes for $g_V = 3$, $M_V = 2$ TeV and $c_F = 4$ (all the other parameters are fixed to their value in model A). The notation is the same as in Figure 6.6.

the enhanced BRs, model B evades bounds from direct searches more and more compared to model A which remains close to the excluded region, and bounds from EWPT constrain model B more than model A. The last two features are due to the larger value of c_H predicted by model B, corresponding to a region which is very difficult to access with direct searches.

A second interesting way to present the experimental limits is to focus on explicit models and draw exclusion curves in the plane of their input parameters. In both models A and B we have two parameters, the coupling and the mass of the new vector. The limits in the (M_V, g_V) plane are reported in Figure 6.7. We find similar exclusions in the two models at low g_V , where the limit is dominated by leptonic final state searches, but the situation changes radically for large coupling. In particular the limit in model B is rather weak and barely competitive with EWPT already for intermediate couplings $g_V \sim 3$ and it disappears when the coupling is large.

Finally we want to check that, as expected from the discussion of section 6.2.1, the parameters c_{VVW} , c_{VVV} and c_{VVHH} affect the exclusion only marginally. We thus plot the same constraints shown in Figure 6.6, in the (c_H, c_{VVW}) , (c_H, c_{VVV}) and (c_H, c_{VVHH}) planes in Figure 6.8 for the benchmark models A and B at $g_V = 3$. The plots represent a horizontal slice at $c_F = 4$ in the second plot of Figure 6.6 using the same colouring as previously. We find c_{VVW} and c_{VVV} indeed to be sub-leading with no variation in their direction. A slight tilt can be observed in the direction of c_{VVHH} , on the other hand. This is due to the enhanced sensitivity on c_{VVHH} induced by the term $(1 - 4c_{VVHH}\zeta^2)^2$ in the width in eq. (6.31) for relatively large ζ . The correction induced by this term can be of the order of 20% for $c_H \sim -0.5$ ($\zeta \approx 0.4$). One could expect the same enhancement in the central plot, due to the term $(1 + c_H c_{VVV}\zeta^2)^2$ in the width in eq. (6.31). However, the absence of the factor of four only gives an effect of the order of the percent for $c_H \sim -0.5$, not clearly observable in the central plot.

6.2.3.3 Limit setting for finite widths

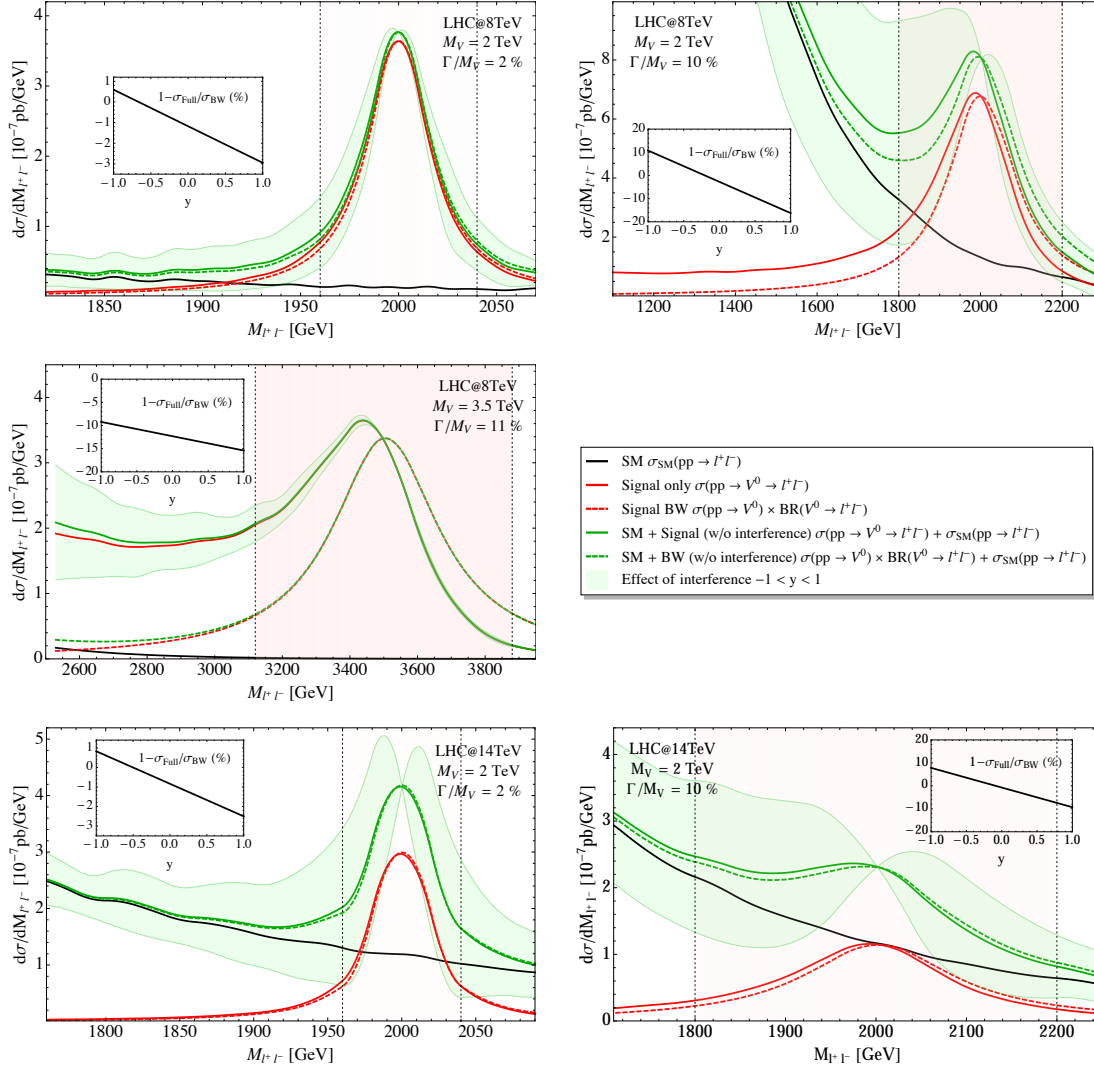


Figure 6.9 – Di-lepton invariant mass distribution for different choices of M_0 and Γ_0/M_0 at the LHC at 8 TeV (first three plots) and 14 TeV (last two plots) c.o.m energy. The Figures show the dependence of the difference between the full $2 \rightarrow 2$ calculation and a simple BW distribution normalized to the on-shell production cross-section and multiplied by the corresponding BR into di-leptons on Γ_0/M_0 . The “inset” plots show the percentage agreement between the cross-sections obtained by integrating the full simulation with a y -dependent interference in the shaded “bin” (varying continuously from fully constructive ($y = 1$) to fully deconstructive ($y = -1$)) and the simple sum of the BW plus the background.

The final goal of a resonance search is to set experimental limits, for either exclusion or discovery, on the resonance production cross-section times the BR into the relevant final states for different mass hypotheses. This way of presenting the experimental results is obviously the simplest and most convenient, as it is completely model-independent and can be very easily interpreted in any given model as we did above. However whether this

goal can be really achieved or not, and with which accuracy, can depend crucially on the details of the analysis and on the assumed total width of the resonance. The aim of this section is to illustrate two kinds of effects associated with the finite particle width that can make the extraction of $\sigma \times \text{BR}$ limits from an experimental search rather involved. Both effects are well-known. Recent discussions can be found in Refs. [296, 301, 334]. Here we will quantify their importance for heavy vector searches at the LHC and propose some strategies to minimise their impact. The results of this section are obviously not conclusive. A detailed analysis of these issues and their impact on the searches should be performed by the experimental collaborations. The final goal should be to quantify, and minimise, the systematic uncertainties associated with the determination of $\sigma \times \text{BR}$.

The example of the di-lepton invariant mass

Let us study the width effects in detail by focusing on the simple case of di-lepton searches for the neutral vector. The relevant observable is the di-lepton invariant mass distribution which we show in Figure 6.9 for different V^0 masses, widths and collider energies. We took a vector resonance with a mass of 2 TeV, both narrow ($\Gamma/M_V = 2\%$) and broad ($\Gamma/M_V = 10\%$) at the LHC at 8 TeV (first row of plots) and 14 TeV (last row of plots) as reference. Finally, in the central plot we show the example of a resonance at 3.5 TeV with $\Gamma/M_V \sim 11\%$ at the 8 TeV LHC.

The first effect to be discussed is the distortion of the signal shape which can depart significantly from the prediction of the BW formula. This can be seen in the Figure by comparing the dashed red curves, which are obtained by the BW distribution normalized to $\sigma \times \text{BR}$, where σ is defined by eq. (6.34) with the red solid lines obtained by MADGRAPH5 simulations of the $2 \rightarrow 2$ process $pp \rightarrow V_0^* \rightarrow l^+ l^-$. We see that in the peak region the distortion is rather mild when the resonance is light (2 TeV) at both the 8 and 14 TeV LHC. The effect is barely visible for $\Gamma/M = 2\%$ and more pronounced for a broad resonance $\Gamma/M = 10\%$. The distortion is more significant for a 3.5 TeV mass but the deviation is still under control. This can be seen by comparing the area of the two curves in the interval $[M - \Gamma, M + \Gamma]$ depicted as a shadowed region in the plots. The relative deviation is depicted in the inset plots for $y = 0$. We see that it is of around 10% in the worst case of $M_V = 3.5$ TeV and $\Gamma/M_V \sim 11\%$. Outside the peak, on the contrary, the situation is worrisome already for $M_V = 2$ TeV. The simulated signal has a long tail extending towards small invariant masses which is due to the steep fall of the parton luminosities.

By focusing on the peak, where the signal is well approximated by the BW prediction, extracting the limit on $\sigma \times \text{BR}$ is straightforward. For instance one could simply measure the cross-section of the $2 \rightarrow 2$ process integrated in a window around the resonance mass and convert it into a bound on $\sigma \times \text{BR}$ by rescaling for the fraction of events that, according to the BW distribution, are expected to fall in the selected window. Alternatively, one

could perform a shape analysis by assuming a BW signal shape and extract a limit on its normalisation. Also in this second case the analysis should be restricted to the peak region because the tail is not well-described by the BW formula. Notice in particular that the total area of the simulated signal, that gives the total $2 \rightarrow 2$ cross-section, can differ considerably from $\sigma \times \text{BR}$. The low-mass tail, which extends in a wide range of masses, can indeed give a sizeable contribution to the total integral.

In order to understand the effect in more detail, let us briefly remind the reader of the assumption under which the BW formula is derived. The measured signal is $pp \rightarrow l^+ l^-$ whose partonic cross-section is

$$\hat{\sigma}_S(\hat{s}) = \frac{4\pi\hat{s}}{3M_V^2} \frac{\Gamma_{V \rightarrow q_i q_j} \Gamma_{V \rightarrow l^+ l^-}}{(\hat{s} - M_V^2)^2 + M_V^2 \Gamma^2}. \quad (6.35)$$

After convoluting with the PDFs, and using $\hat{s} = M_{l^+ l^-}^2$, the total differential cross-section reads

$$\frac{d\sigma_S}{dM_{l^+ l^-}^2} = \sum_{i,j} \frac{4\pi}{3} \frac{\Gamma_{V \rightarrow q_i q_j} \Gamma_{V \rightarrow l^+ l^-}}{(M_{l^+ l^-}^2 - M_V^2)^2 + M_V^2 \Gamma^2} \frac{M_{l^+ l^-}^2}{M_V^2} \frac{dL_{ij}}{d\hat{s}} \bigg|_{\hat{s}=M_{l^+ l^-}^2}. \quad (6.36)$$

In the peak region, namely for $M_{l^+ l^-} - M_V \sim \Gamma$, and only in that region, it is reasonable to approximate

$$\frac{M_{l^+ l^-}^2}{M_V^2} \frac{dL_{ij}}{d\hat{s}} \bigg|_{\hat{s}=M_{l^+ l^-}^2} \simeq \frac{dL_{ij}}{d\hat{s}} \bigg|_{\hat{s}=M_V^2}, \quad (6.37)$$

from which, using eq. (6.34), the differential cross-section can be written in terms of the on-shell $\sigma \times \text{BR}$, times a universal function

$$\frac{d\sigma_S}{dM_{l^+ l^-}^2} = \sigma \times \text{BR}_{V \rightarrow l^+ l^-} \text{BW}(M_{l^+ l^-}^2; M_V, \Gamma), \quad (6.38)$$

where BW denotes the standard relativistic BW distribution

$$\text{BW}(\hat{s}; M_V, \Gamma) = \frac{1}{\pi} \frac{\Gamma M_V}{(\hat{s} - M_V^2)^2 + M_V^2 \Gamma^2}. \quad (6.39)$$

Whether eq. (6.38) is a good description of the $2 \rightarrow 2$ shape or not depends on how accurately the assumption (6.37) holds, namely it depends on how fast the parton luminosities vary in the peak region. Therefore the agreement is better for smaller widths when the peak is narrower. But the level of agreement also depends on the resonance mass and decreases when the resonance approaches the kinematical production threshold of the collider. This is because after a certain threshold the parton luminosities start to decrease extremely fast, more than exponentials, so that regarding them as constants is less and less justified even for a narrow width. This threshold corresponds, in Figure 6.3,

6.2. A Simple Simplified Model for a Heavy Vector Triplet

to the point where the luminosities become concave functions in logarithmic scale around 3 or 3.5 TeV at the 8 TeV LHC. This explains why the peak distortion is so pronounced at the 3.5 TeV mass point. Notice that the peak distortion could be modelled, starting from eq. (6.36), and the agreement with the simulated signal improved by employing a “distorted” BW shape. We will not discuss this possibility because we consider the BW description to be sufficiently accurate in the cases at hand. However such an improvement could be helpful in order to deal with more problematic situations.

The second important effect to be taken into account originates from the quantum mechanical interference of the resonance production diagrams with those of the SM background. Differently from before the strength of this second effect crucially depends on the amount of background which is present in the peak region or, more precisely, on the signal to background ratio. Notice that only the strictly irreducible backgrounds matter, because interference can only occur among processes with the exact same initial and final states at the partonic level. In Figure 6.9, the upper and lower boundaries of the green shaded region are the result of two complete simulations, including interference, of the $pp \rightarrow l^+l^-$ process as obtained at two different points of the parameter space of our model. For each mass and collider energy the two points are chosen to have identical production rates and partial widths but, respectively, constructive and destructive interference. The two points are simply related by flipping the relative sign of c_q and c_l , which leads to identical rates and widths but opposite interference. The green solid lines correspond instead to the “signal plus background” prediction, obtained by ignoring the interference and summing the background, reported in black, with the “signal only” line in red. In dashed green we show the signal plus background curves obtained by the BW prediction of the signal. Notice that the interference never vanishes in any model so that the signal-plus-background shape does not represent any point of the parameter space. However the interference could be reduced, and most of the shaded region could be populated by some explicit model. Therefore, imagining for simplicity that the interference can be continuously varied from constructive to destructive we define

$$\frac{d\sigma_{\text{Full}}}{dM_{l^+l^-}}(y) = \frac{d\sigma_{\text{B}}}{dM_{l^+l^-}} + \frac{d\sigma_{\text{S}}}{dM_{l^+l^-}} + y \frac{d\sigma_{\text{I}}}{dM_{l^+l^-}}. \quad (6.40)$$

By varying y among -1 and 1 we can get a rough idea of how much the interference effect can change the shape in different regions of the parameter space.

We see in the Figure that the shape distortion due to the interference is considerable, and in most cases more significant than the one due to the PDFs. Notice however that we are voluntarily considering pessimistic cases where the interference distortion is enhanced. The idea is that if we manage to deal with these situations we will have no problems in covering more favourable cases. As mentioned above, the interference distortion depends on the signal to background ratio, therefore for a given mass and collider energy, where the background is fixed, the effect is maximal for the smallest possible signal cross-section. For

the plots in Figure 6.9 we thus selected the minimal cross-sections that can be excluded at the 8 TeV LHC with 20 fb^{-1} and at 14 TeV with 100 fb^{-1} . Stated in a different way, we placed ourselves at the boundary of the excluded $\sigma \times \text{BR}$ region for each mass hypothesis. In the bulk of the excluded region, where $\sigma \times \text{BR}$ is well above the one assumed in the plots, the signal shape would grow and the interference effect would become relatively less important. With this choice, the interference is more important at 14 than at 8 TeV because with the assumed luminosity the exclusion will be set in a region where the background is larger. For the 3.5 TeV mass point the interference is negligible because the background is very small and the distortion is mainly due to the PDF effect as described above.

Notice that, differently from the PDF effect, the distortion due to the interference can not be modelled in any simple way. Namely, it is impossible to cast it in a way that only depends on the production rate and on the widths, indeed we saw above that it depends on other parameter combinations. Obviously it could be computed by a simulation, but the resulting shape would depend in a complicated way on all the model parameters and could not be taken as a universal template. Therefore by proceeding in this way it would not be possible to set model-independent limits on $\sigma \times \text{BR}$ and the comparison of the model with the data should be performed by scanning the parameter space with simulations on a grid of points.

Two different attitudes could be taken towards this problem. One could insist with a shape analysis, assuming a BW signal, and accept the intrinsic systematic uncertainty associated with this assumption. Of course the uncertainty should be quantified by comparing with the limits obtained with the “true” shape, taken for instance from eq. (6.40) for different values of y . Alternatively, one could turn to a simpler cut-and-count experiment and try to reduce the impact of the interference by exploiting the following observation. In general, the interference contribution to the partonic cross-section has the functional form

$$\hat{\sigma}_I(\hat{s}) \propto \frac{(\hat{s} - M_V^2)}{(\hat{s} - M_V^2)^2 + M_V^2 \Gamma^2}, \quad (6.41)$$

so that it vanishes exactly at $\hat{s} = M_V^2$ as is odd around this point. This explains why the shaded green region shrinks to a point for an invariant mass equal to the resonance mass. After PDF convolution one can show that, provided the approximation of constant parton luminosities in eq. (6.37) holds accurately enough, the interference contribution to the signal shape is also an odd function around $M_{l+l-} = M_V$ and thus it cancels when integrated over a symmetric interval. The signal in the $[M_V - \Gamma, M_V + \Gamma]$ region is thus much less sensitive to the interference than the shape itself.¹⁴ This is confirmed by the

¹⁴For a complete cancellation one should consider a domain which is symmetric in the squared invariant mass variable. The cancellation is only approximate in the window we have chosen. However we prefer to stick to this simpler prescription of a symmetric domain in M_{l+l-} , because the cancellation would not be exact anyhow due to the PDF variation in the peak region.

inset plots, where we report the relative deviation of the total signal in the window, compared to the BW signal plus background prediction as a function of the parameter y . We see that the deviation is typically below 10% even in cases where the shape distortion due to the interference is considerable.

In view of the above results, let us briefly discuss the limit setting procedure employed by CMS [233] and ATLAS [234] in the di-lepton searches. After suitable selection and identification cuts, both analyses perform a shape analysis on the di-lepton invariant mass distribution based on an un-binned (CMS) or binned (ATLAS) likelihood. The only relevant difference among the two methods is the choice of the assumed signal distribution and the mass-range where the analysis is performed. CMS employs a gaussian shape obtained by convoluting a narrow resonance peak with the detector resolution function and the analysis is performed in an invariant mass window around the resonance mass. If the resonance is assumed to be extremely narrow, the CMS strategy is definitely correct and leads to an accurate determination of $\sigma \times \text{BR}$. However, no finite width effect is taken into account with this method. It is not even clear, and we plan to study this and related aspects in a future publication, how narrow the resonance must be in order to make this method reliable. Notice that asking for a width below the experimental resolution might not be sufficient as the distortion effects outlined above take place already in the theoretical distribution and are completely unrelated with the detector resolution. Furthermore, assuming a too small width might be inconsistent with the amount of signal needed for exclusion. A given DY cross-section requires, at fixed mass, a given $q\bar{q}$ partial width and thus a minimal total width. Moreover, a non-vanishing BR into di-leptons is needed, leading to a larger minimal width. By exploiting this observation it is possible to compute the minimal width needed, at a given mass, for 3 or more signal events at the 8 TeV LHC. For a mass of 3.5 TeV, for instance, the minimal width is $\Gamma/M_V \gtrsim 10\%$ and therefore it would be inconsistent to set an exclusion limit for a very narrow resonance at this mass. The existence of a minimal width is the reason why we have not considered the case of a narrow 3.5 TeV resonance in Figure 6.9. The ATLAS strategy is different from CMS in two respects. First, it performs the shape analysis in the full mass range rather than around the peak. In light of the above discussion, this is definitely a limitation. Second, it employs a template signal shape obtained by a sequential Z' model [290]. In this manner ATLAS somehow takes the effect of the width into account, but in a rather incomplete way because at each mass point the width is the one predicted by the sequential Z' model. In other scenarios, with larger g_V , the width could be larger and the limit could change significantly. One might argue that at least the ATLAS limit, differently from the CMS one, is strictly correct within the specific model assumed in the simulation. However this is questionable as the interference effects, which are relevant close to the exclusion limit as shown above, are not included in the simulations.

The case of lepton-neutrino

In the discussion above we focused on the simple example of the di-lepton final state, however our considerations are more general and apply to all those searches where the resonance invariant mass distribution can be reconstructed. This clearly includes di-jets [315, 322] and di-bosons in the hadronic channels [239], but also searches with one leptonic W and reconstructed neutrino momentum [235, 236]. In all these cases, the invariant mass distribution approximately follows the BW formula and the distortions due to the PDF and interference effects could be analysed along the lines described above. Of course we expect that in these more complicated examples the experimental resolution, which we could safely ignore for di-leptons, could play an important role and should be taken into account. However, no qualitative difference is expected.

A radically different situation is instead encountered when the invariant mass can not be reconstructed, as in the CMS search [231] in the lepton-neutrino final state. Setting a model-independent limit on $\sigma \times \text{BR}$ might seem hopeless in this case, because one can not rely on the BW formula which of course only describes the invariant mass distribution while the relevant observable is now the transverse mass M_T . This problem has been studied in detail in Ref. [301] with the conclusion that indeed a model-independent limit can not be set and that the search must be reinterpreted in each given model separately. However, there could be a way out. Any pair of massless leptons, of any chirality, produced by the DY mechanism through the s -channel exchange of one vector, are characterised by a universal angular distribution relative to the beam direction in the center of mass frame. Namely, the angular dependence of the partonic cross-section is effectively $1 + \cos^2 \theta$ because the term linear in $\cos \theta$ cancels out for a symmetric proton-proton collider such as the LHC.¹⁵ Given that the angular dependence is fixed, the p_T distribution of the final states can be uniquely computed and expressed, as usual in the limit (6.37) of slowly varying PDFs, in terms of $\sigma \times \text{BR}$. If the resonance is produced at rest in the transverse plane, which we expect to be a good approximation when it is sufficiently heavy, we have $M_T = 2p_T$ and we predict

$$\frac{d\sigma}{dM_T^2} = \sigma \times \text{BR}_{V \rightarrow l\nu} \text{TBW}(M_T; M_V, \Gamma) \quad (6.42)$$

where we denote as TBW a “transverse BW” distribution defined by the following integral

$$\text{TBW}(M_T; M_V, \Gamma) = \frac{3\Gamma}{8\pi M_V} \int_{M_T^2}^s \frac{d\hat{s}}{\sqrt{\hat{s} - M_T^2}} \frac{2\hat{s} - M_T^2}{(\hat{s} - M_V^2)^2 + \Gamma^2 M_V^2} \frac{1}{\sqrt{\hat{s}}} . \quad (6.43)$$

Needless to say, eq. (6.42) is obtained by neglecting the interference, and in the approxi-

¹⁵Of course it does not cancel for asymmetric beams and this is why Z boson asymmetries could be studied at the Tevatron.

6.2. A Simple Simplified Model for a Heavy Vector Triplet

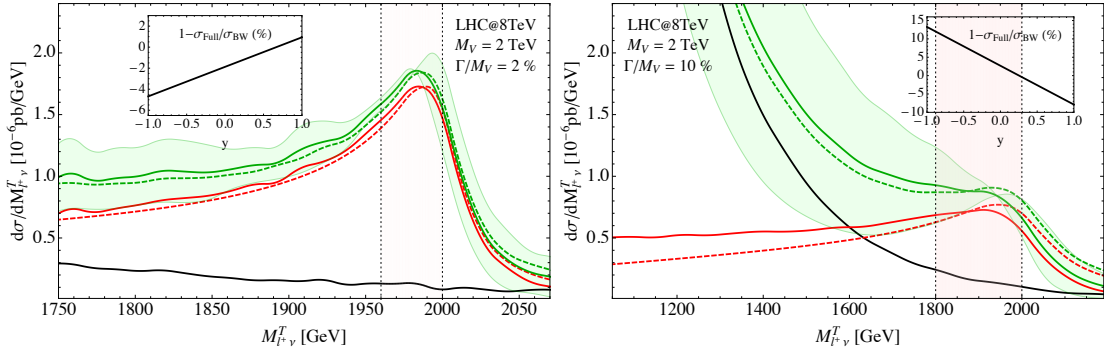


Figure 6.10 – Lepton-neutrino transverse mass distribution for the choices of M_+ and Γ_+/M_+ analogous to the ones of the first two plots of Figure 6.9 at the LHC at 8 TeV. The Figures show the dependence on Γ_+/M_+ of the difference between the full $2 \rightarrow 2$ calculation and a simple TBW distribution normalized to the on-shell production cross-section and multiplied by the corresponding BR into lepton-neutrino. The notation (dashing, colouring, “inset” plots) is identical to Figure 6.9.

mation of slowly-varying PDF. The level of agreement with the “true” signal is illustrated by Figure 6.10. We considered the same points of the parameter space that were used in Figure 6.9 for the 2 TeV neutral resonances at the 8 TeV LHC and we show the M_T shape of the associated charged state. We see that the signal, defined as the cross-section in the window $M_T \in [M_V - \Gamma, M_V]$, is described by eq. (6.42) at the 10% level. However in this case, differently from the previous one, most of the signal is lost when restricting to the window we have selected, decreasing the sensitivity of the analysis. One should probably try to enlarge the window, accepting a larger error. Notice however that the interference, which is the dominant distortion effect, has been maximised in Figure 6.10 by choosing the smallest possible rate as described above. The accuracy of the method would improve for higher rates, allowing at least to set a more conservative, but robust and model-independent limit.

6.2.4 Explicit Models

In this section we present two examples of explicit models to populate the parameter space of the Simplified Model. The first one, called model A, describes the vector triplet emerging from the symmetry breaking pattern $SU(2)_1 \times SU(2)_2 \times U(1)_Y \rightarrow SU(2)_L \times U(1)_Y$ achieved through a linear σ -model [286]. The second model, B, describes the vector triplet considered in Ref. [97] based on a non-linearly realised $SO(5)/SO(4)$ global symmetry.

6.2.4.1 Model A: extended gauge symmetry

We consider the gauge theory $SU(2)_1 \times SU(2)_2 \times U(1)_Y$ [286]. The SM fermions are assumed to be charged under $SU(2)_1$ and $U(1)_Y$ with their usual quantum numbers. The SM Higgs doublet transforms as a $(\mathbf{2}, \mathbf{1})_{1/2}$ under the enlarged gauge group. We

also introduce an additional scalar field Φ transforming as a real bidoublet $(\mathbf{2}, \mathbf{2})_0$. The bosonic part of the Lagrangian is

$$\mathcal{L} = -\frac{1}{4g_1^2} W_{1\mu\nu}^a W_1^{a\mu\nu} - \frac{1}{4g_2^2} W_{2\mu\nu}^a W_2^{a\mu\nu} + D_\mu H^\dagger D^\mu H + \text{Tr}(D_\mu \Phi^\dagger D^\mu \Phi) - \mathcal{V}(H, \Phi). \quad (6.44)$$

In order to obtain the SM at low energies we assume the potential \mathcal{V} in eq. (6.44) to be such that Φ obtains a vacuum expectation value

$$\langle \Phi \rangle = \begin{pmatrix} f & 0 \\ 0 & f \end{pmatrix}. \quad (6.45)$$

This VEV breaks the $SU(2)_1 \times SU(2)_2$ gauge symmetry to its vectorial subgroup which is identified with the SM $SU(2)_L$ gauge group. By going to the unitary gauge for the heavy vector triplet one obtains the following mass term from the kinetic term of Φ

$$\text{Tr}(D_\mu \Phi^\dagger D^\mu \Phi) \supset \frac{f^2}{2} (W_{1\mu}^a - W_{2\mu}^a)^2. \quad (6.46)$$

A single gauge invariance under which both W_1 and W_2 shift in the same way is preserved. It is thus useful to perform the following field redefinition

$$W_{2\mu}^a = V_\mu^a + W_{1\mu}^a. \quad (6.47)$$

In this way V transforms as the triplet of section 6.2 and W_1 is just the SM W boson field (the index “1” will be dropped from now on).

The only part of the Lagrangian that transforms non trivially under the field redefinition in eq. (6.47) is the kinetic term of W_2 . One has

$$W_{2\mu\nu}^a = D_{[\mu} V_{\nu]}^a + \epsilon^{abc} V_\mu^b V_\nu^c + W_{\mu\nu}^a, \quad (6.48)$$

which leads to

$$\begin{aligned} W_{2\mu\nu}^a W_2^{a\mu\nu} &= W_{\mu\nu}^a W^{a\mu\nu} + D_{[\mu} V_{\nu]}^a D^{[\mu} V^{a\nu]} + 2W_{\mu\nu}^a D^{[\mu} V^{a\nu]} \\ &\quad + 2\epsilon^{abc} W_{\mu\nu}^a V^{b\mu} V^{c\nu} + O(V^4). \end{aligned} \quad (6.49)$$

After the redefinition, the Lagrangian develops a kinetic mixing between V and W and thus it can be matched with eq. (6.2) only after the mixing is removed by one further redefinition. This is performed in Appendix D.1, starting from a “tilded” field basis in which the kinetic mixing term is present. By identifying

$$g_V \equiv g_2 \quad \text{and} \quad \frac{1}{g^2} \equiv \frac{1}{g_1^2} + \frac{1}{g_2^2}, \quad (6.50)$$

we have

$$\tilde{m}_V = g_V f, \quad \tilde{c}_{VW} = -\tilde{c}_{V\bar{V}W} = \tilde{c}_{VVV} = -1, \quad \tilde{c}_H = \tilde{c}_{VVHH} = \tilde{c}_F = 0, \quad (6.51)$$

from which we obtain the parameters in eq. (6.2) by the relations in eq. (D.4). In particular, we see that in all cases, $g_* \sim g$ or $g_* \gg g$

$$c_H \sim -g^2/g_V^2 \quad \text{and} \quad c_F \sim 1. \quad (6.52)$$

Depending on the precise form of the potential $\mathcal{V}(H, \Phi)$ and in particular depending on the presence of a $\lambda|H|^2 \text{Tr} \Phi^\dagger \Phi$ term, an additional contribution to c_{VVHH} proportional to $\lambda g_2^2 f^2/m_\Phi^2$ is generated by integrating out the physical mode of Φ . We define our benchmark model setting $\lambda = 0$. However, finite λ effects can be easily accounted for by modifying eq. (6.51). We will come back to this point in section 6.2.4.3. Notice that integrating out Φ also generates (irrelevant) contributions to the quartic interaction of V .

6.2.4.2 Model B: Minimal Composite Higgs Model

Models in which the Higgs boson emerges as a light state (a pseudo Nambu-Goldstone boson) from an underlying strong dynamics predict the existence of heavy vector resonances with electroweak quantum numbers. In the case of the Minimal Composite Higgs Model (MCHM), where the Higgs doublet emerges from the spontaneous breaking of a global $SO(5)$ symmetry to an $SO(4)$ subgroup, these resonances have been discussed in Refs. [3, 97]. Here we want to show how the lightest vector resonance in these models can be described by our Simplified Model. In order to enforce the constraints imposed by the underlying symmetry structure a minimal amount of technical complications is required. Here we follow Ref. [97] which uses the Callan-Coleman-Wess-Zumino (CCWZ) formalism reviewed, for instance, in Appendix A of Ref. [240]. The matching with the Lagrangian of the Simplified Model can be found at the end of this section and the reader who is not interested in the derivation can jump there directly.

We introduce a spin 1 field ρ_μ transforming under the unbroken $SO(4)$ subgroup as a $(\mathbf{3}, \mathbf{1})$ irreducible representation

$$\rho_\mu \equiv \rho_\mu^a t^a \rightarrow h_4 \rho_\mu h_4^T - i h_4 \partial_\mu h_4^T \quad \text{for} \quad a = 1, 2, 3, \quad (6.53)$$

where t^a are generators of the $SU(2)_L$ subgroup of $SO(4)$ in the vector representation and h_4 is a non-linear $SO(4)$ transformation whose construction is described in Appendix A of Ref. [240]. We consider the following Lagrangian

$$\mathcal{L}_\rho = -\frac{1}{4\hat{g}^2} (B_{\mu\nu})^2 - \frac{1}{4\hat{g}^2} (W_{\mu\nu}^a)^2 + \frac{f^2}{4} d_\mu^i d^{\mu i} - \frac{1}{4g_\rho^2} (\rho_{\mu\nu}^a)^2 + \frac{m_\rho^2}{2g_\rho^2} (\rho_\mu^a - e_\mu^a)^2. \quad (6.54)$$

The ρ field strength is given by $\rho_{\mu\nu}^a = \partial_\mu \rho_\nu^a - \partial_\nu \rho_\mu^a - \epsilon^{abc} \rho_\mu^b \rho_\nu^c$. The full expressions for the d and e symbols for $SO(5)/SO(4)$ are given in Appendix A of Ref. [240]. Here we will only need approximate formulas in the large f limit

$$d_\mu^i d^{\mu i} = \frac{4}{f^2} |D_\mu H|^2 + \frac{2}{3f^4} [(\partial_\mu |H|^2)^2 - 4|H|^2 |D_\mu H|^2] + O(1/f^6), \quad (6.55)$$

and

$$\rho_\mu^a - e_\mu^a = \rho_\mu^a + W_\mu^a - \frac{i}{f^2} H^\dagger \tau^a \overleftrightarrow{D}_\mu H + \frac{i}{f^4} |H|^2 H^\dagger \tau^a \overleftrightarrow{D}_\mu H + O(1/f^6). \quad (6.56)$$

We can thus define the triplet V , which does not shift under the SM gauge group, as

$$V_\mu^a \equiv \rho_\mu^a + W_\mu^a. \quad (6.57)$$

Under this field redefinition the ρ kinetic term transforms as

$$\rho_{\mu\nu}^a = D_{[\mu} V_{\nu]}^a - \epsilon^{abc} V_\mu^b V_\nu^c - W_{\mu\nu}^a, \quad (6.58)$$

and using the large f expressions in eq. (6.55) and (6.56) it is now straightforward to match \mathcal{L}_ρ with the “tilded” basis of Appendix D.1. By identifying

$$g_V = g_\rho, \quad \frac{1}{g^2} = \frac{1}{\hat{g}^2} + \frac{1}{g_\rho^2} \quad \text{and} \quad g' = \hat{g}', \quad (6.59)$$

and after normalising the kinetic term of V we obtain

$$\tilde{m}_V = m_\rho, \quad \tilde{c}_{VW} = \tilde{c}_{V\bar{V}W} = \tilde{c}_{VVV} = 1, \quad \tilde{c}_H = -\frac{m_\rho^2}{g_\rho^2 f^2} \equiv -a_\rho^2, \quad \tilde{c}_{VVHH} = \tilde{c}_F = 0, \quad (6.60)$$

where a_ρ is an $O(1)$ free parameter as defined in Ref. [97]. Using eq. (D.4) we see that

$$c_H \sim c_F \sim 1. \quad (6.61)$$

The difference with the linear model of the previous section arises from the fact that \tilde{c}_H is now non vanishing.

In order to perform the matching we ignored both higher dimension operators coming from subleading corrections to eq. (6.56) and higher derivative terms which could be added to the Lagrangian in eq. (6.54). We will discuss their effects in the next section.

6.2.4.3 The role of higher dimensional operators

The simple phenomenological Lagrangian in eq. (6.2) has been the starting point of our discussion. Its usefulness stems from the fact that it contains just a handful of parameters due to neglecting all the higher dimensional operators.

As already stressed throughout the chapter eq. (6.2) has to be understood as an intermediate step to compare a more or less complete model of New Physics with the experimental data. That is, not as the leading subset of terms of the effective field theory describing the interactions of V with the SM. From this point of view the fact that eq. (6.2) is all that is needed has to be guaranteed by the underlying theory. We will now check this assumption for the two models we presented in the last two sections.

This discussion is almost straightforward in the context of the linear model. Since the model is renormalizable higher dimensional operators can only be generated by integrating out the heavy physical fluctuations of the scalar field Φ . A hierarchy of masses $m_\Phi \gg m_V$ is understood in order to be allowed to study the vector in isolation. The real bidoublet Φ can be written as

$$\Phi = \frac{\phi_0}{2} + i\tau^a \phi_a. \quad (6.62)$$

In this way eq. (6.45) can be rephrased as $\langle \phi_0 \rangle = 2f$. The three scalar fields ϕ_a are unphysical and only ϕ_0 remains in the spectrum with a mass m_Φ which depends on the parameters in the potential $\mathcal{V}(H, \Phi)$. In the unitary gauge for V_μ , the only relevant ϕ_0 interactions come from the kinetic term of Φ and from a mixed Φ - H quartic coupling which can be present in \mathcal{V}

$$\text{Tr}(D_\mu \Phi^\dagger D^\mu \Phi) - \lambda H^\dagger H \text{Tr}(\Phi^\dagger \Phi) = \frac{1}{2}(\partial_\mu \phi_0)^2 + \frac{g_V^2}{8} \phi_0^2 V_\mu^a V^{\mu a} - \frac{\lambda}{2} \phi_0^2 H^\dagger H. \quad (6.63)$$

By integrating out the heavy ϕ_0 field we obtain the following Lagrangian containing operators up to dimension 6

$$\Delta \mathcal{L}_A = \frac{2\lambda^2 f^2}{m_\Phi^2} |H|^4 - \frac{\lambda g_V^2 f^2}{m_\Phi^2} V_\mu^a V^{\mu a} |H|^2 + \frac{3}{2} \frac{\lambda^2 g_V^2 f^2}{m_\Phi^4} V_\mu^a V^{\mu a} |H|^4 + O(V^4, |H|^6, \dots). \quad (6.64)$$

The first term is an unobservable modification of the Higgs quartic coupling while the second is the contribution to c_{VVHH} that was already anticipated in section 6.2.4.1. It modifies the matching in eq. (6.51) by

$$\tilde{c}_{VVHH} = \frac{\lambda f^2}{m_\Phi^2}. \quad (6.65)$$

The operator

$$\mathcal{O}'_{VVHH} \equiv V_\mu^a V^{\mu a} |H|^4, \quad (6.66)$$

is new and not included in the phenomenological model. It is easy to verify that all its effects, both in the mass matrix and in the couplings of V to W_L , Z_L and h , are suppressed by a factor $\lambda v^2/m_\Phi^2$ with respect to those emerging from \tilde{c}_{VVHH} in eq. (6.65). In a reasonably weakly coupled theory these effects are small and can be safely neglected.

A similar discussion for the non-linear model described in section 6.2.4.2 is necessarily more involved. This is due to its intrinsically finite energy range of validity. In order to have any predictive power the theory has to be endowed with a criterion to estimate the size of the coefficients of the higher dimensional operators. Using this criterion one must be able to show that only a finite number of operators is relevant to achieve a given precision. Here we adopt a slight modification of the *partial UV completion* criterion used in Ref. [97]. We assume that a New Physics mass scale m_* is defined (which could for instance characterise the mass scale of other resonances) such that $m_V \ll m_*$. We furthermore assume that all “composite” states in the theory, which include V , H and the other resonances at m_* , interact with a strength of order g_* when probed at energies of order m_* . More in detail we require that for $E \sim m_*$, amplitudes involving “composite” fields have size $g_* m_*$ and g_*^2 for three and four point functions respectively. Applying this to the scattering amplitude of four Goldstone bosons, it implies in particular that $m_* \sim g_* f$. This criterion has to be extended to estimate the size of those amplitudes involving weakly coupled fields, for instance insertions of the SM gauge bosons. These amplitudes originate from the EW force and not from the strong sector interactions. We thus require them to be suppressed by an additional factor $(g/g_*)^n$ where n is the number of weakly coupled field insertions. In this last point we depart from the prescription of Ref. [97]. The first intuitive consequence of this criterion is the fact that, in order for the model defined by eq. (6.54) to be consistent, it is not only necessary to have $m_V \ll m_*$, but also to have the vector ρ weakly coupled, $g_\rho \ll g_*$.

Before discussing the role of higher derivative terms in the model of section 6.2.4.2, it is worth noticing that the Lagrangian in eq. (6.54) already contains dimension-6 and higher operators which have not been included in the matching with the Simplified Model. The existence of these operators, even in the absence of heavy matter fields to be integrated out, is due to Higgs non-linearities emerging from the σ -model structure. Using eqs. (6.55) and (6.56) one finds at the dimension-6 level

$$\Delta\mathcal{L}_B = \frac{1}{6f^2} \left(1 - \frac{3m_\rho^2}{4g_\rho^2 f^2} \right) [(\partial_\mu |H|^2)^2 - 4|H|^2 |D_\mu H|^2] + \frac{m_\rho^2}{g_\rho f^4} |H|^2 i V_\mu^a H^\dagger \tau^a \overleftrightarrow{D}^\mu H + \dots \quad (6.67)$$

The first term renormalized the Higgs and Goldstones kinetic terms and through this affects all their interactions. However its contribution is suppressed by $\xi = v^2/f^2$ which is necessarily small in this scenario as mentioned already in section 6.2. The second term

6.2. A Simple Simplified Model for a Heavy Vector Triplet

is a new dimension-6 operator

$$\mathcal{O}'_H = |H|^2 i V_\mu^a H^\dagger \tau^a \overleftrightarrow{D}^\mu H, \quad (6.68)$$

with a coefficient of order g_V/f^2 (one should recall that $g_V \equiv g_\rho$ and $m_\rho = a_\rho g_\rho f \sim g_\rho f$). Qualitatively \mathcal{O}'_H has the same effect as the c_H operator both in the mass matrix and in the coupling of V to W_L , Z_L and h and it induces small $O(\xi)$ corrections relative to the latter. Additional operators collectively denoted by “...” in eq. (6.67) and containing extra insertions of $|H|^2$ are always accompanied by more powers of $1/f^2$ so their contribution to the mass matrix and to the decay widths are further suppressed by powers of ξ .

The addition of higher derivative terms to the leading order Lagrangian of the non-linear model is thoroughly discussed in Ref. [97]. The analysis shows that only two CP even operators can give a relative contribution to physical processes which is larger than the typical size of a higher derivative correction, m_V^2/m_*^2 . The two operators are

$$\mathcal{O}_1 = \text{Tr}(\rho_{\mu\nu} i[d_\mu, d_\nu]) \quad \text{and} \quad \mathcal{O}_2 = \text{Tr}(\rho_{\mu\nu} A_{\mu\nu}). \quad (6.69)$$

Here $A_{\mu\nu}$ is defined by

$$A_{\mu\nu} = U^\dagger (T_L^a W_{\mu\nu} + T_R^3 B_{\mu\nu}) U, \quad (6.70)$$

in terms of the Goldstone matrix U and the $\text{SO}(4)$ generators $T_{L,R}^a$, which are defined in Appendix A of Ref. [240]. The two operators can be expanded at order $1/f^2$

$$\text{Tr}(\rho^{\mu\nu} i[d_\mu, d_\nu]) = -\frac{4i}{f^2} \rho^{\mu\nu a} D_\mu H^\dagger \tau^a D_\nu H + O(1/f^4), \quad (6.71)$$

$$\text{Tr}(\rho_{\mu\nu} A_{\mu\nu}) = -W_{\mu\nu}^a \rho_{\mu\nu}^a \left(1 - \frac{|H|^2}{2f^2}\right) + \frac{1}{f^2} B_{\mu\nu} \rho_{\mu\nu}^a H^\dagger \tau^a H + O(1/f^4). \quad (6.72)$$

According to our refined partial UV completion they should appear in the Lagrangian as

$$\Delta\mathcal{L}_B = c_1 \frac{1}{g_\rho g_*} \mathcal{O}_1 + c_2 \frac{1}{g_\rho^2} \mathcal{O}_2, \quad (6.73)$$

with $c_{1,2} \sim 1$. Let us start focusing on \mathcal{O}_1 . Applying the field redefinition in eq. (6.58) and normalising the kinetic term of V , we obtain

$$\Delta\mathcal{L}_B = -\frac{4c_1}{g_* f^2} i D_{[\mu} V_{\nu]}^a D_\mu H^\dagger \tau^a D_\nu H. \quad (6.74)$$

We did not write operators contributing only to 4-point functions involving V , nor operators involving only the SM fields. The main effect of \mathcal{O}_1 is to modify the width of V to longitudinal gauge bosons. Using the equivalence theorem and the field redefinitions

in eqs. (6.28) and (6.29) we obtain the corrections to eq. (6.30)

$$\begin{aligned}
 & -\frac{g_V}{4(1-c_H^2\zeta^2)} \left[4c_1 \frac{M_V^2}{g_\rho^2 f^2} \frac{M_V}{m_*} \right] \epsilon^{abc} V_\mu^a \pi^b \partial^\mu \pi^c \\
 & + \frac{g_V}{2\sqrt{1-c_H^2\zeta^2}} \left[4c_1 \frac{M_V^2}{g_\rho^2 f^2} \frac{M_V}{m_*} \right] h V_\mu^a \partial_\mu \pi^a.
 \end{aligned} \tag{6.75}$$

Relative to the leading term which is proportional to $c_H \sim m_\rho^2/g_\rho^2 f^2$ the above contributions are suppressed even though only by a single power of M_V/m_* , the parameter controlling the derivative expansion.

To discuss the effects of \mathcal{O}_2 , we apply the shift of eq. (6.58) and obtain

$$\begin{aligned}
 \Delta\mathcal{L}_B = & -\frac{c_2}{g_V} D_{[\mu} V_{\nu]}^a W^{\mu\nu a} + c_2 \epsilon_{abc} W^{\mu\nu a} V_\mu^b V_\nu^c \\
 & -\frac{c_2}{2f^2} |H|^2 \epsilon_{abc} W^{\mu\nu a} V_\mu^b V_\nu^c + \frac{c_2}{2g_V f^2} |H|^2 D_{[\mu} V_{\nu]}^a W^{\mu\nu a} \\
 & -\frac{c_2}{f^2} B^{\mu\nu} \epsilon_{abc} H^\dagger \tau^a H V_\mu^b V_\nu^c + \frac{c_2}{g_V f^2} B^{\mu\nu} D_{[\mu} V_{\nu]}^a H^\dagger \tau^a H + \dots
 \end{aligned} \tag{6.76}$$

The first line of eq. (6.76) contains $O(1)$ corrections to the matching conditions in eq. (6.60) which now become

$$\tilde{c}_{VW} = \tilde{c}_{VW} = 1 - 2c_2. \tag{6.77}$$

All the other operators except for the last one in eq. (6.76) induce negligible $O(\xi)$ corrections to the spectrum and to the width of V into transverse gauge bosons. Finally the effect of

$$\mathcal{O}_{VB} = B^{\mu\nu} D_{[\mu} V_{\nu]}^a H^\dagger \tau^a H, \tag{6.78}$$

is qualitatively new. After EWSB it generates a kinetic mixing between the hypercharge gauge boson and V^3

$$\Delta\mathcal{L}_B \supset c_2 \tan \theta_W \zeta \frac{\hat{m}_W}{m_V} \left(\frac{m_V}{g_\rho f} \right)^2 B^{\mu\nu} V_{\mu\nu}^3. \tag{6.79}$$

Such a mixing can be eliminated by a field redefinition of the form given in eq. (6.9) but involving B_μ

$$\begin{cases} B_\mu \rightarrow B_\mu + \alpha V_\mu^3 \\ V_\mu^3 \rightarrow \beta V_\mu^3 \end{cases}, \tag{6.80}$$

with $\alpha \sim m_W/M_V$ and $\beta \sim 1$. It is simple to show that after this field redefinition the spectrum is only modified by corrections of order m_W^2/M_V^2 . The shift also affects the couplings $g_{L,R}^N$ of V^3 to fermions. The corrections are at most of order m_W/M_V , hence

safely negligible.

To summarise, our study of higher derivative terms in the context of the non-linear model shows that the only additional structure to consider is the operator \mathcal{O}_2 . Its effects can be included in the dimension four phenomenological Lagrangian by the modified matching conditions in eq. (6.77). Notice that among those dimension-6 operators that have not been listed in eq. (6.76) because they only involve SM fields one operator is particularly relevant as it contributes to the \hat{S} parameter

$$\Delta\mathcal{L}_B \supset -\frac{c_2}{g_V^2 f^2} B^{\mu\nu} W^{a\mu\nu} H^\dagger \tau^a H, \quad \Delta\hat{S} = c_2 \frac{\hat{m}_W^2}{g_V^2 f^2}. \quad (6.81)$$

If $c_2 \sim 1$ this correction is of the same size as those calculated in Appendix B and can have both signs.

6.3 A Simplified Model for Top Partners

Searches for heavy spin-1/2 resonances with standard and exotic charges are already ongoing (see for instance [335–343] and [344]). Their existence is particularly motivated in the context of composite Higgs models where light coloured fermionic resonances coupling to the top quark, the so-called top partners, are required to explain the observed value of the Higgs mass. Although a simplified Lagrangian approach can be employed to study spin-1/2 resonances, the effective description is fundamentally different from the general approach used for the heavy vector triplet in section 6.2. The main reason lies in the fact that heavy fermions are more sensitive to the Goldstone boson structure of the theory, especially of the Higgs. In addition to the mass term, a Yukawa coupling can be written if the Higgs is not a Goldstone boson and the Lagrangian does not obey the shift symmetry. This leads to a mass splitting within the fermion multiplet resulting in a completely different phenomenology compared to the Goldstone boson case (see for example Refs. [229] and [240] for a detailed discussion of each case). A similar term is present for the vector: c_{VVHH} gives a contribution to the mass and \tilde{c}_{VVHH} is indeed zero in the minimal composite Higgs model as shown in eq. (6.60). However, for the triplet c_{VVHH} can not split the multiplet and hence, even if unsuppressed, would never have such a drastic effect on the phenomenology. A further difference is that a Lagrangian for fermionic resonances can not be truncated at dimension-4. Instead, dimension-5 operators are relevant for single production and need to be included. With this in mind, it seems difficult to find a small set of relevant parameters and to write an as simple and general phenomenological Lagrangian as for the vector triplet. Nonetheless, we want to give a brief summary of current progress in the effective description of heavy fermions based on Refs. [240, 345]. For illustration and to make connection with the exotic charge fermion predicted by the minimally tuned model discussed in section 3, we will restrict here to the composite case with the Higgs emerging as a pNGB in the breaking of $SO(5)$ to

$SO(4)$. We use partial compositeness, described in section 3.2, possibly improved with additional flavour symmetries, as the most promising mechanism to generate a realistic flavour structure.

As before, it is assumed that one $SO(4)$ multiplet of coloured Dirac fermions is parametrically lighter than the other states, living at a scale m_* , which can be integrated out and we remain with an effective Lagrangian for the lightest multiplet. In the literature, resonances transforming as a **5** and **14** of $SO(5)$ have been explored [240]. In order to make connection with the minimally tuned model (with the fermionic degrees of freedom discussed in 3.3.2), we will focus here on the $\mathbf{14}_{2/3}$ of $SO(5) \times U(1)_X$. We restrict to a discussion of the effective description of the $\mathbf{9}_{2/3}$ of $SO(4) \times U(1)_X$ for brevity since it embeds a coloured charge-8/3 resonance, Υ , the most striking prediction of the minimally tuned model.¹⁶ We denote it by $\Psi_q^{\mathbf{9}}$ given explicitly by the (i, j) components of eq. (A.24) with $i, j = 1, \dots, 4$. Following Ref. [345], the most general effective leading order Lagrangian can be written using the CCWZ [138, 346] formalism

$$\begin{aligned} \mathcal{L} = & i\bar{t}_R \not{D} t_R + i\bar{\Psi}_q^{\mathbf{9}} (\not{D} + 2i\phi) \Psi_q^{\mathbf{9}} - M_{\Psi_q} \bar{\Psi}_q^{\mathbf{9}} \Psi_q^{\mathbf{9}} \\ & + c_1 \lambda_L f \bar{\psi}_q^{IJ} U_{Ii} U_{Jj} \Psi_q^{\mathbf{9}ij} + \lambda_L f \bar{\psi}_q^{IJ} U_{I5} U_{J5} t_R \\ & + \frac{c_2}{M_*} \bar{\Psi}_q^{\mathbf{9}ij} d_\mu^i d^{\mu j} t_R + \text{h.c.}, \end{aligned} \quad (6.82)$$

where we have assumed a fully composite t_R . $c_{1,2}$ are dimensionless parameters expected to be $\mathcal{O}(1)$. Remember that U is the Goldstone matrix defined in eq. (3.1) and ψ_q the embedding of q_L in a $\mathbf{14}_{2/3}$ of $SO(5) \times U(1)_X$ given in eq. (3.27). The indices i and I are $SO(4)$ and $SO(5)$ indices respectively. The CCWZ variables $d_\mu^{\hat{a}}$ and e_μ^a are defined in appendix A.1. The ϕ in the kinetic term is needed to respect the $SO(5)$ symmetry while the covariant derivative is given by

$$D_\mu \Psi_q^{\mathbf{9}} = (\partial_\mu - iY g' B_\mu - i g_S G_\mu) \Psi_q^{\mathbf{9}}, \quad (6.83)$$

where g_S is the $SU(3)_c$ gauge coupling and the hypercharge Y depends on the state inside the multiplet and can be read from Table A.1. The first line of the above Lagrangian represents the kinetic term for the t_R and $\Psi_q^{\mathbf{9}}$ and mass term for $\Psi_q^{\mathbf{9}}$. According to partial compositeness, the second line describes linear mixings between the top partners and the elementary fermions. In particular, the second term gives rise to the top quark mass. In the last line we have a direct interaction among the strong resonances and the composite t_R . Note that this is a dimension-5 operator suppressed by the scale of the heavier resonances which are integrated out. In contrast to the heavy vector triplet, here

¹⁶For discussions of other representations along the same lines see for instance Ref. [240].

it is crucial to include higher dimensional operators to ensure the inclusion of all single production channels.

6.3.1 Basic phenomenology

QCD pair production of the top partners is charge-independent and sizeable, ranging (including NLO effects) from 170 (1460) fb for a 600 GeV top partner to 0.001 (0.38) fb for a 1.9 TeV one, at the LHC for 8 (14) TeV center of mass energy. The charge is however crucial to describe single production in association to either a b or t quark. As discussed in Ref. [240] single production is the most relevant process for top partners of higher masses due to the lower kinematical threshold. Furthermore the presence of a forward jet in the final state provides an important experimental handle to reduce the impact of backgrounds. For the particular case of a charge $8/3$ resonance, however, single production via $W^+t \rightarrow \Upsilon W^-$ or $W^+W^+ \rightarrow \Upsilon \bar{t}$ is suppressed either by the scale M_* or an additional power of the weak coupling and a phase space suppression and can therefore be neglected.

The experimental signatures of the top partners depend strongly on their charge. Charge $2/3$ and $-1/3$ resonances decay dominantly into third family quarks with an associated vector or Higgs boson. More rare signals arise from the decay of the charge $5/3$ (χ) and $8/3$ (Υ) fermions. As discussed in detail in Ref. [345], the mass spectrum of the $\Psi_q^{\mathbf{9}}$ is mostly degenerate. Especially, the Υ and χ are exactly degenerate at tree level as they do not mix with the elementary states. Their splitting is induced by electroweak effects at 1-loop and is of order 200 MeV [133]. This implies a relatively straightforward phenomenology since cascade decays are kinematically disfavoured. Although generally two-body decays into a SM fermion and gauge boson dominate, e.g. $\chi \rightarrow Wt$, by charge conservation this is not the case for the Υ . Instead the interactions originating from the kinetic term include a W and a charge $5/3$ state χ , while the last term in eq. (6.82) gives a contact interaction of the form $\bar{\Upsilon} W^+ W^+ t_R$. Consequently, the Υ decays exclusively into $W^+ W^+ t_R$. Hence the decay chain of these exotic quarks will involve the emission of up to three (for the charge $8/3$ top partner) same sign W s resulting in a final state involving up to six W bosons (plus at least 2 b quarks). This results in a sizeable fraction of same-sign di-lepton and tri-lepton events.

6.3.2 Data and Bounds

The actual bounds depend not only on the charge of the top partners but also on their embedding in the $SO(4)$ multiplet. While the partners in the $\mathbf{4}$ are excluded below 600 – 1000 GeV depending on the choice of parameters, the singlet can still be allowed above 440 GeV.¹⁷ For the exotic charges in the $\mathbf{9}$, a rough estimate of the current

¹⁷For a detailed analysis see Ref. [240].

experimental bounds can be inferred from the analysis of Ref. [347] looking for same-sign di-leptons in a sample of 19.6 fb^{-1} from the 8 TeV LHC run. In the analysis the SM is extended by the addition of a single charge $5/3$ Dirac fermion decaying with unit branching ratio into W^+t . A 95% C.L. lower bound of 770 GeV is set on the mass of the fermion. The actual bound will be stronger in the minimally tuned model. Neglecting the other states inside Ψ_q^9 and other $SO(4)$ multiplets, we still have two charge $5/3$ and one charge $8/3$ quarks. The pair production of the charge $5/3$ fermions will give rise to same-sign di-leptons with a branching ratio of 4.5% and to tri-leptons with a branching ratio of 3%.

To date no dedicated searches for a charge $8/3$ resonance have been conducted by the experiments, however, the two same sign lepton searches (ssl) designed for charge $5/3$ resonances can be recast to set bounds on Υ . Following Ref. [345], the most conservative bound can be obtained assuming that only a charge $8/3$ resonance contributes to the signal. This can be modelled by the effective interaction

$$\frac{cg^2}{M_*} \bar{\Upsilon} W_\mu^+ W^{+\mu} t + \text{h.c.}, \quad (6.84)$$

where c is a dimensionless parameter. The Υ thus decays always into W^+W^+t with a subsequent $t \rightarrow W^+b$. Since the W decays hadronically with $BR = 67\%$, the dominant signature of a pair produced charge $8/3$ resonance would be a large number of jets. Searches for multi-particle final states have been performed in the context of microscopic black holes [348, 349] but are not yet sensitive to Υ . Recasting the $2ssl$ analysis in Ref. [347] achieves a better sensitivity and allows one to set a lower bound of 940 GeV at 95% C.L. at 8 TeV and 20 fb^{-1} on the mass of the $8/3$ resonance [345]. The bound is more stringent due to a higher branching fraction of the Υ into $2ssl$ and a higher cut acceptance explained by a larger multiplicity of the decay products. The authors of Ref. [345] furthermore show that a dedicated search for $3ssl$ will not yield competitive bounds despite providing an important independent probe of a charge $8/3$ top partner.

Considering the complete effective Lagrangian for Ψ_q^9 discussed in eq. (6.82) gives similar but slightly more stringent bounds. In addition to the contact interaction, also off-shell decays into χ 's are now present. Summing all possible contributions to a $2ssl$ signal hence leads to $m_\Upsilon \geq 990 \text{ GeV}$ at 95% C.L. for $c_1 = c_2 = 1$, $\xi = 0.1$ and $M_* = 3 \text{ TeV}$. In the minimally tuned model originating from an extra dimension, the coefficients c_1 and c_2 in eq. (6.82) are related and can be obtained by integrating out all multiplets except for Ψ_q^9 . Assuming them to be of order one, the current results already imply some tension with the minimally tuned model predicting m_Υ to be around, or even below, 1 TeV. Potential stronger bounds from forthcoming experiments will push the model into a more fine-tuned corner of parameter space.

6.4 Conclusions

We described a model-independent strategy to study heavy spin one particles in the triplet of the SM gauge group. Our method, depicted as a bridge in Figure 6.1, is based on a Simplified Model Lagrangian, introduced in section 6.2, designed to reproduce a large class of explicit descriptions of the heavy vector in different regions of its parameter space. Two explicit examples, describing vectors with rather different properties and physical origin, are discussed in section 6.2.4. Those are denoted as model A and model B and correspond, respectively, to heavy vectors emerging from an underlying weakly-coupled extensions of the SM gauge group [286] and a strongly coupled Composite Higgs scenario [97].

By studying the Simplified Model we derived a set of generic phenomenological features of the heavy vectors in section 6.2. In particular, we have seen that the charged and neutral states are essentially degenerate in mass and thus have comparable production rates. As discussed in Ref. [282], this fact is a strong motivation for combining the searches of the two charge states. We have also seen that the heavy vector always has a negligible coupling with the transversely polarised EW bosons and the only relevant interactions are with the longitudinals. The longitudinal coupling is generically comparable with the one to the SM fermions in the region of the parameter space that corresponds to weakly coupled models and it becomes dominant in the strongly-coupled case. This is the main phenomenological difference between the two scenarios. Finally, we showed that not all the parameters of the model are equally relevant. The partial decay widths, and in turn the single production rate, are to a good approximation completely determined by the parameter combinations $g_V c_H$ and $g^2 c_F / g_V$. If we assume, for simplicity, a universal coupling to fermions, then the experimental limits on the heavy vector can be conveniently represented, for a given mass, on a two-dimensional plane as we did in Figure 6.6. The dependence on the other parameters is extremely mild and can be safely ignored. Moreover, the phenomenology being controlled by a few parameters implies tight model-independent correlations among different observables. For instance, the relative BRs of the charged and neutral states in different bosonic decay channels, including the ones with the Higgs boson in the final state, are basically fixed. This would make the combination of different experimental searches extremely easy.

In section 6.2.3 we quantified the impact of the present experimental searches. Following the Bridge method we firstly translated the experimental results into limits on the Simplified Model parameters (Figure 6.1) and afterwards converted them into the “fundamental” parameters of the explicit models A and B. The results are shown in Figure 6.7 in a mass-coupling two-dimensional plane. We see that model A is excluded for masses below around 2 or 3 TeV, depending on the coupling, while the limit is weaker in model B. For large coupling, which is expected in model B as this is supposed to represent a strongly-coupled scenario, the exclusion never exceeds 2 TeV and is still comparable with the indirect limits from EWPT.

For our analysis we took all the experimental results at face value, and used the exclusions on $\sigma \times \text{BR}$ at each mass point. However we pointed out in section 6.2.3.3 that this might not be completely correct because of the effects associated with the finite resonance width, which might affect the limit setting procedures adopted by the experimental collaborations. We illustrated the expected impact of these effects on the invariant mass and transverse mass distributions that are employed in the di-lepton and in the lepton-neutrino searches respectively. Our conclusion is that finite-width effects can be considerable and can distort the signal shape in a significant way. In spite of this, we identified some strategies by which their impact could be reduced and a robust model-independent limit on $\sigma \times \text{BR}$ could be extracted. We plan to elaborate more on these aspects in a forthcoming publication.

Our work could be extended in at least three directions. First, one could easily consider other representations of the SM group. Aside from the triplet which we studied in the present chapter, another relevant representation is the singlet, either neutral like a Z' [290–292] or charged like a W' [278]. These particles emerge together in strongly-coupled models where they arise from a $(\mathbf{1}, \mathbf{3})$ representation of the custodial group. Another interesting representation, which is present in models with a Composite pseudo-Nambu-Goldstone boson Higgs, is the doublet with $1/2$ hypercharge [304]. A second limitation of our approach, which could be easily overcome, is the assumption of a linearly realised EW group, broken by the VEV of the Higgs doublet like in the SM. This is clearly a well-motivated assumption, but it might be worth studying also technicolor-like theories where the strong sector condensate breaks the EW symmetry directly. For this purpose our parameterization is insufficient because some higher dimensional operators involving extra powers of the Higgs field would be unsuppressed and should be included in the Simplified Model Lagrangian. Finally, in this chapter we did not discuss the possibility of non-universal fermion couplings $c_F = \{c_l, c_q, c_3\}$ in detail. In particular, c_3 being different from the light fermions couplings $c_{l,q}$ is well-motivated in strongly coupled scenarios with partial fermion compositeness [80]. In this case, the large compositeness of the top quark induces a potentially large coupling to the third family quarks. Its effect on the searches with third family final states should be investigated.

7 Conclusions

Conclusions of the individual projects, including discussions and some further outlook, were already given at the end of each chapter. Here we want to collect the above results to build a physics case for the estimated impact of the LHC and future colliders on the parameter space of a composite Higgs model. Generically, direct and indirect evidence, or the lack thereof, probe the parameter space of a specific model from complementary sides. Lepton colliders are generally more suited to perform precision measurements due to their clean collision environment. The sensitivity on individual couplings and, indirectly, the reach on model-specific parameters are typically large. Hadron colliders can usually reach greater centre of mass energies than lepton colliders and thus probe new particles with high masses. A choice between a future lepton and hadron collider is delicate and needs to be assessed carefully taking current and forthcoming LHC data into account.

In Figure 7.1, we present a summary of the current constraints and expected LHC and future collider reach in the (ξ, m_ρ) plane of the minimal composite Higgs model. This plot has already partly been shown and discussed extensively in section 5.2. Let us briefly summarise the main features. We focus on the interesting parameter region $1 < g_\rho < 4\pi$ for the typical strength of the new physics interactions g_ρ . The constraints from EWPT assuming no loop contribution from heavy states ($\Delta\hat{T} = 0$) are depicted in green. An additional positive contribution to \hat{T} can arise, for example, from loops of light top partners which could open up regions of larger $\xi = v^2/f^2$ [157]. Indirect bounds are discussed in detail in chapter 5. While the LHC is sensitive to $\xi \sim 0.1$ in single Higgs production, double Higgs production is merely visible for ξ of $\mathcal{O}(1)$ at 95% C.L.. Following our analysis of double Higgs production at a future linear collider, such as CLIC, values of ξ at the percent level can be reached. From single Higgs production, a permille sensitivity is expected at CLIC. In addition to the previously discussed plot, we show the current and extrapolated reach from direct heavy vector searches in the lepton neutrino [231, 232] and diboson [235, 236] channels. We focus on heavy $SU(2)_L$ triplets whose current bounds are presented in section 6.2. The leftmost violet region up to ~ 3 TeV shows the parameter space currently excluded by the 8 TeV LHC with 20 fb^{-1} . We extrapolate the current

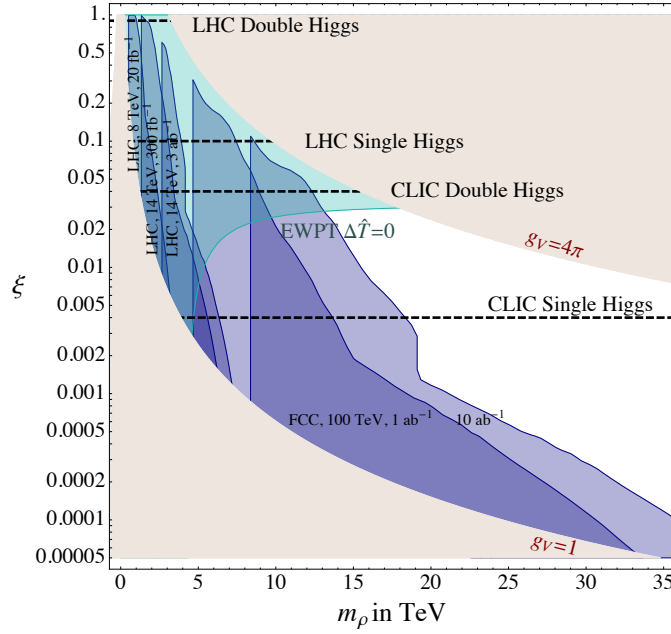


Figure 7.1 – Summary of current constraints and expected sensitivities at 95% C.L. at CLIC, the FCC and the LHC on $\xi = (v/f)^2$ and the mass of the lightest spin-1 resonance m_ρ for $SO(5)/SO(4)$ composite Higgs theories. For a detailed discussion see text.

limits from the lepton neutrino and diboson analyses to bounds expected at higher centre of mass energies and integrated luminosities according to appendix D.4. The LHC at 14 TeV is expected to reach masses up to ~ 5 TeV with 300 fb^{-1} and ~ 7 TeV with 3 ab^{-1} for small values of ξ . A future circular collider with 100 TeV centre of mass energy could exclude vectors up to 30 TeV with 1 ab^{-1} and more than 35 TeV with 10 ab^{-1} . The mass reach is highest for small values of ξ and decreases as ξ is $\mathcal{O}(1)$. Note that the apparent lower cutoff of the bounds arises as an artefact of our rescaling procedure: current limits on heavy vectors start at ~ 500 GeV and are simply mapped to larger masses. This gap is most likely going to be closed in reality. It could, however, be that gaps in direct searches remain for $\xi \sim \mathcal{O}(1)$, since g_ρ varies rapidly in that region and dramatically decreases the production cross section, analogously to the discussion below Figure 6.7. Moreover, large values of g_ρ lead to resonances too broad for direct searches to be sensitive. This region is hence unlikely to be excluded by resonance searches. The gap in this region of parameter space can easily be closed by precision measurements, e.g. single and double Higgs production, at the LHC and future colliders.

As can be seen from the figure, a clear favourite between lepton and hadron collider is impossible to find since both contribute complementary information on the model parameters and access unique regions in parameter space. While the superiority of a 100 TeV FCC is undebatable in terms of direct reach, its sensitivity on ξ via single and double Higgs production is a crucial missing piece of information. Moreover, a careful

assessment of the precision capabilities of the FCC (for example in WW scattering and Higgs production) is necessary to obtain a complete picture. Since the center of mass energy is well above the electroweak scale at which these processes occur, a good sensitivity can be expected, proportionally better than at the LHC. If it were at all comparable to the reach of CLIC, a FCC would probably yield more information on a new strongly coupled sector responsible for electroweak symmetry breaking.

The study of the potential of future colliders is going to continue in the next years. Minimal models, both in the supersymmetric and composite framework, are already in a fine tuned territory. However, to seriously challenge naturalness as a guiding principle we need to go beyond the LHC and, most likely, also beyond the minimal models.

A The Minimal Composite Higgs Model

A.1 The CCWZ chiral Lagrangian

The effective Lagrangian for a spontaneously broken symmetry can be build systematically through the CCWZ construction introduced by Callan, Coleman, Wess and Zumino in Refs. [138, 346].

The gauging of the SM group is realised by first gauging the full $SO(5)$ with the sources A_μ

$$A_\mu = A_\mu^I T^I \rightarrow A_\mu = g (A_\mu + i\partial_\mu) g^T, \quad (\text{A.1})$$

where T^I are the $SO(5)$ generators given in eq. (A.13). The physical gauge fields

$$\begin{aligned} A_\mu = & \frac{g}{\sqrt{2}} W_\mu^+ (T_L^1 + iT_L^2) + \frac{g}{\sqrt{2}} W_\mu^- (T_L^1 - iT_L^2) \\ & + g (\cos \theta_W Z_\mu + \sin \theta_W A_\mu) T_L^3 + g' (\cos \theta_W A_\mu - \sin \theta_W Z_\mu) T_R^3 \end{aligned} \quad (\text{A.2})$$

will later remain dynamical, while the unphysical ones can be set to zero. We can now dress A_μ by the Goldstone boson matrix in eq. (3.1)

$$\bar{A}_\mu = U^T (A_\mu + i\partial_\mu) U, \quad (\text{A.3})$$

which transforms as

$$\bar{A}_\mu \rightarrow \hat{h} (\bar{A}_\mu + i\partial_\mu) \hat{h}^T. \quad (\text{A.4})$$

The shift $i\hat{h}\partial_\mu\hat{h}^T$ lives in the $SO(4)$ subalgebra since $\hat{h} \in H$. \bar{A}_μ can thus be decomposed into broken and unbroken generators

$$\bar{A}_\mu = -d_\mu^{\hat{a}} T^{\hat{a}} - e_\mu^a T^a \quad (\text{A.5})$$

Appendix A. The Minimal Composite Higgs Model

transforming under H as

$$d_\mu \rightarrow \hat{h} d_\mu \hat{h}^T, \quad e_\mu \rightarrow \hat{h} (e_\mu - i \partial_\mu) \hat{h}^T \quad (\text{A.6})$$

Note, that e_μ transforms as a gauge field. Explicitly, the fields are given by

$$\begin{aligned} d_\mu^{\hat{a}} T^{\hat{a}} &= -A_\mu^{\hat{a}} T^{\hat{a}} + \frac{\sqrt{2}}{f} \partial_\mu h^{\hat{a}} T^{\hat{a}} - \frac{\sqrt{2}i}{f} [T^a, T^{\hat{b}}] A_\mu^a h^{\hat{b}} + \dots \\ e_\mu^a T^a &= -A_\mu^a T^a - \frac{i}{f^2} [T^{\hat{a}}, T^{\hat{b}}] h^{\hat{a}} \partial^\mu h^{\hat{b}} - \frac{\sqrt{2}i}{f} [T^{\hat{a}}, T^{\hat{b}}] A_\mu^{\hat{a}} h^{\hat{b}} + \dots \end{aligned} \quad (\text{A.7})$$

While the standard covariant derivative $\nabla_\mu = \partial_\mu - i A_\mu^a T^a$ acts on $d_\mu^{\hat{a}}$, we can define a CCWZ covariant derivative

$$\nabla_\mu = \partial_\mu + i e_\mu^a T^a, \quad (\text{A.8})$$

acting on e_μ^a . It is used to construct the field strength

$$e_{\mu\nu} = \partial_\mu e_\nu - \partial_\nu e_\mu + i [e_\mu, e_\nu], \quad (\text{A.9})$$

transforming as $e_{\mu\nu} \rightarrow \hat{h} e_{\mu\nu} \hat{h}^T$. The chiral Lagrangian can be build from combinations of the covariant variables d_μ , $e_{\mu\nu}$ and their covariant derivative. At order $O(p^2)$, only one operator can be formed

$$\mathcal{L}^{(2)} = \frac{f^2}{4} \text{Tr} (d_\mu d^\mu) \quad (\text{A.10})$$

which can be proven to coincide exactly with the one written in eq. (3.6). At order $O(p^4)$, 10 invariant operators can be built.

A.2 $SO(5)$ generators

A basis for the generators in the fundamental representation of the $SO(5)$ algebra is given by

$$\begin{aligned} (T_R^a)_{IJ} &= \frac{i}{2} \left[\frac{1}{2} \epsilon^{abc} \left(\delta_I^b \delta_J^c - \delta_J^b \delta_I^c \right) + \left(\delta_I^a \delta_J^4 - \delta_J^a \delta_I^4 \right) \right] (-1)^{\delta_2^a}, \\ (T_L^a)_{IJ} &= \frac{i}{2} \left[\frac{1}{2} \epsilon^{abc} \left(\delta_I^b \delta_J^c - \delta_J^b \delta_I^c \right) - \left(\delta_I^a \delta_J^4 - \delta_J^a \delta_I^4 \right) \right] (-1)^{\delta_1^a}, \\ (T_{\hat{1}}^{\hat{a}})_{IJ} &= -\frac{i}{\sqrt{2}} \left(\delta_I^{\hat{a}} \delta_J^5 - \delta_J^{\hat{a}} \delta_I^5 \right), \end{aligned} \quad (\text{A.11})$$

where $I, J = 1, \dots, 5$, while $\hat{a} = 1, \dots, 4$ and $a = 1, 2, 3$. The generators $\{T_{R,L}^a\}$ and $\{T_{\hat{1}}^{\hat{a}}\}$ represent the $SO(4) \cong SU(2)_L \times SU(2)_R$ and the $SO(5)/SO(4)$ subspaces of $SO(5)$

respectively. Here the generators obey the following commutation relations

$$\begin{aligned}
 [T_{L,R}^a, T_{L,R}^b] &= i\epsilon^{abc}T_{L,R}^c & [T_L^a, T_R^b] &= 0 \\
 [T^{\hat{a}}, T^{\hat{4}}] &= \frac{i}{2}\delta^{\hat{a}a}\left((-1)^{\delta_1^a}T_L^a - (-1)^{\delta_2^a}T_R^a\right) & [T^{\hat{a}}, T^{\hat{b}}] &= -\frac{i}{2}\epsilon^{\hat{a}\hat{b}c}\left((-1)^{\delta_1^c}T_L^c + (-1)^{\delta_2^c}T_R^c\right) \\
 [T^{\hat{a}}, T_L^a] &= -\frac{i}{2}(-1)^{\delta_1^a}\left(\delta^{\hat{a}a}T^{\hat{4}} + \epsilon^{\hat{a}ab}T^{\hat{b}}\right) & [T^{\hat{a}}, T_R^a] &= \frac{i}{2}(-1)^{\delta_2^a}\left(\delta^{\hat{a}a}T^{\hat{4}} - \epsilon^{\hat{a}ab}T^{\hat{b}}\right) \\
 [T^{\hat{4}}, T_L^a] &= (-1)^{\delta_1^a}\frac{i}{2}\delta^{a\hat{a}}T^{\hat{a}} & [T^{\hat{4}}, T_R^a] &= -(-1)^{\delta_2^a}\frac{i}{2}\delta^{a\hat{a}}T^{\hat{a}}
 \end{aligned} \tag{A.12}$$

Note that this basis differs from the usual $SO(5)$ basis by the factors $(-1)^{\delta_{1,2}^a}$. This is due to the fact that it is written as the $SO(5)$ subspace of an $SO(6)$ basis of generators. The standard $SO(5)$ generators are given by

$$\begin{aligned}
 (T_{L,R}^a)_{IJ} &= -\frac{i}{2}\left[\frac{1}{2}\epsilon^{abc}\left(\delta_I^b\delta_J^c - \delta_J^b\delta_I^c\right) \pm (\delta_I^a\delta_J^4 - \delta_J^a\delta_I^4)\right], \\
 (T_{\hat{1}}^{\hat{a}})_{IJ} &= -\frac{i}{\sqrt{2}}\left(\delta_I^{\hat{a}}\delta_J^5 - \delta_J^{\hat{a}}\delta_I^5\right),
 \end{aligned} \tag{A.13}$$

A.3 5D implementation in AdS₅ space

In this Appendix we describe the implementation of the MCHM₁₄ in AdS₅ space and illustrate some details about the flat space construction which were not discussed in the text. We consider a 5D space-time with metric

$$ds^2 = a(z)^2 (\eta_{\mu\nu}dx^\mu dx^\nu - dz^2), \tag{A.14}$$

where the coordinate z varies on the interval $[z^{UV}, z^{IR}]$ and the warp function $a(z)$ is a regular and positive function satisfying $a(z_{UV}) = 1$. This parameterization includes flat and AdS₅ spaces with

$$\begin{aligned}
 \text{flat :} \quad & a(z) = 1, \quad z_{UV} = 0, \quad z_{IR} \equiv L, \\
 \text{AdS}_5 : \quad & a(z) = \frac{1}{kz}, \quad z_{UV} = \frac{1}{k}, \quad z_{IR} > z_{UV}.
 \end{aligned} \tag{A.15}$$

A.3.1 Gauge degrees of freedom

The Lagrangian for the gauge fields in terms of the general metric of eq. (A.14) is given by

$$S_{5D}^g = \int d^4x \int_{z_{UV}}^{z_{IR}} dz \sqrt{g} \left[\frac{1}{4g_5^2 L_0} \text{Tr}[F_{MN}^2] + \frac{1}{4g_X^2 L_0} (F_{MN}^X)^2 \right], \tag{A.16}$$

Appendix A. The Minimal Composite Higgs Model

where L_0 has the dimensions of length and is equal to L in flat space and to $1/k$ in AdS_5 . We also add a UV localised term exactly as in eq. (3.48). To derive the effective Lagrangian in AdS_5 , we can follow the same procedure as discussed in section 3.3.1. The whole difference with respect to flat space is encoded in the two form factors Π_V and $\hat{\Pi}_V$ which read in AdS_5

$$\Pi_V(p) = p \frac{J_0(pz_{UV})Y_0(pz_{IR}) - J_0(pz_{IR})Y_0(pz_{UV})}{J_1(pz_{UV})Y_0(pz_{IR}) - J_0(pz_{IR})Y_1(pz_{UV})}, \quad (\text{A.17})$$

$$\hat{\Pi}_V(p) = p \frac{J_1(pz_{IR})Y_0(pz_{UV}) - J_0(pz_{UV})Y_1(pz_{IR})}{J_1(pz_{IR})Y_1(pz_{UV}) - J_1(pz_{UV})Y_1(pz_{IR})}. \quad (\text{A.18})$$

The Higgs decay constant in this case is given by

$$f^2 = \frac{4}{g_5^2} \frac{1}{z_{IR}^2 - z_{UV}^2} \approx \frac{4}{g_5^2} \frac{1}{z_{IR}^2}, \quad (\text{A.19})$$

where, in the last step, we assumed $z_{IR} \gg z_{UV}$. In the same limit the SM gauge couplings can be written as

$$\begin{aligned} \frac{1}{g^2} &= \frac{1}{g_2^2} + \frac{1}{g_5^2} \left(\log \frac{z_{IR}}{z_{UV}} - \frac{3}{8} s_h^2 \right) \approx \frac{1}{g_2^2} + \frac{1}{g_5^2} \log \frac{z_{IR}}{z_{UV}}, \\ \frac{1}{g'^2} &= \frac{1}{g_1^2} + \left(\frac{1}{g_5^2} + \frac{1}{g_X^2} \right) \left(\log \frac{z_{IR}}{z_{UV}} - \frac{3}{8} s_h^2 \frac{g_X^2}{g_5^2 + g_X^2} \right) \approx \frac{1}{g_1^2} + \left(\frac{1}{g_5^2} + \frac{1}{g_X^2} \right) \log \frac{z_{IR}}{z_{UV}}, \end{aligned} \quad (\text{A.20})$$

where we approximated $\log \frac{z_{IR}}{z_{UV}} \gg 1$. In the same limit the W boson mass is given by

$$m_W^2 = \frac{s_h^2}{z_{IR}^2 \log \frac{z_{IR}}{z_{UV}}}. \quad (\text{A.21})$$

The KK mass scale (looking for instance at the W boson tower) is

$$M_{KK} \approx \frac{2.4}{z_{IR}} + O \left(\frac{1}{z_{IR} \log \frac{z_{IR}}{z_{UV}}} \right). \quad (\text{A.22})$$

and the \hat{S} parameter is

$$\hat{S} \approx \frac{3}{8} \frac{s_h^2}{\log \frac{z_{IR}}{z_{UV}}}. \quad (\text{A.23})$$

Note that the inclusion of UV localised kinetic terms for the gauge fields is not strictly necessary to realise partial compositeness in AdS_5 space. The value of g_2 and g_1 may be interpreted as the strength of the gauge coupling at the scale k [350]: when the localised kinetic terms vanish, the gauge fields are strongly coupled at that scale.

A.3.2 Fermionic degrees of freedom

Here we discuss various details about the fermionic sector of the model both in AdS₅ and flat space. The expression of Ψ_q in terms of eigenstates of the SM quantum numbers is

$$\Psi_q = \begin{pmatrix} \frac{1}{2}(\zeta + i\Upsilon - \mathfrak{T}) & \frac{1}{2}(i\zeta + \Upsilon) & \frac{1}{\sqrt{2}}(\mathcal{B} + \mathcal{X}) & \frac{i}{\sqrt{2}}(\mathcal{B}^* + \mathcal{X}^*) & \frac{1}{2}(b^{(1)} + \chi^{(1)}) \\ \frac{1}{2}(i\zeta + \Upsilon) & -\frac{1}{2}(\zeta + i\Upsilon + \mathfrak{T}) & \frac{i}{\sqrt{2}}(\mathcal{B} - \mathcal{X}) & -\frac{1}{\sqrt{2}}(\mathcal{B}^* - \mathcal{X}^*) & \frac{i}{2}(b^{(1)} - \chi^{(1)}) \\ \frac{1}{\sqrt{2}}(\mathcal{B} + \mathcal{X}) & \frac{i}{\sqrt{2}}(\mathcal{B} - \mathcal{X}) & \frac{1}{2}\overline{\mathfrak{T}} + \overline{\mathcal{T}} & i\mathcal{T} & \frac{1}{2}(t^{(1)} + it^{(2)}) \\ \frac{i}{\sqrt{2}}(\mathcal{B}^* + \mathcal{X}^*) & -\frac{1}{\sqrt{2}}(\mathcal{B}^* - \mathcal{X}^*) & i\mathcal{T} & \frac{1}{2}\overline{\mathfrak{T}} - \overline{\mathcal{T}} & \frac{1}{2}(it^{(1)} + t^{(2)}) \\ \frac{1}{2}(b^{(1)} + \chi^{(1)}) & \frac{i}{2}(b^{(1)} - \chi^{(1)}) & \frac{1}{2}(t^{(1)} + it^{(2)}) & \frac{1}{2}(it^{(1)} - t^{(2)}) & \frac{2}{\sqrt{5}}t^{(3)} \end{pmatrix}. \quad (\text{A.24})$$

where the fields $t^{(i)}$, $b^{(i)}$, $\chi^{(i)}$, ζ and Υ have charges $2/3$, $-1/3$, $5/3$, $-4/3$, $8/3$ respectively and

$$\begin{aligned} \mathcal{B}^{(*)} &= \frac{1}{2}(b^{(2)} + {}^{(-)}ib^{(3)}) , \\ \mathcal{X}^{(*)} &= \frac{1}{2}(\chi^{(2)} + {}^{(-)}i\chi^{(3)}) , \\ \mathcal{T} &= \frac{1}{2}(t^{(5)} + t^{(6)}) , \\ \overline{\mathcal{T}} &= \frac{1}{2}(t^{(5)} - t^{(6)}) , \\ \mathfrak{T} &= t^{(4)} + \frac{1}{\sqrt{5}}t^{(3)} , \\ \overline{\mathfrak{T}} &= t^{(4)} - \frac{1}{\sqrt{5}}t^{(3)} . \end{aligned} \quad (\text{A.25})$$

The total 5D action for the fermionic sector of the model is given by

$$S_{\text{total}}^f = S_{5D}^f + S_{\text{IR}}^f + \Delta S_{\text{UV}} + \Delta S_{\text{IR}}, \quad (\text{A.26})$$

where

$$\begin{aligned} S_{5D}^f &= \int d^4x \int_{z_{UV}}^{z_{IR}} \frac{dz}{L_0} \sqrt{g} \left[\frac{i}{2} \text{Tr} \left[\overline{\Psi}^q e_A^M \Gamma^A D_M \Psi^q - (D_M \Psi^{q\dagger}) e_A^M \Gamma^0 \Gamma^A \Psi^q \right] - M_{\Psi_Q} \overline{\Psi}^q \Psi^q \right. \\ &\quad \left. + \frac{i}{2} \left(\overline{\Psi}^u e_A^M \Gamma^A D_M \Psi^u - (D_M \Psi^{u\dagger}) e_A^M \Gamma^0 \Gamma^A \Psi^u \right) - M_{\Psi_u} \overline{\Psi}^u \Psi^u \right], \end{aligned} \quad (\text{A.27})$$

$$\begin{aligned} S_{\text{IR}}^f &= \int d^4x \sqrt{g_{\text{IR}}} \left[\left(m_{11} \overline{\psi}_{qR}^{(1)} \psi_{tL} + \text{h.c.} \right) + \left(ik_1^t \overline{\psi}_{tL} e_a^\mu \gamma^a \partial_\mu \psi_{tL} + ik_1^q \overline{\psi}_{qR}^{(1)} e_a^\mu \gamma^a \partial_\mu \psi_{qR}^{(1)} \right. \right. \\ &\quad \left. \left. + ik_4^q \overline{\psi}_{qL}^{(4)} e_a^\mu \gamma^a \partial_\mu \psi_{qL}^{(4)} + ik_9^q \overline{\psi}_{qL}^{(9)} e_a^\mu \gamma^a \partial_\mu \psi_{qL}^{(9)} \right) \right], \end{aligned} \quad (\text{A.28})$$

$$\Delta S_{\text{UV}} = \frac{1}{L_0} \int d^4x \sqrt{g_{UV}} \frac{1}{2} [\overline{\Psi}_q \Psi_q - \overline{\Psi}_t \Psi_t], \quad (\text{A.29})$$

$$\Delta S_{\text{IR}} = \frac{1}{L_0} \int d^4x \sqrt{g_{\text{IR}}} \frac{1}{2} [\overline{\psi}_q^{(1)} \psi_q^{(1)} - \overline{\psi}_q^{(4)} \psi_q^{(4)} - \overline{\psi}_q^{(9)} \psi_q^{(9)} - \overline{\Psi}^u \Psi^u]. \quad (\text{A.30})$$

Appendix A. The Minimal Composite Higgs Model

L_0 is a length we use to normalise the bulk action in order to have 5D fermions with the same mass dimension as 4D fermions. As in the case of the gauge action it is equal to L in flat space and to $1/k$ in AdS_5 . g_{IR} and g_{UV} are the induced metrics on the IR and UV boundaries respectively. e_A^M is the fünfbein and e_a^μ its projection on the 4D indices. It is given by $\delta_A^M/a(z)$ for flat and AdS_5 metric. Covariant derivatives in S_{5D}^f include both gauge and spin connections. The latter cancel out in the equations of motion. In flat space we also add localised kinetic terms on the UV boundary, as in eq. (3.64), to properly implement partial compositeness.

The bulk equations of motion corresponding to eq. (A.26) are

$$\left[\partial_5 + 2 \frac{\partial_5 a(z)}{a(z)} \pm M_{\Psi^i} a(z) \right] \Psi_{L,R}^i = \pm \not{p} \Psi_{R,L}^i. \quad (\text{A.31})$$

These are supplemented by the following boundary conditions:

- **UV boundary conditions**

$$\Psi_{qL}(z_{UV}) = U \Psi_{qL}^0 U^T \quad \delta \Psi_{qL}(z_{UV}) = \delta \Psi_{qL}^0 = 0, \quad (\text{A.32})$$

with Ψ_{qL}^0 given by eq. (A.24) where all the fields but $t^1 = t_L$ and $b^1 = b_L$ are set to zero while $\Psi_{qR}(z_{UV})$ is free to vary and

$$\Psi_{tR}(z_{UV}) = \Psi_{tR}^0 \quad \delta \Psi_{tR}(z_{UV}) = \delta \Psi_{tR}^0 = 0, \quad (\text{A.33})$$

with $\Psi_{tR}^0 = t_R$ and $\Psi_{tL}(z_{UV})$ free to vary.

- **IR boundary conditions**

$$\Psi_{tR}(z_{IR}) = L_0 m_{11} \psi_{qR}^{(1)}(z_{IR}), \quad \Psi_{tL}(z_{IR}) = -\frac{1}{L_0 m_{11}} \psi_{qL}^{(1)}(z_{IR}), \quad (\text{A.34})$$

$$\psi_{qR}^{(4)}(z_{IR}) = k_4^q \frac{L_0}{a(z_{IR})} \not{p} \psi_{qL}^{(4)}(z_{IR}) \quad \psi_{qR}^{(9)}(z_{IR}) = k_9^q \frac{L_0}{a(z_{IR})} \not{p} \psi_{qL}^{(9)}(z_{IR}). \quad (\text{A.35})$$

where, without loss of generality, we have set $k_1^q = k_1^t = 0$.

The U transformation in the Ψ_{qL} UV boundary condition has been introduced to take the $SO(5)$ transformation in eq. (3.47) into account, needed to rotate the Higgs (A^5) away from the bulk and the IR boundary. The SM quantum numbers and the boundary conditions for all fermionic fields of the 5D model are summarised in Table A.1.

Solving the bulk equations of motion (A.31) with the boundary conditions above, integrating out the bulk fields and matching to the 4D effective action (3.28) gives the form factors as functions of the fermion bulk-to-boundary propagators $G_+(z, m)$ and

A.3. 5D implementation in AdS₅ space

$G_-(z, m)$, which are functions of the metric $g_{\mu\nu}$. Defining $\omega_{q,t}^2 = p^2 - m_{q,t}^2$ in flat space and $\omega_q = 2/(\pi z_{UV})$ and $\omega_t = 2/(\pi z_{IR})$ in AdS₅ the form factors can be written in the form

$$\Pi_0^Q = \frac{G_R^+(z_{UV}, M_{\Psi_q}) - k_9^q p L_0 G_R^-(z_{UV}, M_{\Psi_q})}{p L_0 [G_L^+(z_{UV}, M_{\Psi_q}) - k_9^q p L_0 G_L^-(z_{UV}, M_{\Psi_q})]}, \quad (\text{A.36a})$$

$$\tilde{\Pi}_0^Q = Z_q + \Pi_0^Q, \quad (\text{A.36b})$$

$$\Pi_1^Q = \frac{\omega_q^2 (k_4^q - k_9^q)}{2p^2 [G_L^+(z_{UV}, M_{\Psi_q}) - k_4^q p L_0 G_L^-(z_{UV}, M_{\Psi_q})] [G_L^+(z_{UV}, M_{\Psi_q}) - k_9^q p L_0 G_L^-(z_{UV}, M_{\Psi_q})]}, \quad (\text{A.36c})$$

$$\begin{aligned} \Pi_2^Q = & \frac{\omega_q^2}{4p^2 G_L^+(M_{\Psi_q})} \left[\frac{3k_9^q}{G_L^+(z_{UV}, M_{\Psi_q}) - k_9^q p L_0 G_L^-(z_{UV}, M_{\Psi_q})} \right. \\ & - \frac{8k_4^q}{G_L^+(z_{UV}, M_{\Psi_q}) - k_4^q p L_0 G_L^-(z_{UV}, M_{\Psi_q})} \\ & \left. - \frac{5G_R^+(z_{UV}, M_{\Psi_t})}{p^2 L_0 [G_L^-(z_{UV}, M_{\Psi_q}) G_R^+(z_{UV}, M_{\Psi_t}) + m_{11}^2 L_0^2 G_L^+(z_{UV}, M_{\Psi_q}) G_R^-(z_{UV}, M_{\Psi_t})]} \right], \end{aligned} \quad (\text{A.36d})$$

$$\Pi_0^t = -\frac{G_L^-(z_{UV}, M_{\Psi_q}) G_L^+(z_{UV}, M_{\Psi_t}) + m_{11}^2 L_0^2 G_L^-(z_{UV}, M_{\Psi_t}) G_L^+(z_{UV}, M_{\Psi_q})}{p L_0 [G_L^-(z_{UV}, M_{\Psi_q}) G_R^+(z_{UV}, M_{\Psi_t}) + m_{11}^2 L_0^2 G_L^+(z_{UV}, M_{\Psi_q}) G_R^-(z_{UV}, M_{\Psi_t})]}, \quad (\text{A.36e})$$

$$\tilde{\Pi}_0^t = Z_t + \Pi_0^t, \quad (\text{A.36f})$$

$$M_1^t = \frac{-i\sqrt{5} m_{11} \omega_q \omega_t}{2p^2 [L_0^2 m_{11}^2 G_L^+(z_{UV}, M_{\Psi_q}) G_R^-(z_{UV}, M_{\Psi_t}) + G_L^-(z_{UV}, M_{\Psi_q}) G_R^+(z_{UV}, M_{\Psi_t})]}. \quad (\text{A.36g})$$

The bulk-to-boundary propagators $G_L^\pm(z, m)$ and $G_R^\pm(z, m)$ are given by the following expressions:

- Flat space ($z_{IR} = L$)

$$\begin{aligned} G_L^+(z, m) &= \frac{1}{p} (\omega \cos \omega (L - z) + m \sin \omega (L - z)), \\ G_L^-(z, m) &= \sin \omega (L - z), \\ G_R^+(z, m) &= \sin \omega (L - z), \\ G_R^-(z, m) &= -\frac{1}{p} (\omega \cos \omega (L - z) + m \sin \omega (L - z)). \end{aligned} \quad (\text{A.37})$$

- AdS₅

$$\begin{aligned} G_L^\pm(z, m) &= Y_{ML\mp 1/2}(pz_{IR}) J_{ML+1/2}(pz) - J_{ML\mp 1/2}(pz_{IR}) Y_{ML+1/2}(pz) \\ G_R^\pm(z, m) &= Y_{ML\mp 1/2}(pz_{IR}) J_{ML-1/2}(pz) - J_{ML\mp 1/2}(pz_{IR}) Y_{ML-1/2}(pz). \end{aligned} \quad (\text{A.38})$$

Appendix A. The Minimal Composite Higgs Model

	T_3^L	T_3^R	X	Y	Q	ψ_L BC (UV,IR)	ψ_R BC (UV,IR)
$t^{(1)}$	$+\frac{1}{2}$	$-\frac{1}{2}$	$+\frac{2}{3}$	$+\frac{1}{6}$	$+\frac{2}{3}$	$(t_L, /)$	$(/, k_4^q L_0 \not{p} t_L^{(1)})$
$t^{(2)}$	$-\frac{1}{2}$	$+\frac{1}{2}$	$+\frac{2}{3}$	$+\frac{7}{6}$	$+\frac{2}{3}$	$(0, /)$	$(/, k_4^q L_0 \not{p} t_L^{(2)})$
$t^{(3)}$	0	0	$+\frac{2}{3}$	$+\frac{2}{3}$	$+\frac{2}{3}$	$(0, -\frac{2}{\sqrt{5}} L_0 m_{11} t_L^{(7)})$	$(/, t_R^{(3)})$
$t^{(4)}$	0	0	$+\frac{2}{3}$	$+\frac{2}{3}$	$+\frac{2}{3}$	$(0, /)$	$(/, k_9^q L_0 \not{p} t_L^{(4)})$
$t^{(5)}$	+1	-1	$+\frac{2}{3}$	$-\frac{1}{3}$	$+\frac{2}{3}$	$(0, /)$	$(/, k_9^q L_0 \not{p} t_L^{(5)})$
$t^{(6)}$	-1	1	$+\frac{2}{3}$	$+\frac{5}{3}$	$+\frac{2}{3}$	$(0, /)$	$(/, k_9^q L_0 \not{p} t_L^{(6)})$
$b^{(1)}$	$-\frac{1}{2}$	$-\frac{1}{2}$	$+\frac{2}{3}$	$+\frac{1}{6}$	$-\frac{1}{3}$	$(b_L, /)$	$(/, k_4^q L_0 \not{p} b_L^{(1)})$
$b^{(2)}$	0	-1	$+\frac{2}{3}$	$-\frac{1}{3}$	$-\frac{1}{3}$	$(0, /)$	$(/, k_9^q L_0 \not{p} b_L^{(2)})$
$b^{(3)}$	-1	0	$+\frac{2}{3}$	$+\frac{2}{3}$	$-\frac{1}{3}$	$(0, /)$	$(/, k_9^q L_0 \not{p} b_L^{(3)})$
$\chi^{(1)}$	$+\frac{1}{2}$	$+\frac{1}{2}$	$+\frac{2}{3}$	$+\frac{7}{6}$	$+\frac{2}{3}$	$(0, /)$	$(/, k_4^q L_0 \not{p} \chi_L^{(1)})$
$\chi^{(2)}$	+1	0	$+\frac{2}{3}$	$+\frac{2}{3}$	$+\frac{2}{3}$	$(0, /)$	$(/, k_9^q L_0 \not{p} \chi_L^{(2)})$
$\chi^{(3)}$	0	+1	$+\frac{2}{3}$	$+\frac{5}{3}$	$+\frac{2}{3}$	$(0, /)$	$(/, k_9^q L_0 \not{p} \chi_L^{(3)})$
ζ	-1	-1	$+\frac{2}{3}$	$-\frac{1}{3}$	$-\frac{1}{3}$	$(0, /)$	$(/, k_9^q L_0 \not{p} \zeta_L)$
Υ	+1	+1	$+\frac{2}{3}$	$+\frac{5}{3}$	$+\frac{2}{3}$	$(0, /)$	$(/, k_9^q L_0 \not{p} \Upsilon_L)$
$\Psi^t \equiv t^{(7)}$	0	0	$+\frac{2}{3}$	$+\frac{2}{3}$	$+\frac{2}{3}$	$(/, t_L^{(7)})$	$(t_R, \frac{\sqrt{5}}{2} L_0 m_{11} t_R^{(3)})$

Table A.1 – Quantum numbers of the 5D fermion fields of the model. In the last row the boundary conditions on the UV and IR branes are shown. In **red** (**blue**) we indicate the states with the same SM quantum numbers of the q_L and t_R . The holographic fields are t_L , b_L and t_R .

As the propagators appear only as functions of z_{UV} in eq. (A.36), for clarity we have absorbed a factor of $z^{5/2}$, originating from the G , inside $\omega_{q,t}$.

A.4 The electroweak fit

We use the following experimental determination of the \hat{S} and \hat{T} parameters taken from Ref. [108] where U was constrained to 0 in the fit¹

$$\begin{aligned}\hat{S} &= (0.39 \pm 0.70) 10^{-3} \\ \hat{T} &= (0.60 \pm 0.56) 10^{-3}\end{aligned}\tag{A.39}$$

with the corresponding correlation matrix

$$\rho = \begin{pmatrix} 1 & 0.91 \\ 0.91 & 1 \end{pmatrix}.\tag{A.40}$$

The current world average $m_W = (80.385 \pm 0.015) \text{ GeV}$ [101] was used as input, as well as the latest Tevatron measurement for the top mass $m_t = 173.18 \pm 0.94 \text{ GeV}$. The resulting

¹Note that this is the reason why the fit does not coincide with the one presented in eq. (2.52).

χ^2 function is given by

$$\chi^2(\hat{S}, \hat{T}) = V_i(\sigma^2)_{ij}^{-1} V_j,$$

$$V = (\hat{S} - \hat{S}_0, \hat{T} - \hat{T}_0), \quad \sigma_{ij}^2 = \sigma_i \rho_{ij} \sigma_j. \quad (\text{A.41})$$

The contributions to \hat{S} and \hat{T} in our model are estimated by

$$\hat{S} = \hat{S}_{UV} + \frac{\alpha_{EM}(m_Z)}{48\pi s_W^2} \xi \log \left(\frac{\Lambda^2}{m_h^2} \right), \quad (\text{A.42})$$

$$\hat{T} = -\frac{3\alpha_{EM}(m_Z)}{16\pi c_W^2} \xi \log \left(\frac{\Lambda^2}{m_h^2} \right), \quad (\text{A.43})$$

where Λ is the scale at which the logs are cut off. We fix Λ to be the mass of the first vector KK resonance. \hat{S} and \hat{T} are defined to vanish for a SM Higgs boson with $m_h = 125$ GeV.

B Indirect Probes of NP at the LHC

B.1 Forward $Wb \rightarrow th$ scattering

The forward cross section for the partonic process $Wb \rightarrow th$, defined for example by a cut on $|\eta| > \bar{\eta}$, can be computed for large s in a very simple way. In fact, for this purpose the diagram with top exchange in the s -channel can be neglected, and we only need to look at the diagram with W exchange in the t -channel. In the regime we are interested in, i.e. large s , the longitudinal polarisation of the W dominates. The leading term in the amplitude, which is enhanced at small $|t|$, goes as $\sim s/(t - m_W^2)$ and reads

$$\mathcal{A}_L^{fw} \simeq \frac{g c_V m_W}{\sqrt{2}v} \frac{1}{t - m_W^2} \bar{u}(p_t) p\!\!\!/\!\! W (1 - \gamma_5) u(p_b) \quad (\text{B.1})$$

At large s and generic t , the fermion bilinears relevant to the amplitude read

$$\bar{u}(p_t)(1 - \gamma_5)u(p_b) = 2\sqrt{s} A(t/s, \varphi; \xi_t, \xi_b) + 2m_t B(t/s, \varphi; \xi_t, \xi_b) + \dots \quad (\text{B.2})$$

$$\bar{u}(p_t) p\!\!\!/\!\! W (1 - \gamma_5)u(p_b) = 2s B(t/s, \varphi; \xi_t, \xi_b) + \dots \quad (\text{B.3})$$

where the functions A, B have been defined in eqs. (4.2-4.3), and the dots stand for subleading terms. Thus squaring the amplitude in eq. (B.1), summing and averaging over polarisations (we neglect the contributions of the transverse components of the W) and recalling that we are interested in the region $s \gg |t|$ we find

$$\overline{|\mathcal{A}^{fw}|^2} = \frac{g^2 c_V^2 m_W^2}{3v^2} \left(\frac{s}{t - m_W^2} \right)^2 \quad (\text{B.4})$$

from which we derive the approximate expression of the forward cross section

$$\sigma(|\eta| > \bar{\eta}, s) \simeq \frac{c_V^2 g^2}{48\pi v^2} R(\bar{\eta}, s), \quad R(\bar{\eta}, s) = \frac{(s/2m_W^2)(1 - \tanh \bar{\eta})}{1 + (s/2m_W^2)(1 - \tanh \bar{\eta})} \quad (\text{B.5})$$

Appendix B. Indirect Probes of NP at the LHC

valid for $\tanh \bar{\eta} \approx 1$ (i.e. for large $\bar{\eta}$). We note that as expected, the forward cross section is controlled only by c_V and is insensitive to the value of c_F . As a consequence, the forward cross section is insensitive to the growth with energy of the “hard scattering” amplitude, which takes place for $c_V \neq c_F$ and was discussed in Sec. 4.2. As a numerical example, let us consider $c_V = 1$, a cut $|\eta| > 3$ and let us set the center of mass energy to $\sqrt{s} = 5 \text{ TeV}$. Then computing the cross section without approximations gives

$$\sigma_{\text{full}}(|\eta| > 3) = \{16.3, 16.5, 16.8\} \text{ pb}, \quad \text{for} \quad c_F = \{1, 0, -1\} \quad (\text{B.6})$$

whereas using the approximate formula in (B.5) yields $\sigma(|\eta| > 3, \sqrt{s} = 5 \text{ TeV}) = 16.4 \text{ pb}$, a very accurate result. The factor R has the value $R(\bar{\eta} = 3, \sqrt{s} = 5 \text{ TeV}) \simeq 0.91$.

C Indirect Probes of NP at Future Colliders

C.1 Dimension-8 operators for strong scatterings

At the dimension-8 level, the following three operators can be constructed with two derivatives and six Higgs fields

$$\begin{aligned}
c'_r \mathcal{O}'_r &= \frac{c'_r}{f^2} |H|^4 |D_\mu H|^2 &= |H|^2 c'_r \mathcal{O}_r, \\
c'_H \mathcal{O}'_H &= \frac{c'_H}{2f^2} |H|^2 \partial_\mu |H|^2 \partial^\mu |H|^2 &= |H|^2 c'_H \mathcal{O}_H, \\
c'_T \mathcal{O}'_T &= \frac{c'_T}{2f^2} |H|^2 \left(H^\dagger \overleftrightarrow{D}_\mu H \right) \left(H^\dagger \overleftrightarrow{D}^\mu H \right) &= |H|^2 c'_T \mathcal{O}_T,
\end{aligned} \tag{C.1}$$

which can be found by constructing all possible $SU(2)_L$ -invariant structures and using integration by parts and the identities

$$\begin{aligned}
\sigma_{ij}^A \sigma_{hk}^A &= 2\delta_{ik} \delta_{jh} - \delta_{ij} \delta_{hk}, \\
\sigma_{ij}^2 \sigma_{hk}^2 &= -\delta_{ih} \delta_{jk} + \delta_{jh} \delta_{ik}.
\end{aligned} \tag{C.2}$$

The operators of eq. (C.1) consist of the dimension-6 structures discussed in Ref. [80] extended by two Higgs fields. Note that \mathcal{O}'_T violates custodial symmetry, in analogy to \mathcal{O}_T . At the dimension-8 level there is also the operator $\mathcal{O}_8 = -c_8 (H^\dagger H)^4 / f^2$ defined in eq. (2.30), which involves no derivative. The operator \mathcal{O}_r can be redefined away by the following field redefinition

$$H \rightarrow H + \alpha H \frac{|H|^2}{f^2} + \beta H \frac{|H|^4}{f^4}, \tag{C.3}$$

under which the kinetic term transforms as follows

$$|D_\mu H|^2 \rightarrow |D_\mu H|^2 + \frac{2\alpha}{f^2} \mathcal{O}_r + \frac{\alpha}{f^2} \mathcal{O}_H + \frac{\alpha^2 + 2\beta}{f^4} (\mathcal{O}'_r + 2\mathcal{O}'_H), \tag{C.4}$$

while the dimension-6 operators give

$$\mathcal{O}_T \rightarrow \mathcal{O}_T + \frac{5\alpha}{f^2} \mathcal{O}'_T + \dots, \quad \mathcal{O}_H \rightarrow \mathcal{O}_H + \frac{8\alpha}{f^2} \mathcal{O}'_H + \dots, \quad \mathcal{O}_r \rightarrow \mathcal{O}_r + \frac{8\alpha}{f^2} \mathcal{O}'_r + \frac{2\alpha}{f^2} \mathcal{O}'_H + \dots \quad (\text{C.5})$$

Hence by choosing α and β appropriately both \mathcal{O}_r and \mathcal{O}'_r can be redefined away. We thus remain with only one custodially-invariant operator: \mathcal{O}'_H .

C.2 Double Higgs-strahlung

The differential cross section for double Higgsstrahlung can be expressed in term of the Dalitz variables $x_i \equiv 2E_i/\sqrt{s}$ where $E_{1,2}$ are the energies of the two Higgses and $x_3 \equiv 2E_3/\sqrt{s}$ for the Z boson [269, 270]:

$$\frac{d\sigma}{dx_1 dx_2} = \frac{G_F^3 m_Z^6}{384 \sqrt{2} \pi^3 s} \frac{1 + (1 - 4s_W^2)^2}{(1 - \mu_Z)^2} \mathcal{A}. \quad (\text{C.6})$$

Here \sqrt{s} is the collider center-of-mass energy. We define $\mu_i \equiv m_i^2/s$, $\mu_{ij} \equiv \mu_i - \mu_j$, $y_i \equiv 1 - x_i$, so that $x_3 = 2 - x_1 - x_2$ follows by energy conservation. We have

$$\mathcal{A} = \mathcal{A}_0^2 f_0 + \frac{a^2}{4\mu_Z(y_1 + \mu_{hZ})} \left(\frac{a^2 f_1}{y_1 + \mu_{hZ}} + \frac{a^2 f_2}{y_2 + \mu_{hZ}} + 2\mu_Z \mathcal{A}_0 f_3 \right) + (y_1 \leftrightarrow y_2) \quad (\text{C.7})$$

with

$$\mathcal{A}_0 = 3 \frac{m_h^2}{m_Z^2} \frac{ad_3}{y_3 - \mu_{hZ}} + \frac{2a^2}{y_1 + \mu_{hZ}} + \frac{2a^2}{y_2 + \mu_{hZ}} + \frac{b}{\mu_Z} \quad (\text{C.8})$$

and

$$\begin{aligned} f_0 &= \frac{1}{8} \mu_Z ((y_1 + y_2)^2 + 8\mu_Z), \\ f_1 &= (y_1 - 1)^2 (\mu_Z - y_1)^2 - 4\mu_h y_1 (y_1 + y_1 \mu_Z - 4\mu_Z) + \mu_Z (\mu_Z - 4\mu_h) (1 - 4\mu_h) - \mu_Z^2, \\ f_2 &= (\mu_Z (y_3 + \mu_Z - 8\mu_h) - (1 + \mu_Z) y_1 y_2) (1 + y_3 + 2\mu_Z) \\ &\quad + y_1 y_2 (y_1 y_2 + 1 + \mu_Z^2 + 4\mu_h (1 + \mu_Z)) + 4\mu_h \mu_Z (1 + \mu_Z + 4\mu_h) + \mu_Z^2, \\ f_3 &= y_1 (y_1 - 1) (\mu_Z - y_1) - y_2 (y_1 + 1) (y_1 + \mu_Z) + 2\mu_Z (1 + \mu_Z - 4\mu_h). \end{aligned} \quad (\text{C.9})$$

The kinematical boundaries of the phase space integration are defined by

$$|2(1 - x_1 - x_2 + 2\mu_h - \mu_Z) + x_1 x_2| \leq \sqrt{x_1^2 - 4\mu_h} \sqrt{x_2^2 - 4\mu_h}. \quad (\text{C.10})$$

Using

$$x_1 = \frac{s + m_h^2 - m_{23}^2}{s}, \quad x_2 = \frac{m_{12}^2 + m_{23}^2 - m_h^2 - m_Z^2}{s} \quad (\text{C.11})$$

and

$$\frac{d\sigma}{dx_1 dx_2} = s^2 \frac{d\sigma}{dm_{12}^2 dm_{23}^2}, \quad (\text{C.12})$$

one can obtain the differential cross section as a function of $m_{12} \equiv m_{hh}$ and $m_{23} \equiv m_{hZ}$. Figure 5.9 in particular is derived by integrating over m_{23} and varying m_{hh} .

It is interesting to analyse the enhancement of the differential cross section $d\sigma/dm_{hh}$ near the kinematic boundary $m_{hh} \simeq \sqrt{s}$. As mentioned in footnote 15, the enhancement is due to the singularity associated with the soft emission of a transversely-polarised Z boson in the diagrams in the first row of Fig. 5.7. The leading singular behaviour can be thus isolated by setting $d_3 = 0$, to switch off the Higgs trilinear coupling, and by fixing the couplings a and b to their SM value ($\delta_b = 0$). It is useful to make a change of variables in eq. (C.6) from (x_1, x_2) to $(r \equiv m_{hh}^2/s, x_2)$, where the energy of the Z is related to the invariant mass of the two Higgses by

$$r = 1 - x_3 + \frac{m_Z^2}{s}. \quad (\text{C.13})$$

By integrating x_2 over the interval $r + \epsilon \leq x_2 \leq 1 - \epsilon$ and expanding for $\epsilon = m_Z^2/s$ small, we obtain

$$\frac{d\sigma}{dr} \simeq \frac{G_F^3 m_Z^6 [1 + (1 - 4s_W^2)^2]}{192\sqrt{2}\pi^3 s} \left[(1 - r) + \frac{r}{1 - r} \log(1 - r) - \frac{r}{1 - r} \log \epsilon \right], \quad (\text{C.14})$$

which shows the singularity at $r = 1$. The logarithmic terms in the above formula follow from the collinear singularity also associated with the Z emission. Notice that events with a final longitudinally-polarised Z have no soft singularity. At very large c.o.m. energies the process $e^+e^- \rightarrow hhZ_L$ dominates the total cross section and its leading contribution, which is proportional to δ_b , peaks at $m_{hh}/\sqrt{s} \sim 1/\sqrt{7}$, see eq. (C.22). The left plot of Fig. 5.9 shows that for $\sqrt{s} = 1$ TeV the values of the differential cross section near the kinematic edge increases when going from $\delta_b = 0$ to $\delta_b = 0.5$. This means that the contribution from transversely-polarised final Z bosons is still large in this case, as also shown by the right plot of Fig. 5.8. We have checked that for larger c.o.m. energies (or, similarly, much larger values of δ_b), the differential cross section $d\sigma/dm_{hh}$ eventually peaks at the intermediate values $m_{hh}/\sqrt{s} \sim 1/\sqrt{7}$.

The high-energy limit of the double Higgs-strahlung total cross section can be easily calculated explicitly. In a gauge in which the equivalence theorem is manifest, the diagrams contributing to the leading high-energy behaviour are those depicted in Fig. C.1.

Appendix C. Indirect Probes of NP at Future Colliders

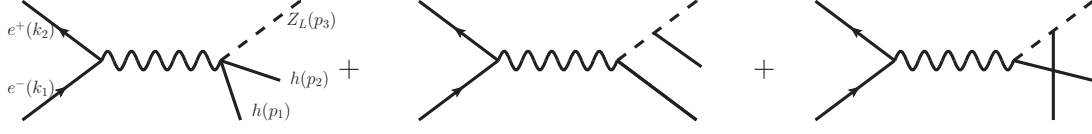


Figure C.1 – Diagrams contributing to the leading high-energy behaviour of the double Higgs-strahlung cross section.

The relevant vertices are found by expanding the Lagrangian of eq. (2.16)

$$\Delta\mathcal{L} = a\frac{h}{v}(\partial_\mu\chi^3)^2 - m_Z\left(2a\frac{h}{v} + b\frac{h^2}{v^2}\right)\partial_\mu\chi^3 Z^\mu. \quad (\text{C.15})$$

Neglecting the masses of the initial state leptons, as well as those of the Higgs and the Z boson, the amplitude can be written as

$$i\mathcal{A}(e^+e^- \rightarrow hhZ_L) \simeq (\sqrt{2}G_F)^{3/2}\frac{2m_Z^2}{s}(b - a^2)\bar{v}(k_2)\not{p}_3(g_V - g_A\gamma^5)u(k_1), \quad (\text{C.16})$$

where k_1 and k_2 are the momenta of the incoming electron and positron, p_3 is the momentum of the outgoing Z boson and s is the center-of-mass energy. The vector and axial-vector couplings of the electron are given by

$$g_V = -\frac{1}{2} + 2s_W^2, \quad g_A = -\frac{1}{2}. \quad (\text{C.17})$$

Squaring and averaging the amplitude over the initial spins one gets

$$\overline{|\mathcal{A}|^2} \simeq 8m_Z^4(\sqrt{2}G_F)^3(g_V^2 + g_A^2)(b - a^2)^2\frac{p_3 \cdot k_1 p_3 \cdot k_2}{s^2}. \quad (\text{C.18})$$

The total cross section is written as

$$\sigma(e^+e^- \rightarrow hhZ_L) = \frac{1}{2} \times \frac{1}{2s} \int \overline{|\mathcal{A}|^2} d\Phi^{(3)}, \quad (\text{C.19})$$

where the extra $1/2$ factor accounts for the two Higgs particles in the final state. The phase space integral can be done by using the recursive formula

$$d\Phi^{(3)}(P; p_1, p_2, p_3) = \int \frac{dp_{12}^2}{2\pi} d\Phi^{(2)}(p_{12}; p_1, p_2) d\Phi^{(2)}(P; p_{12}, p_3). \quad (\text{C.20})$$

Notice that p_{12}^2 is the invariant mass of the two Higgses. Since the amplitude in eq. (C.18) does not depend on the momenta of the two Higgs bosons, p_1 and p_2 , the first phase space integral in eq. (C.20) is trivial and gives

$$d\Phi^{(2)}(p_{12}; p_1, p_2) = \frac{1}{8\pi}. \quad (\text{C.21})$$

Taking into account the energy and angular dependence of the amplitude one obtains

$$\frac{d\sigma}{dm_{hh}^2} \simeq \frac{(\sqrt{2}G_F)^3(g_V^2 + g_A^2)}{1536\pi^3} \frac{m_Z^4}{s} (b - a^2)^2 \left(1 - \frac{m_{hh}^2}{s}\right)^3, \quad (\text{C.22})$$

and integrating over $0 \leq m_{hh}^2 \leq s$ it follows

$$\sigma \simeq \frac{(\sqrt{2}G_F)^3(g_V^2 + g_A^2)}{6144\pi^3} m_Z^4 (b - a^2)^2 = 0.15 \text{ fb } (b - a^2)^2. \quad (\text{C.23})$$

D Direct Probes of NP

D.1 The tilded basis

The field redefinition in eq. (6.9) allows many equivalent Lagrangian description of the Simplified Model. In all but one of them a kinetic mixing between V and W is present. We define each of these bases by the same Lagrangian in eq. (6.2) with all the couplings replaced by “tilded” ones

$$c \rightarrow \tilde{c}, \quad m_V \rightarrow \tilde{m}_V, \quad (D.1)$$

and with the addition of the kinetic mixing term

$$\tilde{c}_{VW} \frac{g}{2g_V} D_{[\mu} V_{\nu]}^a W^{\mu\nu a}. \quad (D.2)$$

Using the field redefinition of eq. (6.9) with

$$\alpha = \frac{g \tilde{c}_{VW}}{\sqrt{g_V^2 - \tilde{c}_{VW}^2 g^2}} \quad \text{and} \quad \beta = \frac{g_V}{\sqrt{g_V^2 - \tilde{c}_{VW}^2 g^2}}, \quad (D.3)$$

we get the following relations between the parameters in the two bases

$$\begin{aligned}
 m_V^2 &= \frac{g_V^2}{g_V^2 - \tilde{c}_{VW}^2 g^2} \tilde{m}_V^2, \\
 c_{V VW} &= \frac{g_V^2}{g_V^2 - \tilde{c}_{VW}^2 g^2} \left[\tilde{c}_{V VW} - \frac{g^2}{g_V^2} \tilde{c}_{VW}^2 \right], \\
 c_{V V V} &= \frac{g_V^3}{(g_V^2 - \tilde{c}_{VW}^2 g^2)^{3/2}} \left[\tilde{c}_{V V V} - \frac{g^2}{g_V^2} \tilde{c}_{VW} (\tilde{c}_{V VW} + 2) + 2 \frac{g^4}{g_V^4} \tilde{c}_{VW}^3 \right], \\
 c_H &= \frac{g_V}{\sqrt{g_V^2 - \tilde{c}_{VW}^2 g^2}} \left[\tilde{c}_H + \frac{g^2}{g_V^2} \tilde{c}_{VW} \right], \\
 c_{V V H H} &= \frac{g_V^2}{g_V^2 - \tilde{c}_{VW}^2 g^2} \left[\tilde{c}_{V V H H} + \frac{g^2}{2 g_V^2} \tilde{c}_{VW} \tilde{c}_H + \frac{g^4}{4 g_V^4} \tilde{c}_{VW}^2 \right], \\
 c_F &= \frac{g_V}{\sqrt{g_V^2 - \tilde{c}_{VW}^2 g^2}} [\tilde{c}_F + \tilde{c}_{VW}].
 \end{aligned} \tag{D.4}$$

D.2 Electroweak precision tests

In this Appendix we discuss the constraints of EWPT on the Simplified Model parameter space. In order to do this we integrate out the vector triplet and describe the resulting theory as the SM supplemented by higher dimensional operators. We expect all the relevant corrections to be oblique, that is encoded in corrections to the vacuum polarisation of the SM gauge bosons. This is not immediate to see in the basis of eq. (6.2) as V couples, though universally, to the light fermions. It is then useful to remove this coupling through the field redefinition¹

$$W_\mu^a \rightarrow W_\mu^a - c_F \frac{g^2}{g_V} V_\mu^a. \tag{D.5}$$

The resulting Lagrangian reads

$$\begin{aligned}
 \mathcal{L}_V &= -\frac{1}{4} \left(1 + c_F^2 \frac{g^2}{g_V^2} \right) D_{[\mu} V_{\nu]}^a D^{[\mu} V^{\nu]} a + \frac{m_V^2}{2} V_\mu^a V^{\mu a} \\
 &\quad + i g_V \left(c_H - c_F \frac{g^2}{g_V^2} \right) V_\mu^a H^\dagger \tau^a \overleftrightarrow{D}^\mu H + \frac{c_F}{2 g_V} D_{[\mu} V_{\nu]}^a W^{\mu\nu a} \\
 &\quad + g_V^2 \left(c_{V V H H} + \frac{c_F^2}{4} \frac{g^4}{g_V^4} - \frac{c_F c_H}{2} \frac{g^2}{g_V^2} \right) V_\mu^a V^{\mu a} H^\dagger H + \dots,
 \end{aligned} \tag{D.6}$$

while the coupling of V to the light fermions is removed. Notice that a kinetic mixing between the W and V is reintroduced. The dots include terms of order WV^2 , V^3 , V^4 .

¹For convenience we work in the basis in which the gauge coupling appears only in front of the gauge kinetic term.

These are not relevant in the discussion of the EWPT. Normalising the kinetic term gives the leading order equation of motion of V

$$[(\square + \mu_V^2)g_{\mu\nu} - \partial_\mu\partial_\nu] V_\nu^a = -ig_V\gamma_H H^\dagger \tau^a \overleftrightarrow{D}_\mu H + \gamma_F \frac{1}{g_V} D_\nu W_{\nu\mu}^a \equiv \mathcal{J}_\mu^a, \quad (\text{D.7})$$

where

$$\left(1 + c_F^2 \frac{g^2}{g_V^2}\right) \mu_V^2 = m_V^2 + 2 \left(c_{VVHH} + \frac{c_F^2}{4} \frac{g^4}{g_V^4} - \frac{c_F c_H}{2} \frac{g^2}{g_V^2} \right) g_V^2 |H|^2, \quad (\text{D.8})$$

$$\left(1 + c_F^2 \frac{g^2}{g_V^2}\right)^{1/2} \gamma_H = c_H - c_F \frac{g^2}{g_V^2}, \quad (\text{D.9})$$

$$\left(1 + c_F^2 \frac{g^2}{g_V^2}\right)^{1/2} \gamma_F = c_F. \quad (\text{D.10})$$

The solution of eq. (D.7) is

$$V_\mu^a = D_{\mu\nu} \mathcal{J}_\nu^a, \quad D_{\mu\nu} = \frac{g_{\mu\nu} + \partial_\mu\partial_\nu/\mu_V^2}{\square + \mu_V^2}. \quad (\text{D.11})$$

Plugging this solution into eq. (D.6) with a normalised kinetic term and expanding in derivatives we get the leading terms contributing to the EWPT

$$\begin{aligned} \mathcal{L}_V = & -\frac{1}{2\mu_V^2} \left(-ig_V\gamma_H H^\dagger \tau^a \overleftrightarrow{D}_\mu H + \gamma_F \frac{1}{g_V} D_\nu W_{\nu\mu}^a \right)^2 \\ & + \frac{1}{2\mu_V^2} \left(-ig_V\gamma_H H^\dagger \tau^a \overleftrightarrow{D}_\mu H \right) \frac{\square_{\mu\nu}^T}{\mu_V^2} \left(-ig_V\gamma_H H^\dagger \tau^a \overleftrightarrow{D}_\nu H \right) + \dots, \end{aligned} \quad (\text{D.12})$$

where we defined $\square_{\mu\nu}^T = g_{\mu\nu}\square - \partial_\mu\partial_\nu$. All other terms in the expansion, represented by the dots, give subleading contributions to the EWPT in a \hat{m}_W^2/μ_V^2 expansion. Following Ref. [132] we rewrite the quadratic part of \mathcal{L}_V as

$$\mathcal{L} = -\frac{1}{2} W_\mu^3 \Pi_{33}(p^2) W^{\mu 3} - \frac{1}{2} B_\mu \Pi_{00}(p^2) B^\mu - W_\mu^3 \Pi_{30}(p^2) B^\mu - W_\mu^+ \Pi_\pm(p^2) W^{\mu -}. \quad (\text{D.13})$$

The various form factors are then expanded in powers of p^2

$$\Pi(p^2) = \Pi(0) + p^2 \Pi'(0) + \frac{p^4}{2} \Pi''(0) + \dots \quad (\text{D.14})$$

Starting from eq. (D.12) and following the procedure we outlined above we get the leading order contributions (as in the text we define $z \equiv g_V \hat{v}/2\mu_V$, $\hat{m}_W = g\hat{v}/2$ and

Appendix D. Direct Probes of NP

$$t_W \equiv \tan \theta_W = g'/g$$

$$\begin{aligned}\Pi_{00}(0) &= \Pi_{33}(0) = \Pi_{\pm}(0) = -\Pi_{30}(0) = -\frac{\hat{v}^2}{4} (1 - z^2 \gamma_H^2), \\ \Pi'_{00}(0) &= \frac{1}{g'^2} \left(1 + t_W^2 \gamma_H^2 z^2 \frac{\hat{m}_W^2}{\mu_V^2} \right), \\ \Pi'_{30}(0) &= \frac{1}{g^2} \left(\gamma_H^2 z^2 \frac{\hat{m}_W^2}{\mu_V^2} - \gamma_H \gamma_F \frac{\hat{m}_W^2}{\mu_V^2} \right), \\ \Pi'_{\pm}(0) &= \Pi'_{33}(0) = \frac{1}{g^2} \left(1 + \gamma_H^2 z^2 \frac{\hat{m}_W^2}{\mu_V^2} + 2\gamma_H \gamma_F \frac{\hat{m}_W^2}{\mu_V^2} \right), \\ \Pi''_{\pm}(0) &= \Pi''_{33}(0) = \frac{1}{g^2 \hat{m}_W^2} \left(2\gamma_F^2 \frac{g^2}{g_V^2} \frac{\hat{m}_W^2}{\mu_V^2} \right).\end{aligned}\tag{D.15}$$

We thus obtain the following relations

$$\begin{aligned}v^2|_{\text{exp}} &\equiv -4\Pi_{\pm}(0) = \hat{v}^2 (1 - z^2 \gamma_H^2), \\ \frac{1}{g^2}|_{\text{exp}} &\equiv \Pi'_{\pm}(0) = \frac{1}{g^2} \left(1 + \gamma_H^2 z^2 \frac{\hat{m}_W^2}{\mu_V^2} + 2\gamma_H \gamma_F \frac{\hat{m}_W^2}{\mu_V^2} \right), \\ \frac{1}{g'^2}|_{\text{exp}} &\equiv \Pi'_{00}(0) = \frac{1}{g'^2} \left(1 + t_W^2 \gamma_H^2 z^2 \frac{\hat{m}_W^2}{\mu_V^2} \right).\end{aligned}\tag{D.16}$$

The relevant custodial invariant oblique parameters are defined by

$$\hat{S} = g^2 \Pi'_{30}(0), \quad W = \frac{g^2 \hat{m}_W^2}{2} \Pi''_{33}(0).\tag{D.17}$$

The natural size of the coefficients γ_H and γ_F is $\gamma_H \sim \gamma_F \sim 1$. This implies that the oblique parameters will be at most of order \hat{m}_W^2/μ_V^2 , while

$$g|_{\text{exp}} = g + O(\hat{m}_W^2/\mu_V^2), \quad g'|_{\text{exp}} = g' + O(\hat{m}_W^2/\mu_V^2),\tag{D.18}$$

so that the corrections to g and g' can be neglected in the calculation of the oblique parameters. Notice on the other hand that \hat{v} can depart from its measured value 246 GeV by $O(1)$ corrections

$$v^2|_{\text{exp}} = \hat{v}^2 (1 - \gamma_H^2 z^2).\tag{D.19}$$

One thus finds

$$\hat{S} = \gamma_H^2 z^2 \frac{\hat{m}_W^2}{\mu_V^2} - \gamma_H \gamma_F \frac{\hat{m}_W^2}{\mu_V^2}, \quad W = \gamma_F^2 \frac{g^2}{g_V^2} \frac{\hat{m}_W^2}{\mu_V^2}.\tag{D.20}$$

where one has still to express \hat{v} in terms of the physical $v \simeq 246$ GeV. Notice that under the assumption that $\gamma_F \sim 1$ the correction to the V kinetic term which is present in eq. (D.6) is always subleading in a \hat{m}_W^2/μ_V^2 expansion and can be neglected.

D.3 Tools provided with this chapter

In addition to the present section we provide a set of tools useful to perform analyses using the Simplified Model. We make them available on the webpage of this project [324].

The Simplified Model Lagrangian in eq. (6.2) in the mass eigenstate basis and in the unitary gauge was implemented into different Matrix Element Generators (MEG) using the FeynRules [351, 352] MATHEMATICA package. Model files for the CalcHEP [353, 354] and MADGRAPH5 [189] MEG and the FeynRules source model are registered in the HEPMDB model database [355] with the unique number hepmdb:0214.0151 and are available at the link [356].

The model was implemented into FeynRules taking α_{EW} , G_F and M_Z as SM electroweak input parameters and the mass of the neutral heavy vector M_0 , the overall coupling g_V and all the parameters c_i 's as described in this section as the new vector input parameters. The Higgs mass is also an input parameter, that we fixed to a default value of 125.5 GeV. All the other parameters are dependent parameters, defined as functions of the aforementioned inputs. Free parameters a, b, c, d_3, d_4 for the Higgs sector were also implemented with the notation of Ref. [64]. For $a = b = c = d_3 = d_4 = 1$ the Higgs sector is exactly SM like.

In addition to the MEG model files, we made available a Computable Document Format CDF© [357] notebook at the webpage [324]. This is an interactive web interface to a MATHEMATICA notebook which allows the user to compute the dependent parameters, the widths and the BRs in the model and to plot the relevant cross-sections at 8, 14 and 100 TeV by simply inputting the independent parameters. It also automatically generates the MADGRAPH5 “param_card.dat” for the chosen point of the parameter space. Further information and possibly additional tools can be found directly at the webpage of this project [324].

D.4 Extrapolation of experimental bounds

In order to extrapolate the current LHC bounds on heavy vectors, obtained at a centre of mass energy $\sqrt{s_0}$ and integrated luminosity L_0 , to future colliders with a different, increased centre of mass energy \sqrt{s} and integrated luminosity L , we use the following rescaling procedure. The exclusion bounds on $\sigma \times BR$ given by the experimental collaborations contain information only on the background cross section. The excluded signal can be inferred from $N_S/\sqrt{N_B} = 3$, the definition of the exclusion bound for non-zero background. This implies

$$\frac{\sigma_S(s_0, \hat{s}_0)L_0}{\sqrt{\sigma_B(s_0, \hat{s}_0)L_0}} = \frac{\sigma_S(s, \hat{s})L}{\sqrt{\sigma_B(s, \hat{s})L}}, \quad (\text{D.21})$$

Appendix D. Direct Probes of NP

where each cross section depends not only on the center of mass energy s , but also on the scale \hat{s} at which the parton luminosities are computed (see Figures 6.3). Solving gives

$$\sigma_S(s, \hat{s}) = \sqrt{\frac{L_0}{L}} \sqrt{\frac{\sigma_B(s, \hat{s})}{\sigma_B(s_0, \hat{s}_0)}} \sigma_S(s_0, \hat{s}_0). \quad (\text{D.22})$$

At this point, we assume that the background cross section rescales with the parton luminosities as

$$\sigma_B(s, \hat{s}) = k \frac{dL}{d\hat{s}}(s, \hat{s}). \quad (\text{D.23})$$

Substituting into eq. (D.21) yields

$$\sigma_S(s, \hat{s}) = \sqrt{\frac{L_0}{L}} \sqrt{\frac{\frac{dL}{d\hat{s}}|_{s, \hat{s}}}{\frac{dL}{d\hat{s}}|_{s_0, \hat{s}_0}}} \sigma_S(s_0, \hat{s}_0). \quad (\text{D.24})$$

From eq. (D.23), the following relations can be inferred by multiplying and dividing by the corresponding integrated luminosities

$$\frac{L}{L_1} \frac{\sigma_B(s, \hat{s})}{\frac{dL}{d\hat{s}}|_{s, \hat{s}}} = \frac{L}{L_0} \frac{\sigma_B(s_0, \hat{s}_0)}{\frac{dL}{d\hat{s}}|_{s_0, \hat{s}_0}}, \quad \Rightarrow \quad \frac{N_B(s, \hat{s}, L)}{L \frac{dL}{d\hat{s}}|_{s, \hat{s}}} = \frac{N_B(s_0, \hat{s}_0, L_0)}{L_0 \frac{dL}{d\hat{s}}|_{s_0, \hat{s}_0}}. \quad (\text{D.25})$$

Now, when the number of background events at the old and new collider and old and new centre of mass are the same, $N_B(s, \hat{s}, L) = N_B(s_0, \hat{s}_0, L_0)$, which corresponds to the same number of excluded signal events, $N_S(s, \hat{s}, L) = N_S(s_0, \hat{s}_0, L_0)$, this equation gives

$$\frac{\frac{dL}{d\hat{s}}|_{s, \hat{s}}}{\frac{dL}{d\hat{s}}|_{s_0, \hat{s}_0}} = \frac{L_0}{L}, \quad (\text{D.26})$$

which is universal and does not depend on the way the signal rescales. Plugging this equation into eq. (D.24) we finally obtain the rescaling relation

$$\sigma_S(s, \hat{s}) = \frac{L_0}{L} \sigma_S(s_0, \hat{s}_0). \quad (\text{D.27})$$

In practise, this means that the excluded signal cross section for a vector of mass $M_0 = \sqrt{\hat{s}_0}$ obtained at a collider with s_0 and L_0 gets mapped into a limit on a vector of mass M at a collider with s and L . M is obtained from M_0 by evaluating the parton luminosities at \hat{s}_0 for a collider s_0 , rescaling them by the ratio of the luminosities L_0/L and finding the corresponding mass $M = \sqrt{\hat{s}}$ of this value at the new collider with s .

Acknowledgements

Not only have I learned most of what I know and many of the most fundamental ideas in physics from my advisors, Riccardo Rattazzi and Christophe Grojean, but also the enthusiasm, patience and genuine curiosity needed for solid research. I am incredibly grateful for showing me a critical and healthy approach towards science and for teaching me the importance of asking a relevant question.

I want to thank Duccio Pappadopulo, who adopted me in the early stages of my Ph.D., and very patiently and confusedly brought me closer to the mysteries of particle phenomenology, and Riccardo Torre, for searching with me every possible missing minus sign and reading many versions of this manuscript. Thanks not only for having been the most hands-on support in moments of crisis but also for being great friends. To many more fiorentinas!

I am especially grateful to Luigi Del Debbio, for his encouragement to go into phenomenology, to Roberto Contino and Andrea Wulzer from whom I still hope to learn a lot, and to my collaborators and friends Marco, Francesco, Paolo, Sasha and particularly Ennio for many discussions about physics, life and such.

Besides physics, I want to thank my friends and officemates Benjamin, without whom the parallel thesis writing would have been way less cheerful, Davide and Lucio for their supportive understanding due to experience and of course fantastic colour suggestions to make my plots significantly more stylish, Thomas, Valentin, Tamas, Boaz, Davide and Solomon, who all made the seventh floor unique. Finally, a hearty thanks to my flatmates, Fanny, Momchil and Benoit, who never stopped proposing a drink despite my temporary lack of social energy.

Ein allerherzlichstes Dankeschön an Diana, Julia und Theresa dafür, dass sie immer da sind und mir ab und zu den Kopf zurecht rücken. Für stete moralische Unterstützung in allen Lebenslagen möchte ich mich auch bei Johanna bedanken. Und Kathrin verdanke ich das täglich benötigte jahrelange Durchhaltevermögen, geprobt durch vielen Stunden am Klavier.

Nicht zuletzt möchte ich mich herzlichst bei meinen Eltern und Großeltern bedanken, die mich ausnahmslos in jedem nur erdenklichen Sinne unterstützen.

Lausanne, 22 July 2014

Andrea Thamm

Bibliography

- [1] D. Pappadopulo, A. Thamm, and R. Torre, “A minimally tuned composite Higgs model from an extra dimension”, *JHEP* **1307** (2013) 058, [arXiv:1303.3062](#). [[Inspire](#)].
- [2] M. Farina, C. Grojean, F. Maltoni, E. Salvioni, and A. Thamm, “Lifting degeneracies in Higgs couplings using single top production in association with a Higgs boson”, *JHEP* **1305** (2013) 022, [arXiv:1211.3736](#). [[Inspire](#)].
- [3] R. Contino, C. Grojean, D. Pappadopulo, R. Rattazzi, and A. Thamm, “Strong Higgs Interactions at a Linear Collider”, *JHEP* **1402** (2014) 006, [arXiv:1309.7038](#). [[Inspire](#)].
- [4] D. Pappadopulo, A. Thamm, R. Torre, and A. Wulzer, “Heavy Vector Triplets: Bridging Theory and Data”, [arXiv:1402.4431](#). [[Inspire](#)].
- [5] P. W. Higgs, “Broken Symmetries and the Masses of Gauge Bosons”, *Phys.Rev.Lett.* **13** (1964) 508–509. [[Inspire](#)].
- [6] G. Guralnik, C. Hagen, and T. Kibble, “Global Conservation Laws and Massless Particles”, *Phys.Rev.Lett.* **13** (1964) 585–587. [[Inspire](#)].
- [7] F. Englert and R. Brout, “Broken Symmetry and the Mass of Gauge Vector Mesons”, *Phys.Rev.Lett.* **13** (1964) 321–323. [[Inspire](#)].
- [8] **ATLAS** Collaboration, G. Aad *et al.*, “Measurement of the Higgs boson mass from the $H \rightarrow \gamma\gamma$ and $H \rightarrow ZZ^* \rightarrow 4\ell$ channels with the ATLAS detector using 25 fb⁻¹ of pp collision data”, [arXiv:1406.3827](#). [[Inspire](#)].
- [9] **CMS** Collaboration, “Precise determination of the mass of the Higgs boson and studies of the compatibility of its couplings with the standard model”, [[CMS-PAS-HIG-14-009](#)].
- [10] G. ’t Hooft, “Naturalness, chiral symmetry, and spontaneous chiral symmetry breaking”, *NATO Adv.Study Inst.Ser.B Phys.* **59** (1980) 135. [[Inspire](#)].
- [11] R. Rattazzi, V. S. Rychkov, E. Tonni, and A. Vichi, “Bounding scalar operator dimensions in 4D CFT”, *JHEP* **0812** (2008) 031, [arXiv:0807.0004](#). [[Inspire](#)].
- [12] **ATLAS** Collaboration, G. Aad *et al.*, “Observation of a new particle in the search for the Standard Model Higgs boson with the ATLAS detector at the LHC”, *Phys. Lett. B* **716** (2012) 1, [arXiv:1207.7214](#). [[Inspire](#)].
- [13] **CMS** Collaboration, S. Chatrchyan *et al.*, “Observation of a new boson at a mass of 125 GeV with the CMS experiment at the LHC”, *Phys. Lett. B* **716** (2012) 30,

- [arXiv:1207.7235](#). [[Inspire](#)].
- [14] Y. Nambu, “Quasiparticles and Gauge Invariance in the Theory of Superconductivity”, *Phys.Rev.* **117** (1960) 648–663. [[Inspire](#)].
 - [15] P. W. Anderson, “Plasmons, Gauge Invariance, and Mass”, *Phys. Rev.* **130** (1963) 439–442. [[Inspire](#)].
 - [16] Y. Nambu, “Axial vector current conservation in weak interactions”, *Phys.Rev.Lett.* **4** (1960) 380–382. [[Inspire](#)].
 - [17] P. W. Higgs, “Broken symmetries, massless particles and gauge fields”, *Phys.Lett.* **12** (1964) 132–133. [[Inspire](#)].
 - [18] R. Haag, J. T. Lopuszanski, and M. Sohnius, “All Possible Generators of Supersymmetries of the s Matrix”, *Nucl.Phys.* **B88** (1975) 257. [[Inspire](#)].
 - [19] S. R. Coleman and J. Mandula, “All Possible Symmetries of the S Matrix”, *Phys.Rev.* **159** (1967) 1251–1256. [[Inspire](#)].
 - [20] R. Barbieri and G. Giudice, “Upper Bounds on Supersymmetric Particle Masses”, *Nucl.Phys.* **B306** (1988) 63. [[Inspire](#)].
 - [21] S. Dimopoulos and G. Giudice, “Naturalness constraints in supersymmetric theories with nonuniversal soft terms”, *Phys.Lett.* **B357** (1995) 573–578, [hep-ph/9507282](#). [[Inspire](#)].
 - [22] G. Dvali and A. Pomarol, “Anomalous $U(1)$ as a mediator of supersymmetry breaking”, *Phys.Rev.Lett.* **77** 3728–3731, [hep-ph/9607383](#). [[Inspire](#)].
 - [23] M. Papucci, J. T. Ruderman, and A. Weiler, “Natural SUSY Endures”, *JHEP* **1209** (2012) 035, [arXiv:1110.6926](#). [[Inspire](#)].
 - [24] R. T. D’Agnolo, E. Kuflik, and M. Zanetti, “Fitting the Higgs to Natural SUSY”, *JHEP* **1303** (2013) 043, [arXiv:1212.1165](#). [[Inspire](#)].
 - [25] A. Arvanitaki, M. Baryakhtar, X. Huang, K. van Tilburg, and G. Villadoro, “The Last Vestiges of Naturalness”, *JHEP* **1403** (2014) 022, [arXiv:1309.3568](#). [[Inspire](#)].
 - [26] A. Arvanitaki, N. Craig, S. Dimopoulos, and G. Villadoro, “Mini-Split”, *JHEP* **1302** (2013) 126, [arXiv:1210.0555](#). [[Inspire](#)].
 - [27] **ATLAS** Collaboration. [[Summary plots from the ATLAS Supersymmetry physics group](#)].
 - [28] M. Czakon, A. Mitov, M. Papucci, J. T. Ruderman, and A. Weiler, “Closing the stop gap”, [arXiv:1407.1043](#). [[Inspire](#)].
 - [29] **OPAL** Collaboration, G. Abbiendi *et al.*, “Search for R-Parity Violating Decays of Scalar Fermions at LEP”, *Eur. Phys. J. C* **33** (2004) 149–172, [hep-ex/0310054](#). [[Inspire](#)].
 - [30] **CDF** Collaboration, T. Aaltonen *et al.*, “Search for pair-production of strongly-interacting particles decaying to pairs of jets in $p\bar{p}$ collisions at $\sqrt{s} = 1.96$ TeV”, *Phys. Rev. Lett.* **111** (2013) 031802, [arXiv:1303.2699](#). [[Inspire](#)].
 - [31] **ATLAS** Collaboration. [[Summary of ATLAS searches for electroweak production of charginos and neutralinos](#)].
 - [32] **CMS** Collaboration. [[Summary of observed limits for WEKino models](#)].
 - [33] S. Dimopoulos and J. Preskill, “Massless Composites With Massive Constituents”,

- Nucl.Phys.* **B199** (1982) 206. [Inspire].
- [34] D. B. Kaplan, H. Georgi, and S. Dimopoulos, “Composite Higgs Scalars”, *Phys. Lett.* **B136** (1984) 187. [Inspire].
- [35] D. B. Kaplan and H. Georgi, “ $SU(2) \times U(1)$ Breaking by Vacuum Misalignment”, *Phys. Lett.* **B136** (1984) 183. [Inspire].
- [36] H. Georgi and D. B. Kaplan, “Composite Higgs and Custodial $SU(2)$ ”, *Phys. Lett.* **B145** (1984) 216. [Inspire].
- [37] H. Georgi, D. B. Kaplan, and P. Galison, “Calculation of the Composite Higgs Mass”, *Phys. Lett.* **B143** (1984) 152. [Inspire].
- [38] M. J. Dugan, H. Georgi, and D. Kaplan, “Anatomy of a Composite Higgs Model”, *Nucl.Phys.* **B254** (1985) 299. [Inspire].
- [39] T. Banks, “Constraints on $SU(2) \times U(1)$ breaking by vacuum misalignment”, *Nucl.Phys.* **B243** (1984) 125. [Inspire].
- [40] R. Contino, Y. Nomura, and A. Pomarol, “Higgs as a Holographic Pseudo-Goldstone Boson”, *Nucl. Phys.* **B 671** (2003) 148–174, [hep-ph/0306259](#). [Inspire].
- [41] K. Agashe, R. Contino, and A. Pomarol, “The Minimal Composite Higgs Model”, *Nucl. Phys.* **B 719** (2005) 165–187, [hep-ph/0412089](#). [Inspire].
- [42] K. Agashe and R. Contino, “The Minimal Composite Higgs Model and Electroweak Precision Tests”, *Nucl. Phys.* **B 742** (2006) 59–85, [hep-ph/0510164](#). [Inspire].
- [43] R. Contino, L. Da Rold, and A. Pomarol, “Light custodians in natural composite Higgs models”, *Phys. Rev.* **D 75** (2007) 055014, [hep-ph/0612048](#). [Inspire].
- [44] G. Panico, M. Serone, and A. Wulzer, “A Model of Electroweak Symmetry Breaking from a Fifth Dimension”, *Nucl. Phys.* **B739** (2006) 186–207, [hep-ph/0510373](#). [Inspire].
- [45] R. Barbieri, B. Bellazzini, S. Rychkov, and A. Varagnolo, “The Higgs boson from an extended symmetry”, *Phys. Rev.* **D76** (2007) 115008, [arXiv:0706.0432](#). [Inspire].
- [46] R. Contino, “Tasi 2009 lectures: The Higgs as a Composite Nambu-Goldstone Boson”, [arXiv:1005.4269](#). [Inspire].
- [47] G. Panico, M. Redi, A. Tesi, and A. Wulzer, “On the Tuning and the Mass of the Composite Higgs”, *JHEP* **1303** (2013) 051, [arXiv:1210.7114](#). [Inspire].
- [48] A. Pomarol and F. Riva, “The Composite Higgs and Light Resonance Connection”, *JHEP* **08** (2012) 135, [arXiv:1205.6434](#). [Inspire].
- [49] D. Marzocca, M. Serone, and J. Shu, “General Composite Higgs Models”, *JHEP* **08** (2012) 013, [arXiv:1205.0770](#). [Inspire].
- [50] H. Baer, T. Barklow, K. Fujii, Y. Gao, A. Hoang, *et al.*, “The International Linear Collider Technical Design Report - Volume 2: Physics”, [arXiv:1306.6352](#). [Inspire].
- [51] L. Linssen, A. Miyamoto, M. Stanitzki, and H. Weerts, “Physics and Detectors at CLIC: CLIC Conceptual Design Report”, [arXiv:1202.5940](#). [Inspire].
- [52] M. Koratzinos, A. Blondel, R. Aleksan, O. Brunner, A. Butterworth, *et al.*, “TLEP: A High-Performance Circular e^+e^- Collider to Study the Higgs Boson”,

- [arXiv:1305.6498](#). [Inspire].
- [53] **LHC New Physics Working Group** Collaboration, D. Alves *et al.*, “Simplified Models for LHC New Physics Searches”, *J. Phys. G* **39** (2012) 105005, [arXiv:1105.2838](#). [Inspire].
 - [54] S. Glashow, “Partial Symmetries of Weak Interactions”, *Nucl.Phys.* **22** (1961) 579–588. [Inspire].
 - [55] S. Weinberg, “A Model of Leptons”, *Phys.Rev.Lett.* **19** (1967) 1264–1266. [Inspire].
 - [56] A. Salam, “Weak and Electromagnetic Interactions”, *Conf.Proc.* **C680519** (1968) 367–377. [Inspire].
 - [57] A. Strumia and F. Vissani, “Neutrino masses and mixings and...”, [hep-ph/0606054](#).
 - [58] S. Weinberg, “Implications of Dynamical Symmetry Breaking”, *Phys.Rev.* **D13** (1976) 974–996. [Inspire].
 - [59] S. Dimopoulos and L. Susskind, “Mass Without Scalars”, *Nucl.Phys.* **B155** (1979) 237–252. [Inspire].
 - [60] E. Farhi and L. Susskind, “Technicolor”, *Phys.Rept.* **74** (1981) 277. [Inspire].
 - [61] T. Appelquist and C. W. Bernard, “Strongly Interacting Higgs Bosons”, *Phys.Rev.* **D22** (1980) 200. [Inspire].
 - [62] A. C. Longhitano, “Heavy Higgs Bosons in the Weinberg-Salam Model”, *Phys.Rev.* **D22** (1980) 1166. [Inspire].
 - [63] A. C. Longhitano, “Low-Energy Impact of a Heavy Higgs Boson Sector”, *Nucl.Phys.* **B188** (1981) 118. [Inspire].
 - [64] R. Contino, C. Grojean, M. Moretti, F. Piccinini, and R. Rattazzi, “Strong Double Higgs Production at the LHC”, *JHEP* **05** (2010) 089, [arXiv:1002.1011](#). [Inspire].
 - [65] V. Koulovassilopoulos and R. S. Chivukula, “The Phenomenology of a nonstandard Higgs boson in $W(L)W(L)$ scattering”, *Phys.Rev.* **D50** (1994) 3218–3234, [hep-ph/9312317](#). [Inspire].
 - [66] C. Burgess, J. Matias, and M. Pospelov, “A Higgs or not a Higgs? What to do if you discover a new scalar particle”, *Int.J.Mod.Phys.* **A17** (2002) 1841–1918, [hep-ph/9912459](#). [Inspire].
 - [67] B. Grinstein and M. Trott, “A Higgs-Higgs bound state due to new physics at a TeV”, *Phys.Rev.* **D76** (2007) 073002, [arXiv:0704.1505](#). [Inspire].
 - [68] E. Halyo, “Technidilaton or Higgs?”, *Mod.Phys.Lett.* **A8** (1993) 275–284. [Inspire].
 - [69] W. D. Goldberger, B. Grinstein, and W. Skiba, “Distinguishing the Higgs boson from the dilaton at the Large Hadron Collider”, *Phys.Rev.Lett.* **100** (2008) 111802, [arXiv:0708.1463](#). [Inspire].
 - [70] L. Vecchi, “Phenomenology of a light scalar: the dilaton”, *Phys.Rev.* **D82** (2010) 076009, [arXiv:1002.1721](#). [Inspire].
 - [71] B. A. Campbell, J. Ellis, and K. A. Olive, “Phenomenology and Cosmology of an Electroweak Pseudo-Dilaton and Electroweak Baryons”, *JHEP* **1203** (2012) 026, [arXiv:1111.4495](#). [Inspire].
 - [72] Z. Chacko, R. Franceschini, and R. K. Mishra, “Resonance at 125 GeV: Higgs or Dilaton/Radion?”, *JHEP* **04** (2013) 015, [arXiv:1209.3259](#). [Inspire].

-
- [73] B. Bellazzini, C. Csaki, J. Hubisz, J. Serra, and J. Terning, “A Higgslike Dilaton”, *Eur. Phys. J. C* **73** (2013) 2333, [arXiv:1209.3299](#). [[Inspire](#)].
- [74] P. P. Giardino, K. Kannike, I. Masina, M. Raidal, and A. Strumia, “The universal Higgs fit”, *JHEP* **1405** (2014) 046, [arXiv:1303.3570](#). [[Inspire](#)].
- [75] S. Weinberg, “The Quantum Theory of Fields”, *Cambridge University Press* **2** (1995) .
- [76] S. Weinberg, “Baryon and Lepton Nonconserving Processes”, *Phys.Rev.Lett.* **43** (1979) 1566–1570. [[Inspire](#)].
- [77] C. Csaki, Y. Shirman, and J. Terning, “A Seiberg Dual for the MSSM: Partially Composite W and Z”, *Phys.Rev.* **D84** (2011) 095011, [arXiv:1106.3074](#). [[Inspire](#)].
- [78] O. Domenech, A. Pomarol, and J. Serra, “Probing the SM with Dijets at the LHC”, *Phys.Rev.* **D85** (2012) 074030, [arXiv:1201.6510](#). [[Inspire](#)].
- [79] A. Pomarol and F. Riva, “Towards the Ultimate SM Fit to Close in on Higgs Physics”, *JHEP* **1401** (2014) 151, [arXiv:1308.2803](#). [[Inspire](#)].
- [80] G. F. Giudice, C. Grojean, A. Pomarol, and R. Rattazzi, “The Strongly-Interacting Light Higgs”, *JHEP* **06** (2007) 045, [hep-ph/0703164](#). [[Inspire](#)].
- [81] C. Burges and H. J. Schnitzer, “Virtual Effects of Excited Quarks as Probes of a Possible New Hadronic Mass Scale”, *Nucl.Phys.* **B228** (1983) 464. [[Inspire](#)].
- [82] C. N. Leung, S. Love, and S. Rao, “Low-Energy Manifestations of a New Interaction Scale: Operator Analysis”, *Z.Phys.* **C31** (1986) 433. [[Inspire](#)].
- [83] W. Buchmuller and D. Wyler, “Effective Lagrangian Analysis of New Interactions and Flavor Conservation”, *Nucl.Phys.* **B268** (1986) 621–653. [[Inspire](#)].
- [84] R. Rattazzi, “Anomalous Interactions at the Z^0 Pole”, *Z.Phys.* **C40** (1988) 605–611. [[Inspire](#)].
- [85] B. Grzadkowski, Z. Hioki, K. Ohkuma, and J. Wudka, “Probing anomalous top quark couplings induced by dimension-six operators at photon colliders”, *Nucl.Phys.* **B689** (2004) 108–126, [hep-ph/0310159](#). [[Inspire](#)].
- [86] C. Grojean, W. Skiba, and J. Terning, “Disguising the oblique parameters”, *Phys.Rev.* **D73** (2006) 075008, [hep-ph/0602154](#). [[Inspire](#)].
- [87] P. J. Fox, Z. Ligeti, M. Papucci, G. Perez, and M. D. Schwartz, “Deciphering top flavor violation at the LHC with B factories”, *Phys.Rev.* **D78** (2008) 054008, [arXiv:0704.1482](#). [[Inspire](#)].
- [88] J. Aguilar-Saavedra, “A Minimal set of top anomalous couplings”, *Nucl.Phys.* **B812** (2009) 181–204, [arXiv:0811.3842](#). [[Inspire](#)].
- [89] J. Aguilar-Saavedra, “A Minimal set of top-Higgs anomalous couplings”, *Nucl.Phys.* **B821** (2009) 215–227, [arXiv:0904.2387](#). [[Inspire](#)].
- [90] B. Grzadkowski, M. Iskrzynski, M. Misiak, and J. Rosiek, “Dimension-Six Terms in the Standard Model Lagrangian”, *JHEP* **1010** (2010) 085, [arXiv:1008.4884](#). [[Inspire](#)].
- [91] R. Contino, M. Ghezzi, C. Grojean, M. Muhlleitner, and M. Spira, “Effective Lagrangian for a light Higgs-like scalar”, *JHEP* **1307** (2013) 035, [arXiv:1303.3876](#). [[Inspire](#)].

- [92] J. Elias-Miro, J. Espinosa, E. Masso, and A. Pomarol, “Higgs windows to new physics through $d=6$ operators: constraints and one-loop anomalous dimensions”, *JHEP* **1311** (2013) 066, [arXiv:1308.1879](#). [[Inspire](#)].
- [93] R. S. Gupta, A. Pomarol, and F. Riva, “BSM Primary Effects”, [arXiv:1405.0181](#). [[Inspire](#)].
- [94] G. D’Ambrosio, G. Giudice, G. Isidori, and A. Strumia, “Minimal flavor violation: An Effective field theory approach”, *Nucl.Phys.* **B645** (2002) 155–187, [hep-ph/0207036](#). [[Inspire](#)].
- [95] M. S. Chanowitz and M. K. Gaillard, “The TeV Physics of Strongly Interacting W’s and Z’s”, *Nucl.Phys.* **B261** (1985) 379. [[Inspire](#)].
- [96] A. Wulzer, “An Equivalent Gauge and the Equivalence Theorem”, [arXiv:1309.6055](#). [[Inspire](#)].
- [97] R. Contino, D. Marzocca, D. Pappadopulo, and R. Rattazzi, “On the effect of resonances in composite Higgs phenomenology”, *JHEP* **10** (2011) 081, [arXiv:1109.1570](#). [[Inspire](#)].
- [98] M. Farina, C. Grojean, and E. Salvioni, “(Dys)Zphilia or a custodial breaking Higgs at the LHC”, *JHEP* **1207** (2012) 012, [arXiv:1205.0011](#). [[Inspire](#)].
- [99] CMS Collaboration, “Combination of standard model Higgs boson searches and measurements of the properties of the new boson with a mass near 125 GeV”, [[Inspire](#)].
- [100] ATLAS Collaboration, “Combined coupling measurements of the Higgs-like boson proton-proton collision data”, [[Inspire](#)].
- [101] CDF Collaboration, D0 Collaboration Collaboration, T. E. W. Group, “2012 Update of the Combination of CDF and D0 Results for the Mass of the W Boson”, [arXiv:1204.0042](#). [[Inspire](#)].
- [102] M. Antonelli, V. Cirigliano, G. Isidori, F. Mescia, M. Moulson, *et al.*, “An Evaluation of $|V_{us}|$ and precise tests of the Standard Model from world data on leptonic and semileptonic kaon decays”, *Eur.Phys.J.* **C69** (2010) 399–424, [arXiv:1005.2323](#). [[Inspire](#)].
- [103] CMS Collaboration, S. Chatrchyan *et al.*, “Search for new physics in final states with a lepton and missing transverse energy in pp collisions at the LHC”, *Phys.Rev* **D87** (2013) 072005, [arXiv:1302.2812](#). [[Inspire](#)].
- [104] DELPHI Collaboration, J. Abdallah *et al.*, “Measurements of CP-conserving Trilinear Gauge Boson Couplings WWV ($V = \gamma, Z$) in e^+e^- Collisions at LEP2”, *Eur.Phys.J.* **C66** (2010) 35–56, [arXiv:1002.0752](#). [[Inspire](#)].
- [105] G. Brooijmans, R. Contino, B. Fuks, F. Moortgat, P. Richardson, *et al.*, “Les Houches 2013: Physics at TeV Colliders: New Physics Working Group Report”, [arXiv:1405.1617](#). [[Inspire](#)].
- [106] CMS Collaboration, S. Chatrchyan *et al.*, “Search for a Higgs boson decaying into a Z and a photon in pp collisions at $\sqrt{s} = 7$ and 8 TeV”, *Phys.Lett.* **B726** (2013) 587–609, [arXiv:1307.5515](#). [[Inspire](#)].
- [107] ATLAS Collaboration, “Search for the Standard Model Higgs boson in the

- $H \rightarrow Z\gamma$ decay mode with pp collisions at $\sqrt{s} = 7$ and 8 TeV”, [ATLAS-CONF-2013-009].
- [108] M. Baak, M. Goebel, J. Haller, A. Hoecker, D. Kennedy, *et al.*, “The Electroweak Fit of the Standard Model after the Discovery of a New Boson at the LHC”, *Eur.Phys.J. C* **72** (2012) 2205, [arXiv:1209.2716](#). [Inspire].
 - [109] J. Erler, “Tests of the Electroweak Standard Model”, *J.Phys.Conf.Ser.* **485** (2014) 012010, [arXiv:1209.3324](#). [Inspire].
 - [110] B. Batell, S. Gori, and L.-T. Wang, “Higgs Couplings and Precision Electroweak Data”, *JHEP* **1301** (2013) 139, [arXiv:1209.6382](#). [Inspire].
 - [111] M. Ciuchini, E. Franco, S. Mishima, and L. Silvestrini, “Electroweak Precision Observables, New Physics and the Nature of a 126 GeV Higgs Boson”, *JHEP* **08** (2013) 106, [arXiv:1306.4644](#). [Inspire].
 - [112] **ALEPH Collaboration, DELPHI Collaboration, L3 Collaboration, OPAL Collaboration, SLD Collaboration, LEP Electroweak Working Group, SLD Electroweak Group, SLD Heavy Flavour Group** Collaboration, S. Schael *et al.*, “Precision electroweak measurements on the Z resonance”, *Phys.Rept.* **427** (2006) 257–454, [hep-ex/0509008](#). [Inspire].
 - [113] M. E. Peskin and T. Takeuchi, “Estimation of oblique electroweak corrections”, *Phys. Rev. D* **46** (1992) 381–409. [Inspire].
 - [114] R. Barbieri, A. Pomarol, R. Rattazzi, and A. Strumia, “Electroweak symmetry breaking after LEP1 and LEP2”, *Nucl. Phys. B* **703** (2004) 127–146, [hep-ph/0405040](#). [Inspire].
 - [115] I. Low, R. Rattazzi, and A. Vichi, “Theoretical Constraints on the Higgs Effective Couplings”, *JHEP* **04** (2010) 126, [arXiv:0907.5413](#). [Inspire], and the references cited therein.
 - [116] A. Falkowski, S. Rychkov, and A. Urbano, “What if the Higgs couplings to W and Z bosons are larger than in the Standard Model?”, *JHEP* **1204** (2012) 073, [arXiv:1202.1532](#). [Inspire].
 - [117] M. Golden and L. Randall, “Radiative Corrections to Electroweak Parameters in Technicolor Theories”, *Nucl.Phys. B* **361** (1991) 3–23. [Inspire].
 - [118] R. Barbieri, G. Isidori, and D. Pappadopulo, “Composite fermions in Electroweak Symmetry Breaking”, *JHEP* **0902** (2009) 029, [arXiv:0811.2888](#). [Inspire].
 - [119] C. Grojean, O. Matsedonskyi, and G. Panico, “Light top partners and precision physics”, *JHEP* **1310** (2013) 160, [arXiv:1306.4655](#). [Inspire].
 - [120] A. Azatov, R. Contino, A. Di Iura, and J. Galloway, “New Prospects for Higgs Compositeness in $h \rightarrow Z\gamma$ ”, *Phys.Rev.* **2013** (2013) 075019, [arXiv:1308.2676](#). [Inspire].
 - [121] M. S. Carena, E. Ponton, J. Santiago, and C. E. Wagner, “Light Kaluza Klein States in Randall-Sundrum Models with Custodial $SU(2)$ ”, *Nucl.Phys. B* **759** (2006) 202–227, [hep-ph/0607106](#). [Inspire].
 - [122] P. Lodone, “Vector-like quarks in a ‘composite’ Higgs model”, *JHEP* **0812** (2008) 029, [arXiv:0806.1472](#). [Inspire].

- [123] M. Gillioz, “A Light composite Higgs boson facing electroweak precision tests”, *Phys.Rev.* **D80** (2009) 055003, [arXiv:0806.3450](#). [[Inspire](#)].
- [124] A. Pomarol and J. Serra, “Top Quark Compositeness: Feasibility and Implications”, *Phys.Rev.* **D78** (2008) 074026, [arXiv:0806.3247](#). [[Inspire](#)].
- [125] A. Freitas and Y.-C. Huang, “Electroweak two-loop corrections to $\sin^2\theta_{eff}^{b\bar{b}}$ and R_b using numerical Mellin-Barnes integrals”, *JHEP* **1208** (2012) 050, [arXiv:1205.0299](#). [[Inspire](#)].
- [126] D. Guadagnoli and G. Isidori, “BR($B_s \rightarrow \mu^+ \mu^-$) as an electroweak precision test”, *Phys.Lett.* **B724** (2013) 63–67, [arXiv:1302.3909](#). [[Inspire](#)].
- [127] **CDF Collaboration, D0 Collaboration** Collaboration, T. Aaltonen *et al.*, “Combination of the top-quark mass measurements from the Tevatron collider”, *Phys.Rev.* **D86** (2012) 092003, [arXiv:1207.1069](#).
- [128] S. Alekhin, A. Djouadi, and S. Moch, “The top quark and Higgs boson masses and the stability of the electroweak vacuum”, *Phys.Lett.* **B716** (2012) 214–219, [arXiv:1207.0980](#). [[Inspire](#)].
- [129] B. Holdom and J. Terning, “Large corrections to electroweak parameters in technicolor theories”, *Phys.Lett.* **B247** (1990) 88–92. [[Inspire](#)].
- [130] G. Altarelli and R. Barbieri, “Vacuum polarization effects of new physics on electroweak processes”, *Phys.Lett.* **B253** (1991) 161–167. [[Inspire](#)].
- [131] G. Altarelli, R. Barbieri, and F. Caravaglios, “Nonstandard analysis of electroweak precision data”, *Nucl.Phys.* (1993) 3–23. [[Inspire](#)].
- [132] G. Cacciapaglia, C. Csaki, G. Marandella, and A. Strumia, “The Minimal Set of Electroweak Precision Parameters”, *Phys. Rev. D* **74** (2006) 033011, [hep-ph/0604111](#). [[Inspire](#)].
- [133] M. Cirelli, N. Fornengo, and A. Strumia, “Minimal Dark Matter”, *Nucl.Phys.* **B753** (2005) 178–194, [hep-ph/0512090](#). [[Inspire](#)].
- [134] R. Barbieri, “Ten Lectures on the ElectroWeak Interactions”, [arXiv:0706.0684](#). [[Inspire](#)].
- [135] A. Orgogozo and S. Rychkov, “Exploring T and S parameters in Vector Meson Dominance Models of Strong Electroweak Symmetry Breaking”, *JHEP* **1203** 046, [arXiv:1111.3534](#). [[Inspire](#)].
- [136] R. Barbieri, D. Buttazzo, F. Sala, D. Straub, and A. Tesi, “A 125 GeV composite Higgs boson versus flavour and electroweak precision tests”, [arXiv:1211.5085](#). [[Inspire](#)].
- [137] D. B. Kaplan, “Flavor at SSC energies: A new mechanism for dynamically generated fermion masses”, *Nucl. Phys. B* **365** (1991) 259. [[Inspire](#)].
- [138] C. G. Callan, S. Coleman, J. Wess, and B. Zumino, “Structure of Phenomenological Lagrangians. II”, *Phys. Rev.* **177** (1969) 2247–2250. [[Inspire](#)].
- [139] B. Keren-Zur, P. Lodone, M. Nardecchia, D. Pappadopulo, R. Rattazzi, and L. Vecchi, “On Partial Compositeness and the CP asymmetry in charm decays”, *Nucl.Phys.* **B867** (2013) 429–447, [arXiv:1205.5803](#). [[Inspire](#)].
- [140] K. Agashe, R. Contino, L. Da Rold, and A. Pomarol, “A Custodial symmetry for

- $Zb\bar{b}$ ", *Phys.Lett.* **B641** (2006) 62–66, [hep-ph/0605341](#). [[Inspire](#)].
- [141] J. Mrazek, A. Pomarol, R. Rattazzi, M. Redi, J. Serra, and A. Wulzer, "The Other Natural Two Higgs Doublet Model", *Nucl.Phys.* **B 853** (2011) 1–48, [arXiv:1105.5403](#). [[Inspire](#)].
 - [142] S. R. Coleman and E. J. Weinberg, "Radiative Corrections as the Origin of Spontaneous Symmetry Breaking", *Phys. Rev.* **D 7** (1973) 1888–1910. [[Inspire](#)].
 - [143] J. M. Maldacena, "The Large N limit of superconformal field theories and supergravity", *Adv.Theor.Math.Phys.* **2** (1998) 231–252, [hep-th/9711200](#). [[Inspire](#)].
 - [144] C. Csaki, "TASI lectures on extra dimensions and branes", [hep-ph/0404096](#). [[Inspire](#)].
 - [145] G. D. Kribs, "TASI 2004 lectures on the phenomenology of extra dimensions", [hep-ph/0605325](#). [[Inspire](#)].
 - [146] G. Panico and A. Wulzer, "Effective Action and Holography in 5D Gauge Theories", *JHEP* **05** (2007) 060, [hep-th/0703287](#). [[Inspire](#)].
 - [147] R. Contino and A. Pomarol, "Holography for fermions", *JHEP* **11** (2004) 058, [hep-th/0406257](#). [[Inspire](#)].
 - [148] M. Serone, "Holographic Methods and Gauge-Higgs Unification in Flat Extra Dimensions", *New J. Phys.* **12** (2010) 075013, [arXiv:0909.5619](#). [[Inspire](#)].
 - [149] C. Scrucca, M. Serone, and L. Silvestrini, "Electroweak symmetry breaking and fermion masses from extra dimensions", *Nucl.Phys.* **B669** (2003) 128–158, [hep-ph/0304220](#). [[Inspire](#)].
 - [150] R. Barbieri, A. Pomarol, and R. Rattazzi, "Weakly coupled Higgsless theories and precision electroweak tests", *Physics Letters B* **591** (2003) 141–149, [hep-ph/0310285](#). [[Inspire](#)].
 - [151] G. Panico, M. Safari, and M. Serone, "Simple and Realistic Composite Higgs Models in Flat Extra Dimensions", *JHEP* **1102** (2011) 103, [arXiv:1012.2875](#). [[Inspire](#)].
 - [152] E. Witten, "Some Inequalities Among Hadron Masses", *Phys. Rev. Lett.* **51** (1983) 2351. [[Inspire](#)].
 - [153] C. Vafa and E. Witten, "Restrictions on symmetry breaking in vector-like gauge theories", *Nucl. Phys.* **B 234** (1984) 173. [[Inspire](#)].
 - [154] G. Panico and A. Wulzer, "The Discrete Composite Higgs Model", *JHEP* **1109** (2011) 135, [arXiv:1106.2719](#). [[Inspire](#)].
 - [155] S. D. Curtis, M. Redi, and A. Tesi, "The 4D Composite Higgs", *JHEP* **1204** (2012) 042, [arXiv:1110.1613](#). [[Inspire](#)].
 - [156] M. Redi and A. Tesi, "Implications of a Light Higgs in Composite Models", *JHEP* **1210** (2012) 166, [arXiv:1205.0232](#). [[Inspire](#)].
 - [157] O. Matsedonskyi, G. Panico, and A. Wulzer, "Light Top Partners for a Light Composite Higgs", *JHEP* **1301** (2013) 164, [arXiv:1204.6333](#). [[Inspire](#)].
 - [158] A. Strumia, "The fine-tuning price of the early LHC", *JHEP* **1104** (2011) 073, [arXiv:1101.2195](#). [[Inspire](#)].
 - [159] R. Barbieri and G. F. Giudice, "Upper bounds on supersymmetric particle masses",

- Nucl. Phys. B* **306** (1988) 63. [Inspire].
- [160] G. F. Giudice and R. Rattazzi, “Living Dangerously with Low-Energy Supersymmetry. ”, *Nucl. Phys. B* **757** (2006) 19–46, [hep-ph/0606105](#). [Inspire].
- [161] **ATLAS** Collaboration, “Search for exotic same-sign dilepton signatures (b’ quark, $T_{5/3}$ and four top quarks production) in 4.7/fb of pp collisions at $\sqrt{s} = 7$ TeV with the ATLAS detector”, [[ATLAS-CONF-2012-130](#)].
- [162] **CMS** Collaboration, “Search for RPV supersymmetry with three or more leptons and b-tags”, [[CMS-PAS-SUS-12-027](#)].
- [163] A. Falkowski, F. Riva, and A. Urbano, “Higgs At Last”, *JHEP* **1311** (2013) 111, [arXiv:1303.1812](#). [Inspire].
- [164] D. Zeppenfeld, R. Kinnunen, A. Nikitenko, and E. Richter-Was, “Measuring Higgs boson couplings at the CERN LHC”, *Phys. Rev. D* **62** (2000) 013009, [hep-ph/0002036](#). [Inspire].
- [165] **ATLAS** Collaboration, M. Dührssen, “Prospects for the measurement of Higgs boson coupling parameters in the mass range from 110 - 190 GeV”, [[ATL-PHYS-2003-030](#)].
- [166] M. Dührssen, S. Heinemeyer, H. Logan, D. Rainwater, G. Weiglein, and D. Zeppenfeld, “Extracting Higgs boson couplings from CERN LHC data”, *Phys. Rev. D* (2004) 113009, [hep-ph/0406323](#). [Inspire].
- [167] R. Lafaye, T. Plehn, M. Rauch, D. Zerwas, and M. Dührssen, “Measuring the Higgs Sector”, *JHEP* **0908** (2009) 009, [arXiv:0904.3866](#). [Inspire].
- [168] D. Carmi, A. Falkowski, E. Kuflik, and T. Volansky, “Interpreting LHC Higgs Results from Natural New Physics Perspective”, *JHEP* **1207** (2012) 136, [arXiv:1202.3144](#). [Inspire].
- [169] A. Azatov, R. Contino, and J. Galloway, “Model-Independent Bounds on a Light Higgs”, *JHEP* **1204** (2012) 127, [arXiv:1202.3415](#). [Inspire].
- [170] J. R. Espinosa, C. Grojean, M. Mühlleitner, and M. Trott, “Fingerprinting Higgs Suspects at the LHC”, *JHEP* **1205** (2012) 097, [arXiv:1202.3697](#). [Inspire].
- [171] **ATLAS** Collaboration, “Updated coupling measurements of the Higgs boson with the ATLAS detector using up to 25 fb^{-1} of proton-proton collision data”, [[ATLAS-CONF-2014-009](#)].
- [172] A. Azatov, R. Contino, D. D. Re, J. Galloway, M. Grassi, and S. Rahatlou, “Determining Higgs couplings with a model-independent analysis of $h \rightarrow \text{gamma gamma}$ ”, *JHEP* **1206** (2012) 134, [arXiv:1204.4817](#). [Inspire].
- [173] **ATLAS** Collaboration, “Search for the Standard Model Higgs boson produced in association with top quarks and decaying into bb in pp collisions at $\sqrt{s} = 8$ TeV with the ATLAS detector at the LHC”, [[ATLAS-CONF-2014-011](#)].
- [174] **CMS** Collaboration, “Search for ttH production using the Matrix Element Method”, [[CMS-PAS-HIG-14-010](#)].
- [175] W. Beenakker, S. Dittmaier, M. Kramer, B. Plumper, M. Spira, and P. M. Zerwas, “Higgs radiation off top quarks at the Tevatron and the LHC”, *Phys. Rev. Lett.* **87** (2001) 201805, [hep-ph/0107081](#). [Inspire].

- [176] S. Dawson, L. H. Orr, L. Reina, and D. Wackeroth, “Associated top quark Higgs boson production at the LHC”, *Phys. Rev.* **D67** (2003) 071503, [hep-ph/0211438](#). [[Inspire](#)].
- [177] R. Frederix, S. Frixione, V. Hirschi, F. Maltoni, R. Pittau, and P. Torrielli, “Scalar and pseudoscalar Higgs production in association with a top-antitop pair”, *Phys.Lett.* **2011** (B701) 427–433, [arXiv:1104.5613](#). [[Inspire](#)].
- [178] M. V. Garzelli, A. Kardos, C. G. Papadopoulos, and Z. Trocsanyi, “Standard Model Higgs boson production in association with a top anti-top pair at NLO with parton showering”, *Europhys.Lett.* **96** (2011) 11001, [arXiv:1108.0387](#). [[Inspire](#)].
- [179] C. Degrande, J. M. Gerard, C. Grojean, F. Maltoni, and G. Servant, “Probing Top-Higgs Non-Standard Interactions at the LHC”, *JHEP* **1207** (2012) 036, [arXiv:1205.1065](#). [[Inspire](#)].
- [180] F. Maltoni, K. Paul, T. Stelzer, and S. Willenbrock, “Associated production of Higgs and single top at hadron colliders”, *Phys. Rev.* **D64** (2001) 094023, [hep-ph/0106293](#). [[Inspire](#)].
- [181] T. M. P. Tait and C. P. Yuan, “Single top quark production as a window to physics beyond the standard model”, *Phys. Rev.* **D63** (2000) 014018, [hep-ph/0007298](#). [[Inspire](#)].
- [182] V. Barger, M. McCaskey, and G. Shaughnessy, “Single top and Higgs associated production at the LHC”, *Phys. Rev.* **D81** (2010) 034020, [arXiv:0911.1556](#). [[Inspire](#)].
- [183] S. Biswas and E. Gabrielli and B. Mele, “Single top and higgs associated production as a probe of the htt coupling sign at the lhc”, *JHEP* **1301** (2013) 088, [arXiv:1211.0499](#). [[Inspire](#)].
- [184] S. Biswas, E. Gabrielli, F. Margaroli, and B. Mele, “Direct constraints on the top-Higgs coupling from the 8 TeV LHC data”, *JHEP* **07** (2013) 073, [arXiv:1304.1822](#). [[Inspire](#)].
- [185] S. Dawson, “The effective W approximation”, *Nucl. Phys.* **B 249** (1985) 42. [[Inspire](#)].
- [186] G. L. Kane, W. W. Repko, and W. B. Rolnick, “The Effective W^\pm, Z^0 Approximation for High-Energy Collisions”, *Phys. Lett.* **B148** (1984) 367–372. [[Inspire](#)].
- [187] T. Appelquist and M. S. Chanowitz, “Unitarity Bound on the Scale of Fermion Mass Generation”, *Phys. Rev. Lett.* **59** (1987) 2405. [[Inspire](#)].
- [188] F. Maltoni, J. M. Niczyporuk, and S. Willenbrock, “The Scale of fermion mass generation”, *Phys. Rev.* **D65** (2002) 033004, [hep-ph/0106281](#). [[Inspire](#)].
- [189] J. Alwall, M. Herquet, F. Maltoni, O. Mattelaer, and T. Stelzer, “MadGraph 5: going beyond”, *JHEP* **06** (2011) 128, [arXiv:1106.0522](#). [[Inspire](#)].
- [190] J. Pumplin, D. R. Stump, J. Huston, H. L. Lai, P. M. Nadolsky, and W. K. Tung, “New generation of parton distributions with uncertainties from global QCD analysis”, *JHEP* **0207** (2002) 012, [hep-ph/0201195](#). [[Inspire](#)].
- [191] R. Frederix, S. Frixione, F. Maltoni, and T. Stelzer, “Automation of next-to-leading

- order computations in QCD: The FKS subtraction”, *JHEP* **0910** (2009) 003, [arXiv:0908.4272](#). [[Inspire](#)].
- [192] V. Hirschi, R. Frederix, S. Frixione, M. V. Garzelli, F. Maltoni, and R. Pittau, “Automation of one-loop QCD corrections”, *JHEP* **1105** (2011) 044, [arXiv:1103.0621](#). [[Inspire](#)].
- [193] [[AMC@NLO](#)].
- [194] **ATLAS** Collaboration, G. A. *et al.*, “Jet energy resolution in proton-proton collisions at $\sqrt{s} = 7$ TeV recorded in 2010 with the ATLAS detector”, *EPJ Web Conf.* **C73** (2013) 2306, [arXiv:1210.6210](#). [[Inspire](#)].
- [195] J. R. Espinosa and C. Grojean and M. Mühlleitner and M. Trott, “First glimpses at higgs’ face”, *JHEP* **1212** (2012) 045, [arXiv:1207.1717](#). [[Inspire](#)].
- [196] **CMS** Collaboration, “Search for associated production of a single top quark and a Higgs boson in events where the Higgs boson decays to two photons at $\sqrt{s} = 8$ TeV”, [[CMS-PAS-HIG-14-001](#)].
- [197] **ATLAS** Collaboration, “Search for $H \rightarrow \gamma\gamma$ produced in association with top quarks and constraints on the top quark-Higgs boson Yukawa coupling using data taken at 7 TeV and 8 TeV with the ATLAS detector”, [[ATLAS-CONF-2014-043](#)].
- [198] R. Frederix, E. Re, and P. Torrielli, “Single-top t-channel hadroproduction in the four-flavour scheme with POWHEG and aMC@NLO”, *JHEP* **1209** (2012) 130, [arXiv:1207.5391](#). [[Inspire](#)].
- [199] R. Gröber and M. Mühlleitner, “Composite Higgs Boson Pair Production at the LHC”, *JHEP* **1106** (2011) 020, [arXiv:1012.1562](#). [[Inspire](#)].
- [200] R. Contino, M. Ghezzi, M. Moretti, G. Panico, F. Piccinini, and A. Wulzer, “Anomalous Couplings in Double Higgs Production”, *JHEP* **1208** (2012) 154, [arXiv:1205.5444](#). [[Inspire](#)].
- [201] M. Gillioz, R. Grober, C. Grojean, M. Muhlleitner, and E. Salvioni, “Higgs Low-Energy Theorem (and its corrections) in Composite Models”, *JHEP* **10** (2012) 004, [arXiv:1206.7120](#). [[Inspire](#)].
- [202] R. Aaij *et al.*, “First evidence for the decay $B_s \rightarrow \mu^+ \mu^-$ ”, *Phys. Rev. Lett.* **110** (2013) 021801, [arXiv:1211.2674](#). [[Inspire](#)].
- [203] A. J. Buras, J. Girrbach, D. Guadagnoli, and G. Isidori, “On the Standard Model prediction for $\text{BR}(B_s, d \rightarrow \mu^+ \mu^-)$ ”, *Eur. Phys. J. C* **72** (2012) 2172, [arXiv:1208.0934](#). [[Inspire](#)].
- [204] A. D. Roeck, J. Ellis, C. Grojean, S. Heinemeyer, K. Jakobs, *et al.*, “From the LHC to Future Colliders”, *Eur. Phys. J. C* **66** (2010) 525–583, [arXiv:0909.3240](#). [[Inspire](#)].
- [205] E. Todesco and F. Zimmermann, “Proceedings, EuCARD-AccNet-EuroLumi Workshop: The High-Energy Large Hadron Collider, Malta, Republic of Malta, 14 - 16 Oct 2010”, [arXiv:1111.7188](#). [[Inspire](#)].
- [206] O. Brüning, B. Goddard, M. Mangano, S. Myers, L. Rossi, E. Todesco, and F. Zimmermann, “High Energy LHC Document prepared for the European HEP strategy update”, [[CERN-ATS-2012-237](#)].

-
- [207] **CLIC Physics Working Group** Collaboration, E. Accomando *et al.*, “Physics at the CLIC multi-TeV linear collider”, [hep-ph/0412251](#). [[Inspire](#)].
- [208] P. Lebrun, L. Linssen, A. Lucaci-Timoce, D. Schulte, F. Simon, *et al.*, “The CLIC Programme: Towards a Staged e^+e^- Linear Collider Exploring the Terascale : CLIC Conceptual Design Report”, [arXiv:1209.2543](#). [[Inspire](#)].
- [209] V. Barger, T. Han, P. Langacker, B. McElrath, and P. Zerwas, “Effects of genuine dimension-six Higgs operators”, *Phys. Rev.* **D67** (2003) 115001, [hep-ph/0301097](#). [[Inspire](#)].
- [210] J. Bagger, V. D. Barger, K.-m. Cheung, J. F. Gunion, T. Han, *et al.*, “The Strongly interacting W W system: Gold plated modes”, *Phys.Rev.* **D49** (1994) 1246–1264, [hep-ph/9306256](#). [[Inspire](#)].
- [211] J. Bagger, V. D. Barger, K.-m. Cheung, J. F. Gunion, T. Han, *et al.*, “CERN LHC analysis of the strongly interacting W W system: Gold plated modes”, *Phys.Rev.* **D52** (1995) 3878–3889, [hep-ph/9504426](#). [[Inspire](#)].
- [212] A. Ballestrero, G. Bevilacqua, D. B. Franzosi, and E. Maina, “How well can the LHC distinguish between the SM light Higgs scenario, a composite Higgs and the Higgsless case using VV scattering channels?”, *JHEP* **0911** (2009) 126, [arXiv:0909.3838](#). [[Inspire](#)].
- [213] A. Ballestrero, G. Bevilacqua, and E. Maina, “A Complete parton level analysis of boson-boson scattering and ElectroWeak Symmetry Breaking in $l\nu$ + four jets production at the LHC”, *JHEP* **0905** (2009) 015, [arXiv:0812.5084](#). [[Inspire](#)].
- [214] **CMS Collaboration** Collaboration, P. Govoni, “Study of V V-scattering processes as a probe of electroweak symmetry breaking”, *AIP Conf.Proc.* **1078** (2009) 229–231. [[Inspire](#)].
- [215] E. Accomando, A. Ballestrero, A. Belhouari, and E. Maina, “Boson fusion and Higgs production at the LHC in six fermion final states with one charged lepton pair”, *Phys.Rev.* **D75** (2007) 113006, [hep-ph/0603167](#). [[Inspire](#)].
- [216] J. Butterworth, B. Cox, and J. R. Forshaw, “WW scattering at the CERN LHC”, *Phys. Rev.* **D65** (2002) 096014, [hep-ph/0201098](#). [[Inspire](#)].
- [217] T. Han, D. Krohn, L.-T. Wang, and W. Zhu, “New Physics Signals in Longitudinal Gauge Boson Scattering at the LHC”, *JHEP* **1003** (2010) 082, [arXiv:0911.3656](#). [[Inspire](#)].
- [218] D. Espriu and B. Yenko, “Longitudinal WW scattering in light of the “Higgs boson” discovery”, *Phys. Rev.* **D87** (2013) 055017, [arXiv:1212.4158](#). [[Inspire](#)].
- [219] A. Freitas and J. Gainer, “High Energy WW Scattering at the LHC with the Matrix Element Method”, *Phys. Rev.* **D88** (2013) 017302, [arXiv:1212.3598](#). [[Inspire](#)].
- [220] T. Corbett, O. Eboli, J. Gonzalez-Fraile, and M. Gonzalez-Garcia, “Robust Determination of the Higgs Couplings: Power to the Data”, *Phys.Rev.* **D87** (2013) 015022, [arXiv:1211.4580](#). [[Inspire](#)].
- [221] A. Azatov and J. Galloway, “Electroweak Symmetry Breaking and the Higgs Boson: Confronting Theories at Colliders”, *Int.J.Mod.Phys.* **A28** (2013) 1330004, [arXiv:1212.1380](#). [[Inspire](#)].

- [222] J. Ellis and T. You, “Updated Global Analysis of Higgs Couplings”, *JHEP* **1306** (2013) 103, [arXiv:1303.3879](#). [[Inspire](#)].
- [223] CMS Collaboration, “CMS at the High-Energy Frontier. Contribution to the Update of the European Strategy for Particle Physics”, [[CMS-NOTE-2012-006](#)].
- [224] ATLAS Collaboration, “Physics at a High-Luminosity LHC with ATLAS (Update)”,
- [225] R. Barbieri, G. Isidori, V. S. Rychkov, and E. Trincherini, “Heavy Vectors in Higgs-less models”, *Phys. Rev. D* **78** (2008) 036012, [arXiv:0806.1624](#). [[Inspire](#)].
- [226] R. Barbieri, A. E. Cárcamo Hernández, G. Corcella, R. Torre, and E. Trincherini, “Composite vectors at the Large Hadron Collider”, *JHEP* **03** (2010) 068, [arXiv:0911.1942](#). [[Inspire](#)].
- [227] A. Carcamo Hernandez and R. Torre, “A ‘Composite’ scalar-vector system at the LHC”, *Nucl.Phys. B* **841** (2010) 188–204, [arXiv:1005.3809](#). [[Inspire](#)].
- [228] A. Falkowski, C. Grojean, A. Kaminska, S. Pokorski, and A. Weiler, “If no Higgs then what?”, *JHEP* **11** (2011) 028, [arXiv:1108.1183](#). [[Inspire](#)].
- [229] R. Contino, T. Kramer, M. Son, and R. Sundrum, “Warped/composite phenomenology simplified”, *JHEP* **0705** (2007) 074, [hep-ph/0612180](#). [[Inspire](#)].
- [230] M. Redi and A. Weiler, “Flavor and CP Invariant Composite Higgs Models”, *JHEP* **11** (2011) 108, [arXiv:1106.6357](#). [[Inspire](#)].
- [231] CMS Collaboration, “Search for leptonic decays of W' bosons in pp collisions at $\sqrt{s} = 8$ TeV”, [[CMS-PAS-EXO-12-060](#)].
- [232] ATLAS Collaboration, “Search for high-mass states with one lepton plus missing transverse momentum in pp collisions at $\sqrt{s} = 8$ TeV with the ATLAS detector”, [[ATLAS-CONF-2014-017](#)].
- [233] CMS Collaboration, “Search for Resonances in the Dilepton Mass Distribution in pp Collisions at $\sqrt{s} = 8$ TeV”, [[CMS-PAS-EXO-12-061](#)].
- [234] ATLAS Collaboration, G. Aad *et al.*, “Search for high-mass dilepton resonances in pp collisions at $\sqrt{s} = 8$ TeV with the ATLAS detector”, [arXiv:1405.4123](#). [[Inspire](#)].
- [235] CMS Collaboration, V. Khachatryan *et al.*, “Search for new resonances decaying via WZ to leptons in proton-proton collisions at $\sqrt{s} = 8$ TeV”, [arXiv:1407.3476](#). [[Inspire](#)].
- [236] ATLAS Collaboration, G. Aad *et al.*, “Search for WZ resonances in the fully leptonic channel using pp collisions at $\sqrt{s} = 8$ TeV with the ATLAS detector”, [arXiv:1406.4456](#). [[Inspire](#)].
- [237] CMS Collaboration, “Search for new resonances decaying to $WW \rightarrow \ell\nu q\bar{q}$ in the final state with a lepton, missing transverse energy, and single reconstructed jet”, [[CMS-PAS-EXO-12-021](#)].
- [238] CMS Collaboration, “Search for a narrow spin-2 resonance decaying to Z bosons in the semileptonic final state”, [[CMS-PAS-EXO-12-022](#)].
- [239] CMS Collaboration, “Search for heavy resonances in the W/Z -tagged dijet mass spectrum in pp collisions at 8 TeV”, [[CMS-PAS-EXO-12-024](#)].

- [240] A. De Simone, O. Matsedonskyi, R. Rattazzi, and A. Wulzer, “A First Top Partner’s Hunter Guide”, *JHEP* **04** (2013) 004, [arXiv:1211.5663](#). [[Inspire](#)].
- [241] A. Azatov and J. Galloway, “Light Custodians and Higgs Physics in Composite Models”, *Phys.Rev.* **D85** (2012) 055013, [arXiv:1110.5646](#). [[Inspire](#)].
- [242] C. Delaunay, C. Grojean, and G. Perez, “Modified Higgs Physics from Composite Light Flavors”, *JHEP* **1309** (2013) 090, [arXiv:1303.5701](#). [[Inspire](#)].
- [243] M. Montull, F. Riva, E. Salvioni, and R. Torre, “Higgs Couplings in Composite Models”, *Phys.Rev.* **D88** (2013) 095006, [arXiv:1308.0559](#). [[Inspire](#)].
- [244] M. S. Chanowitz and W. Kilgore, “Complementarity of Resonant and Nonresonant Strong WW Scattering at the LHC”, *Phys. Lett.* **B 322** (1993) 147–153, [hep-ph/9311336](#). [[Inspire](#)].
- [245] M. S. Chanowitz and W. B. Kilgore, “ W^+Z and $W^+\gamma^*$ backgrounds to strong W^+W^+ scattering at the LHC”, *Phys.Lett.* **B347** (1995) 387–393, [hep-ph/9412275](#). [[Inspire](#)].
- [246] M. S. Chanowitz, “Strong $W W$ scattering at the end of the 90’s: Theory and experimental prospects”, [hep-ph/9812215](#). [[Inspire](#)].
- [247] R. Casalbuoni, P. Chiappetta, A. Deandrea, S. De Curtis, D. Dominici, *et al.*, “Vector resonances from a strong electroweak sector at linear colliders”, *Z.Phys.* **C60** (1993) 315–326, [hep-ph/9303201](#). [[Inspire](#)].
- [248] W. Bernreuther and T. Schroder, “Strongly interacting Higgs sector and W pair production in e^+e^- collisions”, *Z.Phys.* **C62** (1994) 615–622. [[Inspire](#)].
- [249] D. Dominici, “Tests for a strong electroweak sector at future e^+e^- high-energy colliders”, *Riv.Nuovo Cim.* **20N11** (1997) 1–64, [hep-ph/9711385](#). [[Inspire](#)].
- [250] P. Poulose, S. Rindani, and L. Sehgal, “Lepton spectra from $e^+e^- \rightarrow W^+W^-$ in the BESS model”, *Phys.Lett.* **B525** (2002) 71–80, [hep-ph/0111134](#). [[Inspire](#)].
- [251] T. L. Barklow, “Strong symmetry breaking at e^+e^- linear colliders”, *eConf* **C010630** (2001) E3067, [hep-ph/0112286](#). [[Inspire](#)].
- [252] B. Ananthanarayan, M. Patra, and P. Poulose, “Probing strongly interacting W ’s at the ILC with polarized beams”, *JHEP* **1203** (2012) 060, [arXiv:1112.5020](#). [[Inspire](#)].
- [253] **CLIC Detector and Physics Study Collaboration** Collaboration, H. Abramowicz *et al.*, “Physics at the CLIC e^+e^- Linear Collider – Input to the Snowmass process 2013”, [arXiv:1307.5288](#). [[Inspire](#)].
- [254] S. Dutta, K. Hagiwara, and Y. Matsumoto, “Measuring the Higgs-Vector boson Couplings at Linear e^+e^- Collider”, *Phys.Rev.* **D78** (2008) 115016, [arXiv:0808.0477](#). [[Inspire](#)].
- [255] M. E. Peskin, “Comparison of LHC and ILC Capabilities for Higgs Boson Coupling Measurements”, [arXiv:1207.2516](#). [[Inspire](#)].
- [256] M. Klute, R. Lafaye, T. Plehn, M. Rauch, and D. Zerwas, “Measuring Higgs Couplings at a Linear Collider”, *Europhys.Lett.* **101** (2013) 51001, [arXiv:1301.1322](#). [[Inspire](#)].
- [257] G. Ferrera, J. Guasch, D. Lopez-Val, and J. Sola, “Triple Higgs boson production

- in the Linear Collider”, *Phys. Lett.* **B659** (2008) 297–307, [arXiv:0707.3162](#). [[Inspire](#)].
- [258] A. Belyaev, A. Oliveira, R. Rosenfeld, and M. C. Thomas, “Multi Higgs and Vector boson production beyond the Standard Model”, *JHEP* **1305** (2013) 005, [arXiv:1212.3860](#). [[Inspire](#)].
- [259] T. Binoth, S. Karg, N. Kauer, and R. Ruckl, “Multi-Higgs boson production in the Standard Model and beyond”, *Phys.Rev.* **D74** (2006) 113008, [hep-ph/0608057](#). [[Inspire](#)].
- [260] V. D. Barger, K.-m. Cheung, T. Han, and R. Phillips, “Probing strongly interacting electroweak dynamics through W^+W^- / ZZ ratios at future e^+e^- colliders”, *Phys.Rev.* **D52** (1995) 3815–3825, [hep-ph/9501379](#). [[Inspire](#)].
- [261] T. Han, “Higgs boson and $W(L)W(L)$ scattering at e^-e^- colliders”, *Int.J.Mod.Phys.* **A11** (1996) 1541–1550, [hep-ph/9601393](#). [[Inspire](#)].
- [262] E. Boos, H. He, W. Kilian, A. Pukhov, C. Yuan, *et al.*, “Strongly interacting vector bosons at TeV e^+e^- linear colliders”, *Phys.Rev.* **D57** (1998) 1553, [hep-ph/9708310](#). [[Inspire](#)].
- [263] V. D. Barger and T. Han, “Double Higgs Boson Production via WW Fusion in TeV e^+e^- Collisions”, *Mod.Phys.Lett.* **A5** (1990) 667–674. [[Inspire](#)].
- [264] E. Asakawa, D. Harada, S. Kanemura, Y. Okada, and K. Tsumura, “Higgs boson pair production in new physics models at hadron, lepton, and photon colliders”, *Phys.Rev.* **D82** (2010) 115002, [arXiv:1009.4670](#). [[Inspire](#)].
- [265] T. Han, Y.-P. Kuang, and B. Zhang, “Anomalous gauge couplings of the Higgs boson at high energy photon colliders”, *Phys.Rev.* **D73** (2006) 055010, [hep-ph/0512193](#). [[Inspire](#)].
- [266] W. Kilian, T. Ohl, and J. Reuter, “WHIZARD: Simulating Multi-Particle Processes at LHC and ILC”, *Eur. Phys. J.* **C71** (2011) 1742, [arXiv:0708.4233](#). [[Inspire](#)].
- [267] G. Gounaris, D. Schildknecht, and F. Renard, “Test of Higgs Boson Nature in $e^+e^- \rightarrow HHZ$ ”, *Phys.Lett.* **B83** (1979) 191. [[Inspire](#)].
- [268] V. D. Barger, T. Han, and R. Phillips, “Double Higgs Boson Bremsstrahlung From W and Z Bosons at Supercolliders”, *Phys.Rev.* **D38** (1988) 2766. [[Inspire](#)].
- [269] A. Djouadi, H. Haber, and P. Zerwas, “Multiple production of MSSM neutral Higgs bosons at high-energy e^+e^- colliders”, *Phys.Lett.* **B375** (1996) 203–212, [hep-ph/9602234](#). [[Inspire](#)].
- [270] A. Djouadi, W. Kilian, M. Muhlleitner, and P. Zerwas, “Testing Higgs selfcouplings at e^+e^- linear colliders”, *Eur.Phys.J.* **C10** (1999) 27–43, [hep-ph/9903229](#). [[Inspire](#)].
- [271] S. S. Biswal, D. Choudhury, R. M. Godbole, and Mamta, “Role of polarization in probing anomalous gauge interactions of the Higgs boson”, *Phys.Rev.* **D79** (2009) 035012, [arXiv:0809.0202](#). [[Inspire](#)].
- [272] R. Killick, K. Kumar, and H. E. Logan, “Learning what the Higgs boson is mixed with”, *Phys.Rev.* **D88** (2013) 033015, [arXiv:1305.7236](#). [[Inspire](#)].
- [273] C. W. Bauer, Z. Ligeti, M. Schmaltz, J. Thaler, and D. G. E. Walker, “Supermodels

- for early LHC”, *Phys. Lett. B* **690** (2010) 280–288, [arXiv:0909.5213](#). [[Inspire](#)].
- [274] R. Barbieri and R. Torre, “Signals of single particle production at the earliest LHC”, *Phys. Lett. B* **695** (2011) 259–263, [arXiv:1008.5302](#). [[Inspire](#)].
- [275] T. Han, I. Lewis, and Z. Liu, “Colored Resonant Signals at the LHC: Largest Rate and Simplest Topology”, *JHEP* **12** (2010) 085, [arXiv:1010.4309](#). [[Inspire](#)].
- [276] E. Accomando, A. S. Belyaev, L. Fedeli, S. F. King, and C. H. Shepherd-Themistocleous, “ Z' physics with early LHC data”, *Phys. Rev. D* **83** (2012) 075012, [arXiv:1010.6058](#). [[Inspire](#)].
- [277] M. Schmaltz and C. Spethmann, “Two Simple W' Models for the Early LHC”, *JHEP* **07** (2011) 046, [arXiv:1011.5918](#). [[Inspire](#)].
- [278] C. Grojean, E. Salvioni, and R. Torre, “A weakly constrained W' at the early LHC”, *JHEP* **07** (2011) 002, [arXiv:1103.2761](#). [[Inspire](#)].
- [279] C.-W. Chiang, N. D. Christensen, G.-J. Ding, and T. Han, “Discovery in Drell-Yan Processes at the LHC”, *Phys. Rev. D* **85** (2012) 015023, [arXiv:1107.5830](#). [[Inspire](#)].
- [280] R. Torre, “Limits on leptophobic W' after 1 fb^{-1} of LHC data: a lesson on parton level simulations”, [arXiv:1109.0890](#). [[Inspire](#)].
- [281] R. Torre, “An isosinglet W' at the LHC: updated bounds from direct searches”, *PoS CORFU2011* (2011) 036, [arXiv:1204.4364](#). [[Inspire](#)].
- [282] J. de Blas, J. M. Lizana, and M. Perez-Victoria, “Combining searches of Z' and W' bosons”, *JHEP* **01** (2013) 166, [arXiv:1211.2229](#). [[Inspire](#)].
- [283] M. Buchkremer, G. Cacciapaglia, A. Deandrea, and L. Panizzi, “Model Independent Framework for Searches of Top Partners”, *Nucl. Phys. B* **876** (2013) 376–417, [arXiv:1305.4172](#). [[Inspire](#)].
- [284] J. A. Aguilar-Saavedra, R. Benbrik, S. Heinemeyer, and M. Perez-Victoria, “A handbook of vector-like quarks: mixing and single production”, *Phys. Rev. D* **88** (2013) 094010, [arXiv:1306.0572](#). [[Inspire](#)].
- [285] J. M. Lizana and M. Perez-Victoria, “Vector triplets at the LHC”, *EPJ Web Conf.* **60** (2013) 17008, [arXiv:1307.2589](#). [[Inspire](#)].
- [286] V. Barger, W.-Y. Keung, and E. Ma, “Gauge model with light W and Z bosons”, *Phys. Rev. D* **22** (1980) 727. [[Inspire](#)].
- [287] J. L. Hewett and T. G. Rizzo, “Low-energy phenomenology of superstring-inspired E_6 models”, *Phys. Rept.* **183** (1989) 193–381. [[Inspire](#)].
- [288] M. Cvetič and S. Godfrey, “Discovery and Identification of Extra Gauge Bosons”, In **Barklow, T.L. (ed.) et al.: Electroweak symmetry breaking and new physics at the TeV scale** (1995) 383–415, [hep-ph/9504216](#). [[Inspire](#)].
- [289] T. G. Rizzo, “ Z' Phenomenology and the LHC”, [hep-ph/0610104](#). [[Inspire](#)].
- [290] P. Langacker, “The Physics of Heavy Z' Gauge Bosons”, *Rev. Mod. Phys.* **81** (2009) 119–1228, [arXiv:0801.1345](#). [[Inspire](#)].
- [291] E. Salvioni, G. Villadoro, and F. Zwirner, “Minimal Z' models: present bounds and early LHC reach”, *JHEP* **11** (2009) 068, [arXiv:0909.1320](#). [[Inspire](#)].
- [292] E. Salvioni, A. Strumia, G. Villadoro, and F. Zwirner, “Non-universal minimal Z'

- models: present bounds and early LHC reach”, *JHEP* **03** (2010) 010, [arXiv:0911.1450](#). [[Inspire](#)].
- [293] E. Salvioni, “Minimal Z' models and the early LHC”, *Frascati Phys.Ser.* **51** (2010) 1–6, [arXiv:1007.0490](#). [[Inspire](#)].
- [294] M. S. Chanowitz, “A heavy little Higgs and a light Z' under the radar”, *Phys. Rev. D* **84** (2011) 035014, [arXiv:1102.3672](#). [[Inspire](#)].
- [295] E. Salvioni, “Some Z-prime and W-prime models facing current LHC searches”, *20th International Workshop on Deep-Inelastic Scattering and Related Subjects (DIS 2012) Proceeding* (2012) 609–612. [[Inspire](#)].
- [296] E. Accomando, D. Becciolini, A. S. Belyaev, S. Moretti, and C. H. Shepherd-Themistocleous, “ Z' at the LHC: Interference and Finite Width Effects in Drell-Yan”, *JHEP* **10** (2013) 153, [arXiv:1304.6700](#). [[Inspire](#)].
- [297] P. Langacker and S. U. Sankar, “Bounds on the mass of W_R and the $W_L - W_R$ mixing angle ζ in general $SU(2)_L \times SU(2)_R \times U(1)$ models”, *Phys. Rev. D* **40** (1989) 1569–1585. [[Inspire](#)].
- [298] Z. Sullivan, “Fully differential W' production and decay at next-to-leading order in QCD”, *Phys. Rev. D* **66** (2002) 075011, [hep-ph/0207290](#). [[Inspire](#)].
- [299] T. G. Rizzo, “The Determination of the Helicity of W' Boson Couplings at the LHC”, *JHEP* **05** (2007) 037, [arXiv:0704.0235](#). [[Inspire](#)].
- [300] M. Frank, A. Hayreter, and I. Turan, “Production and Decays of W_R bosons at the LHC”, *Phys. Rev. D* **83** (2011) 035001, [arXiv:1010.5809](#). [[Inspire](#)].
- [301] E. Accomando, D. Becciolini, S. de Curtis, D. Dominici, L. Fedeli, and C. H. Shepherd-Themistocleous, “Interference effects in heavy W' -boson searches at the LHC”, *Phys. Rev. D* **85** (2011) 115017, [arXiv:1110.0713](#). [[Inspire](#)].
- [302] K. Agashe, H. Davoudiasl, S. Gopalakrishna, T. Han, G.-Y. Huang, G. Perez, Z.-G. Si, and A. Soni, “LHC Signals for Warped Electroweak Neutral Gauge Bosons”, *Phys. Rev. D* **76** (2007) 115015, [arXiv:0709.0007](#). [[Inspire](#)].
- [303] K. Agashe, S. Gopalakrishna, T. Han, G.-Y. Huang, and A. Soni, “LHC signals for warped electroweak charged gauge bosons”, *Phys. Rev. D* **80** (2009) 075007, [arXiv:0810.1497](#). [[Inspire](#)].
- [304] K. Agashe, A. Azatov, T. Han, Y. Li, Z.-G. Si, and L. Zhu, “LHC Signals for Coset Electroweak Gauge Bosons in Warped/Composite PGB Higgs Models”, *Phys. Rev. D* **81** (2010) 096002, [arXiv:0911.0059](#). [[Inspire](#)].
- [305] B. Bellazzini, C. Csaki, J. Hubisz, J. Serra, and J. Terning, “Composite Higgs Sketch”, *JHEP* **11** (2012) 003, [arXiv:1205.4032](#). [[Inspire](#)].
- [306] E. Accomando, L. Fedeli, S. Moretti, S. D. Curtis, and D. Dominici, “Charged di-boson production at the LHC in a 4-site model with a composite Higgs boson”, *Phys. Rev. D* **86** (2012) 115006, [arXiv:1208.0268](#). [[Inspire](#)].
- [307] A. E. Cárcamo Hernández, C. O. Dib, and A. R. Zerwekh, “The Effect of Composite Resonances on Higgs decay into two photons”, *Eur. Phys. J. C* **74** (2014) 2822, [arXiv:1304.0286](#). [[Inspire](#)].
- [308] R. Barbieri, V. S. Rychkov, and R. Torre, “Signals of composite

- electroweak-neutral Dark Matter: LHC/Direct Detection interplay”, *Phys. Lett. B* **688** (2010) 212–215, [arXiv:1001.3149](#). [[Inspire](#)].
- [309] A. E. Cárcamo Hernández and R. Torre, “A ‘composite’ scalar-vector system at the LHC”, *Nucl. Phys. B* **841** (2010) 188, [arXiv:1005.3809](#). [[Inspire](#)].
- [310] A. E. Cárcamo Hernández, “Top quark effects in composite vector pair production at the LHC”, *Eur. Phys. J. C* **72** (2012) 2154, [arXiv:1008.1039](#). [[Inspire](#)].
- [311] O. Catà, G. Isidori, and J. F. Kamenik, “Drell-Yan production of Heavy Vectors in Higgsless models”, *Nucl. Phys. B* **822** (2009) 230, [arXiv:0905.0490](#). [[Inspire](#)].
- [312] E. Accomando, D. Becciolini, S. D. Curtis, D. Dominici, and L. Fedeli, “ W' production at the LHC in the 4-site Higgsless model”, *Phys. Rev. D* **84** (2011) 115014, [arXiv:1107.4087](#). [[Inspire](#)].
- [313] **ATLAS** Collaboration, G. Aad *et al.*, “Measurement of $W\gamma$ and $Z\gamma$ production cross sections in pp collisions at $\sqrt{s} = 7$ TeV and limits on anomalous triple gauge couplings with the ATLAS detector”, *Phys. Lett. B* **717** (2012) 49–69, [arXiv:1205.2531](#). [[Inspire](#)].
- [314] **ATLAS** Collaboration, G. Aad *et al.*, “Measurement of WZ production in proton-proton collisions at $\sqrt{s} = 7$ TeV with the ATLAS detector”, *Eur. Phys. J. C* **72** (2012) 2173, [arXiv:1208.1390](#). [[Inspire](#)].
- [315] **ATLAS** Collaboration, G. Aad *et al.*, “Search for new phenomena in the dijet mass distribution using pp collision data at $\sqrt{s} = 8$ TeV with the ATLAS detector”, [arXiv:1407.1376](#). [[Inspire](#)].
- [316] **ATLAS** Collaboration, “Search for resonant ZZ production in the $ZZ \rightarrow llqq$ channel with the ATLAS detector using 7.2 fb $^{-1}$ of $\sqrt{s} = 8$ TeV pp collision data”, [[ATLAS-CONF-2012-150](#)].
- [317] **ATLAS** Collaboration, “A search for high-mass ditau resonances decaying in the fully hadronic final state in pp collisions at $\sqrt{s} = 8$ TeV with the ATLAS detector”, [[ATLAS-CONF-2013-066](#)].
- [318] **ATLAS** Collaboration, “A search for $t\bar{t}$ resonances in the lepton plus jets final state with ATLAS using 14 fb $^{-1}$ of pp collisions at $\sqrt{s} = 8$ TeV”, [[ATLAS-CONF-2013-052](#)].
- [319] **ATLAS** Collaboration, “Search for $W' \rightarrow t\bar{b}$ in proton-proton collisions at a centre-of-mass energy of $\sqrt{s} = 8$ TeV with the ATLAS detector”, [[ATLAS-CONF-2013-050](#)].
- [320] **CMS** Collaboration, “Search for Anomalous Top Quark Pair Production in the Boosted All-Hadronic Final State using pp Collisions at $\sqrt{s} = 8$ TeV”, [[CMS-PAS-B2G-12-005](#)].
- [321] **CMS** Collaboration, “Search for Heavy Resonances Decaying into bb and bg Final States in pp Collisions at $\sqrt{s} = 8$ TeV”, [[CMS-PAS-EXO-12-023](#)].
- [322] **CMS** Collaboration, “Search for Narrow Resonances using the Dijet Mass Spectrum with 19.6 fb $^{-1}$ of pp Collisions at $\sqrt{s} = 8$ TeV”, [[CMS-PAS-EXO-12-059](#)].
- [323] **CMS** Collaboration, “Search for narrow $t + b$ resonances in the leptonic final state at $\sqrt{s} = 8$ TeV”, [[CMS-PAS-B2G-12-010](#)].

- [324] D. Pappadopulo, A. Thamm, R. Torre, and A. Wulzer, “Tools for the study of heavy vector triplets”, <http://heidi.pd.infn.it/html/vector/index.html>.
- [325] F. del Aguila, J. de Blas, and M. Perez-Victoria, “Electroweak Limits on General New Vector Bosons”, *JHEP* **09** (2010) 033, [arXiv:1005.3998](#). [[Inspire](#)].
- [326] R. Torre, *Signals of composite particles at the LHC*. PhD thesis, Università di Pisa, 2011. [arXiv:1110.3906](#). [[Inspire](#)].
- [327] P. Borel, R. Franceschini, R. Rattazzi, and A. Wulzer, “Probing the Scattering of Equivalent Electroweak Bosons”, *JHEP* **06** (2012) 122, [arXiv:1202.1904](#). [[Inspire](#)].
- [328] T. Han, P. Langacker, Z. Liu, and L.-T. Wang, “Diagnosis of a New Neutral Gauge Boson at the LHC and ILC for Snowmass 2013”, [arXiv:1308.2738](#). [[Inspire](#)].
- [329] D. Hayden, R. Brock, and C. Willis, “Z Prime: A Story”, [arXiv:1308.5874](#). [[Inspire](#)].
- [330] S. Godfrey and T. Martin, “Z’ Discovery Reach at Future Hadron Colliders: A Snowmass White Paper”, [arXiv:1309.1688](#). [[Inspire](#)].
- [331] A. Katz, M. Son, and B. Tweedie, “Jet Substructure and the Search for Neutral Spin-One Resonances in Electroweak Boson Channels”, *JHEP* **03** (2011) 011, [arXiv:1010.5253](#). [[Inspire](#)].
- [332] A. Katz, M. Son, and B. Tweedie, “Ditau-Jet Tagging and Boosted Higgses from a Multi-TeV Resonance”, *Phys. Rev. D* **83** (2011) 114033, [arXiv:1011.4523](#). [[Inspire](#)].
- [333] M. Son, C. Spethmann, and B. Tweedie, “Diboson-Jets and the Search for Resonant Zh Production”, *JHEP* **08** (2012) 160, [arXiv:1204.0525](#). [[Inspire](#)].
- [334] D. Choudhury, R. M. Godbole, and P. Saha, “Dijet resonances, widths and all that”, *JHEP* **01** (2012) 155, [arXiv:1111.1054](#). [[Inspire](#)].
- [335] **ATLAS** Collaboration, “Search for pair production of heavy top-like quarks decaying to a high-pT W boson and a b quark in the lepton plus jets final state in pp collisions at $\sqrt{s} = 8$ TeV with the ATLAS detector”, [[ATLAS-CONF-2013-060](#)].
- [336] **ATLAS** Collaboration, “Search for pair production of new heavy quarks that decay to a Z boson and a third generation quark in pp collisions at $\sqrt{s} = 8$ TeV with the ATLAS detector”, [[ATLAS-CONF-2013-056](#)].
- [337] **ATLAS** Collaboration, “Search for anomalous production of events with same-sign dileptons and b jets in 14.3 fb^{-1} of pp collisions at $\sqrt{s} = 8$ TeV with the ATLAS detector”, [[ATLAS-CONF-2013-051](#)].
- [338] **ATLAS** Collaboration, “Search for heavy top-like quarks decaying to a Higgs boson and a top quark in the lepton plus jets final state in pp collisions at $\sqrt{s} = 8$ TeV with the ATLAS detector”, [[ATLAS-CONF-2013-018](#)].
- [339] **CMS** Collaboration, S. C. *et al.*, “Inclusive search for a vector-like T quark with charge 2/3 in pp collisions at $\sqrt{s} = 8$ TeV”, *Phys. Lett. B* **729** (2014) 149–171, [arXiv:1311.7667](#). [[Inspire](#)].
- [340] **CMS** Collaboration, “Search for Vector-Like b' Pair Production with Multilepton Final States in pp collisions at $\sqrt{s} = 8$ TeV”, [[CMS-PAS-B2G-13-003](#)].
- [341] **CMS** Collaboration, “Search for pair-produced vector-like quarks of charge $-1/3$

- in lepton+jets final state in pp collisions at $\sqrt{s} = 8$ TeV”, [CMS-PAS-B2G-12-019].
- [342] CMS Collaboration, “Search for pair-produced vector-like quarks of charge $-1/3$ in dilepton+jets final state in pp collisions at $\sqrt{s} = 8$ TeV”, [CMS-PAS-B2G-12-021].
- [343] CMS Collaboration, “Inclusive search for top partners in single- and multiple-lepton final states at $\sqrt{s} = 8$ TeV”, [CMS-PAS-B2G-12-015].
- [344] CMS Collaboration, S. C. *et al.*, “Search for top-quark partners with charge $5/3$ in the same-sign dilepton final state”, [arXiv:1312.2391](#). [Inspire].
- [345] O. Matsedonskyi, F. Riva, and T. Vantalón, “Composite Charge $8/3$ Resonances at the LHC”, *JHEP* **1404** (2014) 059, [arXiv:1401.3740](#). [Inspire].
- [346] S. Coleman, J. Wess, and B. Zumino, “Structure of Phenomenological Lagrangians. I”, *Phys. Rev.* **177** (1969) 2239–2247. [Inspire].
- [347] CMS Collaboration, “Search for $T_{5/3}$ top partners in same-sign dilepton final state”, [CMS-PAS-B2G-12-012].
- [348] CMS Collaboration, S. C. *et al.*, “Search for microscopic black holes in pp collisions at $\sqrt{s} = 8$ TeV”, *JHEP* **1307** (2013) 178, [arXiv:1303.5338](#). [Inspire].
- [349] ATLAS Collaboration, G. A. *et al.*, “Search for microscopic black holes in a like-sign dimuon final state using large track multiplicity with the ATLAS detector”, *Phys. Rev. D* **88** (2013) 072001, [arXiv:1308.4075](#). [Inspire].
- [350] K. Agashe, A. Delgado, and R. Sundrum, “Gauge coupling renormalization in RS1”, *Nucl. Phys.* **B643** (2002) 172–186, [hep-ph/0206099](#). [Inspire].
- [351] A. Alloul, N. D. Christensen, C. Degrande, C. Duhr, and B. Fuks, “FeynRules 2.0 - A complete toolbox for tree-level phenomenology”, [arXiv:1310.1921](#). [Inspire].
- [352] C. Duhr, N. D. Christensen, and B. Fuks, “FeynRules - A Mathematica package to calculate Feynman rules”, <http://feynrules.irmp.ucl.ac.be>.
- [353] A. Belyaev, N. D. Christensen, and A. Pukhov, “CalcHEP 3.4 for collider physics within and beyond the Standard Model”, *Comput. Phys. Commun.* **184** (2013) 1729–1769, [arXiv:1207.6082](#). [Inspire].
- [354] A. Belyaev, N. Christensen, and A. Pukhov, “CalcHEP - a package for calculation of Feynman diagrams and integration over multi-particle phase space”, [Web page of the package](#).
- [355] “High energy physics models database”, <http://hepmdb.soton.ac.uk>.
- [356] D. Pappadopulo, A. Thamm, R. Torre, and A. Wulzer, “Vector triplet (bridge model)”, <http://hepmdb.soton.ac.uk/hepmdb:0214.0151>.
- [357] Wolfram, “Computable document format”, <http://www.wolfram.com/cdf/>.

Da steh' ich nun, ich armer Tor,
Und bin so klug als wie zuvor!
— Johann Wolfgang von Goethe

ANDREA THAMM

ADDRESS

École Polytechnique Fédérale de Lausanne
Institut de Théorie des Phénomènes Physiques
CH - 1015 Lausanne
Switzerland

E-MAIL

andrea.thamm@epfl.ch
andrea.thamm@cern.ch

DATE OF BIRTH 2 July 1987, Rostock, Germany
NATIONALITY German

PH.D. AT ÉPFL (LAUSANNE, SWITZERLAND)

09/2010 - 08/2014	pursuing Ph.D. in beyond the Standard Model phenomenology Topic: Effective Lagrangian approach to electroweak symmetry breaking Supervisors: Prof. Riccardo Rattazzi and Prof. Christophe Grojean
02/2012 - present	teaching assistant for Quantum Field Theory course by Prof. Riccardo Rattazzi
09/2010 - 08/2012	Marie Curie (ITN) Fellow at CERN UNILHC Grant

EDUCATION AT THE UNIVERSITY OF EDINBURGH (UK)

09/2008 - 06/2010	Degree of Master of Physics with First Class Honours in Mathematical Physics Master Thesis: Decoupling in Effective Field Theories Supervisor: Prof. Luigi Del Debbio
09/2006 - 08/2008	Direct entry into second year, pursuing Master of Physics with Honours Computational Physics Change of degree specialisation to Mathematical Physics

EDUCATION IN LEIPZIG (GERMANY)

09/2002 - 06/2006	Wilhelm-Ostwald-Gymnasium, secondary school with emphasis on mathematics and natural sciences Graduation with <i>Abitur</i> , average grade 1.0 (highest possible grade)
-------------------	--

LIST OF PUBLICATIONS

1. G. Brooijmans *et al.* *Les Houches 2013: Physics at TeV Colliders: New Physics Working Group Report*, [arXiv:1405.1617](#) [[Inspire](#)]
2. D. Pappadopulo, A. Thamm, R. Torre and A. Wulzer, *Heavy Vector Triplets: Bridging Theory and Data*, [arXiv:1402.4431](#) [[Inspire](#)]
3. R. Contino, C. Grojean, D. Pappadopulo, R. Rattazzi and A. Thamm, *Strong Higgs Interactions at a Linear Collider*, [JHEP 1402 \(2014\) 006](#), [arXiv:1309.7038](#) [[Inspire](#)]
4. H. Abramowicz *et al.* [CLIC Detector and Physics Study Collaboration], *Physics at the CLIC e^+e^- Linear Collider – Input to the Snowmass process 2013*, [arXiv:1307.5288](#) [[Inspire](#)]
5. D. Pappadopulo, A. Thamm and R. Torre, *A minimally tuned composite Higgs model from an extra dimension*, [JHEP 1307 \(2013\) 058](#), [arXiv:1303.3062](#) [[Inspire](#)]
6. A. De Simone, A. Monin, A. Thamm and A. Urbano, *On the effective operators for Dark Matter annihilations*, [JCAP 1302 \(2013\) 039](#), [arXiv:1301.1486](#) [[Inspire](#)]
7. M. Farina, C. Grojean, F. Maltoni, E. Salvioni and A. Thamm, *Lifting degeneracies in Higgs couplings using single top production in association with a Higgs boson*, [JHEP 1305 \(2013\) 022](#), [arXiv:1211.3736](#) [[Inspire](#)]

PROCEEDINGS

1. A. Thamm, *Strong multiple Higgs production at CLIC*, [PoS CORFU 2011 \(2011\) 035](#) [[Inspire](#)]

Heavy Vector Triplets: Bridging Theory and Data

Seminar, Universität Mainz, Germany, 3 June 2014

Seminar, Universitat Autònoma de Barcelona, Spain, 9 May 2014

Workshop: After the Discovery, Benasque, Spain, 17 April 2014

Anomalous Higgs couplings in composite models at the LHC and beyond

Phenomenology seminar, Scuola Normale Superiore, Italy, 11 December 2013

Theoretical physics seminar, Vrije Universiteit Brussel, Belgium, 28 November 2013

Invited seminar, Université catholique de Louvain, Belgium, 27 November 2013

High energy theory seminar, Padova University, Italy, 22 November 2013

High energy theoretical physics seminar, EPFL, Switzerland, 04 November 2013

Effective operators for dark matter annihilations

25th Rencontres des Blois 2013, Blois, France, 29 May 2013

A minimally tuned composite Higgs model from an extra dimension

Planck 2013, Bonn, Germany, 22 May 2013

Strong Higgs production at CLIC

TASI 2012, University of Colorado, Boulder, USA, 20 June 2012

Planck 2012, Warsaw, Poland, 30 May 2012

School on Strongly Coupled Physics, ICTP, Trieste, Italy, 20 January 2012

1st School of ITN: Unification in the LHC Era, Corfu, Greece, 8 September 2011

1st Future Hadron Collider Workshop

CERN, Switzerland, 26 – 28 May 2014

After the Discovery: Hunting for a Non-Standard Higgs Sector

Centro de Ciencias de Benasque Pedro Pascual, Benasque, Spain, 6 – 18 April 2014

BSM physics opportunities at 100 TeV

CERN, Switzerland, 11 – 12 February 2014

PiTP 2013: LHC Physics

IAS, Princeton, USA, 15 – 26 July 2013

GGI Workshop: Beyond the Standard Model after the first run of the LHC

The Galileo Galilei Institute for Theoretical Physics, Florence, Italy, 03 – 21 June 2013

25th Rencontres des Blois 2013

Blois, France, 26 – 31 May 2013

Planck 2013: From the Planck Scale to the Electroweak Scale

Bonn, Germany, 20 – 24 May 2013

62th Lindau Nobel Laureate Meeting

Lindau, Germany, 01 – 06 July 2012

Planck 2012: From the Planck Scale to the Electroweak Scale

Warsaw, Poland, 28 May – 01 June 2012

School and Workshop on Strongly Couple Physics Beyond the Standard Model

ICTP, Trieste, Italy, 16 – 27 January 2012

1st Summer School of ITN: Unification in the LHC Era

Corfu, Greece, 04 – 15 September 2011

Theoretical Physics to Face the Challenge of the LHC

Les Houches, France, 01 – 26 August 2011

Planck 2011: From the Planck Scale to the Electroweak Scale

Lisbon, Portugal, 30 May – 03 June 2011

UNILHC Training Workshop on Science Communication

SISSA, Trieste, Italy, 20 – 26 March 2011